

Xuezhong He

# Development of Hollow Fiber Carbon Membranes for CO<sub>2</sub> Separation

Thesis for the degree of Philosophiae Doctor

Trondheim, May 2011

Norwegian University of Science and Technology  
Faculty of Natural Sciences and Technology  
Department of Chemical Engineering



**NTNU – Trondheim**  
Norwegian University of  
Science and Technology

**NTNU**

Norwegian University of Science and Technology

Thesis for the degree of Philosophiae Doctor

Faculty of Natural Sciences and Technology  
Department of Chemical Engineering

© Xuezhong He

ISBN 978-82-471-2606-6 (printed ver.)  
ISBN 978-82-471-2607-3 (electronic ver.)  
ISSN 1503-8181

Doctoral theses at NTNU, 2011:42

Printed by NTNU-trykk

## **Abstract**

CO<sub>2</sub> capture from flue gases by membrane technology in post combustion power plants could be used for the reducing of CO<sub>2</sub> emissions. Previous work has demonstrated that the carbon membrane can achieve a high separation performance with respect to high CO<sub>2</sub> permeability and selectivity over the other gases, such as N<sub>2</sub> and O<sub>2</sub>. The focus of the current work was to find a low-cost precursor and develop a simple process for the preparation of high performance hollow fiber carbon membranes (HFCMs) for CO<sub>2</sub> separation.

The cellulose acetate (CA) hollow fibers were spun from a dope solution of CA / Polyvinylpyrrolidone (PVP) / N-methyl-2-pyrrolidone (NMP) (22.5 % / 5 % / 72.5 %) using an optimal spinning condition: bore fluid (water + NMP (85 %)), air gap (25 mm), bore flow rate (40 % of dope flow rate) and temperature of quench bath (50 °C). The cellulosic hollow fibers, regenerated from the spun CA fibers by deacetylation, were used as the precursors for preparation of HFCMs. The experimental results indicated that the precursors would influence significantly the separation performances of the prepared HFCMs. Therefore, the deacetylation process needed to be optimized, and the optimal deacetylation condition was found to be: soaking CA hollow fibers in a 10 % glycerol solution for 24 h, and then treated by immersion in a 0.075 M NaOH (96 % ethanol) solution for 2 h.

The carbonization parameters were also found to affect the separation properties of the HFCMs significantly. The carbonization condition was optimized based on an orthogonal experimental design method and statistical analysis. The optimal carbonization procedure was found to be: CO<sub>2</sub> as purge gas, a final temperature of 823K, a heating rate of 4K/min and a final soak time of 2h (CO<sub>2</sub>-823K-4K/min-2h), and the importance of the investigated carbonization parameters was sorted out with respect to their influence on carbon membrane separation performances. The order of importance for the carbonization parameters was found to be: purge gas > final temperature > heating rate > final soak time. It was hence concluded that the purge gas was the most important parameter affecting the final carbon membrane performance, and CO<sub>2</sub> was found to be the most effective purge gas for preparation of the high performance cellulosic derived carbon membranes.

A symmetric structure for the prepared HFCMs with a typical thickness of 25 um was identified from the scanning electronic microscopy (SEM) images, and a great shrinkage compared to the precursor could be seen. The Fourier Transform Infrared

(FTIR) spectra showed the decomposition and break down of the chemical groups in precursors in various carbonization environments, leading to the release of volatile gases. A typical d-spacing of the carbon membranes was found to be 4 Å from the X-ray diffraction (XRD) characterization. CO<sub>2</sub> and N<sub>2</sub> adsorption equilibrium isotherms were obtained by the gravimetric sorption measurements. A higher adsorption affinity of CO<sub>2</sub>, obtained by fitting the experimental data using Langmuir-Freundlich model, indicated that CO<sub>2</sub> is more adsorbable than N<sub>2</sub>. Two type of hollow fiber carbon membrane (HFCM-A and HFCM-B) has been prepared in the current work. The micropore volume and average pore size for the carbon membrane HFCM-B are around 0.17 cm<sup>3</sup>/g and 5.6 Å, respectively, which are slightly larger than that of the HFCM-A (0.15 cm<sup>3</sup>/g and 5.2 Å). The kinetic rate constants were also determined from the CO<sub>2</sub> kinetic adsorption experiments, and the higher kinetic rate constant of HFCM-B indicates the more open structure.

Gas permeation tests were conducted with single gases (H<sub>2</sub>, CO<sub>2</sub>, O<sub>2</sub>, N<sub>2</sub> and CH<sub>4</sub>) as well as gas mixtures. The single gas permeation tests confirmed that the permeability values decreased with increasing kinetic diameter of the gas molecules, which indicated that the molecular sieving mechanism was dominating in the carbon membrane separation processes. The results also showed that the kinetic diameter had a larger effect than the Lennard-Jones well depth, which indicated that the diffusion was dominated by a molecular sieving process and that the sorption had relatively little influence. The gas permeability increased with temperature due to the activated transport process for the molecular sieve mechanism. The gas molecules with larger activation energy (e.g. CH<sub>4</sub> and N<sub>2</sub>) were affected by the temperature more significantly, comparing to that with lower activation energy (e.g. CO<sub>2</sub>). The strongly adsorbed CO<sub>2</sub> showed a more significant decrease of permeability with pressure compared to N<sub>2</sub>, reflecting a stronger concentration dependence for the diffusion coefficient of CO<sub>2</sub>. The gas permeability decreased with the presence of water vapor which might be caused by the pore blocking. The aging test results indicated that the permeability of carbon membrane decreased over time when exposed to air, and needed to be regenerated. The gas mixture measurements showed that the significant effects of the operating parameters, especially the feed pressure, on the membrane performance based on the fractional factorial design method and statistical analysis. Therefore, the operating conditions need to be optimized for the specific applications.

The single stage membrane processes for CO<sub>2</sub> capture from flue gases with feed compression, permeate evacuation, and their combination were investigated using Aspen HYSYS simulation tool integrated with an in-house membrane simulation model called ChemBrane. The simulation results indicated that the single stage membrane process could not achieve high CO<sub>2</sub> purity and CO<sub>2</sub> recovery simultaneously using these HFCMs. The plotted characteristic diagrams could be easily used to identify the required operating conditions and membrane areas to accomplish specific targets for a given separation process. A two stage membrane system was also designed for the evaluation of process feasibility, and the simulation results indicated that a CO<sub>2</sub> purity of 90 % and a recovery of 80 % could be achieved by optimizing of the process conditions. Although the cost of carbon membranes is still unknown, the membrane/module cost could be greatly reduced by further improving the membrane separation performance (especially increasing the gas permeance by reducing the wall thickness of HFCMs) and simplifying the membrane production process. The capital cost estimation for two-stage cascade membrane process indicated that the potential application for carbon membrane technique could be promising compared to chemical absorption.

## **Acknowledgements**

First, I would like to thank my supervisor Professor May-Britt Hägg for giving me the opportunity to do the PhD program in Memfo group. I wish to thank her for her encouragement, support and patience in my experiments, courses, articles and thesis during the last four years.

Second, I wish to thank all the members in Memfo group - Jon, Arne, Marius, Tom-Nils, Taek-Joong, Qiang, Lily, Tom-Göran, Washim, Inger Lise, Jamil, Arshad, Janga, Karen, Vajiheh, Lei, David, Khalim, Edel and Martin for their nice help in different situations and interesting discussions. I would especially like to thank Edel and Jon to help me for the preparation of my first hollow fiber carbon membrane. I also want to thank Arne for the helping with my experimental setup and instruments.

I am grateful to Jan Morten Roel, Frode Sundseth, Harry Trygve Brun and Arne Fossum at Department of Chemical Engineering for their technical assistance during my PhD program. I would also thank Lisbeth Blekkan Roel for her patient supports. Appreciation also goes to Dr. Yingda Yu in SEM-Lab for the help of using SEM as well as the Analytische Laboratorien in Germany for the element analysis.

I would like to acknowledge the NanoGloWa project for the funding (EUs 6<sup>th</sup> framework program) of my PhD work

Finally, I wish to thank my dear wife Yunhan Chu. She always supports me both on my life and scientific research. I am also thankful to the rest of my family for their patience and showing interest in my work.

Trondheim, March 2011



Xuezhong He

## List of presentations and publications

### Presentations in international conferences

- [1] **Xuezhong He**, Jon Arvid Lie, Edel Sheridan, May-Britt Hägg. Preparation and Characterization of Hollow Fiber Carbon Membranes based on a Cellulosic Precursor. ICOM 2008, Honolulu, Hawaii USA 2008.
- [2] Edel Sheridan, Jon Arvid Lie, **Xuezhong He**, May-Britt Hägg. Production of Carbon Membranes with an Online Regeneration Technique. ICOM 2008, Honolulu, Hawaii USA 2008.
- [3] **Xuezhong He**, May-Britt Hägg. Gas Separation through Hollow Fiber Carbon Membranes. NYM 10th conference, Berlin, Germany 2008.
- [4] **Xuezhong He**, Jon Arvid Lie, Edel Sheridan, May-Britt Hägg. CO<sub>2</sub> Capture by Hollow Fibre Carbon Membranes: Experiments and Process Simulations. GHGT-9, Washington DC USA 2008 (Poster).
- [5] May-Britt Hägg, Jon Arvid Lie, **Xuezhong He**. Carbon Molecular Sieve Membranes. NanoMemCourse, Lillestrøm, Norway, March 2009.
- [6] **Xuezhong He**, May-Britt Hägg, Using Orthogonal Experimental Design for Spinning Defect-free Hollow Fiber Membranes. ECI Advanced Membrane Technology IV 2009, Trondheim, Norway
- [7] **Xuezhong He**, May-Britt Hägg, Preparation and Characterization of High Performance Hollow Fiber Carbon Membranes - Discussion of Results and Potential Applications. Euromembrane 2009, Montpellier, France
- [8] **Xuezhong He**, May-Britt Hägg, Hollow Fiber Carbon Membranes: Investigations for CO<sub>2</sub> Capture. NAMS 2010, Washington D.C., USA 2010.
- [9] **Xuezhong He**, May-Britt Hägg, Carbon Membranes in Energy Applications. 5<sup>th</sup> KIFEE International Symposium on Environment, Energy and Materials, Kyoto, Japan 2011.

### Presentations in NanoGloWa project meeting

- [1] **Xuezhong He**, May-Britt Hägg. Preparation of Carbon Membranes Based on Optimal Carbonization Conditions. NanoGloWa project meeting, Aachen Germany, Oct. 27-28th 2008.
- [2] **Xuezhong He**, May-Britt Hägg. Hollow Fiber Carbon Membranes: Experimental Results and Process Simulation. NanoGloWa project meeting, Trondheim Norway, June 4-5th 2009
- [3] **Xuezhong He**, May-Britt Hägg. Hollow Fiber Carbon Membranes: Experimental Results and Discussions. University of Twente, the Netherlands. Nov. 3-4th 2009

- [4] **Xuezhong He**, May-Britt Hägg. Hollow Fiber Carbon Molecular Sieve Membranes for Gas Separation. NanoGloWa project meeting, Haifa Israel, Nov. 15-17th 2010.

#### Publications

- [1] **He X**, Lie JA, Sheridan E, Hägg M-B. CO<sub>2</sub> Capture by Hollow Fibre Carbon Membranes: Experiments and Process Simulation. *Energy Procedia*, 2009, 1, 261-268
- [2] **He X**, Lie JA, Sheridan E, Hägg M-B. Preparation and Characterization of Hollow Fiber Carbon Membranes from Cellulose Acetate Precursors. *Industrial & Engineering Chemistry Research*, 2011, 50, (4), 2080-2087.
- [3] **He X**, Hägg M-B. Hollow Fiber Carbon Membranes: Investigations for CO<sub>2</sub> Capture. *Journal of Membrane Science*. Article in Press.
- [4] **He X**, Hägg M-B. Optimization of Carbonization Process for Preparation of High Performance Hollow Fiber Carbon Membranes, Submitted to *Industrial & Engineering Chemistry Research*.
- [5] **He X**, Hägg M-B. Structural, Kinetic and Performance Characterization of Hollow Fiber Carbon Membranes. Submitted to *Journal of Membrane Science*.
- [6] **He X**, Hägg M-B. Hollow Fiber Carbon Membranes: from Material to Application. Submitted to *AIChE Journal*.
- [7] Hägg M-B. **He X**, Carbon Molecular Sieve Membranes, Book Chapter of Membrane Engineering for the Treatment of Gases, Enrico Drioli, Giuseppe Barbieri, Eds., to be published by RSC in 2011.

## Table of contents

<b>Abstract</b> .....	i
<b>Acknowledgements</b> .....	iv
<b>List of presentations and publications</b> .....	v
<b>Table of contents</b> .....	vii
<b>Nomenclature</b> .....	xi
<b>1 Introduction and motivation</b> .....	1
1.1 Background .....	1
1.2 Research objectives .....	2
1.3 Outline of thesis .....	3
1.4 References .....	4
<b>2 Membranes for gas separation</b> .....	6
2.1 Different membrane materials and properties .....	6
2.1.1. Polymer membranes .....	6
2.1.2. Carbon molecular sieve membranes .....	9
2.2 Membrane gas separation principles .....	10
2.2.1. General gas transport model .....	11
2.2.2. Transport through dense polymer membranes .....	12
2.2.3. Transport through FSC membranes .....	14
2.2.4. Transport through mixed matrix membranes .....	15
2.2.5. Transport through carbon membranes .....	16
2.2.6. System operating conditions .....	18
2.3 Membranes relevant for CO <sub>2</sub> separation .....	20
2.3.1. CO <sub>2</sub> capture from flue gases .....	20
2.3.2. Natural gas sweetening .....	21
2.3.3. Biogas upgrading .....	22
2.3.4. H <sub>2</sub> / CO <sub>2</sub> separation from pre-combustion process .....	23
2.4 References .....	25
<b>3 Carbon molecular sieve membranes</b> .....	29
3.1 Production of CMS membranes .....	30
3.1.1. Material selection .....	31
3.1.2. Material functionalization .....	32
3.1.3. Precursor preparation .....	33
3.1.4. Pretreatment .....	34

3.1.5.	Carbonization.....	34
3.1.6.	Post treatment .....	38
3.2	Characterization for CMS membranes.....	38
3.2.1.	General characterization techniques .....	38
3.2.2.	Gas sorption.....	41
3.2.3.	Gas permeation .....	42
3.2.4.	Aging and regeneration .....	45
3.3	Carbon membrane module construction .....	47
3.4	Potential industrial applications for CMS membranes.....	48
3.4.1.	Biogas .....	48
3.4.2.	Natural gas.....	49
3.4.3.	Flue gas.....	50
3.4.4.	Air separation .....	51
3.4.5.	Petrochemical industry .....	52
3.4.6.	High-temperature applications .....	53
3.5	References .....	55
4	Experimental equipments, procedures and membrane preparation.....	63
4.1	Materials .....	63
4.1.1.	Membrane materials .....	63
4.1.2.	Gases.....	63
4.2	Equipments and methods.....	63
4.2.1.	Dope solution formation.....	63
4.2.2.	Spinning.....	64
4.2.3.	Deacetylation .....	65
4.2.4.	Carbonization.....	66
4.2.5.	Gas chromatograph (GC).....	67
4.2.6.	Thermogravimetric analysis-Mass spectroscopy (TGA-MS).....	67
4.2.7.	Scanning electron microscopy (SEM).....	68
4.2.8.	Fourier Transform Infrared (FTIR) .....	69
4.2.9.	Element analysis.....	71
4.2.10.	X-ray diffraction (XRD).....	71
4.2.11.	Gas gravimetric sorption .....	72
4.2.12.	Gas permeation .....	73

4.2.13. Orthogonal experimental design and conjoint analysis .....	74
4.3 Membrane module construction .....	75
4.4 References .....	76
5 Results and discussions-precursors, spinning conditions .....	78
5.1 Spinning hollow fiber membranes .....	78
5.1.1. Optimization of spinning condition .....	78
5.1.2. Conjoint analysis .....	79
5.2 Optimization of deacetylation process .....	83
5.2.1. Investigation of deacetylation conditions .....	83
5.2.2. Optimization of deacetylation condition .....	84
5.3 Conclusions .....	88
5.4 References .....	89
6 Results and discussions-preparation and characterization carbon membranes .....	90
6.1 Effect of precursors.....	90
6.2 Carbonization procedure.....	93
6.3 Transport mechanism investigation .....	94
6.4 Optimization of carbonization parameters.....	96
6.4.1. Carbonization condition investigation.....	96
6.4.2. Orthogonal experimental design and results .....	96
6.4.3. Analysis for OED .....	98
6.5 Characterization by general techniques .....	100
6.5.1. TGA and SEM .....	101
6.5.2. FTIR.....	103
6.5.3. XRD.....	104
6.5.4. Element analysis.....	104
6.6 Gas sorption .....	105
6.6.1. Structure characterization .....	105
6.6.2. Kinetic measurements.....	108
6.7 Single gas tests.....	110
6.7.1. Effects of temperature .....	110
6.7.2. Effects of pressure .....	112
6.7.3. Effects of humidity .....	112
6.7.4. Aging and durability tests.....	113
6.8 Gas mixture tests.....	113
6.9 Gas mixture tests.....	114

6.9.1. CO <sub>2</sub> separation from synthetic flue gas .....	114
6.9.2. CO <sub>2</sub> separation from sythentic biogas .....	117
6.10 Conclusions .....	118
6.11 References .....	120
7 Process simulation .....	122
7.1 Process design and simulation basis .....	122
7.2 Capital cost evaluation .....	124
7.3 Results and discussion .....	125
7.3.1. Effect of feed and permeate pressures .....	125
7.3.2. Characteristic diagrams .....	127
7.3.3. Process feasibility evaluation .....	130
7.4 Conclusions .....	132
7.5 References .....	133
8 Conclusions .....	134
9 Future work .....	136
Appendix list .....	137

## Nomenclature

Symbol	Explanation	Unit / value
<b>Latin characters</b>		
<i>A</i>	membrane area; constant of polymer-penetrant system	cm <sup>2</sup> ; -
<i>a</i>	constant	-
<i>B</i>	constant of polymer-penetrant system	-
<i>b</i>	Langmuir affinity parameter; constant	Bar <sup>-1</sup> ; -
<i>C</i>	capital cost	\$
<i>c</i>	concentration of component <i>i</i> ; constant	mol m <sup>-3</sup> ; -
<i>D</i>	diffusion coefficient	m <sup>2</sup> s <sup>-1</sup>
<i>d</i>	kinetic diameter; d-spacing	nm; Å
<i>E</i>	activation energy	kJ mol <sup>-1</sup>
<i>e</i>	electron charge	1.602×10 <sup>-19</sup> C
<i>F</i>	module factor; mass flow	-; t/h
<i>f</i>	fugacity	bar
<i>h</i>	Planck constant	6.626×10 <sup>-34</sup> J s
<i>J</i>	flux	mol m <sup>-2</sup> s <sup>-1</sup>
<i>K</i>	Boltzmann constant	1.381×10 <sup>-23</sup> J K <sup>-1</sup>
<i>k</i>	kinetic rate constant	s <sup>-1</sup>
<i>L</i>	average micropore width	Å
<i>l</i>	effective membrane thickness	µm
<i>m</i>	mass	g
<i>N</i>	Knudsen number	-
<i>n</i>	shape factor	-
<i>P</i>	permeability	Barrer
<i>p</i>	pressure	Bar, or mbar
<i>q</i>	absorption amount; flow rate	g g <sup>-1</sup> ; kmol h <sup>-1</sup>
<i>R</i>	molar gas constant	8.314 J K <sup>-1</sup> mol <sup>-1</sup>
<i>S</i>	entropy; solubility	J K <sup>-1</sup> ; mol m <sup>-3</sup> bar <sup>-1</sup>
<i>T</i>	temperature	K
<i>t</i>	time	s or h
<i>V</i>	volume	cm <sup>3</sup>
<i>w</i>	micropore volume	cm <sup>3</sup> g <sup>-1</sup>
<i>x</i>	mole composition	-
<i>y</i>	mole composition	-
<b>Greek Characters</b>		
$\Delta$	delta (finite difference)	-
$\Pi$	permeation number	-
$\Phi$	volume fraction; pressure ratio	-
$\alpha$	selectivity	-

Symbol	Explanation	Unit / value
$\varepsilon$	microporosity; Lennard-Jones well depth	-; J
$\theta$	diffraction angle; stage-cut	°; %
$\lambda$	mean free path	m
$\rho$	density	g cm <sup>-3</sup>
$\tau$	tortuosity	-

### Subscripts

<i>A</i>	component A
<i>AC</i>	complex of component A and carrier C
<i>a</i>	activation
<i>BM</i>	bare module
<i>bal</i>	balance
<i>c</i>	continuous phase
<i>d</i>	diffusion; dispersed phase
<i>e</i>	effective
<i>exp.</i>	experimental
<i>F</i>	feed stream
<i>H, L</i>	high, low pressure side
<i>i, j</i>	component <i>i, j</i>
<i>l</i>	distance in the transport direction
<i>MS</i>	molecular sieve
<i>P</i>	permeate stream
<i>p</i>	preexponential
<i>R</i>	retentate stream
<i>S</i>	sample
<i>SC+S</i>	sample container together with sample
<i>s</i>	solution
<i>TM</i>	total module
0	usually presents pre-exponential

### Abbreviations

BTL	Bradley-Terry-Luce
CA	cellulose acetate
CCS	CO <sub>2</sub> capture and storage
CMR	carbon membrane reactor
CMS	carbon molecular sieve
CMSMs	carbon molecular sieve membranes
DHF	deacetylated hollow fiber
DR	Dubinín and Radushkevich
DS	degree of substitution

Symbol	Explanation	Unit / value
ELM	emulsion liquid membrane	
FFV	fractional free volume	
FSC	fixed-site-carrier	
FTIR	Fourier transform infrared	
GC	gas chromatograph	
GHG	greenhouse gases	
HF	hollow fiber	
HFCMs	hollow fiber carbon membranes	
ID	inner diameter, mm	
IMP	importance score	
LDF	linear driving force	
MEA	monoethanolamine	
MMMs	mixed matrix membranes	
MSB	magnetic suspension balance	
NanoGloWa	Nano-structured membranes against global warming	
NMP	N-methyl-2-pyrrolidone	
OD	outer diameter, mm	
OED	orthogonal experimental design	
PSD	pore size distribution	
PVP	polyvinylpyrrolidone	
SEM	scanning electron microscopy	
SLM	supported liquid membrane	
SMR	steam methane reforming	
SPSS	statistical product and service solutions	
SSF	selective surface flow	
TGA-MS	thermogravimetric analysis-mass spectrascopy	
XPS	X-ray photoelectron spectroscopy	
XRD	X-ray diffraction	

Unit for permeability: 1 Barrer=  $10^{-10} \text{ cm}^3 \text{ (STP).cm} / (\text{cm}^2 \cdot \text{s.cmHg})$

Unit for permeance:  $\text{m}^3 \text{ (STP)} / (\text{m}^2 \cdot \text{h.bar})$

Software: CAPCOST, HYSYS, LabVIEW, Minitab, Origin, Sigmaplot, SPSS



# 1 Introduction and motivation

## 1.1 Background

Energy Information Administration (EIA) 2010 predicted a 49 % increase of energy demand from 2007 to 2035 following more and more countries becoming industrialized [1]. The International Energy Outlook 2010 (IEO 2010) reference case reported that the world energy-related carbon dioxide (CO<sub>2</sub>) emissions increased from 29.7 billion metric tons in 2007 to 33.8 billion metric tons in 2020 and 42.4 billion metric tons in 2035 [1]. The control of anthropogenic emissions of greenhouse gases (GHG) is one of the most challenging environmental issues owing to the implications of GHG for global climate change. Climate models referenced by the IPCC project that global surface temperatures are likely to increase by 1.1 to 6.4 °C between 1990 and 2100 [2]. This increase in global temperatures is likely to result in many negative events such as rising sea levels, changes in ecosystems, loss of biodiversity and so on. These effects can be partially alleviated by the reduction of greenhouse gases such as CO<sub>2</sub>, released into the atmospheres which are produced in a variety of ways, particularly in fossil fired power plants (roughly 40 % of total CO<sub>2</sub> emissions). Three options were reported to reduce the total CO<sub>2</sub> emission into the atmosphere, i.e. to reduce energy consumption, to reduce fossil fuel usage, and to capture and store the CO<sub>2</sub>. The first two options require efficient usage of energy and switch to using non-fossil fuels such as hydrogen and renewable energy respectively, while the third option requires the development of new efficient technologies for CO<sub>2</sub> capture and storage (CCS). The key attraction for CCS is that we may continue to use fossil fuels but without causing significant CO<sub>2</sub> emissions, which could be the ultimate way to reduce the CO<sub>2</sub> emissions as required by the Kyoto protocol.

There are several different techniques which can be used for CO<sub>2</sub> capture, such as chemical and physical absorption, adsorption, cryogenics and membrane separation, but the choice of a suitable method will, to a large extent, mainly depend on the characteristics of the gas to be treated as well as the process conditions. Membranes are already an alternative and competitive technology for selected gas separation processes such as air separation, natural gas sweetening, biogas upgrading, and hydrogen production during the last two decades. It will become steadily more attractive due to the energy efficiency and low economical costs.

There are many authors reporting research work on CO<sub>2</sub> capture by membrane technology, examples are: [3-10]. Although the polymeric membranes are dominating the current industrial use for gas separation, the trade-off of permeability / selectivity as

well as the limitation of operation temperature and adverse conditions such as the presence of acid gases SO<sub>2</sub> and NO<sub>x</sub>, may direct the polymeric membrane development into the alternative carbon membranes. Up to now, different precursor materials such as polyimide [11-12], polyacrylonitrile (PAN) [13], poly(phthalazinone ether sulfone ketone) (PPESK) [14], poly(phenylene oxide) (PPO) [15] have been tested for fabrication of carbon membranes. Recently, strong interests have been taken in the preparation of the carbon membranes for gas separation, from hollow fiber precursors, as these membranes provide better selectivity, thermal and chemical stability than the polymeric ones [16-18].

As partly of the EU 6<sup>th</sup> framework program: NanoGloWa (Nano-structured membranes against global warming), which is mainly focused on the development of the high performance hollow fiber carbon membranes (HFCMs) for CO<sub>2</sub> capture from flue gases. The HFCMs with high CO<sub>2</sub> permeability and good selectivity for CO<sub>2</sub> over the other gas species such as N<sub>2</sub> and O<sub>2</sub> were prepared and investigated within my project.

## **1.2 Research objectives**

The principal objective for this project has been to develop high performance HFCMs for CO<sub>2</sub> separation from a mixed gas stream. The main studies within this project were focused on the choice for polymeric materials as the precursors, optimization for spinning process and carbonization conditions, preparation and characterization of HFCMs, durability measurements and process simulation. These activities are summarized as follows:

- To develop a stable hollow fiber carbon membrane for selective removal of CO<sub>2</sub>
- To prepare the high performance HFCMs by optimization of the carbonization conditions
- To characterize the prepared HFCMs using different techniques such as Fourier transform infrared (FTIR), scanning electron microscopy (SEM), X-ray diffraction (XRD), thermogravimetric analysis-mass spectrometry (TGA-MS), element analysis and gas gravimetric sorption
- To test the performance of HFCMs by the gas permeation measurements for selected single gases (CO<sub>2</sub>, N<sub>2</sub>, O<sub>2</sub>, H<sub>2</sub>, CH<sub>4</sub>) and mixed gases (CO<sub>2</sub>-N<sub>2</sub>:10% / 90%, CO<sub>2</sub>-O<sub>2</sub>-N<sub>2</sub>: 15% / 81% / 4%, CO<sub>2</sub>-CH<sub>4</sub>: 35% / 65%).
- To document durability and stability by medium term performance measurements
- To evaluate the process feasibility for CO<sub>2</sub> capture from flue gases by HFCMs based on process simulation

### 1.3 Outline of thesis

This thesis includes 9 chapters. Chapter 1 gives a brief introduction to the project background, and the motivation to use the membrane for gas separation. Chapter 2 summarizes different types of membranes for gas separation from the materials, properties and transport mechanism. Chapter 3 describes the carbon molecular sieve membranes in detail from the preparation to the industrial application. Chapter 4 describes in detail the experimental equipments, methods and procedures for preparation of the carbon membranes. Chapter 5 presents the results and discussions for the precursors. Chapter 6 presents the results and discussion for the carbon membranes. Chapter 7 presents the results of CO<sub>2</sub> capture from flue gases by the carbon membranes based on the process simulation. Chapter 8 summarizes the main work and conclusions and Chapter 9 gives recommendation for the future work of the carbon membranes.

Some supporting information and publications are attached in the appendices.

- Appendix A: Example of the measurement for single gas permeability
- Appendix B: Durability test for the carbon membranes, NanoGlowa report
- Appendix C: Carbon membrane tests at ITM-CNR, NanoGlowa report
- Appendix D: Preparation and Characterization of Hollow Fiber Carbon Membranes from Cellulose Acetate Precursors (published article in *I&EC Res.*)
- Appendix E: Optimization of Carbonization Process for Preparation of High Performance Hollow Fiber Carbon Membranes (article submitted to *I&EC Res.*)
- Appendix F: Structural, Kinetic and Performance Characterization of Hollow Fiber Carbon Membranes (article submitted to *J. Membr. Sci.*)
- Appendix G: Hollow Fiber Carbon Membranes: Investigations for CO<sub>2</sub> Capture (published article in *J. Membr. Sci.*)
- Appendix H: Hollow Fiber Carbon Membranes: from Material to Application (article submitted to *AICHE Journal*)

#### 1.4 References

- [1] International Energy Outlook 2010 - Highlights. [cited 2010 September 28]; Available from: <http://www.eia.doe.gov/oiaf/ieo/highlights.html>
- [2] IPCC, 2007: Summary for Policymakers. In: Climate Change 2007: The Physical Science Basis. Contribution of Working Group I to the Fourth Assessment Report of the Intergovernmental Panel on Climate Change. Solomon, S., Qin, D., Manning, M., Chen, Z., Marquis, M., Averyt, K.B., Tignor, M., Miller, H.L. ed. Cambridge, United Kingdom and New York, USA: Cambridge University Press 2007.
- [3] Bredesen R, Jordal K, Bolland O. High-temperature membranes in power generation with CO<sub>2</sub> capture. *Chem Eng Process*. 2004;43(9):1129-58.
- [4] Deng L, Kim T-J, Hägg M-B. Facilitated transport of CO<sub>2</sub> in novel PVAm/PVA blend membrane. *J Membr Sci*. 2009;340(1-2):154-63.
- [5] Hagg MB, Lindbrathen A. CO<sub>2</sub> Capture from Natural Gas Fired Power Plants by Using Membrane Technology. *Ind Eng Chem Res*. 2005;44(20):7668-75.
- [6] Huang J, Zou J, Ho WSW. Carbon Dioxide Capture Using a CO<sub>2</sub>-Selective Facilitated Transport Membrane. *Ind Eng Chem Res*. 2008;47(4):1261-7.
- [7] Lin H, Freeman BD. Materials selection guidelines for membranes that remove CO<sub>2</sub> from gas mixtures. *J Mol Struct*. 2005;739(1-3):57-74.
- [8] Reijerkerk SR. Polyether based block copolymer membranes for CO<sub>2</sub> separation [PhD]. Enschede: University of Twente; 2010.
- [9] Sandru M, Haukebo SH, Hägg M-B. Composite hollow fiber membranes for CO<sub>2</sub> capture. *J Membr Sci*. 2010;346(1):172-86.
- [10] Yang H, Xu Z, Fan M, Gupta R, Slimane RB, Bland AE, et al. Progress in carbon dioxide separation and capture: A review. *J Environ Sci*. 2008;20:14-27.
- [11] Suda H, Haraya K. Gas Permeation through Micropores of Carbon Molecular Sieve Membranes Derived from Kapton Polyimide. *J Phys Chem B*. 1997;101(20):3988-94.
- [12] Steel KM, Koros WJ. Investigation of porosity of carbon materials and related effects on gas separation properties. *Carbon*. 2003;41(2):253-66.
- [13] David LIB, Ismail AF. Influence of the thermastabilization process and soak time during pyrolysis process on the polyacrylonitrile carbon membranes for O<sub>2</sub>/N<sub>2</sub> separation. *J Membr Sci*. 2003;213(1-2):285-91.
- [14] Zhang B, Wang T, Zhang S, Qiu J, Jian X. Preparation and characterization of carbon membranes made from poly(phthalazinone ether sulfone ketone). *Carbon*. 2006;44(13):2764-9.

- [15] Yoshimune M, Fujiwara I, Haraya K. Carbon molecular sieve membranes derived from trimethylsilyl substituted poly(phenylene oxide) for gas separation. *Carbon*. 2007;45(3):553-60.
- [16] Barsema JN. Carbon membranes precursor, preparation and functionalization [PhD]. Enschede: University of Twente; 2007.
- [17] Favvas EP, Kapantaidakis GC, Nolan JW, Mitropoulos AC, Kanellopoulos NK. Preparation, characterization and gas permeation properties of carbon hollow fiber membranes based on Matrimid(R) 5218 precursor. *J Mater Process Tech*. 2007;186(1-3):102-10.
- [18] Lie JA. Synthesis, performance and regeneration of carbon membranes for biogas upgrading-a future energy carrier [PhD]. Trondheim: Norwegian University of Science and technology; 2005:152.

## 2 Membranes for gas separation

This chapter describes different types of membranes used for gas separation based on the various separation mechanism and material properties. The membranes relevant for CO<sub>2</sub> separation were also reviewed.

### 2.1 Different membrane materials and properties

The choice of a membrane material for gas separation is typically based on the physical and chemical properties of the materials [1]. These membrane materials can be tailored to accomplish the specific gas separation processes. The gas separation properties through the membrane materials are mainly dependent on:

- Membrane separation performance (permeability, selectivity)
- Membrane structure (stability, and lifetime)
- Membrane configuration (flat-sheet, hollow fiber, tube)
- Module and process design

The different materials show various separation properties, thermal, chemical, and mechanical stability as well as the cost. An overview for the properties of the different membranes is listed in Table 2.1.

#### 2.1.1. Polymer membranes

Dense polymer membranes have been widely used for commercial large scale gas separation processes due to their good separation performance, good mechanical stability and easy module construction. The most important polymer membranes employed for gas separation in commercial system are summarized in Table 2.2 [2]. Among them, the cellulose acetate, polysulfone and polyimides are the most important polymers for gas separation membranes by far [3].

In a polymer membrane, the pores and channels have a broad distribution of the size and topologies, and the free volume plays an important role on the transport properties for the small gas molecules. Most of the industrial gas separation processes are using glassy polymers due to their high selectivity and good mechanical properties. However, the glassy polymers usually exhibit a small fractional free volume, and a large amount of free volume (up to 20%) becomes “frozen”. Typically, the rubbery polymers have high free volume, e.g. polydimethylsiloxane (PDMS), which result in higher permeability but lower selectivity, this is mainly determined by the differences of the condensability of the gases. However, there are some glassy polymers such as poly (1-trimethylsilyl-1-propyne) (PTMSP), Poly (4-methyl-2-pentyne) (PMP) which present a very high free volume compared to the traditional glassy and rubbery polymers (Table 2.3) [1].

Table 2.1 The comparison of different membrane materials

Materials	Advantages	Challenges
Polymer membranes	Easy for module production Good mechanical strength Low cost	Limited separation performance Plasticization Low chemical and thermal stability
Facilitated transport membranes	Good mechanical strength High separation performance Easy for module production	Plasticization Low thermal stability
Mixed matrix membranes (MMMs)	Enhanced separation performance, Good mechanical stability Reduced plasticization and compression at high pressure	Thermal and chemical stability depends on the polymeric matrix Decrease performance in the absorbable environment
Carbon molecular sieve membranes (CMSMs)	Higher separation performance Higher chemical and thermal stability	High production cost Aging Brittle, challenging for module construction

The gas permeability through a polymer membrane depends on a thermodynamic factor (solubility of penetrates in the membrane) and a kinetic factor (diffusivity of gas species through the membrane). The selectivity for the membrane is a key parameter to achieve a high purity product under a given separation condition. Normally, the polymer membranes have relatively high selectivity but lower permeability compared to microporous membranes. There is a trade-off limitation between permeability and selectivity for most polymer membranes as reported by Robeson [4]. Therefore, the polymer membranes related to the solution-diffusion transport mechanism can not exceed the upper bound to get higher permeability /selectivity combination unless the membranes involve other transport mechanisms (such as facilitated transport or surface selective flow as in membranes).

Table 2.2 Important polymer membranes used in industrial gas separation process[2]

Polymer materials	Company	Module	Application
Cellulose acetate	UOP, GMS, Natco	Spiral-wound hollow fiber	Natural gas
Polysulfone	Air Products	Hollow fiber	Large gas companies
Polyimide	Praxair	Hollow fiber	Hydrogen separation
Poly (phenylene oxide)	Parker-Hannifin	Hollow fiber	Vapor/gas, Air separation
Polycarbonate	MG	-	Air separation
Polydimethylsiloxane	GKSS, MTR	Plate and frame spiral-wound	Dehydration

Table 2.3 Representative polymer membranes with high FFV and permeability [1].

Polymer	FFV (%)	O <sub>2</sub> permeability (Barrer)	O <sub>2</sub> /N <sub>2</sub> selectivity
PTMSP	32-34	6100	1.8
PMP	28	2700	2
Teflon AF 2400	33	1600	2
PIM-1*	22-24	370	4

\*: PIM represents polymer of intrinsic microporosity.

Facilitated transport membranes. The fixed-site-carrier (FSC) membranes, one type of facilitated transport membranes, for gas separation such as CO<sub>2</sub> capture from flue gas, biogas upgrading and natural gas sweetening have attracted much attention due to the high separation performance based on the facilitated transport mechanism. CO<sub>2</sub> can react with the carrier and be transported through the FSC membrane both by solution-diffusion and facilitated transport, while the non-reactive gases such as N<sub>2</sub> and CH<sub>4</sub> only transport via the solution- diffusion. The carrier is chemically bonded into the polymer matrix via covalent bond, and shows high mechanical stability compared to the other type of facilitated transport membranes such as supported liquid membrane (SLM) and emulsion liquid membrane (ELM). Yoshikawa et. al. developed a high CO<sub>2</sub> selective FSC membranes with an amine moiety [5]. Zou et.al reported a high performance polyallylamine (PAAm) / poly (vinyl alcohol) (PVA) blend membrane for CO<sub>2</sub> separation from H<sub>2</sub>, N<sub>2</sub> and CO [6]. Recently, a PVA / polyvinyl amine (PVAm) FSC membrane was developed by the Memfo group at NTNU [7-9]. They report that the prepared FSC membranes present very high separation performance for CO<sub>2</sub> removal,

which can exceed the Robeson upper bound. Although the FSC membranes showed very high separation performance and good stability exposed to the acid gases such as SO<sub>2</sub> and NO<sub>x</sub> in a given process, the durability tests over long term needed to be further documented.

Mixed matrix membranes, comprising rigid permeable or impermeable particles, such as zeolites, carbon molecular sieves, silica and carbon nanotubes, dispersed in a continuous polymeric phase presents an interesting material for improving the separation performance of traditional dense polymer membranes [10]. One type of MMMs with microporous fillers could improve the selectivity on the basis of molecular sieve or surface flow transport mechanism, while the other type of MMMs with nonporous nanoparticles could improve the permeability by increasing free-volume. Therefore, choosing the proper materials for both polymers and inorganic particles is fundamentally important for preparation of MMMs. Chung et. al reported that both the polymer and inorganic filler properties will affect the morphology and separation performance of MMM [11]. Usually the glassy polymers are better to use as the polymeric matrix than the rubbery polymers because of their higher selectivity due to the rigid structure. However, the adhesion between the polymer phase and the external surface of the inorganic particles is a challenging problem when glassy polymers are used for preparation of mixed matrix membranes. Moreover, the thermal and chemical stability of the MMMs depend on the polymeric matrix, which may also be suffered by the presence of the acid gas.

#### 2.1.2. Carbon molecular sieve membranes

Carbon molecular sieve membranes (CMSMs) are ultramicroporous inorganic membranes prepared by carbonization of the polymeric precursors. The CMSMs consist primary of carbon atoms, but usually also involve a small amount of oxygen, nitrogen, and hydrogen. Typically, the carbon membranes form a graphitic or turbostratic structure. Table 2.4 shows the representative properties of the cellulose-based carbon fibers [12], which indicates a high strength and moderate modulus comparing to the graphitized fibers.

When the gas molecules transport through a carbon membrane, the physisorption and chemisorption are usually taken place between the gas species and the carbon matrix. The chemisorption are usually high (40 – 400 kJ/mol) compared to the physisorption (4 - 40 kJ/mol). Normally, CO<sub>2</sub> will physically absorb into the carbon matrix, and desorption is revisable. Oxygen is chemisorbed more readily than the other gas species such as N<sub>2</sub>, CH<sub>4</sub> and CO<sub>2</sub>. Basic surface oxides are produced when the carbon matrix surface is cleaned at high carbonization temperature and then exposed to the oxygen at

low testing temperature, e.g. 30 °C. The oxygen was chemisorbed onto the carbon matrix and formed a pyrone-like structure [13]. Marsh et.al reported that the oxygen had surface mobility resulting in “spillover” of oxygen from the edge to basal-plane sites [14]. The oxygen within the graphene layer is non-desorbable which causes a significant influence to the carbon reactivity. Therefore, aging is a typical challenge for most carbon membranes, which causes the decrease of the membrane performance over time. The most relevant aging effects are summarized in Table 2.5. Moreover, the carbon membranes also present a brittle structure, which is challenging for the construction of a membrane module.

Table 2.4 Representative properties of carbon fibers [12]

Parameter	Carbon fibers	Graphitized fibers
Tensile strength (MPa)	500-8000	300-4500
Young's modulus (GPa)	30-300	70-90
Electrical resistivity ( $10^{-5} \Omega \text{ m}$ )	0.4-70	0.002-0.4
Density ( $10^3 \text{ kg m}^{-3}$ )	1.3-1.7	1.3-2.1
Surface area ( $\text{m}^2 \text{ g}^{-1}$ )	0.3-2000	0.1-3
Thermal expansion co. ( $10^6 \text{ K}^{-1}$ )	4	2

Table 2.5 Effects on the carbon membrane separation performance exposure to different environments

Gas/vapor	Aging effect	Mechanism
O <sub>2</sub>	Permeance and selectivity decrease	Chemisorption
N <sub>2</sub>	Deceleration of aging	Physisorption
CO <sub>2</sub>	Permeance decrease	Physisorption
H <sub>2</sub> O	Permeance decrease	Physisorption
Propylene	Permeance increase	Physisorption

## 2.2 Membrane gas separation principles

Gas separation by membrane technology has become a rapid growing interest and alternative to the other traditional gas separation methods the last 30 years. Membrane technique is a low cost, energy efficient process with simple, compact and easily operated equipments. Moreover, there is no requirement for solvents and other chemicals for this environment friendly process. However, the biggest challenge with membrane technology is the requirement for pre-treatment of the feed gas stream as well as the membrane lifetime. Membrane for gas separation is characterized by using

the membrane to accomplish a separation of a particular gas mixture. The membrane is a selective barrier that has the ability to transport one component more readily through the membrane than the others due to the differences in physical and/or chemical properties between the membrane matrix and the penetrants. The gas transport through the membrane takes place as a result of a driving force of the trans-membrane pressure. However, there are several different transport mechanisms while the gas passes through different types of membranes: dense polymer membranes, fixed-site-carrier membranes, mixed matrix membranes and carbon membranes.

### 2.2.1. General gas transport model

The most common configuration for the gas transport through a membrane is the complete mixing model, which is shown in Fig. 2.1. The movement of the gas molecules in a membrane can be well described by Fick's first law which gives for the unidimensional flux  $J_i$  for component  $i$  through the membrane

$$J_i = -D_i \frac{dc_i}{dx_i} \quad (2.1)$$

Here  $D_i$  is the diffusion coefficient for component  $i$  and  $dc_i/dx_i$  is the driving force. For ideal systems, where the gas solubility is independent of the concentration and can be described by Henry's law ( $c = S \times p$ ). Thus, the flux of component  $i$ ,  $J_i$  ( $\text{m}^3(\text{STP})/(\text{m}^2 \cdot \text{h})$ ), can be modified by,

$$J_i = \frac{P_i}{l} \Delta p_i = \frac{P_i}{l} (p_H x_{i,F} - p_L y_{i,P}) \quad (2.2)$$

Where  $P_i$  is permeability (Barrer) for component  $i$  [15],  $l$  is membrane thickness (m),  $\Delta p$  is the driving force,  $p$  is total gas pressure (subscripts  $H$  and  $L$  represent the high pressure- and low pressure side respectively) (bar).  $x_{i,F}$  and  $y_{i,P}$  are the mole fraction of  $i$  on the feed and permeate side, respectively. The ideal selectivity is defined as,

$$\alpha = \frac{P_i}{P_j} \quad (2.3)$$

However, for gas mixture separation process, the process selectivity (or the separation factor),  $\alpha$ , is described as follows,

$$\alpha_{i/j} = \frac{y_{i,P} / y_{j,P}}{x_{i,F} / x_{j,F}} \quad (2.4)$$

Stage-cut is defined as:  $\theta = q_P / q_F \times 100\%$ , which is an important economic index. The stage-cut is typically higher in the commercial processes comparing to the lab scale tests. Therefore, choose a correct stage-cut is essential since it will directly influence the purity and yield of the product.

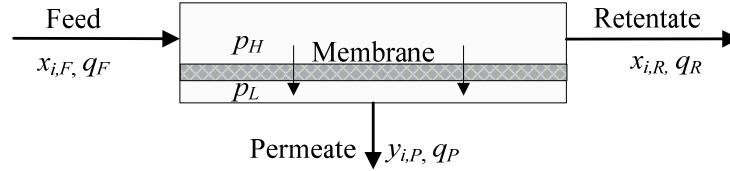


Fig. 2.1 Schematic diagram for a gas membrane separation process

### 2.2.2. Transport through dense polymer membranes

The dense polymer membranes are typically used for gas separation. The solution-diffusion mechanism is used to describe the gas transport mechanism through the dense polymer membranes, and consists of three steps:

- 1) Gas molecules absorb at the higher pressure side,
- 2) Gas molecules diffuse through the membrane to the low pressure side,
- 3) Gas molecules desorb at the low pressure side.

According to the solution-diffusion mechanism, the gas permeability transport through the polymer membrane can be described as [16-17],

$$P = S \times D \quad (2.5)$$

The solubility ( $S$ ) of a gas molecule is described by Henry's law which indicates a linear relationship between the concentration and the pressure inside a membrane ( $c = S \times p$ ). The solubility is a thermodynamic parameter and provides a measurement of the gas absorbed in the membrane at equilibrium, while the diffusivity ( $D$ ) is a kinetic parameter which determines how fast the gas molecules transport through the membranes. Thus, the ideal selectivity in equation 2.3 can also be expressed as,

$$\alpha_{ij} = \frac{S_i}{S_j} \times \frac{D_i}{D_j} \quad (2.6)$$

The solubility selectivity reflects the relative condensabilities of two gas species, and the diffusivity selectivity indicates the difference in size of gas molecules. Both the solubility and diffusivity of the gas molecules vary with polymer materials. Baker reported that the significant difference of gas diffusivity in rubber and glass polymers, and the diffusivity in glass polymers decreases much more rapidly with increasing the kinetic diameter of the gas molecules compared to that in the rubbery polymers [18]. Therefore, the diffusivity selectivity always favors the small gas molecules to pass through the membranes. Van Amerongen et. al reported the solubility selectivity favors the large gas molecules (more condensable) to pass through the membranes [19]. However, the difference of solubility in the rubbery and glassy polymers is much smaller than the difference for diffusivity. Therefore, the permeability values in rubbery

and glassy polymers are different as shown in Fig. 2.4 [18]. In glassy polymer membranes, the diffusivity selectivity is usually dominant, thus, the permeability will decrease with increasing size of gas molecules. However, in rubbery polymer membranes, the permeability will increase with increasing the size of gas molecules since the solubility is dominant-this will however also depend on the temperature.

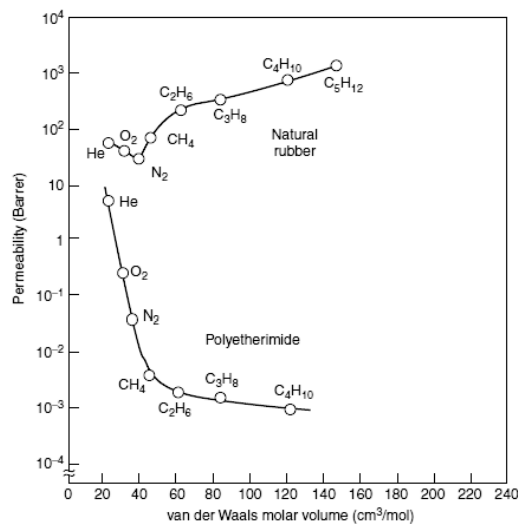


Fig. 2.4 Permeability as a function of molar volume for a rubbery and glassy polymer membranes [18]

Effect of temperature, the transport through the dense polymer membranes may be considered as an activated process which can typically described by Arrhenius equation [20],

$$P = P_0 \exp\left(\frac{-E_p}{RT}\right) = S_0 D_0 \exp\left(-\frac{\Delta H_s + E_d}{RT}\right) \quad (2.7)$$

where  $P_0$ ,  $S_0$  and  $D_0$  are the preexponential factor, respectively, and the  $\Delta H_s$  and  $E_d$  are the heat of solution and activation energy for diffusion separately. The temperature has a significant effect on the gas permeability. For small non-interactive gas molecules the temperature effect on the gas permeability is mainly determined by diffusion since the temperature has minor influence on the solubility. However, for large gas molecules, the temperature effects on the solubility and diffusivity are opposing, therefore, the gas permeability will be determined by the dominated parameter.

Free volume theory, the pores or transient gaps are still present even through in the dense materials which are usually caused by the localized thermal fluctuation of the

chain segments. The small scale openings generated by these motions allow the gas molecules transport through the polymer material with small jumps. The frequency and distance for these jumps are dependent on the kinetic diameter of gas molecules, the mobility and packing density of the polymer chains, and also the cohesive energy. For glassy polymer, the mobility of the chain segments is extremely limited and the thermal energy is too small to rotate the main chain. However, above the glass transition temperature, i.e. in the rubbery state, the mobility of the chain segments is increased. The density and specific volume is changed at the glass transition temperature. The free volume ( $V_f$ ) may be defined as [20],

$$V_f = V_T - V_0 \quad (2.8)$$

where  $V_T$  is the observed volume at a temperature of  $T$ , and  $V_0$  is the volume occupied by the polymer molecules at 0 K. the fractional free volume (FFV) is defined as,

$$FFV = \frac{V_f}{V_T} \quad (2.9)$$

The gas molecules can only jump or diffuse where there is sufficient empty space or free volume. Therefore, the gas diffusivity will mainly depend on the fractional free volume of the materials, which can be described as [21],

$$D = A \exp\left(-\frac{B}{FFV}\right) \quad (2.10)$$

where  $A$  and  $B$  are constant for the characteristics of the polymer-penetrant system.  $A$  is dependent on the size and shape of the gas molecules while  $B$  is related to the minimum local free volume necessary to allow a displacement. By combining the eqs. 2.5 and 2.10, the permeability is expressed as,

$$P = A_p \exp\left(-\frac{B}{FFV}\right) \quad (2.11)$$

where  $A_p$  is a preexponential factor equal to  $A \times S$ . Thus, the gas selectivity of eq. 2.6 can be rewritten as,

$$\alpha_{ij} = \frac{A_{p,i}}{A_{p,j}} \exp\left(-\frac{B_i - B_j}{FFV}\right) \quad (2.12)$$

Therefore, the gas selectivity is mainly dependent on the properties of the membrane and the penetrants.

### 2.2.3. Transport through FSC membranes

The facilitated transport mechanism is usually employed to describe the gas transport through two types of carrier facilitated membranes, i.e. SLM and ELM. In which the penetrant transport couples the solution-diffusion with a carrier-mediated transport, resulting in both high permeability and selectivity [8]. One component (A) absorbed

into the membrane and react with the carrier (C) forming a complex (AC). The flux of the reactive component  $A$  will be the sum of both solution-diffusion and carrier-mediated diffusion, which can be expressed as follows [7, 22],

$$J_A = \frac{D_A}{l}(c_{A,0} - c_{A,l}) + \frac{D_{AC}}{l}(c_{AC,0} - c_{AC,l}) \quad (2.13)$$

where  $D_A$  and  $D_{AC}$  are the diffusion coefficient of Fickian diffusion and carrier mediated diffusion, respectively, and  $l$  is the membranes thickness of the selective layer. For the non-reactive components the transportation can only via the solution diffusion mechanism [7]. However, the instability of the SLM and ELM is a major challenge for their application in large scale [18, 23]. An alternative way is to use fixed-site-carrier (FSC) membrane where the carrier is chemically or physically bonded to the polymer matrix. Cussler et. al developed a hopping mechanism for FSC membranes [24]. They indicated that the polymeric chains must have a certain mobility degree and the concentration of the carrier must be higher than the percolation threshold. Noble reported that the dual solution-diffusion mechanism can be well used to describe the neutral gas molecules such as  $O_2$  transport through the FSC membranes [25]. Kim et. al reported the  $CO_2$  transport through a PVAm FSC membrane [7]. A schematic diagram for the  $CO_2$  separation from through a FSC membrane is shown in Fig. 2.5, where the  $CO_2$  can pass through the membrane both by facilitated transport and solution-diffusion mechanism. However, the non-reactive gas molecules such as  $N_2$  and  $CH_4$  can only transport via solution-diffusion.

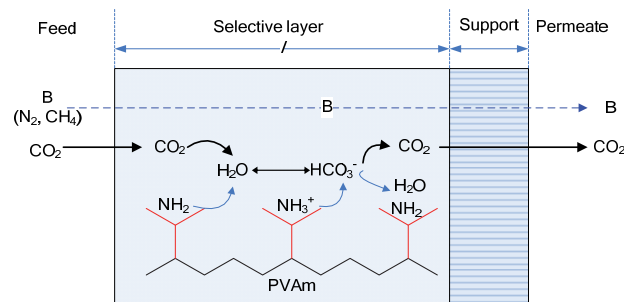


Fig. 2.5 Gas transport through the PVAm FSC membrane

#### 2.2.4. Transport through mixed matrix membranes

The gas transportation in the MMMs presents a complex problem, and a frequently used model describing gas permeation properties through MMMs is Maxwell model. For the MMMs with nonporous nanoparticles, the permeability of the composite membrane ( $P_{MMM}$ ) is described by

$$P_{MMM} = P_c \left( \frac{1 - \phi_d}{1 + \frac{1}{2} \phi_d} \right) \quad (2.14)$$

where  $\phi_d$  and  $P_c$  represent the volume fraction of dispersed phase and gas permeability in the continuous phase. The gas permeability through the MMMs with microporous fillers was predicted by a modified Maxwell model as a function of the gas permeability in the continuous and disperse phases [26], that is,

$$P_{MMM} = P_c \left[ \frac{nP_d + (1-n)P_c - (1-n)\phi_d(P_c - P_d)}{nP_d + (1-n)P_c + n\phi_d(P_c - P_d)} \right] \quad (2.15)$$

where  $P_c$  and  $P_d$  represent the gas permeability values in the continuous and dispersed phases, and  $n$  is the shape factor of the disperse phases. The limit of  $n=0$  corresponds to the parallel transport through a mixed matrix membrane made of side-by-side layers of the two phases, while the limit of  $n=1$  corresponds to the transport through two phases in series.

Ideally, the gas permeability through the MMMs is a function of the intrinsic properties of the continuous and dispersed phases. However, the addition of the dispersed phase may cause the undesirable voids at the interface or change the property of the surrounding polymer. Therefore, the Maxwell's model should be modified in order to predict the transport properties of the MMMs with non-ideal interphases. A detail review was conducted by Borge [27].

### 2.2.5. Transport through carbon membranes

The ability of the ultramicroporous carbon membranes to separate gases depends on the pore size of the membrane, the physiochemical properties of the gases and surface properties of the membrane pore. The pore size of a carbon fiber for gas separation is usually within the range of 3.5 – 10 Å; depending on the conditions for preparation of the membrane during the carbonization or treatment afterwards (post oxidation or chemical vapor deposition). The transport mechanism for the carbon membranes are basically taking place according to one of the three mechanisms listed below, and as described by Hägg et al in [28]:

- Knudsen diffusion; hence the square root of the ratio of the molecular weights will give separation factor.
- Selective surface diffusion governed by a selective adsorption of the larger non-ideal components on the pore surface, hence retaining the smaller components from permeation.
- Molecular sieving; hence the smallest molecules will permeate, the larger being retained.

Knudsen diffusion. For Knudsen diffusion to take place, the lower limit for pore diameter has usually been set to  $d_p > 20\text{\AA}$  [29]. Gilron and Soffer [30] have however discussed thoroughly how Knudsen diffusion may contribute to transport in even smaller pores, and from a model considering pore structure, shown that contributions to transport may both come from activated transport and Knudsen through one specific fiber. It may thus be difficult to know exactly when transport due to Knudsen diffusion is taking place. One way to approach this problem is to calculate the Knudsen number,  $N_{Kn}$ , for the system, which is  $\lambda/d_p$ , where  $\lambda$  is the mean free path. If  $N_{Kn} \geq 10$ , then the separation can be assumed to take place according to Knudsen diffusion [31]. Therefore, if the preparation of the carbon membranes has been unsuccessful, one may get Knudsen diffusion.

Selective Surface Flow (SSF). The driving force for separation according to a surface selective flow is basically the difference in the concentration of the adsorbed phase of the diffusing components. This means that a large driving force can be attained even with a small partial pressure difference for the permeating component. The larger molecules (more condensable, e.g. hydrocarbon) in a gas mixture will be selectively adsorbed, hence the smaller molecules will be retained due to reduced pore size. The pore size region where selective surface flow is expected to take place is about  $5\text{\AA} < d_p < 10\text{\AA}$ ; or up to  $3 \times (\text{diameter of molecule})$  [29]. The transport of gas molecules through a carbon membrane can also be described by Fick's first law as given in Eq. 2.2, and the activated diffusion was described by an Arrhenius type of equation:

$$D_a = D_0 \cdot \exp(-E_d / RT) \quad (2.16)$$

where  $E_d$  is the activation energy for diffusion. Now if Henry's law is assumed to apply, the integrated flux equation is written as in eq. 2.17:

$$J_a = \frac{\Delta p}{RT \cdot l} D_0 \cdot \exp\left\{-\frac{(E_{a,s} - E_{ads})}{RT}\right\} = \frac{\Delta p}{RT \cdot l} D_0 \cdot \exp\left(\frac{-\Delta E_s}{RT}\right) \quad (2.17)$$

$\Delta E_s$ , the difference in transport activation energy and adsorption energy may be positive or negative. When  $\Delta E_s < 0$ , transport due to SSF will increase with decreasing temperature; with  $\Delta E_s > 0$  it will decrease on the opposite way.

Molecular sieving. Molecular sieving is the dominating transport mechanism where carbon membranes are applied; this has also given the name to these membranes, CMS. The pore size is usually within the range of a few Angstrom (3-5)  $\text{\AA}$ . The dimensions of a molecule are usually described either with the Lennard-Jones radii or the Van der Waal radii. The sorption selectivity has little influence on the separation when molecular sieving is considered. Eq. 2.16 is still valid for the activated transport, but

now attention should be drawn to the pre-exponential term,  $D_0$  ( $D_0 = e\lambda^2 kT/h \exp(S_{a,d}/R)$ ) [32]. So the flux for single component can be expressed as,

$$J_a = \frac{\Delta p}{RT \cdot l} D_0 \cdot \exp\left(\frac{-E_{a,MS}}{RT}\right) \quad (2.18)$$

where  $E_{a,MS}$  is the activation energy for diffusion in the molecular sieving process for CMS membranes. Nguyen et al reported that the CMS membrane presents reasonable sieving effect for gas molecules with different kinetic diameters, which suggests that the CMS membrane is predominantly microporous with no major contribution from Knudsen diffusion or viscous flow in its overall mass transfer [33].

#### 2.2.6. System operating conditions

The gas separation performance for a given membrane system is mainly dependent on the membrane permeability and selectivity. However, the operating conditions for a specific process can also affect the membrane separation performance. One of the most important parameters is the pressure ratio across the membranes, which is defined as the ratio between the pressures in the feed and permeate side. The component  $i$  can only transport through the membrane when the partial pressure in the feed side ( $p_H$ ) is higher than in the permeate side ( $p_L$ ), so,

$$x_{i,F} p_H > y_{i,P} p_L \quad \text{or} \quad \frac{y_{i,P}}{x_{i,F}} < \frac{p_H}{p_L} = \phi \quad (2.19)$$

Eq. 2.19 indicates that the enrichment of component  $i$  can never exceed the pressure ratio regardless of the membrane selectivity [34]. The relationship between the pressure ratio and the membrane selectivity can be derived from the Eqs. 2.2, 2.4 and 2.19 [18, 22].

$$y_{i,P} = \frac{\phi}{2} \left[ x_{i,F} + \frac{1}{\phi} + \frac{1}{\alpha - 1} + \sqrt{\left( x_{i,F} + \frac{1}{\phi} + \frac{1}{\alpha - 1} \right)^2 - 4 \frac{\alpha x_{i,F}}{(\alpha - 1)\phi}} \right] \quad (2.20)$$

If the membrane selectivity ( $\alpha$ ) is much larger than the pressure ratio ( $\phi$ ), that is,  $\alpha \gg \phi$ , thus, the equation 2.20 can be simplified as

$$y_{i,P} = x_{i,F} \phi \quad (2.21)$$

This is we normally called the pressure-ratio-limited region, and the membrane separation performance is mainly controlled by the pressure ratio cross the membranes while the selectivity have only minor effects.

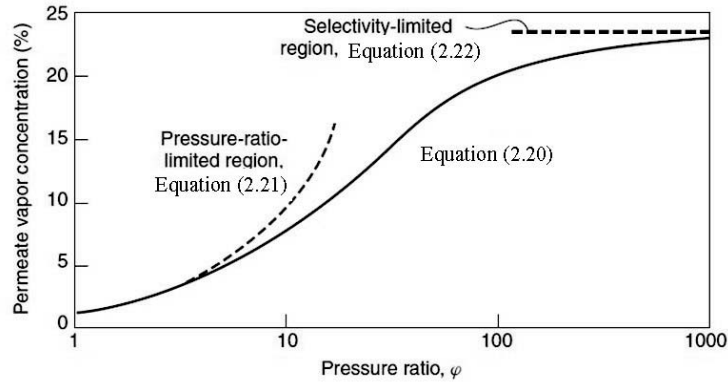


Fig. 2.2 The dependence of the permeate vapor concentration on the pressure ratio at a vapor/nitrogen selectivity of 30 and a feed vapor concentration of 1%. Below the pressure ratio of about 10, the separation is controlled by the pressure ratio across the membrane. Above the pressure ratio of 100, the separation is controlled by the membrane selectivity [22]

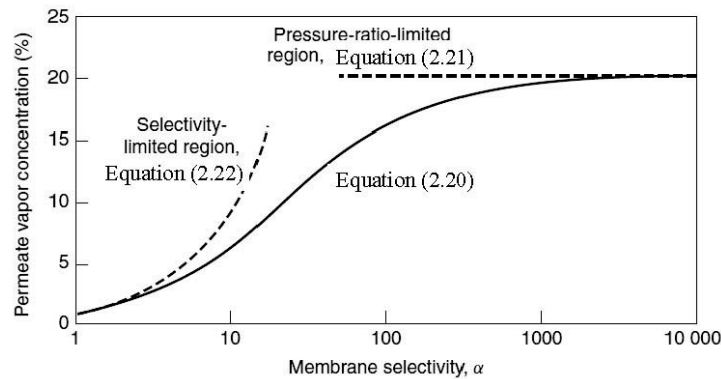


Fig. 2.3 The dependence of the permeate vapor concentration on the membrane selectivity at a pressure ratio of 20 and a feed vapor concentration of 1%. Below the membrane selectivity of about 10, the separation is controlled by the membrane selectivity. Above the membrane selectivity of 100, the separation is controlled by the pressure ratio across the membrane [22]

However, if the membrane selectivity is much smaller than the pressure ratio ( $\alpha \ll \phi$ ), the equation 2.20 becomes,

$$y_{i,P} = \frac{\alpha x_{i,F}}{1 - x_{i,F}(1 - \alpha)} \quad (2.22)$$

This is the membrane-selectivity-limited region, and the membrane separation performance is mainly controlled by the membrane selectivity while the pressure ratio has minor effects. In between, both the pressure ratio and the membrane selectivity will influence the membrane performance.

An example for the dependence of the permeate concentration versus the pressure ratio and selectivity was reported by Paul et. al, as shown in Figures 2.2 and 2.3 [22]. The pressure ratio is very important for gas separation processes in industrial scale due to the practical limitation of the pressure ratio. Achieving the high pressure ratios by compressing the feed side to high pressure or drawing a high vacuum in the permeate side will significantly increase the energy cost. Therefore, the practical pressure ratios are typically in the range 5-20 [34].

### 2.3 Membranes relevant for CO<sub>2</sub> separation

The major industrial applications for CO<sub>2</sub> separation by the membrane technology include the CO<sub>2</sub> capture from flue gases, natural gas sweetening, biogas upgrading and H<sub>2</sub> / CO<sub>2</sub> separation from pre-combustion process. The CO<sub>2</sub> concentration in the flue gas, natural gas and biogas are relative lower comparing to the other gas components such as CH<sub>4</sub> and N<sub>2</sub> as illustrated in Table 2.6. Therefore, it is desired to have a higher CO<sub>2</sub>-selective membrane to reduce the required membrane area.

Table 2.6 Typical gas composition from different sources

Process	Composition (vol, %)						H <sub>2</sub> S/SO <sub>2</sub> (ppm)	Reference
	CO <sub>2</sub>	H <sub>2</sub>	CH <sub>4</sub>	N <sub>2</sub>	O <sub>2</sub>	H <sub>2</sub> O		
Post-combustion	10-12	-	-	78-80	2-3	6-8	180-250	[35]
Natural gas sweetening	9.6	-	90	0.1	-	-	-	[1]
Farm biogas plant	37-38	-	55-58	<2	<1	4-7	32-169	[36]
Sewage digester	38.6	-	57.8	3.7	0	4-7	62.9	[37]
Landfill	37-41	-	47-57	<1	<1	4-7	36-115	[36]
Pre-combustion	38.8	50.4	-	~8.6	-	-	Assumed 0	[38]

#### 2.3.1. CO<sub>2</sub> capture from flue gases

CO<sub>2</sub> capture from flue gases is quite challengeable due to the relative low CO<sub>2</sub> concentration, low feed pressure (1.01bar), huge volume flow rate (10<sup>6</sup> Nm<sup>3</sup>/h for a typical 400 MW power plant) as well as small content of SO<sub>2</sub> and NO<sub>x</sub>. The most mature technique for CO<sub>2</sub> removal from different gas streams is the chemical absorption with amine solutions such as MEA. However, the high energy costs and the potentially environmental unfriendly process directs the development into the alternative membrane

technology. Yang et al reviewed the progress for CO<sub>2</sub> separation and capture, and they concluded that the membrane process is energy-saving, space-saving, easy to scale-up, and could be the future technology for CO<sub>2</sub> separation [39]. However, a high performance membrane with low cost is required for the membrane system in order to compete with the traditional chemical absorption method. The trade-off between the selectivity of CO<sub>2</sub> / N<sub>2</sub> and CO<sub>2</sub> permeability is shown in Fig. 2.6 [1]. Choosing a suitable membrane will mainly depend on the separation requirements [9]. If the higher productivity purity is required, the higher membrane selectivity is preferred. If the larger flow rate of gas needs to be treated, the higher permeability will be preferred. Some literature therefore recommended to use different membranes for CO<sub>2</sub> capture [39-44].

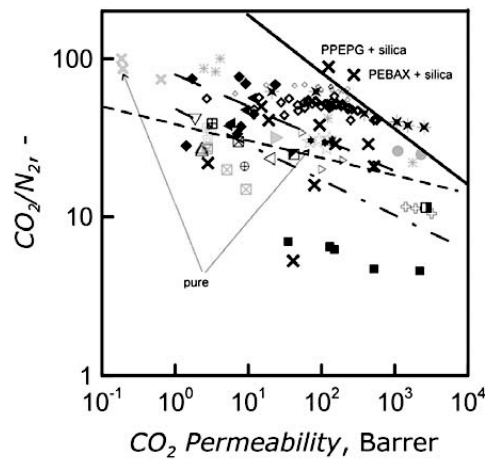


Fig. 2.6 Robeson's diagram for the CO<sub>2</sub>/N<sub>2</sub> separation [1]

### 2.3.2. Natural gas sweetening

CO<sub>2</sub> separation from natural gas (natural gas sweetening) is mandatory to meet the natural gas network grid specifications since CO<sub>2</sub> reduces the heating values of natural gas, is corrosive, and easily forms hydrates which can clog equipment or damage pumps [1]. The membrane technology is attractive for the removal of CO<sub>2</sub> from natural gas due to the high CO<sub>2</sub> permeability compared to the other gas species for most membranes. Moreover, the process can be accomplished with a high CH<sub>4</sub> recovery (e. g. > 94 %). A representative for natural gas sweetening process is shown in Fig. 2.7 [1]. The membrane system is much more favorable for the small size applications (< 6000 Nm<sup>3</sup>/h). Some commercial membranes used for natural gas sweetening are summarized in Table 2.7.

Table 2.7 Representative commercial membranes for CO<sub>2</sub> removal from natural gas

Membrane	Company	Module	Reference
Cellulose acetate	UOP	Spiral wound	[45]
Cynara <sup>®</sup>	NATCO	Hollow fiber	[46]
Prism <sup>®</sup>	Air Products	Hollow fiber	[47]
Composite membrane	MTR	-	[48]

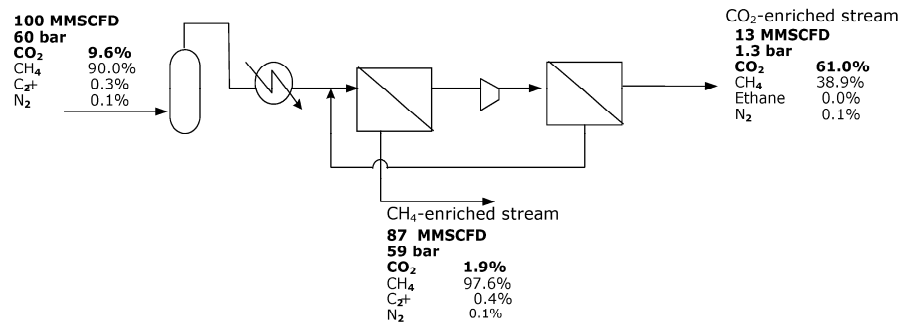


Fig. 2.7 Natural gas sweetening with two-stage membrane process [1]

### 2.3.3. Biogas upgrading

Biogas is produced in anaerobic digesters from biodegradable wastes such as sewage sludge, manure, organic fraction of household and industrial waste. The composition of biogas varies depending on the origin of the anaerobic digestion process. The main components are methane (CH<sub>4</sub>) and carbon dioxide (CO<sub>2</sub>) as indicated in Table 2.6. Biogas has a very high-energy potential due to the presence of methane (CH<sub>4</sub>) and thus is a great source for energy production. Many countries have shown interest in collection and subsequent use of biogas to reduce Green house gas (GHG) emissions from the landfill and to replace the fossil fuels [49]. Biogas can be used as a renewable energy source for heating, combined heat and power (CHP) generation, vehicle fuel, fuel cell and substitute natural gas. However, depending on the different end use, the specific biogas treatment should be executed. For the application as vehicle fuel and natural gas grid injection, the biogas upgrading, defined as removal of the energy diluting components (mainly CO<sub>2</sub>) from the gas, is necessary in order to increase the heating / calorific value of biogas which is direct proportion to the methane concentration. However, the upgrading process adds more costs to the biogas production. Therefore, it is important to find an optimized upgrading process in terms of lower energy consumption and higher efficiency which providing high methane content

in the upgraded gas. Moreover, the methane loss in the upgrading process should be minimized since the methane has a greenhouse effect of 23 times higher than that of CO<sub>2</sub>. Therefore, minimum emission of CH<sub>4</sub> should also be considered.

The most common upgrading techniques include pressure swing adsorption (PSA), physical absorption (e.g. water scrubbing [50]), chemical absorption (e.g. amines) [51-52] and membrane separation. The choice of a suitable technology is mainly dependent on the specific condition at the plant, such as the availability of low price for heating, electricity and water, as well as the amount of gas to be handled. The characteristics for these techniques are compared by Urban [53]. Most biogas upgrading plants in Sweden were using PSA although the methane content in the upgraded gas is low (96%) and the methane loss is quite high (3-10%). The upgrading plants with water scrubbing process will produce a lot of waste water, and the electricity consumption is also quite high. The membrane process as energy-saving, space-saving, easy to scale-up, could be the future technology for CO<sub>2</sub> separation [39-40, 42-43]. Deng et al. reported the biogas upgrading using FSC membranes [54]. Their results indicated that a CH<sub>4</sub> recovery of 99% at a low running cost could be obtained to meet the natural gas network specification, which makes this green process more competitive compared with other conventional technologies currently used. Moreover, a new carbon membrane company MemfoACT (<http://www.memfoact.no>) was launched in 2008 in Norway, which mainly focuses on the biogas upgrading using the carbon membrane technology [55]. Their contribution could be promising to bring this technique into the commercial application in near future.

#### 2.3.4. H<sub>2</sub> / CO<sub>2</sub> separation from pre-combustion process

Integrated gasification combined cycles (IGCC) is considered as one of the most environmentally friendly and potentially energy efficient means of power generation from coal [38]. A typical process essentially consists of coal gasification to syngas, syngas clean-up, gas turbines, heat recovery and steam turbines. Firstly, a mixture of coke, O<sub>2</sub> and steam is gasified at 25 bar and 1500 °C in a gasifier to produce syngas. The syngas is then cooled, producing intermediate pressure (IP) steam, to 235 °C before fly ash is removed by filtration and scrubbing. The scrubbed gas then enters the desulphurization section, which consists of a COS hydrolyser to convert COS to H<sub>2</sub>S and a MDEA absorber unit to separate the H<sub>2</sub>S. A mixture mainly contains CO<sub>2</sub>, H<sub>2</sub>, CO and N<sub>2</sub> by water-gas shift reaction is produced. The CO<sub>2</sub> is removed by a separation unit, and then compressed to pipeline. The hydrogen rich stream is heated by heat exchanger and humidified before being mixed with nitrogen in order to lower the combustion temperature in the gas turbine. The heat exchange integration for the whole process should be executed by process system synthesis and the thermal efficiencies (lower

heating value) can arrive in the region of 46–47%, and it may arrive as high as 55 % due to the implementation of new technology in the future, as predicted by the IEA. Grainger et. al reported that a scheme of heat integration network with CO<sub>2</sub> capture by FSC membrane unit as shown in Fig. 2.8 [38]. They concluded that the FSC membranes could be used to H<sub>2</sub> / CO<sub>2</sub> separation in IGCC power plants. However, the shifted syngas should be cooled down to a certain low temperature (e.g. 35 °C) before fed into the polymer / FSC membrane system for CO<sub>2</sub> separation, and the H<sub>2</sub> rich stream should be reheated to high temperature and send to the gas turbine, which could reduce the whole thermal efficiency. Therefore, the alternative of carbon molecular sieve membrane could be more suitable for this high temperature application.

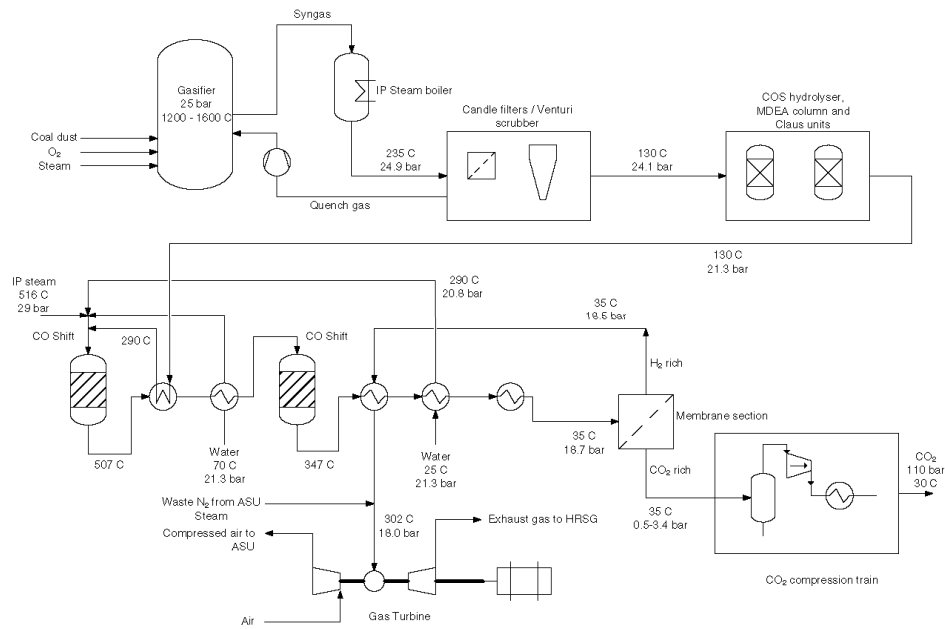


Fig. 2.8 Heat integration scheme for IGCC process with CO<sub>2</sub> capture by FSC membranes [38]

## 2.4 References

- [1] Bernardo P, Drioli E, Golemme G. Membrane Gas Separation: A Review/State of the Art. *Ind Eng Chem Res.* 2009;48(10):4638-63.
- [2] Baker RW. Future Directions of Membrane Gas Separation Technology. *Ind Eng Chem Res.* 2002;41(6):1393-411.
- [3] Peinemann KV, Nunes SP. Membrane technology in the chemical industry. Weinheim: Wiley-VCH 2001.
- [4] Robeson LM. The upper bound revisited. *J Membr Sci.* 2008;320(1-2):390-400.
- [5] Yoshikawa M, Fujimoto K, Kinugawa H, Kitao T, Kamiya Y, Ogata N. Specialty polymeric membranes. V. Selective permeation of carbon dioxide through synthetic polymeric membranes having 2-(N,N-dimethyl)aminoethoxycarbonyl moiety. *J Appl Polym Sci.* 1995;58(10):1771-8.
- [6] Zou J, Ho WSW. CO<sub>2</sub>-selective polymeric membranes containing amines in crosslinked poly(vinyl alcohol). *J Membr Sci.* 2006;286(1-2):310-21.
- [7] Kim T-J, Li B, Hägg M-B. Novel fixed-site-carrier polyvinylamine membrane for carbon dioxide capture. *J Polym Sci Part B: Polym Phys.* 2004;42(23):4326-36.
- [8] Deng L. Development of novel PVAm/PVA blend FSC membrane for CO<sub>2</sub> capture. Trondheim: Norwegian University of Science and Technology; 2009:138.
- [9] Sandru M. Development of a FSC membrane for selective CO<sub>2</sub> capture. Trondheim: Norwegian University of Science and Technology; 2009:164.
- [10] Aroon MA, Ismail AF, Matsuura T, Montazer-Rahmati MM. Performance studies of mixed matrix membranes for gas separation: A review. *Sep Purif Technol.* 2010;75(3):229-42.
- [11] Chung T-S, Jiang LY, Li Y, Kulprathipanja S. Mixed matrix membranes (MMMs) comprising organic polymers with dispersed inorganic fillers for gas separation. *Prog Polym Sci.* 2007;32(4):483-507.
- [12] Rodríguez-Reinoso F, Marsh H. Sciences of carbon materials. [Alicante]: Universidad de Alicante 2000.
- [13] Voll M, Boehm HP. Basische Oberflächenoxide auf Kohlenstoff--IV. Chemische Reaktionen zur Identifizierung der Oberflächengruppen. *Carbon.* 1971;9(4):481-8.
- [14] Marsh H, O'Hair TE. Graphite oxidation--the mobile surface-oxide intermediate. *Carbon.* 1969;7(6):702, IN17-IN18, 3.
- [15] Koros WJ, Ma H, Shimidzu T. Terminology for membranes and membrane processes (IUPAC Recommendation 1996). *J Membr Sci.* 1996;120(2):149-59.

- [16] Koros WJ, Fleming GK. Membrane-based gas separation. *J Membr Sci.* 1993;83(1):1-80.
- [17] Mulder M. Basic principles of membrane technology. Dordrecht: Kluwer 1996.
- [18] Baker R. Membrane Technology and Applications. 2nd ed: McGraw-Hill 2004.
- [19] Van Amerongen GJ. The Permeability of Different Rubbers to Gases and Its Relation to Diffusivity and Solubility. *J Appl Phys.* 1946;17(11):972-85.
- [20] Mulder M. Basic principles of membrane technology, 2nd Ed. 1996:496-8.
- [21] Ghosal K, Freeman BD. Gas separation using polymer membranes: an overview. *Polym Advan Technol.* 1994;5(11):673-97.
- [22] Paul DR, Jampol'skij JP. Polymeric gas separation membranes. Boca Raton, Fla.: CRC Press 1994.
- [23] Koros WJ, Mahajan R. Pushing the limits on possibilities for large scale gas separation: which strategies? *J Membr Sci.* 2000;175(2):181-96.
- [24] Cussler EL, Aris R, Bhowan A. On the limits of facilitated diffusion. *J Membr Sci.* 1989;43(2-3):149-64.
- [25] Noble RD. Analysis of facilitated transport with fixed site carrier membranes. *J Membr Sci.* 1990;50(2):207-14.
- [26] Bouma RHB, Checchetti A, Chidichimo G, Drioli E. Permeation through a heterogeneous membrane: the effect of the dispersed phase. *J Membr Sci.* 1997;128(2):141-9.
- [27] Borge T. Development of hybride membrane materials (mixed matrix membranes). Trondheim: Norwegian University of Science and Technology; 2010:18.
- [28] Hagg M-B, Lie JA, Lindbrathen A. Carbon Molecular Sieve Membranes. A Promising Alternative for Selected Industrial Applications. *Ann Ny Acad Sci.* 2003;984(1):329-45.
- [29] Rao MB, Sircar S. Performance and pore characterization of nanoporous carbon membranes for gas separation. *J Membr Sci.* 1996;110(1):109-18.
- [30] Gilron J, Soffer A. Knudsen diffusion in microporous carbon membranes with molecular sieving character. *J Membr Sci.* 2002;209(2):339-52.
- [31] Geankoplis CJ. Transport Processes and Unit Operations. 3rd ed: Prentice-Hall, Englewood Cliffs 1993.
- [32] Glasstone S, Laidler KJ, Eyring H. The Theory of Rate Processes. 1 ed. New York: McGraw-Hill Book Co. 1941.
- [33] Nguyen C, Do DD, Haraya K, Wang K. The structural characterization of carbon molecular sieve membrane (CMSM) via gas adsorption. *J Membr Sci.* 2003;220(1-2):177-82.

- [34] Baker RW. Membrane technology and applications. Chichester: Wiley 2004.
- [35] Flue gas composition. [cited 2011 January 20th]; Available from: [http://www.habmigern2003.info/19\\_flue-gas-contents.html](http://www.habmigern2003.info/19_flue-gas-contents.html)
- [36] Rasi S, Veijanen A, Rintala J. Trace compounds of biogas from different biogas production plants. *Energy*. 2007;32(8):1375-80.
- [37] Spiegel RJ, Preston JL. Technical assessment of fuel cell operation on anaerobic digester gas at the Yonkers, NY, wastewater treatment plant. *Waste Manage*. 2003;23(8):709-17.
- [38] Grainger D, Hägg M-B. Techno-economic evaluation of a PVAm CO<sub>2</sub>-selective membrane in an IGCC power plant with CO<sub>2</sub> capture. *Fuel*. 2008;87(1):14-24.
- [39] Yang H, Xu Z, Fan M, Gupta R, Slimane RB, Bland AE, et al. Progress in carbon dioxide separation and capture: A review. *J Environ Sci*. 2008;20:14-27.
- [40] Bredesen R, Jordal K, Bolland O. High-temperature membranes in power generation with CO<sub>2</sub> capture. *Chem Eng Process*. 2004;43(9):1129-58.
- [41] Brunetti A, Scura F, Barbieri G, Drioli E. Membrane technologies for CO<sub>2</sub> separation. *J Membr Sci*. 2010;359(1-2):115-25.
- [42] Hagg MB, Lindbrathen A. CO<sub>2</sub> Capture from Natural Gas Fired Power Plants by Using Membrane Technology. *Ind Eng Chem Res*. 2005;44(20):7668-75.
- [43] Huang J, Zou J, Ho WSW. Carbon Dioxide Capture Using a CO<sub>2</sub>-Selective Facilitated Transport Membrane. *Ind Eng Chem Res*. 2008;47(4):1261-7.
- [44] Hussain A, Hägg M-B. A feasibility study of CO<sub>2</sub> capture from flue gas by a facilitated transport membrane. *J Membr Sci*. 2010;359(1-2):140-8.
- [45] Dortmund D, Doshi K. Recent Developments in CO<sub>2</sub> Removal Membrane Technology. 1999 [cited 2010 November 23]; Available from: <http://www.uop.com/objects/84CO2RemvbyMembrn.pdf>
- [46] Kelly RM, inventor Process for separating CO<sub>2</sub> from other gases. U.S. patent 4659343. 1987.
- [47] CO<sub>2</sub> removal [cited 2010 November 30]; Available from: <http://www.airproducts.com/Products/Equipment/PRISMMembranes/page06.htm>
- [48] CO<sub>2</sub> Removal From Natural Gas. [cited 2010 November]; Available from: [http://www.mtrinc.com/co2\\_removal.html](http://www.mtrinc.com/co2_removal.html)
- [49] Bove R, Lunghi P. Electric power generation from landfill gas using traditional and innovative technologies. *Energy Convers Manage*. 2006;47(11-12):1391-401.
- [50] Rasi S, Lantelä J, Veijanen A, Rintala J. Landfill gas upgrading with countercurrent water wash. *Waste Manage*. 2008;28(9):1528-34.

- [51] Gaur A, Park J-W, Jang J-H. Metal-carbonate formation from ammonia solution by addition of metal salts--An effective method for CO<sub>2</sub> capture from landfill gas (LFG). *Fuel Process Technol.* 2010;91(11):1500-4.
- [52] Gaur A, Park J-W, Maken S, Song H-J, Park J-J. Landfill gas (LFG) processing via adsorption and alkanolamine absorption. *Fuel Process Technol.* 2010;91(6):635-40.
- [53] Urban W. Biogas upgrading to pipeline quality –Technology and costs. Connecting Clean Mobility Conference, Arnhem, the Netherlands. 2007.
- [54] Deng L, Hägg M-B. Techno-economic evaluation of biogas upgrading process using CO<sub>2</sub> facilitated transport membrane. *IJGGC.* 2010;4(4):638-46.
- [55] Membranes for advanced clean technologies. [cited 2010 November]; Available from: <http://www.memfoact.no/>

### 3 Carbon molecular sieve membranes

This chapter describes the carbon molecular sieve membranes: from material to application. This work is partly of a book chapter for “Membrane Engineering for the Treatment of Gases”, and expected to be published by Royal Society of Chemistry (RSC) in 2011.

Carbon molecular sieve (CMS) membranes have been studied in more than twenty years as a promising candidate for energy-efficient gas separation technology. Strong interests have been in the preparation of carbon membranes for gas mixture separation such as CO<sub>2</sub>-N<sub>2</sub>, O<sub>2</sub>-N<sub>2</sub> and CO<sub>2</sub>-CH<sub>4</sub>. The first carbon membranes were prepared from the carbonization of cellulose hollow fibers by Koresh and Soffer [1]. After that, many different polymer precursors were used to prepare the CMS membranes, including polyimide [2-4], polyacrylonitrile (PAN) [5], poly(phthalazinone ether sulfone ketone) [6], poly(phenylene oxide) [7-8] and cellulose derivatives [9-10]. The carbon molecular sieve membranes are more expensive than polymeric membranes due to the increased need for man-hours in the production processes, however, they possess the advantages of better permeability and selectivity as well as higher thermal and chemical stability [6, 11-16]. These key advantages have encouraged many researchers since the 1980s to investigate and develop carbon molecular sieve membranes for gas separation. The attention has focused on the carbon membranes that exhibit molecular sieving properties, which can exceed the Robeson upper boundary of permeability vs. selectivity tradeoff relationship [17] as shown in Fig. 3.1. [7, 15, 18-20] where also the region for industrial applicability is suggested by [21].

Carbon molecular sieve membranes can be divided into two categories: unsupported and supported carbon membranes [22]. Unsupported membranes have three different configurations: flat film, hollow fiber and capillary tubes, while the supported carbon membranes involve two configurations: flat and tube. Detailed descriptions of these two categories can be found in the review of Ismail [23]. The supported carbon membranes have better mechanical stability than the unsupported carbon membranes, but the preparation process is much more complex. The supported carbon membranes are typically prepared by coating the supports with a thin, uniform polymer layer. Although many different techniques can be used such as ultrasonic deposition [24], dip coating [25], vapor deposition [26], spin coating [27] and spray coating [28], there are still some challenges to successfully prepare the supported membrane: 1) control the amount of material being deposited on the support; 2) produce a uniform layer; and 3) produce the defect-free layer. The unsupported carbon membranes, i.e. hollow fibers, are prepared from the unsupported polymeric precursors. The spinning conditions are crucial for

making the precursor fibers, and should be well controlled in order to form a good fiber for carbonization. The choice of supported or unsupported carbon membranes will mainly depend on the application. Normally, the hollow fiber modules are chosen for most of gas separation processes due to the high packing capacity compared to flat-sheet membranes [5]. Hence, also the unsupported hollow fiber carbon membranes are promising for future application.

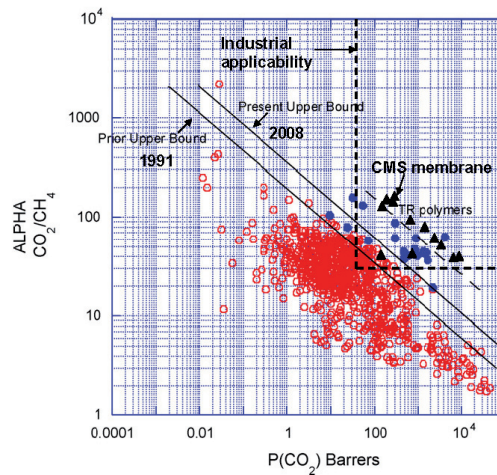


Fig. 3.1 Comparing the  $\text{CO}_2/\text{CH}_4$  Robeson upper bound for dense and thermally rearranged (TR) polymer membranes [17] to the carbon membranes [7, 15, 18-20], and the region for industrial applicability was suggested by [21]. (Data for CMS membranes and industrial applicability region added to the original Robeson plot)

### 3.1 Production of CMS membranes

Preparing a carbon membrane from a precursor is easy, but producing a high performance carbon membrane is a quite difficult task, since it includes many steps that must be well controlled and optimized. The fabrication process for CMS membranes normally consists of six important steps, i.e. material selection, material functionalization, precursor preparation, pretreatment, carbonization and post treatment, as illustrated in Fig. 3.2.

Each step includes many parameters which need to be optimized in order to obtain a high performance membrane. Among these steps, the carbonization process is the most important and can be regarded as the heart of the CMS membrane fabrication process [29]. How to control the carbonization conditions for making an optimized carbon membrane is described in section 3.1.5.

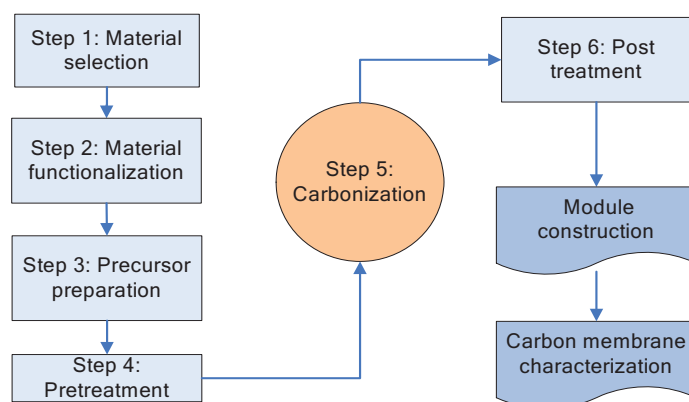


Fig. 3.2 Schematic procedure for preparation of carbon membranes

### 3.1.1. Material selection

The chemical structure and physical properties of the polymer should be primarily considered for the choice of polymer materials. However, there are only a few literature reports on the influences of chemical structure of polymers on the properties of the derived carbon membranes, e.g., by Park [30] and Xiao [31]. The latter reported the structure and properties relationship for polymer based on the experiment and simulation approaches, which provided considerable information for the choice of suitable polymers for carbon membrane preparation in various targeted applications. Hence it would be an efficient way to choose the polymer by investigating the factors of chemical structure and physical properties for determining the carbon membrane performance based on experiments and molecular simulation method.

A suitable polymer material for preparation of carbon membranes should not cause pore-holes or any defects after the carbonization. Up to now, various precursor materials such as polyimide [2-3], polyacrylonitrile (PAN) [5], poly(phthalazinone ether sulfone ketone) [6] and poly(phenylene oxide) [7-8] have been used for the fabrication of carbon molecular sieve membranes. Likewise, aromatic polyimide and its derivatives have been extensively used as precursor for carbon membranes due to their rigid structure and high carbon yields. The membrane morphology of polyimide could be well maintained during the high temperature carbonization process. A commercially available and cheap polymeric material is cellulose acetate (CA, MW 100,000, DS=2.45), this was also used as the precursor material for preparation of carbon membranes by He et. al [18]. They reported that the cellulose acetate can be easily dissolved in many solvents to form the dope solution for spinning the hollow fibers, and the prepared hollow fiber carbon membranes showed nice separation performances.

### 3.1.2. Material functionalization

In order to enhance the selectivity and permeability of the carbon molecular sieve (CMS) membrane, the addition of other components to the carbon matrix is considered. For CMS membranes, two types of additives have been reported: The first kind of additives increases the micropore volume of the carbon membrane by degrading during the carbonization process (temperature range 500-1000°C), and leave behind specific spacing within the mass of the carbon. Such additives are often referred to as porogens and can serve as templates in the formation of microporosity in carbon, for example polyvinylpyrrolidone (PVP) [32-33]. The second kind of additives is the nano-functional additives and can be thought of as thermally stable compounds incorporated into the carbon membrane precursor, either before or after casting or spinning. These components may enhance the gas separation process if the interactions between the additive and the penetrants can be exploited for an enhanced transport rate through the carbon membranes. Obviously, the variety of nano-functional additives which can be incorporated into the CMS membrane is limited due to the high temperatures applied during carbonization which will result in the degradation of all organic components. Possible additives include metals (added as metal salts) which show a high affinity to one of the permeating gas species, silica nano-particles and carbon nanotubes, these are all listed in Table 3.1.

Table 3.1 Representative examples of functionalization additives

Additives	Function	References
Metal nitrates and metal oxides	Fe(NO <sub>3</sub> ) <sub>3</sub> , Cu(NO <sub>3</sub> ) <sub>2</sub> , Ag NO <sub>3</sub> , MgO, CaO, SiO <sub>2</sub> , Fe <sub>2</sub> O <sub>3</sub>	Increase the polarity and / or form interlayer spaces and /or have an affinity towards target gases [34-36]
Alkali metals	Na <sup>+</sup> and Mg <sup>2+</sup>	Cause steric hindrance in the carbon matrix [34]
Transition Metals	Cu <sup>2+</sup> , Ni <sup>2+</sup> or Zn <sup>2+</sup>	Increase macropore volume [34]
Silver	AgNO <sub>3</sub> , AgC <sub>2</sub> H <sub>3</sub> O <sub>2</sub>	Ag nanoclusters behaving as spacers within the carbon matrix [37]
Nickel	nickel nano-particles	a strong chemisorption of the H <sub>2</sub> on the nickel particles [38]
Other metal additives	palladium and platinum	Palladium acting as a gas permeation barrier to other gases [39-40]
Silica nano-particle	SiO <sub>2</sub>	Show molecular sieving properties [41]
Zeolite		Provide transport pathways for specific gasses [42-43]
Carbon nanotube	Single walled or multi-walled nanotube	Changing of charge patterns, used as a compacting agent for the polymer blends [44-46]

The addition of metal nitrates have the additional porogen effect as the nitrates degrade releasing gases during the carbonization procedure [19]. Metal oxides are thought to be unsuitable due to their low solubility in organic solvents such as NMP and their affinity for water which may result in blocking of the metallic sites. The use of nickel for the adsorption of  $\text{CO}_2$  has previously been demonstrated and this may help to enhance  $\text{CO}_2$  transport through the membrane. Also the alkali metals have been found to increase gas selectivity and would be a useful additive if the decrease in permeability could be overcome. Another promising additive appears to be the carbon nanotubes which can be tailored to various sizes and are highly temperature resistant. Example of enhanced separation properties is shown in Fig. 3.3 [19].

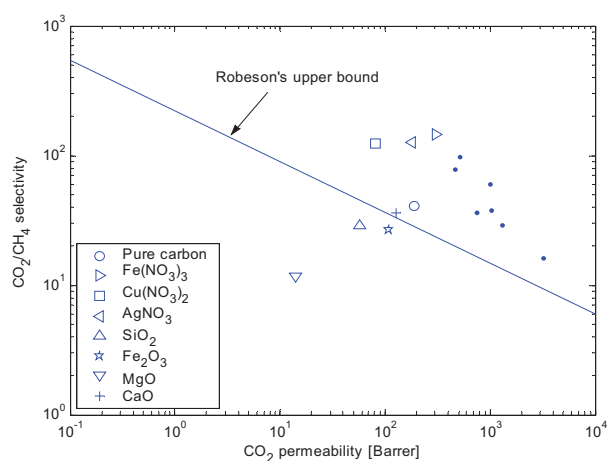


Fig. 3.3 Separation performance of carbon and metal loaded carbon for the  $\text{CO}_2/\text{CH}_4$  gas pair at  $30^\circ\text{C}$ . Dots are literature values for carbonized polyimides [3, 47], the other marks are from a cellulosic precursor

### 3.1.3. Precursor preparation

The general process for preparation of the precursors consists of four steps, i.e. dope formation, casting / spinning, dehydration and post treatment. There are many parameters will affect the precursor properties during the preparation process. An example for the optimization of spinning condition was reported by He et al. they reported that the optimal conditions for spinning cellulose acetate hollow fiber membranes was found to be as follows: bore fluid (water + NMP (85%)), air gap (25mm), bore flow rate (40% of dope flow rate 2.2 ml/min) and temperature of quench bath ( $50^\circ\text{C}$ ) [48].

#### 3.1.4. Pretreatment

The precursor membranes are often pretreated prior to the carbonization/carbonization process. This step can be helpful to ensure the stability of the precursor and retain the chemical structure during the carbonization. In some degree, the performance of CMS membranes can be adjusted by specific pretreatment for a given precursor membrane. Saufi et al. reviewed the pretreatment methods for precursor membranes published in the open literature before 2003 [29]. The pretreatment approaches can be divided into physical and chemical methods.

Physical pretreatment. The physical pretreatment methods for hollow fiber membranes mainly consist of stretching or drawing. This technique used in CMS membranes is sometimes referred to as a post-spinning treatment, which can remove the surface defects and enhance the retention of molecular orientation prior to the carbonization so as to obtain a good balance of stiffness and strength. The draw can take place during the spinning process or after it, and the draw ratios can become very high if the fiber is not ruptured. Yoneyama et al. reported that the drawing can be carried out under conditions which give 3 times or higher total draw by multi-stage drawing method [49].

Chemical pretreatment. Chemical pretreatment includes air oxidation and use of chemical reagents. The oxidation pretreatment is considered very important and can have a substantial effect on the resulting membrane performance, and the aim is to contribute to the stabilization of the asymmetric structure of the precursor and provide sufficient dimensional stability to undergo the high carbonization temperature. Some researchers reported that different oxidation conditions can be applied at various ranges of thermal soak times, depending largely on the precursor choices. The chemical pretreatment can enhance the uniformity of the pore system formed in the carbonization process. The hydrazine, DMF, Hydrogen chloride (HCl) and ammonium chloride (NH<sub>4</sub>Cl) can be used for chemical pretreatment. Schinedler E. et al. reported that an aqueous solution of hydrazine was used to pretreat the acrylic precursor, which can improve the dimensional stability of membrane during the subsequent process [50]. Tin et al. pointed that the as-spun hollow fiber membrane was immersed in the p-xylenediamine/methanol solution in order to form the cross-sectional morphology [51]. The deacetylation of cellulose acetate precursor was carried out by He et. al. to obtain the optimal precursor before the carbonization as reported [18].

#### 3.1.5. Carbonization

The CMS membranes are prepared by carbonizing (under pyrolysing conditions) the precursor membranes in a high temperature tube furnace, as shown in Fig. 3.4 [52]. The

step-by-step method (several dwells) most commonly used as the protocol for the carbonization process is described elsewhere [51, 53].

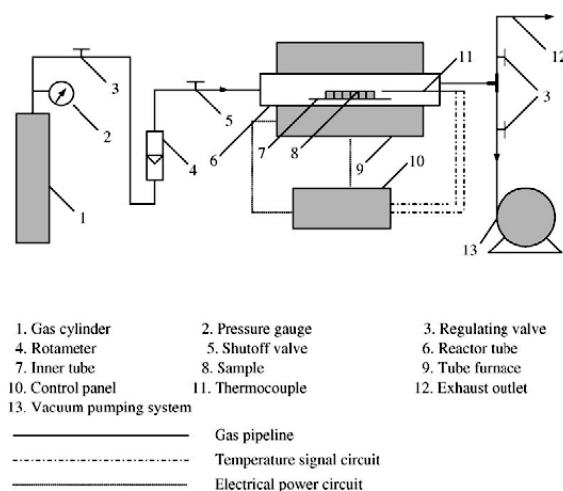


Fig. 3.4 A schematic overview of the furnace set-up [52]

Many researchers report different carbonization conditions in their research works – illustrating very well that each precursor will need different protocols in order to be pore-tailored for the specific applications as summarized in Table 3.2. The carbonization process is the most important step for fabrication of CMS membranes and is used to tailor the pore size and structure of the carbon membranes. Therefore, how to control the carbonization conditions is crucial for the resulting CMS membrane performance. Su et al. reported that the statistical  $2^{4-1}$  factorial experiment design was used to evaluate the influence of carbonization conditions on the membrane transport properties. The parameters of purge gas, carbonization temperature, heating rate and thermal soak time were employed, and the influence of importance for each parameter and interaction between them were found [54]. Wang et al. reported the influence of different carbonization degrees on the carbon membrane performance. They pointed that the  $\text{CO}_2$  diffusion coefficient in the carbon molecular sieve (CMS) membranes depends on the surface heterogeneity of the membrane sample and increases with the degree of carbonization [55]. Geiszler et al. investigated the effect of the polyimide carbonization conditions such as purge gas, purge flow rate and temperature on the carbon membrane performance [56]. They concluded that the vacuum carbonization could prepare more selective but less productive CMS membranes than the inert gas carbonized membranes, and the high purge flow rates could result in a much higher permeability, but lower selectivity membranes. Moreover, by increasing the final temperature, the membranes

become more selective but less productive. In order to systematically investigate the influences of carbonization parameters on the membrane properties, the orthogonal experimental design (OED) and conjoint analysis was executed in this work, a more detail description can be found in Appendix E.

Table 3.2 Representative examples of precursors, carbonization conditions and gas permeation tests for CMS membranes

Precursor	Carbonization conditions (Temperature, Heating rates, Soak times, Purge gas)	Single gas permeation test	Gas mixture test	References
PAN	250–800 °C; 9°C /min; 10–180 min; N <sub>2</sub>	O <sub>2</sub>	O <sub>2</sub> /N <sub>2</sub>	[5]
	600 and 950 °C; 1°C/min; –; N <sub>2</sub>	-	-	[57]
	900 °C; 5 °C /min; –; N <sub>2</sub>	-	-	[58]
	500 °C; –; 10 min -3 h; N <sub>2</sub>	O <sub>2</sub> , N <sub>2</sub>	-	[5]
Cellulose	500–800 °C; –; 12 h; Ar	-	-	[59]
	700 °C; –; –; HCl as catalyst in an inert gas	H <sub>2</sub> , N <sub>2</sub> , O <sub>2</sub> , Cl <sub>2</sub> , HCl, SF <sub>6</sub>	O <sub>2</sub> /N <sub>2</sub> , O <sub>2</sub> /Cl <sub>2</sub> , H <sub>2</sub> /HCl, O <sub>2</sub> /SF <sub>6</sub>	[60]
	120-700 °C; 0.1-0.6 °C /min; –; CO <sub>2</sub> , Ar, N <sub>2</sub> (HCl/NH <sub>4</sub> Cl as the catalyst)	-	-	[61]
Polyimide	500–550 °C; 0.25–13.3 °C/min; 2 h; vacuum	CO <sub>2</sub> , O <sub>2</sub>	H <sub>2</sub> /CH <sub>4</sub> , CO <sub>2</sub> /CH <sub>4</sub> , CO <sub>2</sub> /N <sub>2</sub>	[62-63]
	500–550 °C; 0.25–13.3 °C/min; 2 h; vacuum and inert gas (Ar, He, CO <sub>2</sub> )	H <sub>2</sub> , O <sub>2</sub>	O <sub>2</sub> /N <sub>2</sub> , H <sub>2</sub> / N <sub>2</sub>	[56]
	550 °C; 0.25 °C/min; 2 h; vacuum or He	CO <sub>2</sub>	CO <sub>2</sub> /CH <sub>4</sub>	[16]
	750 °C; –; 60 min; vacuum	C <sub>6</sub> H <sub>6</sub> , Ar, C <sub>6</sub> H <sub>12</sub> , H <sub>2</sub>	C <sub>6</sub> H <sub>6</sub> /Ar, C <sub>6</sub> H <sub>12</sub> /H <sub>2</sub> ,	[64]

Polyimide	600–1000 °C; –; 3.6 min; N <sub>2</sub>	H <sub>2</sub> , CO <sub>2</sub> , O <sub>2</sub> , N <sub>2</sub> , CH <sub>4</sub> , C <sub>2</sub> H <sub>4</sub> , C <sub>2</sub> H <sub>6</sub>	H <sub>2</sub> /CH <sub>4</sub>	[65]
	500–900 °C; –; 0.5s–20min; N <sub>2</sub>	H <sub>2</sub>	H <sub>2</sub> /CH <sub>4</sub>	[66]
	750 °C; 2.6 °C/min; 3 h; N <sub>2</sub> or 850 °C; 2.6 °C/min; 3 h; vacuum	H <sub>2</sub> , He, CH <sub>4</sub> , CO <sub>2</sub> , O <sub>2</sub> , N <sub>2</sub>	CO <sub>2</sub> /CH <sub>4</sub>	[67-68]
	500–700 °C; 5 °C/min; –; N <sub>2</sub>	H <sub>2</sub> , CO <sub>2</sub> , O <sub>2</sub> , N <sub>2</sub> , C <sub>3</sub> H <sub>6</sub> , C <sub>3</sub> H <sub>8</sub>	He/N <sub>2</sub> , CO <sub>2</sub> /N <sub>2</sub> O <sub>2</sub> /N <sub>2</sub> , C <sub>3</sub> H <sub>6</sub> /C <sub>3</sub> H <sub>8</sub>	[69]
	550 °C; –; –; vacuum	H <sub>2</sub> , N <sub>2</sub> , O <sub>2</sub> , Cl <sub>2</sub> , HCl, SF <sub>6</sub>	O <sub>2</sub> /N <sub>2</sub> , O <sub>2</sub> /Cl <sub>2</sub> , H <sub>2</sub> /HCl, O <sub>2</sub> /SF <sub>6</sub>	[60]
P84 co-polyimide	600–900 °C; 1 °C/min; 1 h; N <sub>2</sub>	He, H <sub>2</sub> , O <sub>2</sub> , Ar, O <sub>2</sub> , N <sub>2</sub> , CH <sub>4</sub> , C <sub>2</sub> H <sub>4</sub> , C <sub>2</sub> H <sub>6</sub> , C <sub>3</sub> H <sub>6</sub> , C <sub>3</sub> H <sub>8</sub> , SF <sub>6</sub>	CO <sub>2</sub> /N <sub>2</sub> , O <sub>2</sub> /N <sub>2</sub> , He/x(x: Ar, O <sub>2</sub> , N <sub>2</sub> , CH <sub>4</sub> , C <sub>2</sub> H <sub>4</sub> , C <sub>2</sub> H <sub>6</sub> , C <sub>3</sub> H <sub>6</sub> , C <sub>3</sub> H <sub>8</sub> , SF <sub>6</sub> )	[12]
	650-800 °C; 0,2-3.8 °C/min, 2h; vacuum	CO <sub>2</sub> , CH <sub>4</sub>	CO <sub>2</sub> /CH <sub>4</sub>	[15]
Polyimide/PVP blends	550-700 °C; 3 °C /min; 60min; Ar	H <sub>2</sub> , He, CO <sub>2</sub> , O <sub>2</sub> , N <sub>2</sub>	O <sub>2</sub> /N <sub>2</sub> H <sub>2</sub> /N <sub>2</sub> , He/N <sub>2</sub> , CO <sub>2</sub> /N <sub>2</sub>	[70]
Metal-substituted sulfonated polyimide	600 °C; 3 °C /min; 60 min; Ar	He, O <sub>2</sub> , N <sub>2</sub>	He/N <sub>2</sub> , O <sub>2</sub> /N <sub>2</sub>	[35]
Polyimide Matrimid	500-900 °C; 5 °C/min; 5 min; N <sub>2</sub> , CO <sub>2</sub> , N <sub>2</sub> saturated with water	He, H <sub>2</sub> , CH <sub>4</sub> , Ar, CO <sub>2</sub> , CO, O <sub>2</sub> , N <sub>2</sub>	H <sub>2</sub> /CH <sub>4</sub> , CO <sub>2</sub> /CH <sub>4</sub> , CO <sub>2</sub> /N <sub>2</sub> , O <sub>2</sub> /N <sub>2</sub> , H <sub>2</sub> /CO <sub>2</sub>	[13]
	250-800 °C; 0.2-3 °C /min; 2h; vacuum	CH <sub>4</sub> , CO <sub>2</sub> , O <sub>2</sub> , N <sub>2</sub>	-	[51]
Poly(phenylene Oxide), PPO	550-750 °C; 10 °C/min; –; vacuum	CO <sub>2</sub> , O <sub>2</sub>	O <sub>2</sub> /N <sub>2</sub> , CO <sub>2</sub> /CH <sub>4</sub>	[7]
Mixed matrix of polysulfone/zeolite beta with Matrimid	550-800 °C; 0.2-3.8 °C/min; 2h; vacuum	CH <sub>4</sub> , CO <sub>2</sub> , O <sub>2</sub> , N <sub>2</sub>	CO <sub>2</sub> /CH <sub>4</sub> , O <sub>2</sub> /N <sub>2</sub>	[71]

### 3.1.6. Post treatment

After the carbonization process, the precursor membranes are transformed into the CMS membranes, which have different porosity, structure and separation performance that depend on the carbonization conditions. The CMS membrane performances can be partly adjusted by the application of various post treatment methods, such as post-oxidation, chemical vapor deposition (CVD) [72], coating, post-carbonization. The post-oxidation is the most used method to change the carbon membrane pore structure. Hayashi et. al studied the post-oxidation of a polyimide-derived carbon membrane in the air [25]. They found that the CO<sub>2</sub> permeability increased without any significant change in selectivity. The chemical vapor deposition can be used to introduce the organic species into the carbon matrix and can give three different results: homogeneous deposition, adlayer deposition and in-layer deposition. The coating technique is mainly used to repair the defects in the carbon matrix in order to compose the high selectivity. However, the coating will typically result to the decrease of permeability as reported by Liang et. al [73]. Some literature reported to use the different post treatment methods for altering the membrane structure to improve the membrane performance [66, 74-75].

## 3.2 Characterization for CMS membranes

### 3.2.1. General characterization techniques

*Scanning electron microscopy (SEM)* with high resolution is often used as a standard technique to examine the membrane morphology. The cross-section views the thickness and diameter of the membranes, as shown in Fig. 3.5 [7]. The carbon membrane forms a symmetric structure, and neither voids nor defects were found in carbon membranes. The carbon membranes remained the dense structure after carbonization, but the thickness decrease significantly from 35-38 μm to 23-25 μm.

*Fourier transform infrared (FTIR) spectroscopy* can be used to determine the chemical functional group in the carbon membranes. Fourier transform infrared (FTIR) spectroscopy now is a powerful tool for identifying types of chemical bonds in a molecule by producing an infrared absorption spectrum that is like a molecular "fingerprint". The FTIR spectra of precursor and carbon membranes with different final carbonization temperatures using CO<sub>2</sub> as purge gas as well as in vacuum environment are illustrated in Fig. 3.6. Most peaks disappeared for carbon membranes when the temperature was higher than 550 °C, and the new characteristic absorption peaks were found at 2350 cm<sup>-1</sup> and 670 cm<sup>-1</sup>, which contribute to the CO<sub>2</sub> adsorbed in carbon matrix or C=O bond formed in the membrane surface and the aromatic =C-H out of

plane deformation [15]. In vacuum condition, the characteristic absorption peak of CO<sub>2</sub> also appears in the FTIR spectrum which indicates the CO<sub>2</sub> comes out during the decomposition of deacetylated cellulose acetate and adsorbs strongly in the carbon matrix.

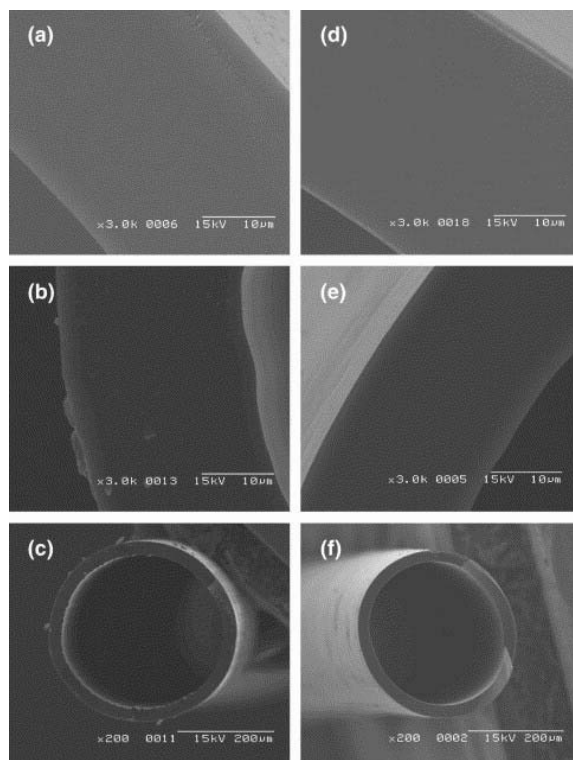


Fig. 3.5 SEM images of the cross sections for (a) P(PPO), (b, c) C(PPO), (d) P(TMS80), and (e, f) C(TMS80). Carbon samples were carbonized at 923 K [7]

*X-ray photoelectron spectroscopy (XPS)* is a powerful tool to study the surface elemental compositions of materials, and can be used to determine the trend of carbon content followed by the change of carbonization temperature. Fig. 3.7 shows the XPS spectra of the original PPESK membrane and the carbon membranes obtained at different carbonization temperatures, revealing that for all membranes, carbon, oxygen, nitrogen and sulfur are the main elements on the membrane's surface as reported by Zhang et. al [6]. They reported that in this carbonization step, rearrangement reactions between the poly- and hetero-cyclic aromatic nitrogen-containing compounds in carbon structure take place.

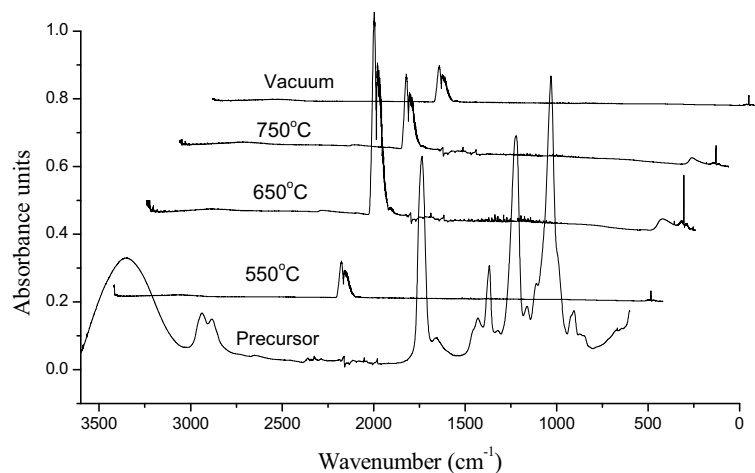


Fig. 3.6 FTIR spectra of precursor and carbon membranes obtained at different conditions

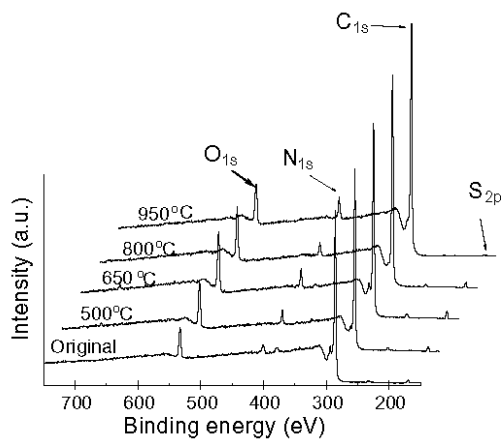


Fig. 3.7 XPS spectra of the original PPESK membrane and as-prepared carbon membranes [6]

X-ray diffraction (XRD) is a useful tool for studying the arrangement of carbon atoms at molecular level. The inter-planar distance and its variation can be monitored by XRD, so it has been well established that the *d*-spacing can serve as indicative of the graphitization degree of the examined carbon membranes since the *d*-spacing of graphite is 0.335 nm. The XRD patterns for the carbon membrane C(PPO) and C(TMS80) are shown in Fig. 3.8 [7]. The average *d*-spacing (*d*<sub>002</sub>) values were calculated from Bragg's equation, providing the interlayer distance of the carbon

membranes as 0.41nm and 0.40nm respectively. The interlayer distance can be considered as a diffusional path for gas molecules through the carbon membranes, which is helpful to evaluate the microstructure of the carbon membranes. The intensity of  $d_{002}$  peak of C(TMS80) was somewhat lower than that of C(PPO), indicating that the microstructure of C(TMS80) is arranged less orderly and tightly.

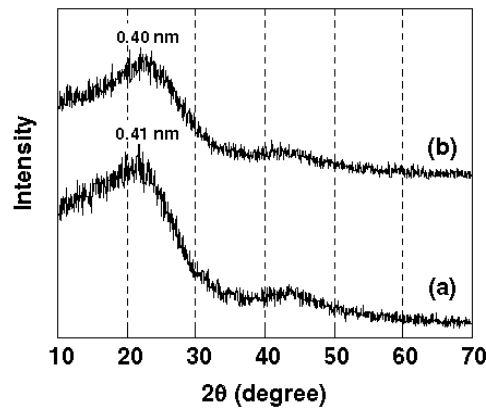


Fig. 3.8 XRD pattern for carbon membranes (a) C(PPO), (b) C(TMS80) [7]

### 3.2.2. Gas sorption

When a gas or vapor is contacted with a solid material, part of it is taken up by the solid. The gas molecules either enter the inside of the solid, or remain on the solid surface. The former phenomenon is termed absorption (or dissolution) and the latter called adsorption. When the phenomena occur simultaneously, the process is termed sorption. The solid that takes up the gas is called the adsorbent, and the gas or vapor taken up on the surface is called the adsorbate. Molecules and atoms can attach themselves onto surfaces in two ways: physisorption and chemisorption.

*In physisorption* (physical adsorption), there is a weak van der Waals attraction of the adsorbate to the surface. The attraction to the surface is weak but long ranged and the energy released upon accommodation to the surface is of the same order of magnitude as an enthalpy of condensation (on the order of 20 kJ/mol).

*In chemisorption* (chemical adsorption), the adsorbate sticks to the solid by the formation of a chemical bond with the surface. This interaction is much stronger than physisorption, and, in general, chemisorption has more stringent requirements for the compatibility of adsorbate and surface site than physisorption.

The gas sorption technique is mainly used to characterize the micropore volume, pore size and pore size distribution (PSD) of the porous inorganic materials. The gas adsorption isotherm is normally obtained by measuring the gas adsorption amount on the material at different pressure by a gravimetric method. At lower pressure, the large pores will be filled with the gas molecules. Following the increase of the pressure, the smaller pores will be filled gradually, and near the saturation pressure all pores are filled. The gas adsorption isotherm data for the carbon membranes can be obtained by a Robotherm magnetic suspension balance (MSB) having a 0.01mg resolution and 0.02 mg reproducibility. The MSB overcomes some disadvantages of other conventional gravimetric sorption instruments by separating the microbalance from the sample and adsorbed gases [76]. The sample is placed in a suspended basket by a permanent magnet through an electromagnet in a closed system. The MSB instrument can perform the sorption measurements within a wide pressure range up to 35 and 150 bar for CO<sub>2</sub> and N<sub>2</sub>, respectively. Moreover, the temperature can be well controlled within the range from 298 to 423 K using a Julabo thermostatic circulator. The system can automatically measure the weight change of the samples over time at a certain temperature and pressure according to the measurement procedure described elsewhere [77]. CO<sub>2</sub> isotherm adsorption at 301 K up to 5 bar was executed by Lagorsse et.al [78]. The adsorption equilibrium isotherms and Dubinin-Radushkevich regression are shown in Fig. 3.9. The micropore volume for the carbon membranes can be determined from the equilibrium adsorption amount near saturation pressure. In order to determine the micropore volume, the Dubinin and Radushkevich (DR) model was used to regress the adsorption equilibrium data,

$$\frac{w}{w_0} = \exp\left(-\left(\frac{RT \ln(p_0/p)}{\beta E_0}\right)^2\right) \quad (3.1)$$

Where  $w$  is the volume adsorbed at a pressure  $p$ ,  $w_0$  is the micropore volume of carbon membrane,  $E_0$  is the adsorption activation energy dependent on the pore structure, and  $\beta$  is the affinity coefficient that is the characteristics of the adsorption capacity [79]. The pore size distribution for the carbon membranes can be further determined by the method proposed by Nguyen and Do [80-81].

### 3.2.3. Gas permeation

Single gas tests are quite important for CMS-membranes as they will also give an indication of the membranes pore size. A time lag method was used to measure the single gas permeabilities [7, 14]. The order of testing was always H<sub>2</sub>, N<sub>2</sub>, CH<sub>4</sub> and finally CO<sub>2</sub> in order to prevent the strongly adsorbing gases from disturbing the performance of the more ideal or non-interacting gases in carbon membranes [14]. The

tests can be run from several minutes to several hours, to ensure that the transient phase of diffusion is passed and a steady state had been obtained ( $dp/dt$  is constant). The gas permeability,  $P$  (Barrer,  $1\text{Barrer}=10^{-10}\text{ cm}^3(\text{STP})\cdot\text{cm}/(\text{cm}^2\cdot\text{s}\cdot\text{cmHg})$ ) can be calculated using standard procedures reported elsewhere [15]. The ideal selectivity is defined as the ratio of the single gas permeabilities and can be evaluated as follows:

$$\alpha_{i/j} = \frac{P_i}{P_j} \quad (3.2)$$

Fig. 3.10 illustrates the gas permeability values of  $\text{H}_2$ ,  $\text{CO}_2$ ,  $\text{O}_2$ ,  $\text{N}_2$  and  $\text{CH}_4$  versus the gas molecule kinetic diameters for the carbon membranes of C(PPO) and C(TMS80) carbonized at 923K [7]. The gas permeability values of the selected gases are in this order:  $\text{H}_2(2.89\text{\AA}) > \text{CO}_2(3.3\text{\AA}) > \text{O}_2(3.46\text{\AA}) > \text{N}_2(3.64\text{\AA}) > \text{CH}_4(3.8\text{\AA})$  at 298K, which clearly indicated that the molecular sieving transport mechanism was dominated for the gas penetrates through the carbon membranes.

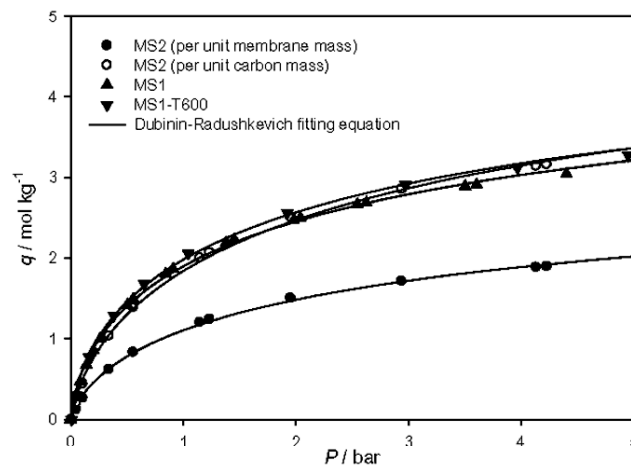


Fig. 3.9. Adsorption equilibrium of  $\text{CO}_2$  on sample MS1 ( $\blacktriangle$ ), MS1-T600 ( $\blacktriangledown$ ) and MS2 ( $\bullet$  and  $\circ$ ) at 301 K. The solid lines correspond to Dubinin–Radushkevich fitting equations [78]

In order to compare the performance for polymeric and carbon membranes, Fig. 3.11 shows a  $\text{CO}_2/\text{CH}_4$  trade-off line for P84 and Matrimid precursors and their carbon membranes as reported by Tin et. al [15]. It is clear that carbon membranes possess excellent permeation properties, where both of the permeability and ideal selectivity access the Robeson upper-bound curve. Moreover, some researchers have also investigated the influence of temperature on the gas permeability [7, 82]. They concluded that the gas permeability values increased with the increase of temperature

due to the activated process for the CMS membranes. They also found that the apparent activation energies for CO<sub>2</sub> calculated from the Arrhenius equation ( $P = P_0 \exp(-E_a/RT)$ ) was much smaller than the other gas species of O<sub>2</sub>, N<sub>2</sub> and CH<sub>4</sub>. Thereby indicating the CO<sub>2</sub> has much higher permeability.

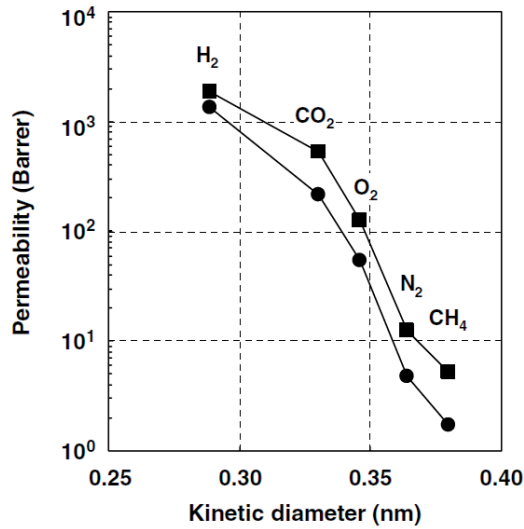


Fig. 3.10 Single gas permeabilities of C(PPO) (●) and C(TMS80) (■) against the kinetic diameter at 298K [7]

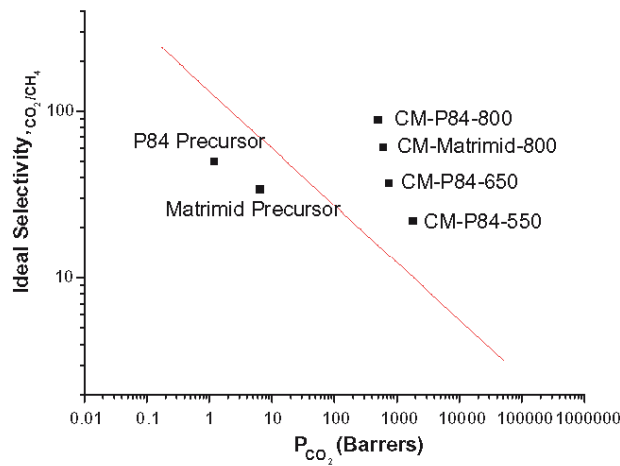


Fig. 3.11 CO<sub>2</sub>/CH<sub>4</sub> trade-off line for P84 and Matrimid precursors and their carbon membranes [15]

Mixed gas measurements, a permeation cell and a gas chromatograph (GC) were combined in order to allow straightforward determination of gas permeability. The permeability of component  $i$  in gas mixture under steady state can be calculated according to the following equations:

$$P_i = \frac{273 \times 10^7 y_i V l (dp/dt)}{76(x_i p_H - y_i p_L) A T_{\text{exp}}} \quad (3.3)$$

$$\bar{x}_i = \frac{x_{F,i} - x_{R,i}}{\ln \left( \frac{x_{F,i}}{x_{R,i}} \right)} \quad (3.4)$$

where  $P_i$  is the permeability of component  $i$ .  $p_H$  and  $p_L$  are the upstream and downstream pressure (bar), and  $x_{F,i}$  is the feed composition of component  $i$ , and  $x_{R,i}$  and  $y_i$  are the molar fraction of component  $i$  in retentate and permeate stream, respectively, which were measured by gas chromatography (GC). The process selectivity ( $\alpha_{ij}$ ) for the gas mixture was calculated using the following equation:

$$\alpha_{ij} = \frac{P_i}{P_j} \text{ or } \frac{y_i/y_j}{x_{F,i}/x_{F,j}} \quad (3.5)$$

The pure gas tests are normally used to indicate the ideal separation performance for carbon membranes. However, the separation properties will be affected by the presence of other penetrants in a gas mixture [15]. Since the transport for gas mixture will be much different from that in pure gas, especially in the presence of strong adsorbable gas like CO<sub>2</sub>. The adsorption of gas molecules in carbon membranes matrix will significantly affect the penetration of other less or non-adsorbable gas molecules. Tin et. al reported the CO<sub>2</sub>/CH<sub>4</sub> separation properties for carbon membrane (CMP84-800) [15], they reported that the selectivity of CO<sub>2</sub>/CH<sub>4</sub> in the binary mixture is about 10% higher than the ideal selectivity. This is due to the ‘‘hindrance effect’’ on the CH<sub>4</sub> permeation brought upon by the CO<sub>2</sub> molecules.

#### 3.2.4. Aging and regeneration

Although the carbon membrane has high thermal and chemical resistance, they may present significant problems related to performance stability which appears to be more vulnerable to oxidation, humidity and blockage of the pores. A small change of the pore size will dramatically affect the permeability. Therefore, the carbon membrane aging should always be investigated, and the corresponding regeneration methods should be conducted to recover the membrane performance periodically.

Humidity effect, aging is the change of membrane performance over time or in different environments. The most relevant aging effects include the physisorption (e.g. N<sub>2</sub>, CO<sub>2</sub>, and water) and chemisorption (Propylene and O<sub>2</sub>). Jones and Koros studied the influences of water vapour on the carbon membrane performance [83]. They found that the performance loss increased with the humidity. The vulnerability of CMS membranes to humidity is a complex phenomenon considering the weak character of the water-carbon dispersion forces and the tendency of water molecules to form hydrogen bonds within the bulk phase [84]. Water will initially adsorb onto hydrophilic sites and further chemisorb the penetrants. The hydrophilic sites are much more reactive than the atoms in the interior of the carbon matrix. Once the first water molecule is adsorbed onto the carbon matrix, the adsorbate-adsorbate interactions will promote the adsorption of further molecules through hydrogen bonds [78]. The water vapor adsorption and the gas permeance exposure to the different relative humidity have been investigated by Lagorsse et. al [84]. They concluded that the humidity effect must not be considered as a pore blocking mechanism associated with a slowly diffusing strongly adsorbed species, but as a competitive multi-component diffusion process.

Chemisorption of oxygen, Lagorsse et. al [85] further reported the long-term exposure to different dry environments, and they concluded that the membrane performance losses were mainly caused by the chemisorption of oxygen. The reaction of oxygen with carbon matrix is believed to involve dissociative adsorption of molecular oxygen to form oxygen surface groups and subsequent desorption of the surface oxides to the carbon monoxide and dioxide.

Regeneration techniques, most carbon membranes do not have a long-time stable permeability, especially not the high flux membranes. The carbon membrane performance will be gradually reduced due to the pore blockage or aging effects on the carbon matrix. This may be compared to the fouling of membranes in liquid separation. Therefore, regular regeneration techniques such as thermal, chemical, electrothermal, ultrasonic, or microwave regeneration are needed. Menendez and Fuertes reported regeneration in vacuum at 600 °C for 1h to improve the N<sub>2</sub> permeance [86], while Jones and Koros investigated the chemical regeneration with propene [87]. They supposed that the propene may interact with the carbon matrix in two ways: Firstly, it may act as a solvent, dissolving the penetrants that are adsorbed in the carbon matrix, secondly, the propene may swell the carbon matrix, and the arrangement of the carbon skeleton may release some of the adsorbed gas molecules. Lie et. al reported that *in-line* electrothermal regeneration method can be used to efficiently desorb the adsorbed CO<sub>2</sub> with a direct current (DC) [9]. A review about the detail regeneration technique can be

found elsewhere [14]. Choosing a suitable regeneration method will mainly depend on the energy demand, operation type and complexity as given in Table 3.3.

Table 3.3 Summary of different regeneration methods [14]

Method	Energy demand	Operation	Complexity
Thermal	High	Offline	Medium
Chemical	Medium	Offline	Medium
Electrothermal	Low	Online	Low
Ultrasonic	Low	Online	Low
Microwaves	Medium	Offline	Low

### 3.3 Carbon membrane module construction

The choice of module design for CMS membranes will typically be the hollow fiber module with counter-current flow. Membrane module construction is, however, seldom referred in open literature as details on this will typically be confidential information for a company producing membrane modules. To date, only tubular and hollow fiber lab-scale modules have been reported for carbon membranes [16, 65, 72]. The potentially industrial use of these membranes were reported by two companies; Carbon Membranes Ltd. (Israel) in the late nineties, and later Blue Membranes GmbH (Germany). Carbon Membranes Ltd. produced hollow fibers on a pilot scale and demonstrated successful separation for various applications, while Blue Membranes developed a new concept based on the honeycomb membrane module configuration (HM) [88] for their carbon membranes. None of these two companies succeeded in taking their CMS membranes all the way to the market. There are, however, new companies which will take advantage of the superior separation properties the CMS membranes have, and will be able to develop them for various applications in the market, as suggested in section 6 below. Saufi S. M. et al. reported that all system designs for module must consider the factors of production cost, maintenance, efficiency [29]. A typical lab-scale module is shown in Fig. 3.12.

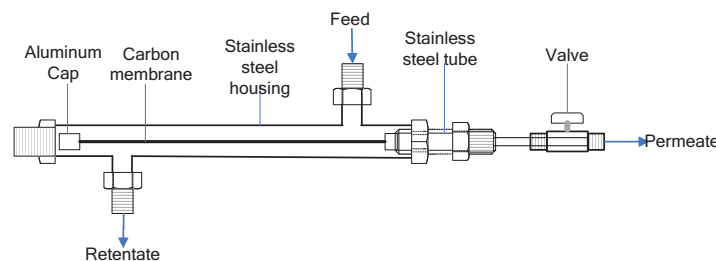


Fig. 3.12 A typical carbon module structure

Although the hollow fiber configuration for module is most commonly used in commercial application [89], their assembly in high packing density modules has also proved to be difficult for the CMS membranes due to the challenge of the relatively brittle fibers. The mechanical strength of the fibers is therefore a main focus for the commercial development of carbon membranes – this can be improved both by choice of a good precursor, and also by developing an optimized carbonization protocol.

### **3.4 Potential industrial applications for CMS membranes**

There are several potential industrial applications for the CMS membranes – some which are close to market, others which may be more future applications. This may be a function of both the volume of the gas streams, and/or challenging process conditions. Closest to market is the upgrading of biogas to vehicle fuel and separation of air by the use of carbon membranes.

#### **3.4.1. Biogas**

Biogas is the gas mixture produced by microbial digestion of organic waste (from households, agriculture, fish industry, waste water treatment...) without the presence of oxygen, also called anaerobic decomposition of organic matter. The biogas consists mainly of CH<sub>4</sub> (50 – 75 %) usually referred to as biomethane, and CO<sub>2</sub>, but will also contain some NH<sub>3</sub> and H<sub>2</sub>S. If produced in a more open landfill, there will also be some N<sub>2</sub> present due to leakage into the system. It is, however, in EU no longer allowed (by 2009) to dispose of organic waste in landfills – handling of the organic waste is strictly regulated. Under controlled conditions the amount of biomethane produced from organic waste can be optimized by using a micro-aerated digester as described by R. Bakke et al. [90] The biomethane is a valuable energy carrier, and the use of this gas gives no net contribution of CO<sub>2</sub> to the atmosphere when burnt. Since CH<sub>4</sub> is a very potent greenhouse gas (around 24 times stronger than CO<sub>2</sub>), an actual reduction in greenhouse gas emissions is achieved when biomethane is burnt.

Biogas is already being utilized in various ways as energy carrier, such as electricity production, being burnt for local heating or combined heat and power generation. By upgrading the biogas to the quality of vehicle fuel and purified natural gas, it may be injected into a natural gas grid or used in the transport sector for cars, buses and trucks. If used for vehicle fuel (ignition engines), the CH<sub>4</sub> content must be minimum 96 %, while it is sufficient with 80-90 % CH<sub>4</sub> for so-called dual fuel engines (tractors, machinery) [91]. The upgrading process to high quality biomethane is illustrated in Fig. 3.13 [92]. As illustrated in the flowsheet, H<sub>2</sub>S and water vapor must be removed before it is lead to the membrane for separating out CO<sub>2</sub> from CH<sub>4</sub>. The compression of the gas may vary depending on whether it goes to the gas grid or will be used for vehicle fuel:

Biomethane for vehicle fuel must be compressed to around 200 bar, while the pressure will be less if injected into the gas grid (<80 bar). The dew point of the final gas should be < -80 °C.

There are several technologies available for upgrading of biogas, such as pressure swing adsorption, physical/chemical absorption and cryogenic separation. These technologies have high energy demands and waste issues, and are not economical for gas streams < 200 Nm<sup>3</sup>/h. The upgrading of biogas using CMS-membranes has, however, been found to be especially favorable for gas streams for these smaller to medium gas streams, and the company MemfoACT [93] is currently starting up production of carbon membrane modules for production of high purity biomethane for a steadily increasing market within the transport sector.

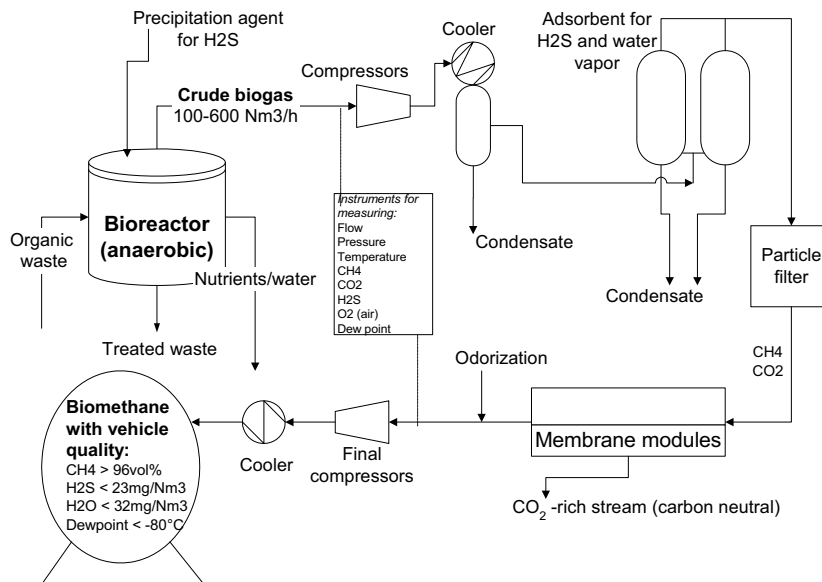


Fig. 3.13 A typical biogas upgrading process [92]

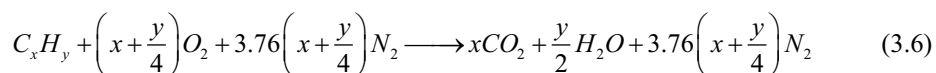
### 3.4.2. Natural gas

The purification of natural gas by removal of CO<sub>2</sub> (natural gas sweetening) is in principle the same separation process as for upgrading of biogas, however, at a much higher feed pressure which is also very favorable for the process. Depending on where in the world the gas production field is found, the pressure, temperature and composition will vary to a large extent. The content of CO<sub>2</sub> is typically very low in the North Sea gas fields (< 5 %), while in other places in the world like the Far East and the

Mexican Gulf, it can be very high (> 40 %). As the driving force for the separation of gases when using a membrane typically is depending on a high partial pressure difference over the membrane, it is usually favorable with a high CO<sub>2</sub> content combined with the high feed pressure of the natural gas (often up to 100 bar). The selectivity for CO<sub>2</sub> / CH<sub>4</sub> measured with hollow fiber carbon membranes prepared from cellulosic precursors, was found to be > 100, and with a CO<sub>2</sub>-permeability around 100 Barrer [18]. For the natural gas, water needs to be removed to avoid formation of hydrates during pipeline transport, and since the CMS-membranes may be sensitive to high contents of water in the gas stream, it is also favorable for the membranes that the gas is being dried. The main challenge for using CMS-membranes in this application will most likely be the price for the membranes since there is usually large gas volumes involved. However, with the very good separation performance these membranes have, a membrane process would potentially be very compact and have a small footprint.

### 3.4.3. Flue gas

In a fossil fuel power plant, the chemical energy stored in coal, fuel oil, natural gas or oil shale is converted successively into thermal energy, mechanical energy and, finally, electrical energy for continuous use and distribution. The complete combustion of fossil fuel using air as the oxygen source is summarized in the following chemical reaction:



The combustion of the hydrocarbon fossil fuels will generate water vapor, carbon dioxide and the non-reactive N<sub>2</sub> when burned. Some byproducts for combustion are sulfur dioxide (predominantly in coal) and oxides of nitrogen. If the combustion is non-complete, the residual O<sub>2</sub> will also be present in the flue gases. Different approaches such as physical absorption (Selexol) and chemical absorption (MEA, DMEA, ammonia) and membrane technology can potentially be used to capture CO<sub>2</sub> from flue gas in post-combustion process. The MEA technology has been widely used in natural gas for over 60 years and produce relatively high purity CO<sub>2</sub> stream. However, if used for CO<sub>2</sub> capture in flue gas, it will be very costly and the challenges will be different from those related to natural gas application. The National Energy Technology Laboratory (NETL) estimates that this method will increase the cost of electricity production by 70% [94]. Some literature reported that an alternative way to use the membrane technology for CO<sub>2</sub> capture in power plant [10, 95-97]. He et. al investigated the application of the hollow fiber carbon membrane for CO<sub>2</sub> capture from flue gas [10]. They reported that the capital cost using the carbon membranes was 197 \$/tonne CO<sub>2</sub> avoided, which is still higher than the traditional chemical method like MEA (59 \$/tonne CO<sub>2</sub> avoided

reported by Rao and Rubin [98]), but the referred carbon membranes had a clear potential of further optimization. In any case, the environmentally friendly technique with further improved membrane performance could promote the hollow fiber carbon membranes as a promising candidate for CO<sub>2</sub> capture in future.

#### 3.4.4. Air separation

Nitrogen production. The feed air is normally compressed to 8-10 bar with a low cost screw compressor and then passed through a bore side hollow-fiber module. In a membrane nitrogen-from-air plant, approximately two-thirds of the total plant cost is associated with the air compressors; 20% or less is associated with the membrane modules, which indicates that reducing the size of the feed gas compressor will significantly decrease the cost for nitrogen production. Baker suggested that the compressor size can be reduced by 20% if the membrane performance for O<sub>2</sub>/N<sub>2</sub> selectivity is improved from 8 to 12 [99]. This might cut nitrogen production costs by 10-15%. From Robeson upper bound (Fig. 3.14) indicated that the O<sub>2</sub>/N<sub>2</sub> selectivity for most of polymeric membranes is below 8 with relative high permeability high than 1 Barrer, which is the commercial interesting area. An alternative way for O<sub>2</sub>/N<sub>2</sub> separation by carbon molecular sieve membranes have been investigated, and Fig. 3.14 gives some representative results [17].

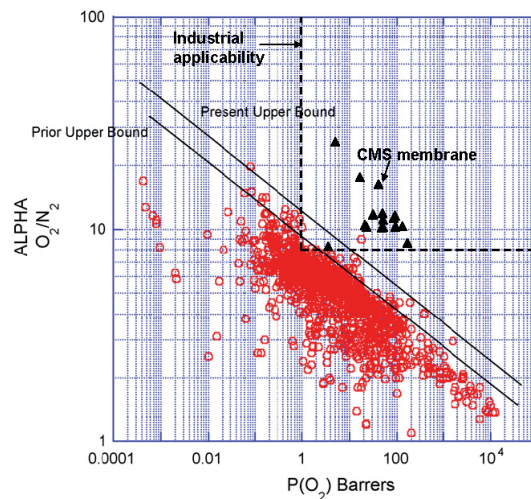


Fig. 3.14 Comparing the O<sub>2</sub>/N<sub>2</sub> Robeson upper bound for dense polymer membranes [17] to the carbon membranes (C(PPO) [7]; C(PPESK) [6]; C(Kapton) [100]; C(Cellulose) [19]; C(Co-polyimide) [37] and C(Cellulose acetate) [18]), and the region for industrial applicability was suggested by [6]. (Data for CMS membranes and industrial applicability region added to the original Robeson plot)

*Oxygen production*, unlike nitrogen production, producing oxygen is more difficult since a certain amount of nitrogen will always permeate together with the oxygen, resulting in oxygen enriched air rather than pure oxygen. This can be easily understood because of the relatively low content of O<sub>2</sub> in air (21%) which will in any process result in a relatively low driving force over the membrane. The pressure differential across the membrane can be evaluated either by pulling a vacuum on the permeation side or using a compressor on the feed side. For the second option, all of the feed air must be compressed, while only a small portion permeates through the membrane as oxygen-enriched product. The energy consumption for a vacuum pump on the permeate side is about one-half that of a feed compressor, because the only gas that needs to pass through the pump is the oxygen-enriched product. However, it should be noted that vacuum operation requires a larger membrane area to produce the same flow of product gas. To make this operating mode economical, high-flux membranes and low-cost membrane modules are required.

#### 3.4.5. Petrochemical industry

At petrochemical plants there are numerous gas streams that contain valuable components which need to be recovered and reused. These are typically non-reacted monomers, by-products from reactors, inerts, solvents and carrier gas. There is a nice potential for using CMS membranes for many of these applications, and thereby also save money if complicated systems with columns, refrigeration and compressors can be avoided. A study on separation of alkanes – alkenes was performed by Hägg et al [101]. Their systems were the separation of propane – propene and propane – ethene. As the alkanes – alkenes are chemically and physically quite similar compounds with almost identical critical properties, they must be separated on the basis of their molecular size. The Lennard-Jones diameter is 4.7 Å and 5.1 Å for propene and propane respectively, hence a carefully tailored CMS-membrane would be able to separate these two components according to the molecular sieving mechanism. A selectivity of 23 for this gas pair was documented at 30°C, and even much higher selectivity at 50°C – this is believed to be a result of a transition of separation mechanisms for propane: at lower temperature propane will permeate faster according to the SSF mechanism, while at higher temperature, it will no longer sorb on the wall, and permeance goes down, selectivity goes up. As the hydrocarbons will more easily clog the membrane at low temperature, it is favorable to run this separation at higher temperature, and possibly regenerate the membrane on-line (see chapter on regeneration).

### 3.4.6. High-temperature applications

Although the dense metal membranes (Pd, Ag, including their alloys) or solid electrolytes can be used for high temperature application such as hydrogen/hydrocarbon/CO<sub>2</sub> separation, they are still found to be too expensive for commercial applications, although they will show high selectivity but low permeability [102]. In a search for a highly selective and relatively inexpensive membrane, the carbon membrane may be a candidate for use in membrane reactors for the hydrogen separation together with equilibrium-limited reaction. The potential interesting applications include hydrocarbon dehydrogenation and steam methane reforming (SMR) for H<sub>2</sub> production. A schematic diagram of the carbon membrane reactor is shown in Fig. 3.15. The reactant is fed into the system from the shell side of the carbon membranes. The driving force for the transport through the carbon membranes can be achieved by compression of the feed stream or using sweep gas or vacuum on permeate side. The membrane reactor can be heated to high working temperature for the application, while there is a cooler in each module end to protect the overheating of the carbon membrane sealing. The sealing of the module at high temperatures is typically not yet solved, so the temperature should be < 150 °C at the ends.

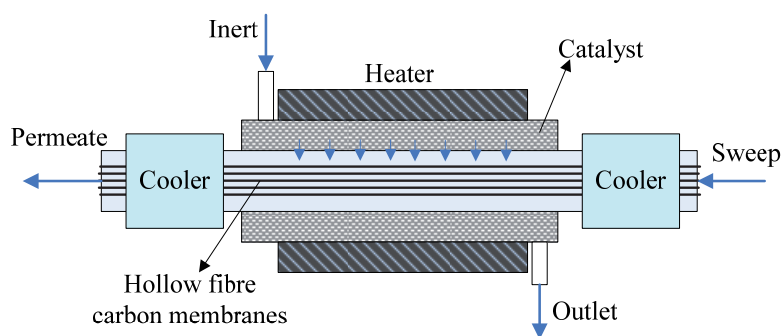


Fig. 3.15 Schematic diagram of hollow fiber carbon membrane reactor

Dehydrogenation. The application of carbon membrane reactors for the dehydrogenation of cyclohexane into benzene was investigated by Itoh and Haraya [64]. They found a higher conversion for the carbon membrane reactor comparing to the normal reactor, which was caused by the chemical reaction shifting to the product side due to the preferential permeation of H<sub>2</sub>. Szejner and Sheintuch studied the dehydrogenation of isobutane to isobutene in a membrane reactor equipped with the carbon membranes. The conversion achieved in the counter-current flow operation

method was achieved a maximum of 85% at 500°C, which is much higher than in the corresponding PFR [103].

*Steam methane reforming.* The steam methane reforming (SMR) technology is the major route to industry's production of merchant H<sub>2</sub> on a worldwide scale. This is a very endothermic reaction (Eq. 10) that operates at 800 °C and at 20 bar pressure in order to achieve near equilibrium conversions and to meet the customers need for high pressure H<sub>2</sub>.



By using a membrane reactor, it can shift the reaction to produce more H<sub>2</sub> at lower operating temperatures. Some literature reported to use the Pd and ceramic membrane reactor for steam methane reforming to H<sub>2</sub> production [104-106]. The results showed that both the overall CH<sub>4</sub> conversion and the conversion to CO, indicative of the extent of the water-gas shift reaction, exceed the thermodynamic equilibrium values. It appear to be greater opportunity for application of membrane reactors with regard to SMR, but some challenges still remain due to the higher cost for membranes based on the process economic analysis [107]. Although the application of the carbon membrane reactor in the steam methane reforming process has not been investigated, a carbon membrane reactor used for methanol steam reforming reaction to generate a product with high-purity H<sub>2</sub> was reported by Zhang et. al [108]. Their results showed that the carbon membrane reactor (CMR) provided a higher methanol conversion than the fixed bed reactor (FBR) at all investigated operating conditions, while the overall yields of hydrogen in the CMR and FBR are identical. However, a CO-free hydrogen stream can be produced with the CMR, which could be directly used in a proton-exchange membrane fuel cell. Therefore, the carbon membranes reactor can also become a promising candidate for the application in high temperature methane steam reforming reaction.

### 3.5 References

- [1] Koresh JE, Soffer A. Molecular sieve carbon membrane Part I: Presentation of a new device for gas mixture separation. *Separ Sci Technol.* 1983;18:723-34.
- [2] Suda H, Haraya K. Gas Permeation through Micropores of Carbon Molecular Sieve Membranes Derived from Kapton Polyimide. *J Phys Chem B.* 1997;101(20):3988-94.
- [3] Steel KM, Koros WJ. Investigation of porosity of carbon materials and related effects on gas separation properties. *Carbon.* 2003;41(2):253-66.
- [4] Barsema JN, van der Vegt NFA, Koops GH, Wessling M. Ag-Functionalized Carbon Molecular-Sieve Membranes Based on Polyelectrolyte/Polyimide Blend Precursors. *Adv Funct Mater.* 2005;15(1):69-75.
- [5] David LIB, Ismail AF. Influence of the thermastabilization process and soak time during pyrolysis process on the polyacrylonitrile carbon membranes for O<sub>2</sub>/N<sub>2</sub> separation. *J Membr Sci.* 2003;213(1-2):285-91.
- [6] Zhang B, Wang T, Zhang S, Qiu J, Jian X. Preparation and characterization of carbon membranes made from poly(phthalazinone ether sulfone ketone). *Carbon.* 2006;44(13):2764-9.
- [7] Yoshimune M, Fujiwara I, Haraya K. Carbon molecular sieve membranes derived from trimethylsilyl substituted poly(phenylene oxide) for gas separation. *Carbon.* 2007;45(3):553-60.
- [8] Lee H-J, Suda H, Haraya K, Moon S-H. Gas permeation properties of carbon molecular sieving membranes derived from the polymer blend of polyphenylene oxide (PPO)/polyvinylpyrrolidone (PVP). *J Membr Sci.* 2007;296(1-2):139-46.
- [9] Lie JA, Hagg M-B. Carbon membranes from cellulose: Synthesis, performance and regeneration. *J Membr Sci.* 2006;284(1-2):79-86.
- [10] He X, Lie JA, Sheridan E, Hägg M-B. CO<sub>2</sub> capture by hollow fibre carbon membranes: Experiments and process simulations. *Energy Procedia.* 2009;1(1):261-8.
- [11] Barsema JN. Carbon membranes precursor, preparation and functionalization [PhD]. Enschede: University of Twente; 2007.
- [12] Barsema JN, van der Vegt NFA, Koops GH, Wessling M. Carbon molecular sieve membranes prepared from porous fiber precursor. *J Membr Sci.* 2002;205(1-2):239-46.
- [13] Favvas EP, Kapantaidakis GC, Nolan JW, Mitropoulos AC, Kanellopoulos NK. Preparation, characterization and gas permeation properties of carbon hollow fiber membranes based on Matrimid(R) 5218 precursor. *J Mater Process Tech.* 2007;186(1-3):102-10.

- [14] Lie JA. Synthesis, performance and regeneration of carbon membranes for biogas upgrading-a future energy carrier [PhD]. Trondheim: Norwegian University of Science and technology; 2005:152.
- [15] Tin PS, Chung T-S, Liu Y, Wang R. Separation of CO<sub>2</sub>/CH<sub>4</sub> through carbon molecular sieve membranes derived from P84 polyimide. *Carbon*. 2004;42(15):3123-31.
- [16] Vu DQ, Koros WJ, Miller SJ. High Pressure CO<sub>2</sub>/CH<sub>4</sub> Separation Using Carbon Molecular Sieve Hollow Fiber Membranes. *Ind Eng Chem Res*. 2002;41(3):367-80.
- [17] Robeson LM. The upper bound revisited. *J Membr Sci*. 2008;320(1-2):390-400.
- [18] He X, Lie JA, Sheridan E, Hägg M-B. Preparation and Characterization of Hollow Fiber Carbon Membranes based on a Cellulosic Precursor. *Conf. on ICOM 2008*. Honolulu, Hawaii USA 2008.
- [19] Lie JA, Hagg M-B. Carbon membranes from cellulose and metal loaded cellulose. *Carbon*. 2005;43(12):2600-7.
- [20] Park HB, Lee YM. Fabrication and Characterization of Nanoporous Carbon/Silica Membranes. *Adv Mater*. 2005;17(4):477-83.
- [21] Hillock AMW, Miller SJ, Koros WJ. Crosslinked mixed matrix membranes for the purification of natural gas: Effects of sieve surface modification. *J Membr Sci*. 2008;314(1-2):193-9.
- [22] Fuertes AB, Centeno TA. Preparation of supported asymmetric carbon molecular sieve membranes. *J Membr Sci*. 1998;144(1-2):105-11.
- [23] Ismail AF, David LIB. A review on the latest development of carbon membranes for gas separation. *J Membr Sci*. 2001;193(1):1-18.
- [24] Shiflett MB, Foley HC. On the preparation of supported nanoporous carbon membranes. *J Membr Sci*. 2000;179(1-2):275-82.
- [25] Hayashi J-i, Mizuta H, Yamamoto M, Kusakabe K, Morooka S. Pore size control of carbonized BPDA-pp' ODA polyimide membrane by chemical vapor deposition of carbon. *J Membr Sci*. 1997;124(2):243-51.
- [26] Wang H, Zhang L, Gavalas GR. Preparation of supported carbon membranes from furfuryl alcohol by vapor deposition polymerization. *J Membr Sci*. 2000;177(1-2):25-31.
- [27] Fuertes AB, Centeno TA. Carbon molecular sieve membranes from polyetherimide. *Micropor Mesopor Mat*. 1998;26(1-3):23-6.
- [28] Acharya M, Foley HC. Spray-coating of nanoporous carbon membranes for air separation. *J Membr Sci*. 1999;161(1-2):1-5.

- [29] Saufi SM, Ismail AF. Fabrication of carbon membranes for gas separation--a review. *Carbon*. 2004;42(2):241-59.
- [30] Park HB, Kim YK, Lee JM, Lee SY, Lee YM. Relationship between chemical structure of aromatic polyimides and gas permeation properties of their carbon molecular sieve membranes. *J Membr Sci*. 2004;229(1-2):117-27.
- [31] Xiao Y, Chung TS, Chng ML, Tamai S, Yamaguchi A. Structure and Properties Relationships for Aromatic Polyimides and Their Derived Carbon Membranes: Experimental and Simulation Approaches. *J Phys Chem B*. 2005;109(40):18741-8.
- [32] Lee H-J, Suda H, Haraya K. Preparation of Carbon Membranes Derived from Polymer Blends in the Presence of a Thermally Labile Polymer. *Separ Sci Technol*. 2007;42(1):59 - 71.
- [33] Kim YK, Park HB, Lee YM. Carbon molecular sieve membranes derived from thermally labile polymer containing blend polymers and their gas separation properties. *J Membr Sci*. 2004;243(1-2):9-17.
- [34] Yoshimune M, Fujiwara I, Suda H, Haraya K. Gas transport properties of carbon molecular sieve membranes derived from metal containing sulfonated poly(phenylene oxide). *Desalination*. 2006;193(1-3):66-72.
- [35] Kim YK, Park HB, Lee YM. Carbon molecular sieve membranes derived from metal-substituted sulfonated polyimide and their gas separation properties. *Journal of Membrane Science*. 2003;226(1-2):145-58.
- [36] Silverstein MS, Najary Y, Lumelsky Y, von Lampe I, Grader GS, Shter GE. Complex formation and degradation in poly(acrylonitrile-co-vinyl acetate) containing metal nitrates. *Polymer*. 2004;45(3):937-47.
- [37] Barsema JN, Balster J, Jordan V, van der Vegt NFA, Wessling M. Functionalized Carbon Molecular Sieve membranes containing Ag-nanoclusters. *Journal of Membrane Science*. 2003;219(1-2):47-57.
- [38] Zhang L, Chen X, Zeng C, Xu N. Preparation and gas separation of nano-sized nickel particle-filled carbon membranes. *J Membr Sci*. 2006;281(1-2):429-34.
- [39] Yoda S, Hasegawa A, Suda H, Uchimar Y, Haraya K, Tsuji T, et al. Preparation of a Platinum and Palladium/Polyimide Nanocomposite Film as a Precursor of Metal-Doped Carbon Molecular Sieve Membrane via Supercritical Impregnation. *Chem Mater*. 2004;16(12):2363-8.
- [40] Suda H, Yoda S, Hasegawa A, Tsuji T, Otake K, Haraya K. Gas permeation properties of carbon molecular sieve membranes dispersed with palladium nano particles via supercritical CO<sub>2</sub> impregnation. *Desalination*. 2006;193(1-3):211-4.

- [41] Park HB, Suh IY, Lee YM. Novel Pyrolytic Carbon Membranes Containing Silica: Preparation and Characterization. *Chem Mater.* 2002;14(7):3034-46.
- [42] Jiang LY, Chung TS, Cao C, Huang Z, Kulprathipanja S. Fundamental understanding of nano-sized zeolite distribution in the formation of the mixed matrix single- and dual-layer asymmetric hollow fiber membranes. *J Membr Sci.* 2005;252(1-2):89-100.
- [43] Liu Q, Wang T, Liang C, Zhang B, Liu S, Cao Y, et al. Zeolite Married to Carbon: A New Family of Membrane Materials with Excellent Gas Separation Performance. *Chem Mater.* 2006;18(26):6283-8.
- [44] Zhou C, Liu T, Wang T, Kumar S. PAN/SAN/SWNT ternary composite: Pore size control and electrochemical supercapacitor behavior. *Polymer.* 2006;47(16):5831-7.
- [45] Kim S, Pechar TW, Marand E. Poly(imide siloxane) and carbon nanotube mixed matrix membranes for gas separation. *Desalination.* 2006;192(1-3):330-9.
- [46] Banerjee S, Murad S, Puri IK. Preferential ion and water intake using charged carbon nanotubes. *Chemical Physics Letters.* 2007;434(4-6):292-6.
- [47] Shao L, Chung T-S, Wensley G, Goh SH, Pramoda KP. Casting solvent effects on morphologies, gas transport properties of a novel 6FDA/PMDA-TMMDA copolyimide membrane and its derived carbon membranes. *J Membr Sci.* 2004;244(1-2):77-87.
- [48] He X, Hägg M-B. Using orthogonal experimental design for spinning defect-free hollow fiber membranes. *Advanced Membrane Technology IV: Membranes for Clean and Sustainable Processes.* Trondheim 2009.
- [49] Yoneyama H, Nishihara Y. Porous hollow carbon fiber film and method of manufacturing the same. EP patent 0394449. 1990.
- [50] Schindler E, Maier F. Manufacture of porous carbon membranes. US patent 4919860. 1990.
- [51] Tin PS, Chung T-S, Kawi S, Guiver MD. Novel approaches to fabricate carbon molecular sieve membranes based on chemical modified and solvent treated polyimides. *Microporous and Mesoporous Materials.* 2004;73(3):151-60.
- [52] Lua AC, Su J. Effects of carbonisation on pore evolution and gas permeation properties of carbon membranes from Kapton® polyimide. *Carbon.* 2006;44(14):2964-72.
- [53] Wallace DW, Staudt-Bickel C, Koros WJ. Efficient development of effective hollow fiber membranes for gas separations from novel polymers. *J Membr Sci.* 2006;278(1-2):92-104.

- [54] Su J, Lua AC. Influence of carbonisation parameters on the transport properties of carbon membranes by statistical analysis. *J Membr Sci.* 2006;278(1-2):335-43.
- [55] Wang K, Loo LS, Haraya K. CO<sub>2</sub> Permeation in Carbon Membranes with Different Degrees of Carbonization. *Ind Eng Chem Res.* 2007;46(4):1402-7.
- [56] Geiszler VC, Koros WJ. Effects of Polyimide Pyrolysis Conditions on Carbon Molecular Sieve Membrane Properties. *Ind Eng Chem Res.* 1996;35(9):2999-3003.
- [57] Linkov VM, Sanderson RD, Jacobs EP. Highly asymmetrical carbon membranes. *J Membr Sci.* 1994;95(1):93-9.
- [58] Linkov VM, Sanderson RD, Jacobs EP. Carbon membranes from precursors containing low-carbon residual polymers. *Polym Int.* 1994;35(3):239-42.
- [59] Soffer A, Koresh J, Saggy S. Separation device. US patent 4685940. 1987.
- [60] Hagg M-B. Membrane purification of Cl<sub>2</sub> gas: II. Permeabilities as function of temperature for Cl<sub>2</sub>, O<sub>2</sub>, N<sub>2</sub>, H<sub>2</sub> and HCl in perfluorinated, glass and carbon molecular sieve membranes. *J Membr Sci.* 2000;177(1-2):109-28.
- [61] Soffer A, Gilron J, Suguee S, Hed-Ofek R, Cohen H. Process for the production of hollow carbon fiber membranes. EP Patent 0671202. 1995.
- [62] Jones CW, Koros WJ. Carbon molecular sieve gas separation membranes-I. Preparation and characterization based on polyimide precursors. *Carbon.* 1994;32(8):1419-25.
- [63] Jones CW, Koros WJ. Characterization of ultramicroporous carbon membranes with humidified feeds. *Ind Eng Chem Res* 1995;34:158-63.
- [64] Itoh N, Haraya K. A carbon membrane reactor. *Catal Today.* 2000;56(1-3):103-11.
- [65] Kusuki Y, Shimazaki H, Tanihara N, Nakanishi S, Yoshinaga T. Gas permeation properties and characterization of asymmetric carbon membranes prepared by pyrolyzing asymmetric polyimide hollow fiber membrane. *J Membr Sci.* 1997;134(2):245-353.
- [66] Yoshinaga T, Shimazaki H, Kusuki Y, Sumiyama Y. Asymmetric hollow filamentary carbon membrane and process for producing the same. EP patent 0459623. 1991.
- [67] Ogawa M, Nakano Y. Gas permeation through carbonized hollow fiber membranes prepared by gel modification of polyamic acid. *J Membr Sci.* 1999;162(1-2):189-98.
- [68] Ogawa M, Nakano Y. Separation of CO<sub>2</sub>/CH<sub>4</sub> mixture through carbonized membrane prepared by gel modification. *J Membr Sci.* 2000;173(1):123-32.

- [69] Okamoto K, Kawamura S, Yoshino M, Kita H, Hirayama Y, Tanihara N, et al. Olefin/Paraffin Separation through Carbonized Membranes Derived from an Asymmetric Polyimide Hollow Fiber Membrane. *Ind Eng Chem Res.* 1999;38(11):4424-32.
- [70] Kim YK, Park HB, Lee YM. Gas separation properties of carbon molecular sieve membranes derived from polyimide/polyvinylpyrrolidone blends: effect of the molecular weight of polyvinylpyrrolidone. *J Membr Sci.* 2005;251(1-2):159-67.
- [71] Jiang LY, Chung T-S, Rajagopalan R. Dual-layer hollow carbon fiber membranes for gas separation consisting of carbon and mixed matrix layers. *Carbon.* 2007;45(1):166-72.
- [72] Lagorsse S, Magalhães FD, Mendes A. Carbon molecular sieve membranes: Sorption, kinetic and structural characterization. *J Membr Sci.* 2004;241(2):275-87.
- [73] Liang C, Sha G, Guo S. Carbon membrane for gas separation derived from coal tar pitch. *Carbon.* 1999;37(9):1391-7.
- [74] Koros WJ, Jones CW. Composite carbon fluid membranes. US patent 5288304. 1994.
- [75] Soffer A, Azariah A, Amar A, Cohem H, Golub D, Saguee S. Method of improving the selectivity of carbon membranes by chemical vapor deposition. US patent 5695818. 1997.
- [76] Dreisbach F, H. RSA, Lösch HW. Gravimetric Measurement of Adsorption Equilibria of Gas Mixture CO/H<sub>2</sub> with a Magnetic Suspension Balance. *Chem Eng Technol.* 2002;25(11):1060-5.
- [77] Belmabkhout Y, Serna-Guerrero R, Sayari A. Adsorption of CO<sub>2</sub> from dry gases on MCM-41 silica at ambient temperature and high pressure. 1: Pure CO<sub>2</sub> adsorption. *Chem Eng Sci.* 2009;64(17):3721-8.
- [78] Lagorsse S, Campo MC, Magalhaes FD, Mendes A. Water adsorption on carbon molecular sieve membranes: Experimental data and isotherm model. *Carbon.* 2005;43(13):2769-79.
- [79] Cazorla-Amoros D, Alcaniz-Monge J, Linares-Solano A. Characterization of Activated Carbon Fibers by CO<sub>2</sub> Adsorption. *Langmuir.* 1996;12(11):2820-4.
- [80] Nguyen C, Do DD. Adsorption of Supercritical Gases in Porous Media: Determination of Micropore Size Distribution. *J Phys Chem B.* 1999;103(33):6900-8.

- [81] Nguyen C, Do DD, Haraya K, Wang K. The structural characterization of carbon molecular sieve membrane (CMSM) via gas adsorption. *J Membr Sci.* 2003;220(1-2):177-82.
- [82] He X, Hägg M-B. Preparation and Characterization of High Performance Hollow Fiber Carbon Membranes - Discussion of Results and Potential Applications *Conf. on Euromembrane 2009* Montpellier, France 2009.
- [83] Jones CW, Koros WJ. Characterization of Ultramicroporous Carbon Membranes with Humidified Feeds. *Ind Eng Chem Res.* 1995;34(1):158-63.
- [84] Lagorsse S, Magalhaes FD, Mendes A. Aging study of carbon molecular sieve membranes. *J Membr Sci.* 2008;310(1-2):494-502.
- [85] Abu-Zahra MRM, Niederer JPM, Feron PHM, Versteeg GF. CO<sub>2</sub> capture from power plants: Part II. A parametric study of the economical performance based on mono-ethanolamine. *IJGGC.* 2007;1(2):135-42.
- [86] Menendez I, Fuertes AB. Aging of carbon membranes under different environments. *Carbon.* 2001;39(5):733-40.
- [87] Jones CW, Koros WJ. Carbon molecular sieve gas separation membranes-II. Regeneration following organic exposure. *Carbon.* 1994;32(8):1427-32.
- [88] Lagorsse S, Leite A, Magalhaes FD, Bischofberger N, Rathenow J, Mendes A. Novel carbon molecular sieve honeycomb membrane module: configuration and membrane characterization. *Carbon.* 2005;43(4):809-19.
- [89] Petersen J, Matsuda M, Haraya K. Capillary carbon molecular sieve membranes derived from Kapton for high temperature gas separation. *J Membr Sci.* 1997;131(1-2):85-94.
- [90] Rathasiri PG, Botheju D, Bakke R. Effects of biofilm formation on oxygen transfer membranes in membrane micro-aerated anaerobic digesters. *Proceedings of the Final MBR-Network Workshop; March/April 2009* Berlin Germany; March/April 2009
- [91] CNG-Power. [cited 2010 September 25]; Available from: <http://www.lupower.at/index.php/CNG-Power>
- [92] Hägg M-B, Lie JA. Upgrading of biogas by membranes for vehicle fuel or injection into the European Gas Network. *ECI Conferences.* Tomar, Portugal 2006.
- [93] Membranes for advanced clean technologies. [cited 2010 November]; Available from: <http://www.memfoact.no/>
- [94] Elwell LC, Grant WS. Technology options for capturing CO<sub>2</sub>. [cited 2010 September 25]; Available from: [http://www.powermag.com/coal/Technology-options-for-capturing-CO2\\_582.html](http://www.powermag.com/coal/Technology-options-for-capturing-CO2_582.html)

- [95] Bredeesen R, Jordal K, Bolland O. High-temperature membranes in power generation with CO<sub>2</sub> capture. *Chem Eng Process*. 2004;43(9):1129-58.
- [96] Hagg MB, Lindbrathen A. CO<sub>2</sub> Capture from Natural Gas Fired Power Plants by Using Membrane Technology. *Ind Eng Chem Res*. 2005;44(20):7668-75.
- [97] Hussain A, Hägg M-B. A feasibility study of CO<sub>2</sub> capture from flue gas by a facilitated transport membrane. *J Membr Sci*. 2010;359(1-2):140-8.
- [98] Rao AB, Rubin ES. A Technical, Economic, and Environmental Assessment of Amine-Based CO<sub>2</sub> Capture Technology for Power Plant Greenhouse Gas Control. *Environ Sci Technol*. 2002;36(20):4467/75.
- [99] Baker RW. Future Directions of Membrane Gas Separation Technology. *Ind Eng Chem Res*. 2002;41(6):1393-411.
- [100] Lua AC, Su J. Effects of carbonisation on pore evolution and gas permeation properties of carbon membranes from Kapton?polyimide. *Carbon*. 2006;44(14):2964-72.
- [101] Hagg M-B, Lie JA, Lindbrathen A. Carbon Molecular Sieve Membranes. A Promising Alternative for Selected Industrial Applications. *Ann Ny Acad Sci*. 2003;984(1):329-45.
- [102] Szejner GA, Efremenko I, Sheintuch M. Carbon membranes for high temperature gas separations: Experiment and theory. *AIChE J*. 2004;50(3):596-610.
- [103] Szejner G, Sheintuch M. Application of a carbon membrane reactor for dehydrogenation reactions. *Chem Eng Sci*. 2004;59(10):2013-21.
- [104] Kikuchi E, Uemiya S, Matsuda T. Hydrogen Production from Methane Steam Reforming Assisted by Use of Membrane Reactor. In: A. Holmen KJJ, Kolboe S, eds. *Studies In Surface Science And Catalysis*: Elsevier 1991:509-15.
- [105] Kikuchi E. Palladium/ceramic membranes for selective hydrogen permeation and their application to membrane reactor. *Catal Today*. 1995;25(3-4):333-7.
- [106] Chen Z, Grace JR, Jim Lim C, Li A. Experimental studies of pure hydrogen production in a commercialized fluidized-bed membrane reactor with SMR and ATR catalysts. *Int J Hydrogen Energ*. 2007;32(13):2359-66.
- [107] Armor JN. Applications of catalytic inorganic membrane reactors to refinery products. *J Membr Sci*. 1998;147(2):217-33.
- [108] Zhang X, Hu H, Zhu Y, Zhu S. Methanol Steam Reforming to Hydrogen in a Carbon Membrane Reactor System. *Ind Eng Chem Res*. 2006;45(24):7997-8001.

## 4 Experimental equipments, procedures and membrane preparation

This chapter describes the experimental materials and equipments. Different techniques used the characterization of the membranes introduced. A brief description for the orthogonal experimental design method and the module construction is also included.

### 4.1 Materials

#### 4.1.1. Membrane materials

- Cellulose acetate (CA, MW 100,000) with an average acetyl content of 39.8% was purchased from the ACROS (USA)
- Polyvinylpyrrolidone (PVP, K10) was supplied by Sigma
- N-methyl-2-pyrrolidone (NMP, >99.5%) was purchased from Merck (Darmstadt, Germany)
- Glycerol (>98%) was purchased from BDH / VWR used for solvent exchange
- NaOH (>99%) used for deacetylation was also supplied from Merck
- Ethanol (96%) provided by Department of Chemical Engineering, NTNU

All materials were used for experiments without further treatment.

#### 4.1.2. Gases

- Single gas

CO<sub>2</sub> (99.999%), O<sub>2</sub> (99.999%), N<sub>2</sub> (99.999%), H<sub>2</sub> (99.999%), CH<sub>4</sub> (99.995%) and helium (99.996%) supplied from AGA and YARA.

- Mixed gas

10%CO<sub>2</sub>-90%N<sub>2</sub>, 15%CO<sub>2</sub>-4%O<sub>2</sub>-81%N<sub>2</sub> and 35%CO<sub>2</sub>-65%CH<sub>4</sub> are supplied from AGA and YARA.

### 4.2 Equipments and methods

#### 4.2.1. Dope solution formation

The dope solution consists of CA/PVP/NMP (22.5% / 5% / 72.5%). The solvent, NMP and the additive, PVP K10, were well mixed by mechanical stirring. The polymer CA was then added gradually into the mixture. The mixture was stirred for 24 h to ensure a homogeneous dope solution. The ultrasonic oscillator was further employed to remove the air bubbles from the dope solution.

#### 4.2.2. Spinning

The hollow fiber membranes were spun using the well-known dry-wet spinning method [1-2]. The dope solution and bore fluid were fed into the spinneret by gearwheel pumps. A schematic diagram for spinning is shown in Fig. 4.1. The extrusion rate for dope and bore fluid were controlled by two gear pumps respectively. Two types of double spinnerets (A53: ID/OD, 0.5/0.7 mm and A54: ID/OD, 0.1/0.2 mm, shown in Fig. 4.2) are used for spinning, and aims to fabricate the even, defect-free hollow fiber membranes by controlling the spinning conditions of dope flow rate, air gap, bore fluid composition, flow rate of bore fluid and temperature of quench bath. The orthogonal experiment design (OED) method was employed to optimize the spinning process to investigate the influences of these parameters systematically. The factors and levels for OED are given in Table 4.1, and the Statistical Product and Service Solutions (SPSS) software is used to generate the experiment plans and analyze the results.

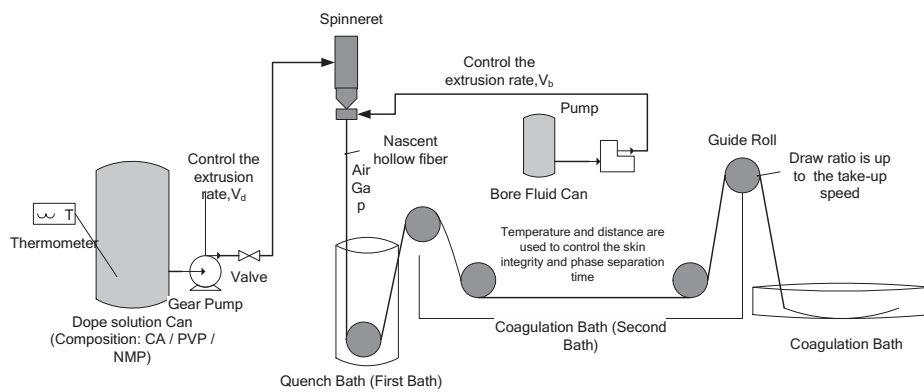


Fig. 4.1 Schematic diagram for spinning process

A double spinneret

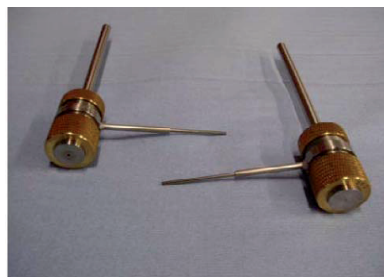
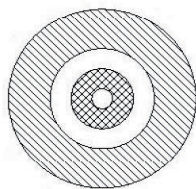


Fig. 4.2 Double spinneret used for spinning of hollow fibers

Table 4.1 Factors and levels for OED of spinning conditions

Level	Bore fluid	Air gap (mm)	Bore flow rate (% of dope flow rate)*	Quench bath temp. (°C)
1	H <sub>2</sub> O	15	20	20
2	H <sub>2</sub> O+NMP (85%)	25	40	50
3		35	60	

\*: dope flow rate 2.2 ml/min with A53 spinneret

#### 4.2.3. Deacetylation

Although some literatures have already reported to prepare the cellulose acetate (CA) fibers [1-6], most of them were mainly used for the dialysis, reverse osmosis (RO) and ultrafiltration (UF). Quite few of the CA hollow fibers were reported to be used as the precursors for preparation of hollow fiber carbon membranes since the CA membranes may form defects or even become dust after carbonization. Therefore, a pretreatment for the CA membranes should be conducted to prepare a suitable precursor for the fabrication of a useful carbon membrane. The alkaline solution such as NaOH and KOH were reported for the deacetylation of cellulose acetate fibers [5-8]. Liu et al. investigated the effects of the reaction time on the deacetylation results [5]. Their results indicated that the deacetylation of CA hollow fibers with NaOH in ethanol solution is much more efficient and complete than that in the aqueous conditions, which producing varying DS (degree of substitution) with no change on the surface, packing, or organization of fibers. Son et al. reported that the deacetylation of CA membranes in KOH ethanol solution (0.5M) after swelling in 25 ml of an acetone-water mixture (V/V 1/1) for 24 h [6]. They concluded that the fibers need to be swelled before the deacetylation. Moreover, they also reported that the deacetylation reaction was very rapid and completed within 20min. The polymer chains could be rearranged with deacetylation, and the crystal structure was converted to that of cellulose. The FTIR was mainly used to characterize the deacetylation results in their studies. Those contributions provide us a valuable clue to investigate the deacetylation of our CA hollow fibers. Therefore, the spun CA hollow fiber membranes were deacetylated by immersion in a certain concentration NaOH ethanol solution for different times at room temperature. The deacetylation reaction of CA with NaOH is shown in eq. 4.1.

The deacetylation was firstly carried out with a 0.2M NaOH in 96% ethanol solution for different reaction time to investigate the complete deacetylation time. The deacetylation was also conducted by immersion in a 0.5M NaOH (50% and 96% ethanol) solution for various reaction times, which was used to investigate the effects of the solution on the deacetylation results. The influences of deacetylation parameters such as NaOH

concentration, solution, deacetylation time, and swelling time on the precursor's properties were systematically investigated on the basis of the orthogonal experimental design (OED) method and statistical analysis. Table 4.2 shows the investigated factors and levels for orthogonal experiment design.

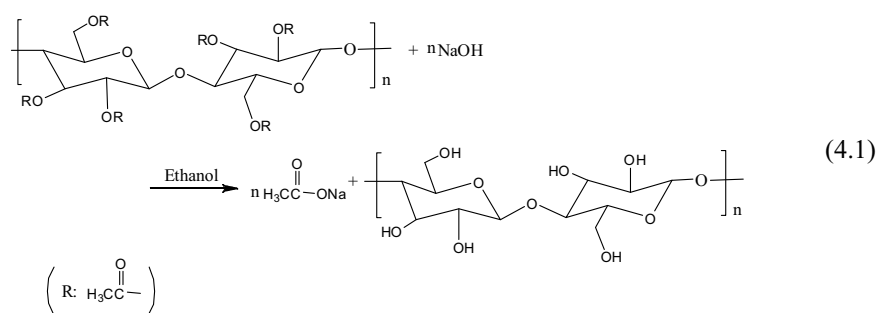


Table 4.2 Factors and levels for OED for the deacetylation conditions

Levels	Swelling time	NaOH concentration	Solution	Reaction time
1	0h	0.05M	96% ethanol	0.5h
2	1h	0.075M	50% ethanol	2h
3	24h	0.1M		4h

#### 4.2.4. Carbonization

The deacetylated precursors were carbonized in a tubular furnace (Carbolite® HZS 12/600E) using a working tube of quartz and a quartz container, which is shown in Fig. 4.3. The flat gasket greased with Molykote® HP-870 was used for sealing between the end of the tube and the steel caps. One end of the tube was connected to a vacuum pump, while the other end of the tube was connected to a mass flow controller. For the carbonization in the environment of CO<sub>2</sub> or N<sub>2</sub> atmosphere, the MKS® mass flow controller up to 500 standard cubic centimeters per minute (SCCM) was used to control the CO<sub>2</sub> or N<sub>2</sub> flow rate. A typical carbonization procedure is summarized as follows:

1. The system is evacuated over 24h to reach a certain vacuum level (e.g. 0.03 mbar);
2. Switch off the vacuum pump, and feed the purge gas of CO<sub>2</sub> or N<sub>2</sub> at a given flow rate (ca. 230 ml/min) for around 1.5 h;
3. Turn on the furnace, and start the carbonization procedure;
4. when carbonization is finished, cool down naturally below to 50 °C
5. Open the furnace and take out the hollow fiber carbon membranes (HFCMs).

The multi-dwell carbonization protocols with various purge gas, heating rate, final temperature and soak time were used as carbonization procedures. An optimal protocol was obtained on the basis of the OED method with respect to the carbon membrane separation performance. The first two dwells are important to remove traces of water and solvent in the precursor as shown in Fig. 4.4. The other dwells are important to rearrange the carbon matrix and form the micropores between the layers of the graphite-like sheets.

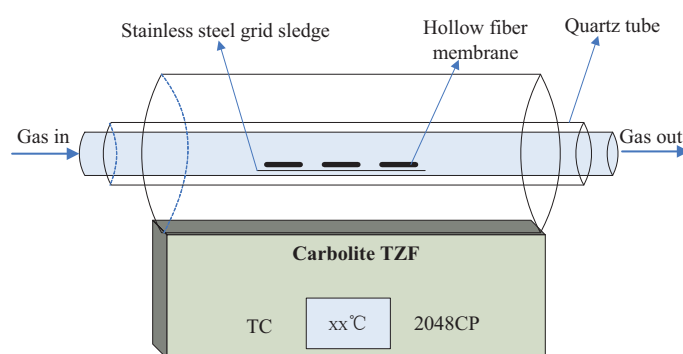


Fig. 4.3 A schematic overview of the furnace set-up

#### 4.2.5. Gas chromatograph (GC)

The gas mixture separation tests were analyzed using an Agilent 6890N gas chromatograph (Agilent Technologies, CA, USA) equipped with a ChemStation software. The gas coming out from the carbon membrane system is sent to the GC by a short 1/16 inch tube. The reason for using small tube is to reduce the time needed for the gas stream transport to the GC and improve the measurement precision. The gas helium and nitrogen (analytical pure) are used as the carrier gas.

#### 4.2.6. Thermogravimetric analysis-Mass spectroscopy (TGA-MS)

Thermogravimetric analyzer (TGA) is usually performed on the samples to determine the amount or rate of weight changes in relation to temperature or time in a controlled atmosphere (He, Air, Ar, or N<sub>2</sub>) at a certain flow rate. Such analysis relies on a high degree of precision in three measurements: weight, temperature, and temperature change, which can determine the composition of the samples and to predict their thermal stability up to a certain temperature (e.g. 1000 °C). Moreover, the TGA can also be employed to determine the drying temperature and time necessary to remove all solvents involved in the samples.

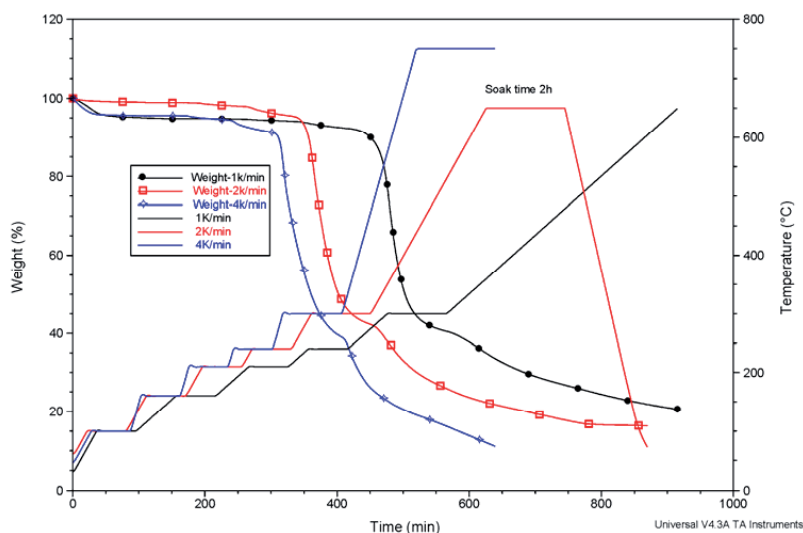


Fig. 4.4 Dependency of weight loss on the various carbonization procedures

In this work, the weight loss during the carbonization process for the precursors was characterized by a TGA Instruments (model Q500, New Castle, USA). Helium is used as the balance gas and purge gas, and the flow rate is controlled at 90 and 10 ml/min, respectively. The data is processed with TA Instruments Universal Analysis 2000 software. A Thermostat<sup>TM</sup> gas analysis system (Pfeiffer Vacuum GmbH, Germany) is coupled to the sample gas outlet of the TGA furnace. The mass spectrum (MS) can be synchronized with the TGA, and the data is analyzed using Quadstar<sup>TM</sup> TG-MS system software (TSTAR\_v7).

#### 4.2.7. Scanning electron microscopy (SEM)

The earliest concept involving the theory of scanning electron microscopy was first introduced in Germany (1935) by M. Knoll. The standard concept of the modern SEM was provided by von Ardenne in 1938 who added scan coils to a transmission electron microscopy. Since then, the SEM design has been modified and many other significant contributions has greatly enhanced and optimized the modern day scanning electron microscopy. The scanning electron microscopy (SEM) can form the images of the samples by scanning the sample surface with a high-energy beam of electrons. The electrons interact with the atoms that make up the sample producing signals that contain information about the sample's surface topography, composition and other properties such as electrical conductivity. The signals produced from the surface when it is scanned by the electron beams include secondary electrons, back-scattered electrons

(BSE), Auger electrons, characteristic X-rays, light (cathodoluminescence), and transmitted electrons (Shown in Fig. 4.5). Among them, the secondary and back-scattered electrons are typically served as the basis of the SEM.

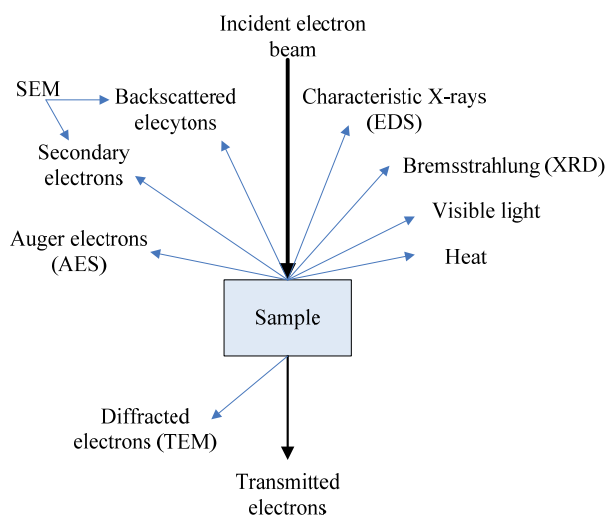


Fig. 4.5 The signals produced by the scanned incident beam to the sample surface

When the impinging electrons interact with the samples molecular composition, the energy of the impinging electrons onto a sample is directly in proportion to the type of electron interaction that is generated from the sample. A series of measurable electron energies can be produced which are analyzed by a sophisticated microprocessor that creates a pseudo three-dimensional image or spectrum of the unique elements that exist in the sample analyzed. For the conventional SEM, the sample must be conductive to prevent the accumulation of the electrostatic charge in the sample surface. Therefore, the non-conductive samples need to coat with a thin conductive material such as gold or carbon.

A Zeiss SUPRA 55VP scanning electron microscopy was used to qualitatively assess structural and morphological characteristics of the samples. Backscatter and secondary electron images were obtained using an acceleration potential of 5 keV. The samples measured had not been used in gas permeation tests, but were taken from the same carbonization batch as those used for the permeation test.

#### 4.2.8. Fourier Transform Infrared (FTIR)

Infrared spectroscopy is a technique for the identification of organic or inorganic functional groups with their characteristic infrared adsorption peaks. The infrared region

of the electromagnetic spectrum is the range of wavelengths from 0.78 to 1000  $\mu\text{m}$ , or 12800 to 10  $\text{cm}^{-1}$  [9]. The IR spectrum is usually subdivided into three regions, the near-, mid- and far- infrared. The near-IR (12800-4000  $\text{cm}^{-1}$ ) can excite overtone or harmonic vibrations. The mid-IR (4000-200  $\text{cm}^{-1}$ ) can be used to investigate the fundamental vibrations and associated rotational-vibrational structure. The far-IR (200-10  $\text{cm}^{-1}$ ) has relative low energy and can be used for the rotational spectroscopy. The most widely used region is the mid-IR which extends from 670  $\text{cm}^{-1}$  to 4000  $\text{cm}^{-1}$ . Here, the absorption, reflection and transmission spectra can be employed for both qualitative and quantitative analysis.

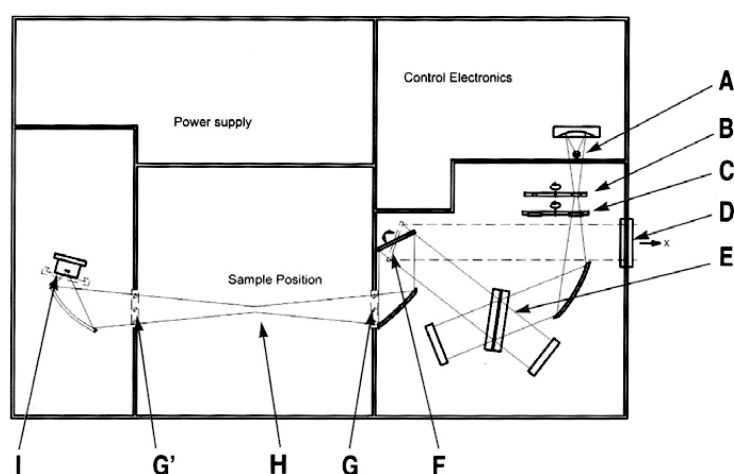


Fig. 4.6 Schematic of Tensor 27 optical bench, IR beam path, and major components. A = mid-IR source, B = aperture wheel, C = filter wheel, D = exit port (not used), E = beamsplitter, F = switch mirror, G = sample compartment window (KBr), G' = optional window (not present), H = sample holder/cell, I = detector (DTGS standard) (Source: Bruker Tensor 27 FT-IR instruction)

Three types of instruments for IR absorption measurements are commonly available: (1) dispersive spectrophotometers with a grating monochromator; (2) Fourier transform spectrometers; (3) nondispersive photometers. Until 1980s, the dispersive spectrophotometers were mostly used for IR measurements. However, this type of instruments has been replaced by Fourier Transform Infrared (FTIR) spectroscopy now, which is a powerful tool for identifying types of chemical bonds in a molecule by producing an infrared absorption spectrum that is like a molecular "fingerprint". A schematic diagram of Bruker Tensor 27 FTIR is shown in Fig. 4.6. The FTIR instruments have signal-to-noise ratios that are better than those of a good-quality dispersive instrument, usually by more than an order of magnitude. The enhanced

signal-to-noise ratio can be traded for rapid scanning with good spectra being attainable in a few seconds in most cases. In FTIR instrument, the IR light is guided through an interferometer instead of recording the amount of energy absorbed when the frequency of the infrared light is changed. By performing a mathematical Fourier transformation on the signals to generate the spectra, which is identical to the conventional infrared spectra (e.g. dispersive IR spectroscopy).

The FTIR spectra for the precursors and prepared HFCMs were obtained by using Bruker Tensor 27 FTIR (available at department of chemical engineering, NTNU). The instrument equips with a room temperature DTGS detector, mid-IR source (4000 to 400  $\text{cm}^{-1}$ ), and a KBr (The crystal has no visible peaks in the infrared spectrum making it transparent in FTIR) beam splitter. Maximum resolution is 1  $\text{cm}^{-1}$ . The samples were grinded as powder for analysis. The OPUS data collection program was used to record the FTIR spectra.

#### 4.2.9. Element analysis

Element analysis is a process where a sample of some material (e.g., chemical compounds) is analyzed for its elemental composition qualitatively or quantitatively. The most common form of elemental analysis, CHN analysis, is conducted by the combustion analysis. For this technique, the sample is burned in an excess of oxygen, and various traps collect the combustion products — carbon dioxide, water, and nitric oxide. The weights of these combustion products can be used to calculate the composition of the unknown sample. The element analysis was used to quantitatively determine the composition of the carbon membranes, which was conducted by combustion of the samples in the Analytische Laboratorien (Germany).

#### 4.2.10. X-ray diffraction (XRD)

X-ray is electromagnetic radiation with the wavelengths between roughly 0.1Å and 100Å, which can be generated by a X-ray tube. X-ray diffraction techniques are a family of non-destructive analytical techniques which reveal information about the crystallographic structure, chemical composition, and physical properties of materials. These techniques are based on observing the scattered intensity of an X-ray beam hitting a sample as a function of incident and scattered angle, polarization, and wavelength or energy. When the x-ray are scattered by the ordered structure of a crystal, the interference (both constructive and destructive) takes place among the scattered rays because the distance between the scattering centers are of the same order of magnitude as the wavelength of the radiation, which resulting to a diffraction pattern. According the XRD pattern, the d-spacing (d) for the samples can be obtained Bragg's equation:

$$n\lambda = 2d \sin \theta \quad (4.2)$$

Where  $n$  is an integer,  $\lambda$  is the wavelength of incident X-ray beam, and  $\theta$  is the diffraction angle. A wide-angle X-ray diffraction (WAXD) of Bruker AXS D8 Focus X-ray (available at NTNU) was used to characterize the d-spacing of the carbon membranes. The carbon powder was filled in the sample holder. A CuK $\alpha$  radiation (1.54 Å) was performed to record the WAXD pattern with  $2\theta$  from 15 ° to 70 °.

#### 4.2.11. Gas gravimetric sorption

Gas sorption isotherms for CO<sub>2</sub> and N<sub>2</sub> were obtained by a RobuTherm magnetic suspension balance (MSB) having a 0.01mg resolution and 0.02 mg reproducibility (Available at NTNU). The MSB overcomes the other conventional gravimetric sorption instruments by separating the microbalance from the sample and adsorbed gases [10]. The sample is placed in a suspended basket by a permanent magnet through an electromagnet in a closed system as shown in Fig. 4.7 [11]. The MSB instrument can perform the sorption measurements within a pressure range from vacuum to 35 bar and 150 bar for CO<sub>2</sub> and N<sub>2</sub>, respectively. Moreover, the temperature can be well controlled within the range of 298K-423K using a Julabo thermostatic circulator. The system can automatically measure the weight change of the samples over time at a certain temperature and pressure according to the measurement procedure described elsewhere [12]. The sample density is determined based on the buoyancy measurement with helium by increasing the pressure from 1bar to 30 bar (change the gas density). The linear regression of the measured balance masses ( $m_{bal}$ ) versus the helium density was carried out to obtain the true density of the sample as follows:

$$m_{bal} = m_{SC+S} - \rho V_{SC+S} \quad (4.3)$$

where the  $m_{SC+S}$  and  $V_{SC+S}$  are the mass and volume of the sample container together with the sample, respectively, which was determined from the intercept and slope of the linear regression. By subtraction of the mass ( $m_{SC} = 4.2249$  g) and volume ( $V_{SC} = 0.55$  ml) for the sample container based on the blank experiments, the mass ( $m_S$ ) and volume ( $V_S$ ) of the sample was obtained. Therefore, the true density of the samples can be calculated ( $\rho_S = m_S/V_S$ ). The CO<sub>2</sub> and N<sub>2</sub> adsorption onto the carbon membranes were executed at different temperatures, flow rates and pressures. In addition, the kinetic measurements were also conducted at a desired pressure with different CO<sub>2</sub> feed flow rates. The weight change, pressure and temperature were measured continuously until the sorption equilibrium was achieved.

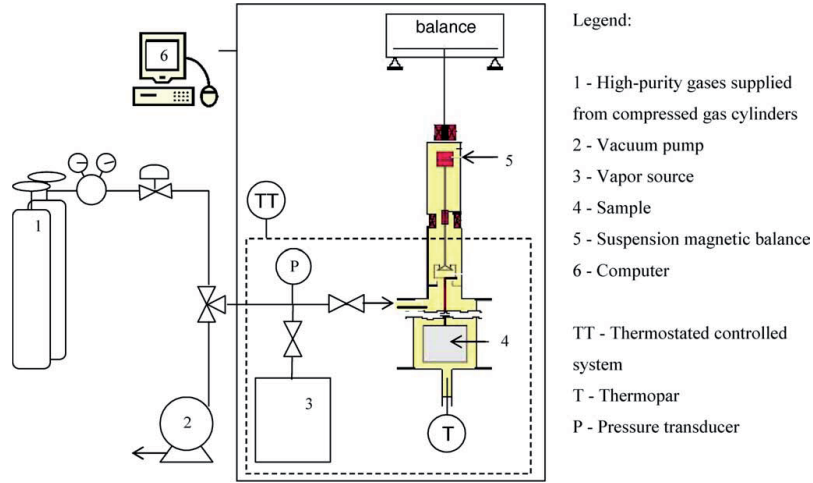


Fig. 4.7 Experimental set up for water vapor adsorption measurements [11]

#### 4.2.12. Gas permeation

The gas permeation measurements were executed using an in-house set-up as shown in Fig. 4.8. Single gas permeation tests were conducted at different temperatures and feed pressures from shell side (maximum 20 mbar in permeate side) in a standard pressure-rise setup (MKS Baratron<sup>®</sup> pressure transducer, 0~100 mbar range) with LabView<sup>®</sup> data logging, which was described in detail elsewhere [13]. The order of testing was always H<sub>2</sub>, N<sub>2</sub>, O<sub>2</sub>, CH<sub>4</sub> and finally CO<sub>2</sub> to prevent the strongly adsorbing gases from disturbing the performance of the carbon membranes to the more ideal or non-interacting gases [13]. The tests were run from several minutes to several hours to ensure that the transient phase of diffusion was passed and a steady state had been achieved ( $dp/dt$  tends to a constant). The gas permeability,  $P$  (Barrer, 1Barrer= $10^{-10}$  cm<sup>3</sup> (STP).cm / (cm<sup>2</sup>.s.cmHg)) is calculated using the following equation:

$$P = \frac{273 \times 10^7 V l (dp/dt)}{76 \Delta p A T_{exp.}} \quad (4.4)$$

where  $V$  is the collection volume (cm<sup>3</sup>) that can be measured with a pre-calibrated permeation cell reported elsewhere [13-14],  $dp/dt$  is the collection volume pressure increase rate (mbar/s),  $l$  and  $A$  are thickness (cm) and total active area of membrane sample (cm<sup>2</sup>) respectively,  $\Delta P$  (bar) is the pressure drop cross the membrane and  $T_{exp}$  the experimental temperature (K). In this work, the ideal selectivity is defined as the ratio of the pure gas permeability values which is evaluated as follows:

$$\alpha_{i/j} = \frac{P_i}{P_j} \quad (4.5)$$

For mixed gas separation measurements, a permeation cell and a gas chromatograph (GC) were combined to analyze the gas composition and calculate the permeability of gas component. The permeability of the gas mixture in steady state is calculated according to the following equations:

$$P_i = \frac{273 \times 10^7 y_i V l (dp/dt)}{76(x_i p_H - y_i p_L) A T_{\text{exp}}} \quad (4.6)$$

$$\bar{x}_i = \frac{x_{F,i} - x_{R,i}}{\ln \left( \frac{x_{F,i}}{x_{R,i}} \right)} \quad (4.7)$$

where  $P_i$  the permeability of component  $i$ ,  $p_H$  and  $p_L$  are the feed and permeate pressure (bar).  $x_{F,i}$  is the feed composition of component  $i$ , and  $x_{R,i}$  and  $y_i$  are the molar fraction of component  $i$  in retentate and permeate stream, respectively, which can be measured by Agilent 6890N GC. The process selectivity is calculated by Eq. 3.5 (See section 3.2.3).

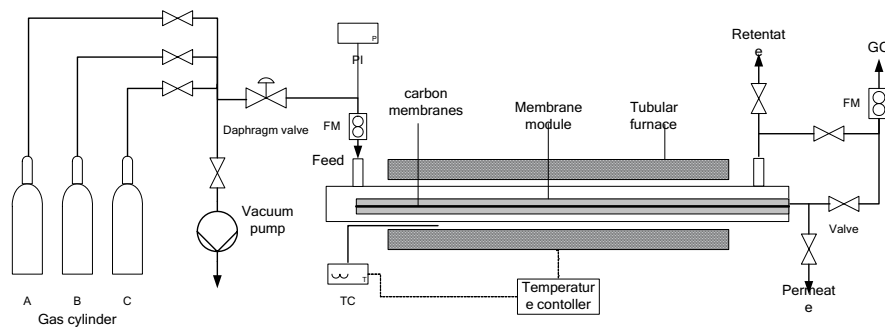


Fig. 4.8 A Schematic diagram for gas permeation test set-up

#### 4.2.13. Orthogonal experimental design and conjoint analysis

Statistical experimental design methods have been widely employed in process engineering and product design area because these methods provide a systematic and efficient plan for experimentation under the consideration of the interactive effects among the control factors. Therefore, many factors can be studied and optimized simultaneously [15]. Among these methods, the orthogonal experimental design (OED) method, developed by Taguchi [16], possesses the advantage that many factors can be examined simultaneously and much quantitative information can be extracted by only a few experimental runs. The variables that have been chosen for an experiment are commonly termed as factors. The number of factors differs from experiment to experiments. Levels of factors can be decided more freely when adjusted by the designer.

When the factors and levels are both set, the orthogonal array can be generated by Statistical Product and Service Solutions (SPSS) software. The conjoint analysis method was employed to analyze the experimental results. The utilities (part-worth) reflect the importance for each factor level. The range (highest minus lowest) of the utility values for each factor provides a measurement of how important the factor is to overall preference. Factors with greater utility ranges play a more significant role than those with smaller ranges. The importance score (*IMP*) for factor *i* (%) is calculated:

$$IMP_i = 100 \frac{Range_i}{\sum_{i=1}^p Range_i} \quad \text{where } p = \text{factor number} \quad (4.8)$$

If there are several subjects used for analysis, the importance for each factor is calculated separately for each subject, and these are then averaged. For prediction, the probability of each simulation ( $p_i$ ) can be estimated according to following methods: The maximum utility model determines the probability as the number of respondents predicted to choose the case divided by the total number of respondents. The BTL (Bradley-Terry-Luce) model determines the probability as the ratio of one case utility to that for all simulation cases [16]. The Logit model is similar to BTL but uses the natural log of the utilities instead of the utilities.

### 4.3 Membrane module construction

The lab-scale carbon membrane modules with ¼ or 3/8 inch stainless steel tube, Swagelok tees and unions were constructed for the gas permeation tests. A representative lab-scale module is shown in Fig. 4.9, and 27 hollow fiber carbon membranes have been mounted into this module.

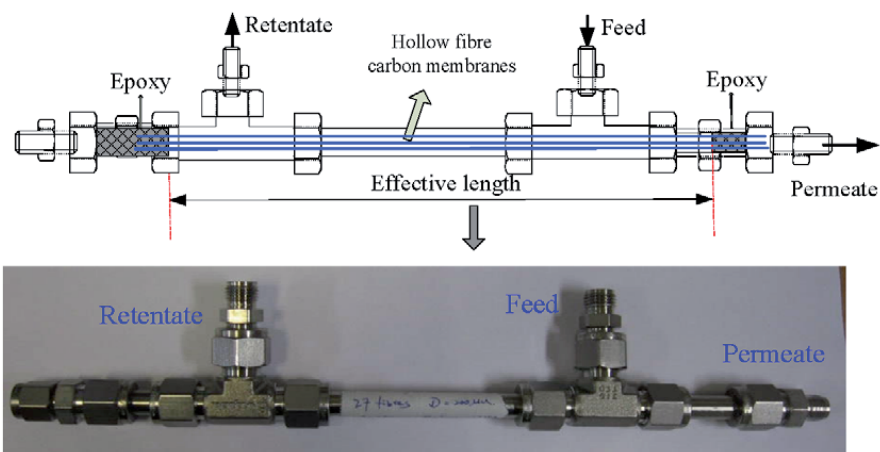


Fig. 4.9 A schematic and lab-scale carbon membrane module

A small pilot scale module (designed by one of the NanoGloWa project partner: HyGear) mounted with 100 carbon fibers was also constructed, which is shown in Fig. 4.10. These carbon membrane modules were used for the gas permeation tests, both for single gas and gas mixture, to characterize the separation performance for the prepared carbon membranes. The single gas permeability tests at different temperature and pressure were mostly conducted by using the lab-scale module. The small pilot scale module was employed to test the gas mixture at a higher permeate flux in order to determine the gas composition more precisely.



Fig. 4.10 A small pilot scale carbon membrane module (Designed by HyGear)

#### 4.4 References

- [1] Jie X, Cao Y, Qin J-J, Liu J, Yuan Q. Influence of drying method on morphology and properties of asymmetric cellulose hollow fiber membrane. *J Membr Sci.* 2005;246(2):157-65.
- [2] Qin J-J, Li Y, Lee L-S, Lee H. Cellulose acetate hollow fiber ultrafiltration membranes made from CA/PVP 360 K/NMP/water. *J Membr Sci.* 2003;218(1-2):173-83.
- [3] Edgar KJ, Buchanan CM, Debenham JS, Rundquist PA, Seiler BD, Shelton MC, et al. Advances in cellulose ester performance and application. *Prog Polym Sci.* 2001;26(9):1605-88.
- [4] Hao J-h, Dai H-p, Yang P-c, Wei J-m, Wang Z. Cellulose acetate hollow fiber performance for ultra-low pressure reverse osmosis. *Desalination.* 1996;107(3):217-21.

- [5] Liu H, Hsieh Y-L. Ultrafine fibrous cellulose membranes from electrospinning of cellulose acetate. *J Polym Sci Part B: Polym Phys.* 2002;40(18):2119-29.
- [6] Son WK, Youk JH, Lee TS, Park WH. Electrospinning of Ultrafine Cellulose Acetate Fibers: Studies of a New Solvent System and Deacetylation of Ultrafine Cellulose Acetate Fibers. *J Polym Sci Part B: Polym Phys.* 2004;42:5-11.
- [7] Olaru N, Olaru L. Cellulose acetate deacetylation in benzene/acetic acid/water systems. *J Appl Polym Sci.* 2004;94(5):1965-8.
- [8] Yamashita Y, Endo T. Deterioration behavior of cellulose acetate films in acidic or basic aqueous solutions. *J Appl Polym Sci.* 2004;91(5):3354-61.
- [9] Skoog DA, Crouch SR, Holler FJ. Principles of instrumental analysis. Belmont, Calif.: Thomson 2007.
- [10] Dreisbach F, H. RSA, Lösch HW. Gravimetric Measurement of Adsorption Equilibria of Gas Mixture CO/H<sub>2</sub> with a Magnetic Suspension Balance. *Chem Eng Technol.* 2002;25(11):1060-5.
- [11] Lagorsse S, Campo MC, Magalhaes FD, Mendes A. Water adsorption on carbon molecular sieve membranes: Experimental data and isotherm model. *Carbon.* 2005;43(13):2769-79.
- [12] Belmabkhout Y, Serna-Guerrero R, Sayari A. Adsorption of CO<sub>2</sub> from dry gases on MCM-41 silica at ambient temperature and high pressure. 1: Pure CO<sub>2</sub> adsorption. *Chem Eng Sci.* 2009;64(17):3721-8.
- [13] Lie JA. Synthesis, performance and regeneration of carbon membranes for biogas upgrading-a future energy carrier [PhD]. Trondheim: Norwegian University of Science and technology; 2005:152.
- [14] Lin W-H, Vora RH, Chung T-S. Gas transport properties of 6FDA-durene/1,4-phenylenediamine (pPDA) copolyimides. *J Polym Sci Part B: Polym Phys.* 2000;38(21):2703-13.
- [15] Houg J-Y, Liao J-H, Wu J-Y, Shen S-C, Hsu H-F. Enhancement of asymmetric bioreduction of ethyl 4-chloro acetoacetate by the design of composition of culture medium and reaction conditions. *Process Biochem.* 2007;42(1):1-7.
- [16] Taguchi G. System of experimental design. In: Engineering methods to optimize quality and minimize costs. New York: Kraus International Publications Of The Astronomical Society Of Australia. 1987.

## 5 Results and discussions-precursors, spinning conditions

The chapter describes the optimization of the spinning and deacetylation processes based on the orthogonal experimental design and statistical analysis method. The precursors from the optimal deacetylation treatment were used for the preparation of the carbon membranes subsequently. This chapter is partly also represent in the article “*Hollow Fiber Carbon Membranes: from Material to Application*” (see Appendix H).

### 5.1 Spinning hollow fiber membranes

The well-known dry-jet wet spinning technology was used to spin cellulose acetate (CA) hollow fiber membranes [1-5]. This process consists of the formation of nascent membrane, followed by the interfacial phase separation within the air gap. After that, the nascent membrane is immersed in a non-solvent quench bath at a certain temperature where phase separation occurs throughout the rest of the membranes. The spinning parameters such as air gap, bore fluid, flow rate of bore fluid, and temperature of quench bath etc., which will affect the structure, morphology and properties of the hollow fibers. Qin [2] and Chung [6] reported the influences of the air gap on the membrane performance. Their results indicated that an increase of the air gap resulted to a significant decrease of the membrane permeation. He et.al reported that the high temperature of the quench bath gives an open structure with a thin skin layer, while low temperature results to forming a dense membrane with a thick skin layer [7]. Moreover, the bore fluid (e.g. mixture of NMP/H<sub>2</sub>O) with high water content results in internal macrovoids, while the high NMP content resulting to form a membrane with much more open sub-structure. Therefore, how to investigate and optimize the spinning parameters in an efficient way becomes a key issue. The orthogonal experiment design (OED) method, as described in section 4.2.13, is well used for multi-factor design and optimization, which can investigate the effects for all parameters systematically whilst reduce the experiment times greatly. Therefore, the OED method was employed to optimize the spinning process.

#### 5.1.1. Optimization of spinning condition

The cellulose acetate hollow fibers were spun using various spinning conditions according to the designed experimental plan (see section 4.2.2 Table 4.1). The spinning parameters were well controlled within a certain region of air gap: 15~35 mm, bore fluid composition: NMP (0 ~ 100 %) +H<sub>2</sub>O, bore flow rate: 20 ~ 60 % of dope flow rate ( $V_b/V_d$ ) and quench (First) bath temperature: 20 ~ 50 °C. The spun fibers were then characterized by FTIR and SEM. The characteristic adsorption peaks of 1030 cm<sup>-1</sup>,

1230  $\text{cm}^{-1}$ , 1740  $\text{cm}^{-1}$  attribute to the ether group ( $\nu_{\text{C-O-C}}$ ), acetyl ester group ( $\nu_{\text{CH}_3\text{-C=O}}$ ) and carbonyl group ( $\nu_{\text{C=O}}$ ) of CA respectively, and the characteristic peak 1665  $\text{cm}^{-1}$  attributes to the carbonyl group of PVP as shown in Fig. 5.1.

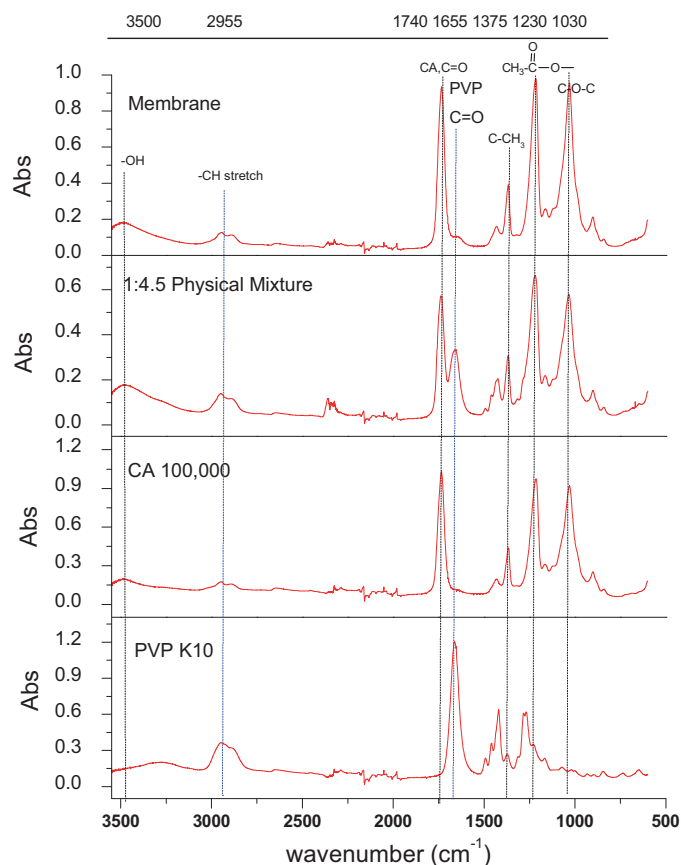


Fig. 5.1 FTIR spectra for CA, PVP, physical mixture of CA and PVP and membrane

The FTIR spectra for the hollow fiber membranes prepared from various spinning conditions are shown in Figs. 5.2 and 5.3. The absorption ratio of 1665  $\text{cm}^{-1}$ /A1030  $\text{cm}^{-1}$  was used to represent the PVP content in the membrane, and the morphology of the prepared hollow fibers were characterized by SEM, which are given in Table 5.1.

#### 5.1.2. Conjoint analysis

The conjoint analysis in SPSS package was used to analyze the results of orthogonal experiment design [8]. The contributions for each factor's level are estimated by the conjoint analysis. The correlations of Pearson's R and Kendall's tau are 0.964 and 0.957

respectively, which indicates that it keeps good consistency between the estimated preferences and experiment results. Table 5.2 shows the utilities (part-worth) for each factor level, and the averaged importance score for each factor. Since the utilities are all expressed in a common unit, they can be added together to give the total utility of any combination. Therefore, a simple comparison for the two combinations of the factor level and the optimal spinning condition is also given in Table 5.3.

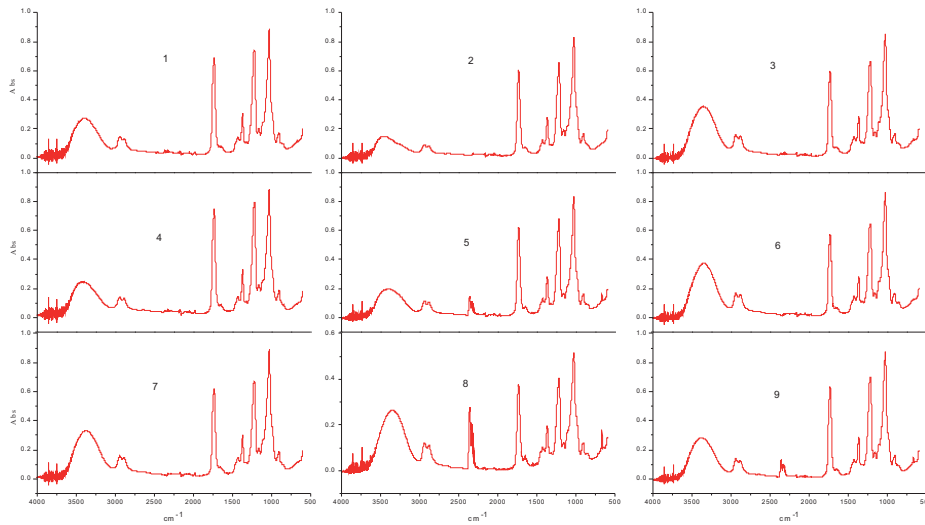


Fig. 5.2 FTIR spectra of the spun hollow fibers using the spinning conditions of experimental plan

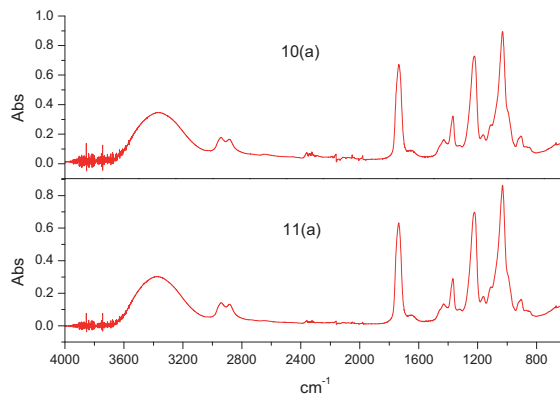
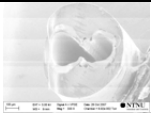
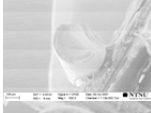
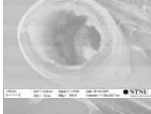
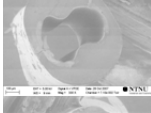
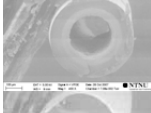
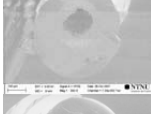
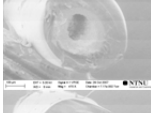
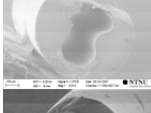
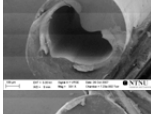
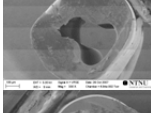
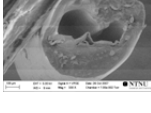


Fig. 5.3 FTIR spectra of spun membranes for holdout experiments

Table 5.1 Results of OED for optimization of spinning conditions

No.	Bore fluid	Air gap	Bore flow rate	Quench bath temperature	PVP content (%)	Membrane morphology*
1	water	15mm	40%	20 °C	9.41	
2	water	35mm	20%	50 °C	9.01	
3	water+NMP(85%)	15mm	60%	50 °C	9.11	
4	water	25mm	60%	20 °C	10.08	
5	water+NMP(85%)	35mm	40%	20 °C	8.59	
6	water+NMP(85%)	25mm	20%	20 °C	8.16	
7	water	25mm	40%	50 °C	9.41	
8	water	15mm	20%	20 °C	10.83	
9	water	35mm	60%	20 °C	7.75	
10(a)	water	15mm	60%	20 °C	7.72	
11(a)	water+NMP(85%)	25mm	60%	20 °C	10.37	
12(b)	water	25mm	40%	20 °C		
13(b)	water+NMP(85%)	25mm	40%	20 °C		

a: Holdout; b: Simulation; \*: SEM images

Table 5.2 Utilities and averaged importance scores for different factors

Factor	Level	Utility	Averaged importance score (%)
Bore fluid	Water	-0.917	28.7
	Water + NMP (85%)	0.917	
Air gap	15mm	-1.111	29.5
	25mm	0.889	
	35mm	0.222	
Bore flow rate (% of the dope flow rate)	20%	-0.778	27.9
	40%	0.889	
	60%	-0.111	
Quench bath Tem.	20 °C	-0.750	13.9
	50 °C	0.750	

Table 5.3 An example for combination of different spinning conditions

Case	Utility				Total utility
	Bore fluid	Air gap (mm)	Bore flow rate (% of dope flow rate)	Quench bath Tem. (°C)	
1	Water (-0.917)	35 (0.222)	60 (-0.111)	20 (-0.75)	4
2*	Water + NMP (85%) (0.917)	25 (0.889)	40 (0.889)	50 (0.75)	9

\*: optimal spinning condition

The range of the utility values (averaged importance score) for each factor provides a measure of how important the factor to overall preference. Factors with greater averaged importance score play a more significant role than those with smaller values. From Table 5.2, one could conclude that the importance for these four spinning factors was sorted as follows:

Air gap > Bore fluid > Bore fluid rate > Quench bath temperature

It is clearly that the air gap is the most important parameter during the dry-wet spinning process which keeps good consistency with the previous reported results [2, 6]. Therefore, the air gap needs to be controlled strictly during the spinning process to prepare the defect-free CA hollow fiber membranes. An optimized spinning condition with bore fluid (water+NMP (85%)), air gap (25 mm), bore flow rate (40 % of dope

flow rate) and temperature of quench bath (50 °C) was also obtained. This result provides the basic guideline for the preparation of defect-free hollow fiber membranes. The prepared hollow fibers need to be pretreated before it can be used as the precursors for carbon membranes.

The real power of conjoint analysis is the ability to predict membrane properties that weren't be executed by the experiments. These are referred to as simulation cases which are included as part of the plan, along with the products from the orthogonal design and any holdout products. The simulation results are given in Table 5.4. The utility of case 2 is larger than that of case 1, and across the two subjects (PVP content and membrane morphology) in this study, all three models of Maximum utility, Bradley-Terry-Luce (BTL) and Logit indicated that simulation case 2 would be preferred. Therefore, the prediction from the conjoint analysis can be used to guide the experiments and spin the defect-free membranes with the specific properties.

Table 5.4 Simulation results by conjoint analysis

Card number	Score	Maximum utility	BTL	Logit
1	5.667	33.3%	43.7%	26.9%
2	7.500	66.7%	56.3%	73.1%

## 5.2 Optimization of deacetylation process

The spun fibers were deacetylated with a NaOH solution to partly convert the cellulose acetate to cellulose. The effects of different deacetylation parameters have been investigated systematically to find the optimal deacetylation condition.

### 5.2.1. Investigation of deacetylation conditions

The cellulose acetate hollow fiber membranes were swelled in 10 % glycerol solution for 24 h first, and the swelled fibers were then deacetylated with a NaOH solutions. In order to investigate the influence of the ethanol solution, the deacetylation using 0.5 M NaOH in (50 % and 96 % ethanol solution with different reaction time were conducted, respectively. The FTIR was used to characterize the properties of the deacetylated precursors. Fig. 5.4 shows the dependence of the residual acetyl content in the deacetylated CA hollow fibers on the reaction time. It can be found that the reaction rate in 50 % ethanol solution is faster than that in 96 % ethanol solution. Based on the above experiments, the deacetylation conditions need to be well controlled to obtain the desired precursors (a certain mount of acetyl group and PVP) for preparation of high performance carbon membranes.

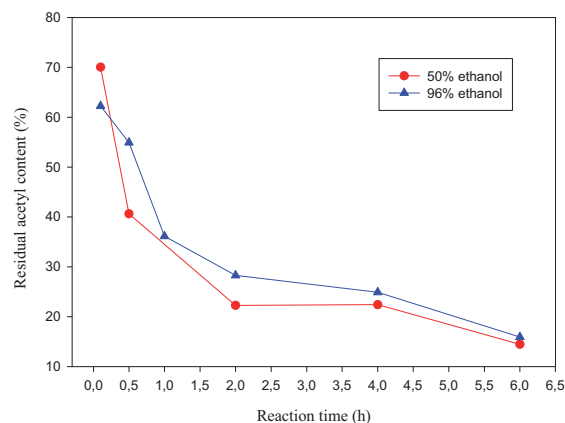


Fig. 5.4 Dependence of residual acetyl content in membranes on the reaction time

### 5.2.2. Optimization of deacetylation condition

Based on the above experimental results, it can be found that the deacetylation parameters such as the NaOH concentration, swelling time, solution and reaction time may affect the deacetylation results greatly. Therefore, a systematic study was conducted to obtain the optimal deacetylation condition. The orthogonal experimental design (OED) method with 4 parameters and 3 levels was studied (see section 4.2.3).

The FTIR was used to characterize the deacetylated precursors as shown in Figs. 5.5 and 5.6. The absorption ratios of  $A_{1740\text{ cm}^{-1}}/A_{1030\text{ cm}^{-1}}$  and  $A_{1665\text{ cm}^{-1}}/A_{1030\text{ cm}^{-1}}$  in FTIR spectra were employed to determine the residual acetyl content and the PVP content of the precursors, respectively, and the results are given in Table 5.5.

Based on the experimental results in Table 5.5, the conjoint analysis in SPSS package was used to investigate the influences of the deacetylation parameters on the precursor's properties. The correlations of Pearson's R and Kendall's tau are 0.989 and 0.914 respectively, which indicates that it keeps good consistency between the estimated properties and experiment results. Table 5.6 shows the utilities (part-worth) for each factor level and averaged importance scores for all factors. Higher utility values indicate better properties. Since the averaged importance scores provides a measure of how important the factor to overall properties of the precursors, thus the factors with greater averaged importance score play a more important role than those with smaller values. From Table 5.6, one could conclude that the importance for these four factors was sorted as follows:

Solution>Swelling time> Reaction time> NaOH concentration

The solution shows a significant effect on the deacetylation results, and the importance of NaOH concentration is relatively small within the studied range. The utilities for all parameter levels are all expressed in a common unit, this values can be added together to present the total contribution of any combinations. Table 5.7 gives a simple comparison between a representative combination and the optimal deacetylation condition (0.075M NaOH in 96 % ethanol solution for 2 h, and the swelled fibers with 24h). This result can be used to guide the deacetylation of CA hollow fiber membranes. The precursors treated with the optimal deacetylation condition was characterized by SEM as shown in Fig. 5.7, which were used to prepare the hollow fiber carbon membranes subsequently.

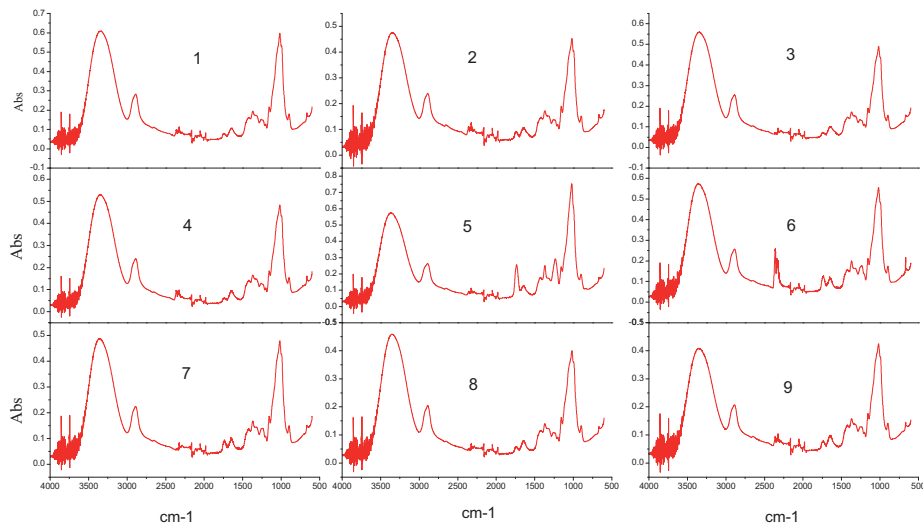


Fig. 5.5 FTIR spectra for the deacetylated hollow fibers of the OED plan's experiments

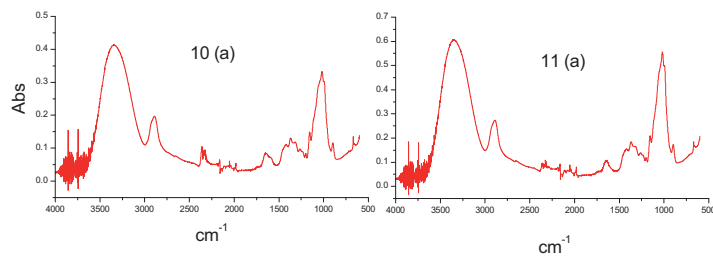


Fig. 5.6 FTIR spectra for the deacetylated hollow fibers of the holdout experiments

Table 5.5 Results of OED for deacetylation of CA membranes

No.	Swelling time	NaOH concentration	Solution	Reaction time	Acetyl content (%) <sup>c</sup>	PVP content (%) <sup>d</sup>
1	0h	0.075M	50% ethanol	4h	14.42	18.83
2	24h	0.075M	50% ethanol	2h	21.44	24.85
3	1h	0.05M	50% ethanol	2h	15.89	21.59
4	24h	0.05M	96% ethanol	4h	13.63	20.20
5	0h	0.05M	50% ethanol	0.5h	34.98	17.43
6	1h	0.075M	96% ethanol	0.5h	23.85	21.53
7	24h	0.1M	50% ethanol	0.5h	20.42	21.04
8	1h	0.1M	50% ethanol	4h	15.55	20.50
9	0h	0.1M	96% ethanol	2h	19.47	24.08
10(a)	24h	0.075M	96% ethanol	4h	14.06	26.40
11(a)	1h	0.05M	96% ethanol	4h	12.00	20.30
12(b)	1h	0.075M	50% ethanol	2h		
13(b)	1h	0.075M	96% ethanol	2h		

<sup>a</sup>: holdout; <sup>b</sup>: simulation; <sup>c</sup>: A1740 cm<sup>-1</sup> / A1030 cm<sup>-1</sup>; <sup>d</sup>: A1655 cm<sup>-1</sup> / A1030 cm<sup>-1</sup>

Table 5.6 Utilities and averaged importance scores for different factors

Factor	Level	Utility	Averaged importance score (%)
Swelling time	0h	-0.889	31.9
	1h	-0.667	
	24h	1.556	
NaOH concentration	0.05M	0.222	14.8
	0.075M	0.333	
	0.1M	-0.556	
Solution	50% ethanol	-1.500	34.4
	96% ethanol	1.500	
Reaction time	0.5h	0	18.9
	2h	0.111	
	4h	-0.111	

Table 5.7 An example for different deacetylation conditions

Case	Utility (Swelling)	Utility (NaOH concentration)	Utility (Solution)	Utility (Reaction time)	Total utility
1	0h (-0.889)	0.05M (0.222)	50% ethanol (-1.5)	0.5h (0)	3.3
2*	24h (1.556)	0.075M (0.333)	96% ethanol (1.5)	2h (0.111)	9.0

\*: optimal deacetylation condition

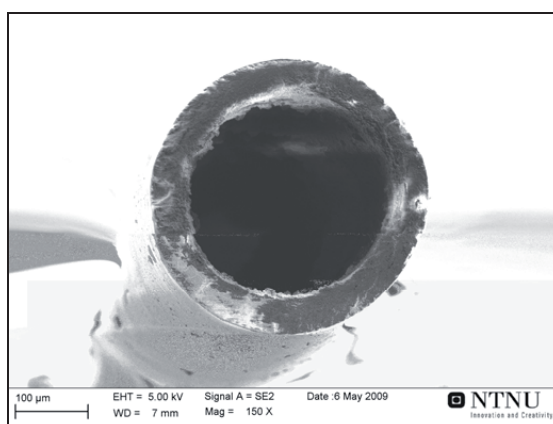


Fig. 5.7 SEM image of cross section for the deacetylated cellulosic precursor

The results based on the conjoint analysis can be used to predict membrane properties that were not executed by the experiments. These are referred to as simulation cases which are included as part of the plan, along with the products from the orthogonal design and any holdout products. Based on the conjoint analysis results of orthogonal experiment design, we can predict the deacetylation results under the other conditions which are not included in plan and holdout experiments. These are referred to as simulation cases. The simulation results were given in Table 5.8. All three models of Maximum utility, BTL and Logit indicated that the simulation case 2 would be preferred. Therefore, the prediction results based on orthogonal experimental design and conjoint analysis could be used to obtain a precursor with the desired properties for the preparation of high performance carbon membranes.

Table 5.8 Simulation results by conjoint analysis

Card Number	Score	Maximum utility	BTL	Logit
1	3.778	0.0%	35.9%	6.9%
2	6.778	100.0%	64.1%	93.1%

### 5.3 Conclusions

CA hollow fiber membranes were prepared from a dope solution containing CA/PVP/NMP using different spinning conditions. The orthogonal experiment design method was used to optimize the spinning conditions. The experiment results indicated that the importance for these 4 parameters could be sorted as follows:

Air gap > Bore fluid > Bore fluid rate > Quench bath temperature

The optimal spinning condition of a bore fluid (water + NMP (85 %)), air gap (25 mm), bore flow rate (40 % of dope flow rate) and temperature of quench bath (50 °C) was also obtained. It could be concluded that the OED method can be well used for the optimization of spinning conditions, and the results can be used to guide the experiments for spinning the defect-free hollow fibers.

The deacetylation of the spun CA hollow fiber membranes was carried out with NaOH solutions. The reaction rate was found to be much fast in ethanol (50 %) solution than in ethanol (96 %) solution. Based on the results of the orthogonal experimental design and statistical analysis, the importance for the deacetylation parameters was sorted as follows:

Solution>Swelling> Reaction time> Concentration

The optimal optimal deacetylation condition with 96 % ethanol solution, swelling 24 h, the concentration of NaOH (0.075 M) and the reaction time (2 h) was also obtained. The deacetylated cellulose acetate fibers can be used as the precursors for the preparation of carbon membranes subsequently.

#### 5.4 References

- [1] Jie X, Cao Y, Qin J-J, Liu J, Yuan Q. Influence of drying method on morphology and properties of asymmetric cellulose hollow fiber membrane. *J Membr Sci.* 2005;246(2):157-65.
- [2] Qin J-J, Li Y, Lee L-S, Lee H. Cellulose acetate hollow fiber ultrafiltration membranes made from CA/PVP 360 K/NMP/water. *J Membr Sci.* 2003;218(1-2):173-83.
- [3] Liu H, Hsieh Y-L. Ultrafine fibrous cellulose membranes from electrospinning of cellulose acetate. *J Polym Sci Part B: Polym Phys.* 2002;40(18):2119-29.
- [4] Son WK, Youk JH, Lee TS, Park WH. Electrospinning of Ultrafine Cellulose Acetate Fibers: Studies of a New Solvent System and Deacetylation of Ultrafine Cellulose Acetate Fibers. *J Polym Sci Part B: Polym Phys.* 2004;42:5-11.
- [5] Hao J-h, Dai H-p, Yang P-c, Wei J-m, Wang Z. Cellulose acetate hollow fiber performance for ultra-low pressure reverse osmosis. *Desalination.* 1996;107(3):217-21.
- [6] Chung T-S, Hu X. Effect of air-gap distance on the morphology and thermal properties of polyethersulfone hollow fibers. *J Appl Polym Sci.* 1997;66(6):1067-77.
- [7] He X, Hägg M-B. Using orthogonal experimental design for spinning defect-free hollow fiber membranes. *Advanced Membrane Technology IV: Membranes for Clean and Sustainable Processes.* Trondheim 2009.
- [8] SPSS Conjoint™ 17.0. [cited 2009 May 15]; Available from: [https://www.washington.edu/uware/spss/docs/SPSS Conjoint 17.0.pdf](https://www.washington.edu/uware/spss/docs/SPSS%20Conjoint%2017.0.pdf)

## 6 Results and discussions-preparation and characterization carbon membranes

This chapter describes the main results for the carbon membranes prepared from the deacetylated cellulose acetate (CA) precursors. Several general characterization techniques, gas sorption measurements and gas permeation tests were used to characterize the carbon membrane properties. The effects of precursors, carbonization condition as well as the operating parameters such as temperature, pressure, humidity on the carbon membrane separation performances are investigated and discussed. These work have been partly included in the articles "*Preparation and Characterization of Hollow Fiber Carbon Membranes from Cellulose Acetate Precursors*" (Appendix D), "*Optimization of Carbonization Process for Preparation of High Performance Hollow Fiber Carbon Membranes*" (Appendix E), and "*Structural, Kinetic and Performance Characterization of Hollow Fiber Carbon Membranes*" (Appendix F).

### 6.1 Effect of precursors

The precursors with different deacetylation conditions were used to prepare the hollow fiber carbon membranes (HFCMs). As indicated in Table 6.1, a significant shrinkage was found for the prepared carbon membranes. The diameter and thickness reduced from a typical 400  $\mu\text{m}$  and 50  $\mu\text{m}$  (the precursors) to 250  $\mu\text{m}$  and 30  $\mu\text{m}$  (the carbon membranes). Moreover, the precursors with short deacetylation time of 0.5 and 1h present a much more significant shrinkage compared to the precursors with longer deacetylation time (>2h).

Table 6.1 Weight loss for precursors with different deacetylation time

Membrane	Deacetylation time(h)	Diameter ( $\mu\text{m}$ )		Thickness ( $\mu\text{m}$ )		Weight loss (%)	Longitudinal shrinkage (%)
		Precursor	Carbon membrane	Precursor	Carbon membrane		
Polymer membrane	0	559		93			
HFCM-0.5	0.5	430	216	65	30	78.0	37.5
HFCM-1	1	400	246	50	29	74.1	32.0
HFCM-2	2	399	250	48	30	73.5	33.3
HFCM-4	4	392	266	48	32	73.6	31.2
HFCM-8	8	390	253	48	25	74.9	32.0

In addition to the thickness and diameter characterization, the weight loss measurement for pyrolysis process was carried out using TGA to mimic the carbonization conditions and hence assess the weight changes of the precursor material during the carbonization

process. The weight loss is larger short deacetylation times (<1 h) than that for longer times (>2 h), which indicates that most acetyl group were reacted with NaOH within 2h, to continuously prolong deacetylation time will not change the degree of substitution for acetyl group ( $DS = 1.62 Acetyl / (43 - 0.42 Acetyl)$ , acetyl content (%)) significantly, as can be seen from Fig. 6.1.

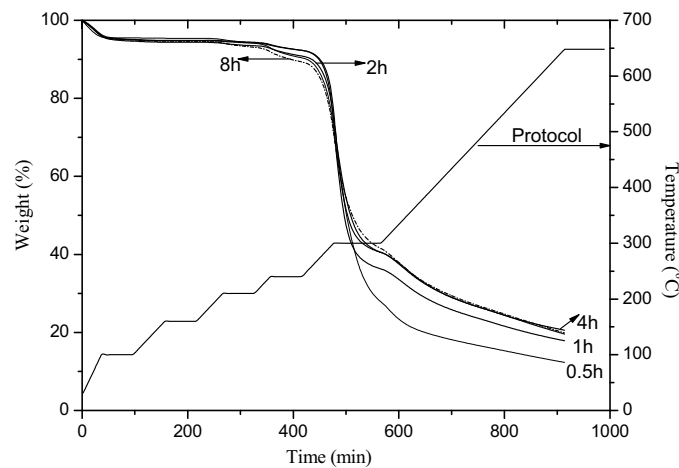


Fig. 6.1 Carbonization procedure and weight loss of the precursor with different deacetylation times

Figure 6.2 illustrates the single gas permeability values of H<sub>2</sub>, CO<sub>2</sub>, N<sub>2</sub> and CH<sub>4</sub> versus the gas molecule kinetic diameters for the prepared HFCMs from the precursors with different deacetylation times (see the detail calculation method in Appendix A). The HFCM-2 with a deacetylation time of 2h shows the highest permeability for the tested gas molecules. Table 6.2 shows the effect of deacetylation time on the carbon membrane performances. When the precursor is pure cellulose acetate, the carbon membrane can not be prepared due to the high acetyl content. Increasing the deacetylation time will convert partly of CA to cellulose, which resulting to a relative low separation performance for the prepared carbon membranes. With longer time, the cellulose acetate can be converted as cellulose completely, and the prepared carbon membrane shows much low performance for both permeability and selectivity. Figs. 6.3 and 6.4 present the permeability and ideal selectivity of CO<sub>2</sub>/N<sub>2</sub> and CO<sub>2</sub>/CH<sub>4</sub> for the carbon membranes prepared from precursors with different deacetylation time. Based on Robeson upper bound as published in 1991 and 2008 [1-2], the hollow fiber carbon membranes exhibit great gas permeability and selectivity properties compared to the precursors and most polymeric membranes.

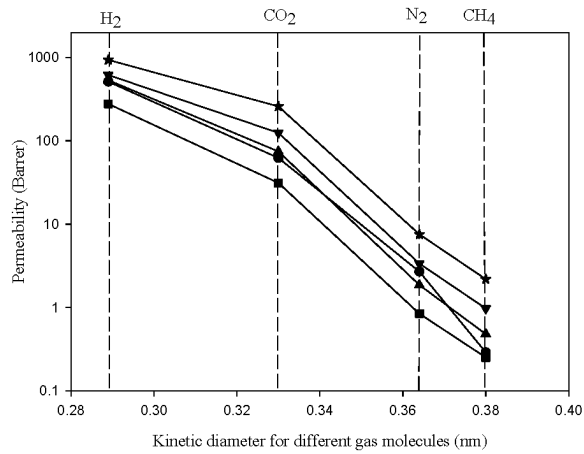


Fig. 6.2 Single gas permeability of (●) HFCM-0.5, (▼) HFCM-1, (★) HFCM-2, (▲) HFCM-4 and (■) HFCM-8 against the kinetic diameter of gas molecules at 303 K and 2 bar

Table 6.2 Effect of deacetylation time

Reaction time	Compounds	DS	Carbon membranes
0	CA	2.45	-
Short, <0.5h	CA/Cellulose	0~2.45	Low performance
Optimal, ~2h	Cellulose / CA	Optimal	High performance
Long, >8h	Cellulose	0	Low permeability

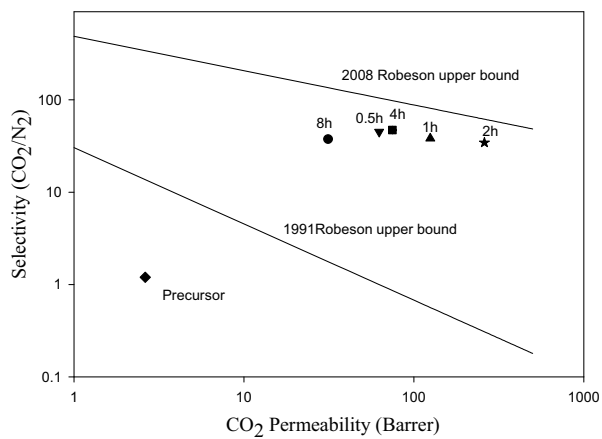


Fig. 6.3 Separation performance for CO<sub>2</sub>/N<sub>2</sub> based on the single gas measurements at 30 °C and 2bar

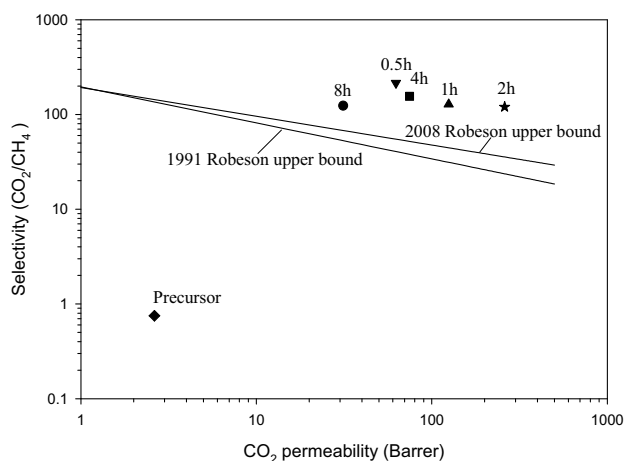


Fig. 6.4 Separation performance for CO<sub>2</sub>/CH<sub>4</sub> based on the single gas measurements at 30 °C and 2 bar

## 6.2 Carbonization procedure

As indicated in Fig. 6.1, the degradation of precursor begins at approximately 240 °C and most of the weight loss occurs at approximately 300 °C, and continues at a slower rate up to 650 °C for all precursors. Some evaporation of absorbed water was also found below 100 °C. Therefore, this carbonization protocol is suitable for the carbonization of the deacetylated CA precursors since the dwells coincide with the range of highest weight loss. The gases evolved during the carbonization were monitored using a mass spectrometer in which the dry helium swept the gas residue into the mass spectrometer (at a flow rate of 90 ml/min). The acquired information is plotted against the weight loss of precursor with deacetylation time of 2h in Fig. 6.3. Wu et al. reported that the cellulose carbonization generates H<sub>2</sub>, CO<sub>2</sub>, CO, H<sub>2</sub>O, CH<sub>4</sub> and other volatiles [3]. In this work, the onset of large weight loss coincided with the increase of H<sub>2</sub>, CO<sub>2</sub>, CO, H<sub>2</sub>O, CH<sub>4</sub> and so on. The main MS peak of H<sub>2</sub>O occurs around 290 - 350 °C, indicating that water is evolved mostly via the chemical dehydration because the physical adsorbed water has been greatly removed in the predrying process (<200 °C) on the basis of the TGA-MS detection. Therefore, the carbonization mechanism is possibly dominated by the dehydration reaction. The thermal cleavages of C-O and C-C linkages can result in the formation of CO and CO<sub>2</sub>. Following the ring opening, the volatiles of the evolution are further eliminated from the glycoside links of the deacetylated cellulose acetate, which can accelerate the conversion from cellulosic structure to the turbostatic carbon

structure that will greatly affect the performance of the resulting hollow fiber carbon membranes.

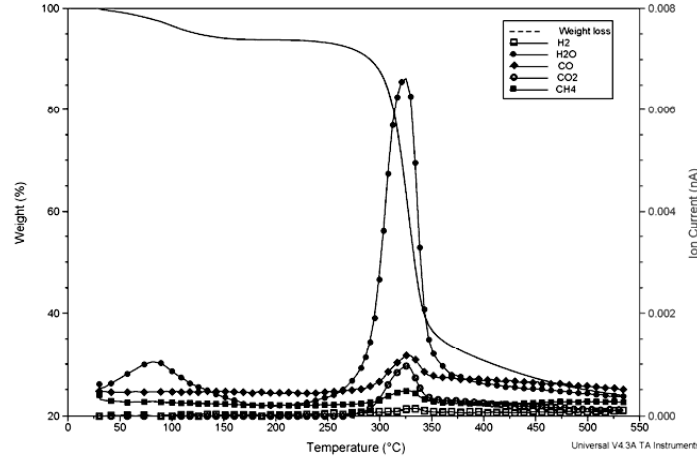


Fig. 6.3 TGA-MS analysis for the carbonization process

### 6.3 Transport mechanism investigation

The gas permeability values of the selected gases were found to be in the following order:  $H_2$  ( $2.89\text{\AA}$ ) >  $CO_2$  ( $3.3\text{\AA}$ ) >  $N_2$  ( $3.64\text{\AA}$ ) >  $CH_4$  ( $3.8\text{\AA}$ ) from Fig. 6.2. The permeability values are decreasing with increasing kinetic diameter of the gases, indicating that the main transport mechanism of HFCMs is molecular sieving. According to the theory of molecular sieving transport mechanism described in section 2.2.5. The most popular approach to linking porosity complexity to intra-particle diffusional behavior is via the so-called tortuosity factor. Thus for a sample of a porous material an effective diffusivity is defined as [4]:

$$D_e = \frac{\varepsilon_p}{\tau} D \quad (6.1)$$

where  $D_e$  is the effective diffusion coefficient,  $\varepsilon_p$  and  $\tau$  represent the microporosity and tortuosity factor, respectively, for carbon membranes. Therefore, the flux for component  $i$  ( $J_i$ ) can be described as follows [5],

$$J_i = \frac{\varepsilon_p \Delta p}{\tau R T L} D_0 \exp\left(\frac{-E_{a,i}}{RT}\right) \quad (6.2)$$

where  $E_{a,i}$  is the activation energy for diffusion in the molecular sieving process for HFCMs,  $D_0$  may be expressed as [6],

$$D_0 = e\lambda^2 \frac{kT}{h} \exp\left(\frac{S_a}{R}\right) \quad (6.3)$$

Combining eq. 6.2 and eq. 6.3, the permeability can be calculated by

$$P_i = \frac{\varepsilon_p e \lambda^2 k}{\tau R h} \exp\left(\frac{S_a}{R}\right) \exp\left(\frac{-E_{a,i}}{RT}\right) \quad (6.4)$$

Suda et. al reported that the activation energy and activation entropy were correlated linearly with kinetic diameter,  $d_k$  and Lennard-Jones well depth,  $\varepsilon/k$  [7]. Therefore, we assumed:

$$E_a = a_1 d_k + b_1, \quad S_a = a_2 \varepsilon / k + b_2 \quad (6.5)$$

Substituting eq. 6.5 into eq. 6.4 and making logarithm for both sides, the equation (6.4) can be modified as,

$$\ln P = c + \frac{-a_1}{RT} d_k + \frac{a_2}{R} \varepsilon / k \quad (6.6)$$

where  $a_1$ ,  $a_2$ , and  $c$  are the constants. Keeping the temperature constant (303K), and plotting the  $\ln P$  versus  $d_k$  and  $\varepsilon/k$ , the corresponding result for HFCM-2 was shown in figure 6.4. The following regression equation was obtained based on the experiment data:

$$\ln P = 25.93 - 67.73 d_k + 0.011 \varepsilon / k \quad (6.7)$$

The negative coefficient of parameter,  $d_k$ , represents that the larger gas molecule kinetic diameters has lower permeability through this carbon membrane. Moreover, eq. 6.7 also indicates that the kinetic diameter is more important due to the larger absolute value comparing to Lennard-Jones well depth, which means that diffusion is dominated by a molecular sieving process and sorption has a relative small influence.

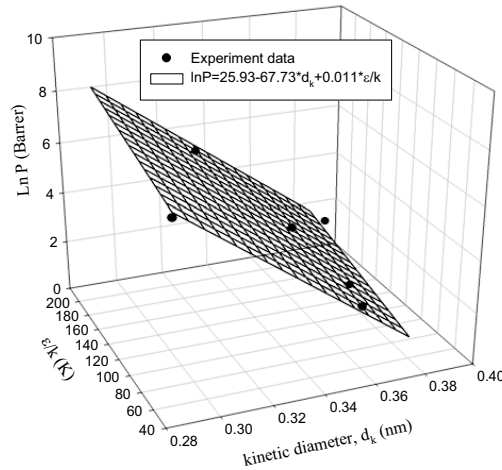


Fig. 6.4 Permeability versus kinetic diameter and Lennard-Jones

## 6.4 Optimization of carbonization parameters

The carbon membranes were prepared by controlling the carbonization conditions. Since many parameters such as purge gas, final temperature, heating rate and soak time, will affect the carbon membrane properties, these parameters need to be optimized in order to produce the high performance carbon for the specific applications.

### 6.4.1. Carbonization condition investigation

The carbon membrane were prepared by controlling the carbonization condition at different final temperatures while keeps the other parameters as constant i.e. CO<sub>2</sub>-4K/min-2h. The carbon membrane performances were tested by single gas of CO<sub>2</sub> and N<sub>2</sub>, and the results were shown in Fig. 6.5. The increasing of final temperature could result to an increase of gas permeance, but decrease of the selectivity. This could be caused by the formation of a much more open structure at higher temperature. In literature it has been reported the influences of carbonizing atmosphere, flow rate of purge gas, heating rate, final thermal temperature and soak time on the carbon membrane properties [8-11], To the knowledge of the authors of the current paper, there has, however, not been reported a systematic approach for optimization of carbonization conditions as presented in the current work.

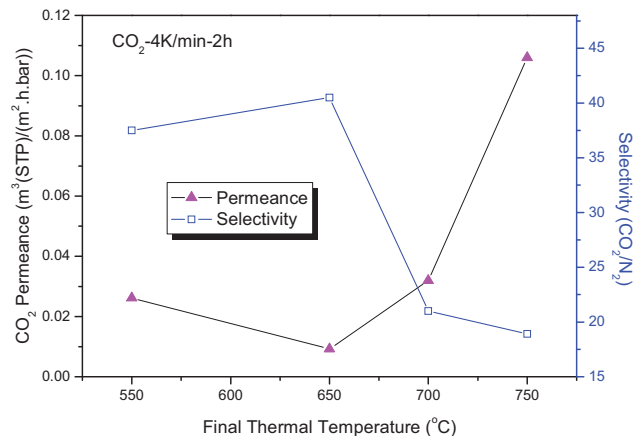


Fig. 6.5 Dependence of CO<sub>2</sub> separation performance on the final carbonization temperature at a constant procedure of CO<sub>2</sub> - 4 K/min - 2 h

### 6.4.2. Orthogonal experimental design and results

In order to investigate the carbonization parameter systematically and reduce the number of experiments but still keep sufficient information, the statistical analysis

method with OED was applied to study the influences of carbonization parameter on the transport properties of carbon membranes. The carbonization parameters of purge gas, heating rate, final temperature and final soak time were examined. Table 6.9 gives the OED's factors and levels of the carbonization protocol for fabrication of HFCMs. A  $L_4^3$  orthogonal experimental design was generated by Statistical Product and Service Solutions (SPSS) software and shown in Table 6.10. A total of nine and four batches of carbon membranes were prepared, named as HFCM1-HFCM13. Cases A and B were only used as simulation and prediction.

Table 6.9 The factors and levels for orthogonal experimental design

Level	Purge gas	Heating rate (K min <sup>-1</sup> )	Final temperature (K)	Final soak time (h)
1	Vacuum	1	823	0
2	Nitrogen	2	923	2
3	Carbon dioxide	4	1023	4

Table 6.10 Experimental design

No.	Purge gas	Heating rate (K min <sup>-1</sup> )	Final temperature (K)	Final soak time (h)	Carbon membranes
1	Vacuum	2	923	2	HFCM-1
2	Nitrogen	1	1023	2	HFCM-2
3	Nitrogen	4	923	0	HFCM-3
4	Nitrogen	2	823	4	HFCM-4
5	Carbon dioxide	4	823	2	HFCM-5
6	Carbon dioxide	1	923	4	HFCM-6
7	Vacuum	1	823	0	HFCM-7
8	Vacuum	4	1023	4	HFCM-8
9	Carbon dioxide	2	1023	0	HFCM-9
10(a)	Vacuum	1	1023	0	HFCM-10
11(a)	Vacuum	2	1023	0	HFCM-11
12(a)	Nitrogen	1	1023	0	HFCM-12
13(a)	Vacuum	1	823	4	HFCM-13
14(b)	Nitrogen	4	823	2	A
15(b)	Carbon dioxide	4	923	4	B

a: Holdout, b: Simulation

### 6.4.3. Analysis for OED

The single gas tests were executed at 30 °C with a feed pressure of 2bar for all prepared carbon membranes. The resulting membrane performances are shown in Fig. 6.6. As can be seen, the results for the carbonized cellulosic-based membranes are for most part of the experiments well above the polymeric precursor (DCA) with respect to selectivity and also permeability, although not yet above the Robeson upper bound. By inclusion of metal salts in the matrix, the separation performance may be lifted above the mentioned upper bound [12]

A statistical analysis method of conjoint analysis in SPSS software was employed to conduct the experimental data. The conjoint procedure is used to estimate the utility (part worth) of the contribution for each factor's level. Two subjects of permeability and selectivity for the prepared HFCMs were used to estimate the membrane performances. The importance for each factor was calculated separately for each subject, and then averaged. The model relationship coefficient was estimated by Pearson's R and Kendall's tau values (0.97 and 0.83 respectively), which indicates that it keeps good consistency between the estimated preferences and experiment results. The Kendall's tau for the holdout experiments displays 0.67, which is only used to check on the validity of the utilities.

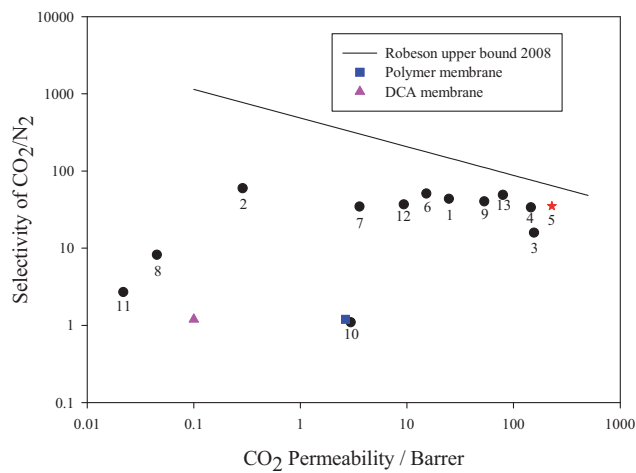


Fig. 6.6 Single gas permeation test results for the OED experiments at 30 °C and 2bar (●) carbon membranes, (▲) deacetylated cellulosic precursor, (■) polymer membrane (CA fibers), and solid line corresponds to upper bound 2008

Table 6.11 shows the utilities (part-worth) for each factor level and averaged importance scores for all factors. Higher utility values indicate greater preference. Therefore, the importance for these four factors is sorted as follows:

Purge gas > Final temperature > Heating rate > Final soak time

So the parameter of *purge gas* will greatly affect the carbon membrane performances, and the parameter of *final soak time* effect has relatively little effect. The optimal carbonization condition of CO<sub>2</sub>-823K-4K/min -2h was hence obtained. Therefore, the CO<sub>2</sub> was used as the most effective purge gas for preparation of cellulose derived carbon membranes. Since the utilities are all expressed in a common unit, they can be added together to give the total utility of any combination. Table 6.12 gives a simple comparison for the three combinations of different factor levels for the carbonization conditions. The purge gas of carbon dioxide shows the highest score comparing to the vacuum and nitrogen, which indicates the carbonization using a purge gas of carbon dioxide can obtain a higher performance carbon membrane. The results indicate that the carbon membranes prepared from condition 3 have better performance than that from conditions 1 and 2.

Table 6.11 Utilities and averaged importance scores for different factors

Factor	Level	Utility	Average importance scores (%)
Purge gas	Vacuum	-2.333	36.1
	Nitrogen	0.970	
	Carbon dioxide	1.364	
Heating rate (K min <sup>-1</sup> )	1	0.364	21.9
	2	0.727	
	4	1.091	
Final temperature (K)	823	1.000	22.5
	923	0.061	
	1023	-1.061	
Final soak time (h)	0	-0.545	19.5
	2	1.121	
	4	-0.576	

As already stated in chapter 5, the real power of conjoint analysis is the ability to predict preference for product profiles that were not rated by the subjects. Based on the conjoint analysis results of orthogonal experiment design, one could predict carbon membrane performances which should be preferred using other carbonization conditions which are not investigated here within the level's range of each factor. These are here referred to as the simulation cases A and B, and the simulation results from using the SPSS

software are given in Table 6.13. with reference to the two subjects (permeability and selectivity) used in this study, all three models of Maximum utility, BTL and Logit indicated that simulation case A would be preferred. In order to validate this simulation result, the carbon membranes were carbonized under both these conditions. The membrane performances tested and illustrated in Table 6.13. It can be found that the permeability for case A is around two times higher than that of case B, and the selectivity is only a little bit lower than that of case B, which kept the consistency with the simulation results by conjoint analysis; higher score corresponds to higher performance. Therefore, the prediction results based on conjoint analysis could be well used as guide for the preparation of high performance carbon membranes.

Table 6.12 An example for different carbonization conditions

Case	Utility				Total utility
	Purge gas	Heating rate	Final temperature	Final soak time	
1	Vacuum (-2.333)	2K min <sup>-1</sup> (0.727)	823k (1.000)	2h (1.121)	4.788
2	Nitrogen (0.970)	2K min <sup>-1</sup> (0.727)	823k (1.000)	2h (1.121)	8.091
3	Carbon dioxide (1.364)	2K min <sup>-1</sup> (0.727)	823k (1.000)	2h (1.121)	8.458

Table 6.13 Simulation and experimental results by conjoint analysis

Case	Score	Preference probabilities from simulations			Experimental results		
		Maximum utility	BTL	Logit	Permeability of CO <sub>2</sub> (Barrer)	Selectivity of CO <sub>2</sub> /N <sub>2</sub>	Average weight loss (%)
A	8.455	90.9%	57.2%	85.9%	96.6	36.9	73.5
B	6.212	9.1%	42.8%	14.1%	45.2	45.4	75.9

## 6.5 Characterization by general techniques

Two batches hollow fibers (HF-A and HF-B) were prepared from different spinning conditions include the spinneret dimension, air gap, flow rate of dope and bore fluid, and coagulation bath temperature as listed in Table 6.14. The spun fibers were placed in the fresh water bath overnight, and subsequently soaked in a 10% glycerol solution for solvent exchange to remove the residual NMP from the fibers. The deacetylation of the fibers were then executed with a 0.075M NaOH (solvent: 96% ethanol) solution for 2h to obtain the precursors of DHF-A and DHF-B separately. The hollow fiber carbon membranes of HFCM-A and HFCM-B were fabricated via the controlled carbonization

procedure with CO<sub>2</sub> purge gas, a heating rate of 4 °C/min, a final thermal temperature of 550 °C and a final soak time of 2h from the precursors of DHF-A and DHF-B, respectively.

Table 6.14 Characteristics of hollow fibers with different spinning conditions

Hollow fibers	Spinneret ID/OD (mm)	Dope flow rate (ml min <sup>-1</sup> )	Bore flow rate (% of dope)	Air gap (mm)	Coagulation bath temp. (°C)
HF-A	0.5 / 0.7	2.2	40	25	50
HF-B	0.1 / 0.2	0.9	140	15	50

### 6.5.1. TGA and SEM

The weight loss for the precursors during the carbonization process was assessed by TGA, as shown in Fig. 6.7. About 70% weight loss was found following the final temperature up to 550 °C.

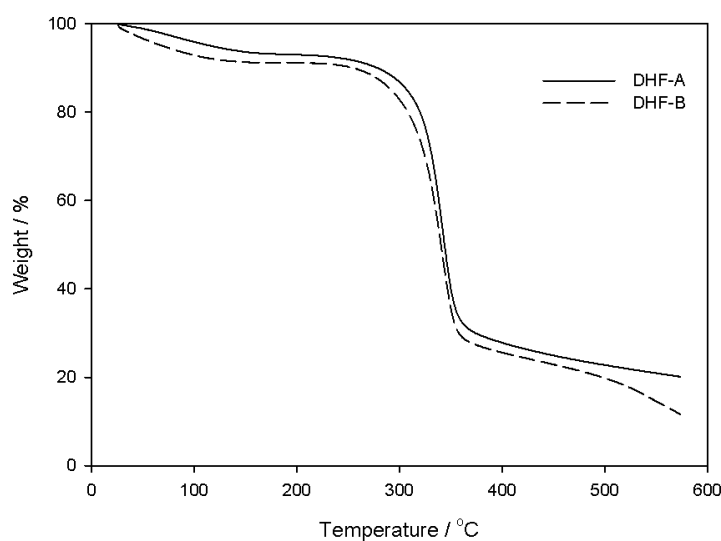


Fig. 6.7 Weight loss of precursors from TGA analysis

SEM is used to characterize the structure and morphology of the materials, and Figs. 6.8 - 6.10 show the cross section images of the precursors and the carbon membranes. Upon examination of SEM images, it was concluded that the HFCMs form a symmetric structure. The outer diameter and wall thickness of the carbon membranes are much smaller comparing to the precursors due to the shrinkage of precursors in the

carbonization process, which was supported by the high weight loss based on the TGA analysis. Moreover, a representative inside structure of the polymer membrane, precursor and carbon membrane was also characterized by SEM as shown in Fig. 6.11.

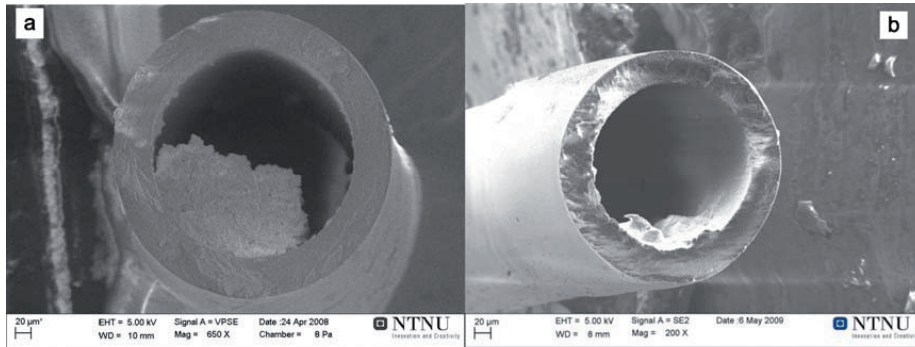


Fig. 6.8 SEM images for cross sections of the precursors (a) DHF-1, (b) DHF-2

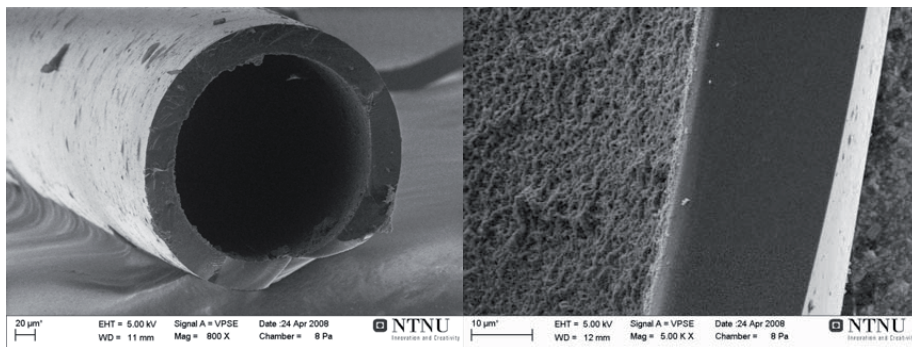


Fig. 6.9 SEM images of the cross section for carbon membrane of HFCM-A

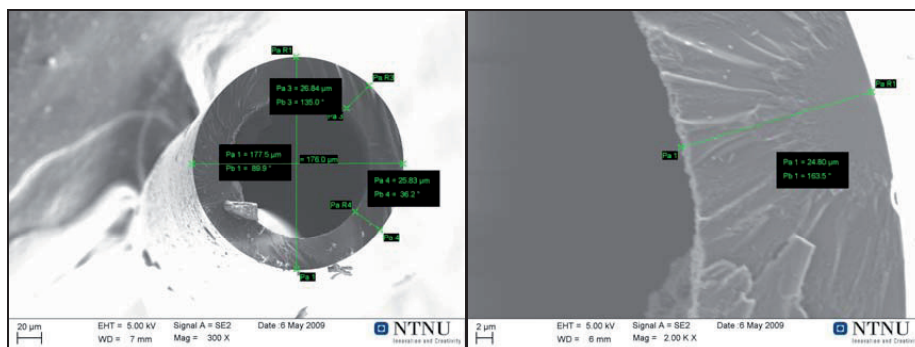


Fig. 6.10 SEM images of the cross section for carbon membranes of HFCM-B

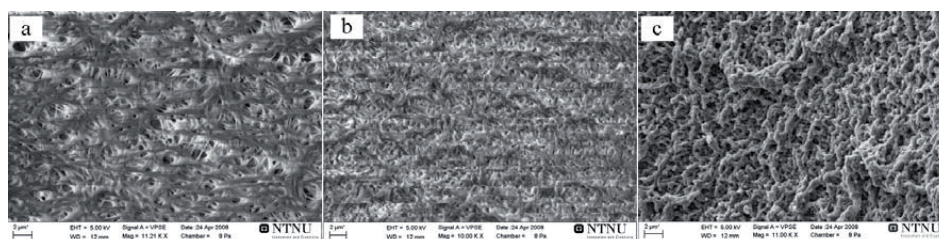


Fig. 6.11 Representative inside structures of the membranes, (a) Hollow fiber, (b) Deacetylated precursor, (c) Carbon membrane

### 6.5.2. FTIR

The FTIR spectra of deacetylated cellulosic precursor and carbon membrane HFCM-A are shown in Fig. 6.12. For precursor, the characteristic absorption peaks of  $1030\text{cm}^{-1}$ ,  $1230\text{cm}^{-1}$ ,  $1740\text{cm}^{-1}$  attribute to the ether group ( $\nu_{C-O-C}$ ), acetyl ester group ( $\nu_{CH_3-C=O}$ ) and carbonyl group ( $\nu_{C=O}$ ) of CA respectively. The C-H bond stretching ( $2950\text{cm}^{-1}$ ) and hydroxyl group ( $3400\text{cm}^{-1}$ ) are also shown in the precursor spectra. The characteristic peak  $1665\text{cm}^{-1}$  attributes to the carbonyl group of PVP which is the additive in the precursor. After carbonization and heat treatment, the intensities of most peaks decreased or even disappeared due to the decomposition and break down of the chemical groups as mentioned above, which could be caused by the release of gases such as  $\text{CO}$ ,  $\text{CO}_2$ ,  $\text{H}_2$  as reported by Wu et. al [3]. For the carbon membranes, the new characteristic absorption peaks were found at  $2350\text{cm}^{-1}$  and  $670\text{cm}^{-1}$ , which contribute to the  $\text{CO}_2$  absorbed in carbon matrix and the aromatic =C-H out of plane deformation as reported by Tin [13].

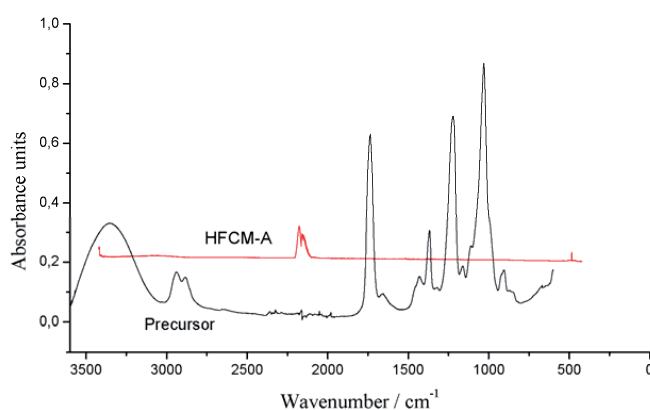


Fig. 6.12 FTIR spectra for the precursor and HFCM-A

### 6.5.3. XRD

The XRD patterns of the carbon membranes were shown in Fig. 6.13. The average d-spacing ( $d_{002}$ ) values were calculated based on the Bragg's equation ( $n\lambda=2d\sin\theta$ ), determining the interlayer distance of carbon matrix. The d-spacing is considered as an effective diffusion path for gas molecules through the carbon membranes, which is used to evaluate the membrane microstructure [14]. The d-spacing values for HFCM-A and HFCM-B were found to be 4 Å and 4.2 Å with the broad asymmetric peaks located in  $2\theta = 21.1^\circ$  and  $22.2^\circ$ , respectively, which is larger than the typical graphitic and turbostratic d-spacing of 3.4 - 3.8 Å. The large difference, which exceeds 4 Å, characterizes linearly organized aliphatic carbon with  $sp$  hybridization [15], which indicates that the carbon membrane forms an amorphous carbon matrix with a mixture of  $sp^2$  and  $sp$  carbon components. The XRD patterns of the carbon membranes exhibit another very weak peak around  $2\theta = 43^\circ$  with a d-spacing value of 2.1 Å, which is also the characteristic peak of the (100) plane in graphite.

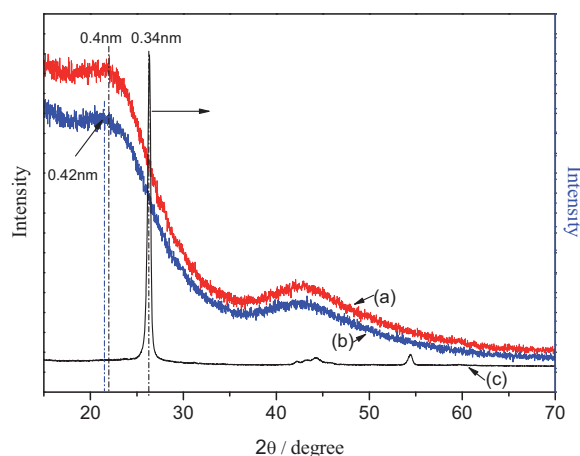


Fig. 6.13 XRD Patterns of (a) HFCM-A, (b) HFCM-B and (c) graphite

### 6.5.4. Element analysis

The results for the carbon membranes obtained from the element analysis are presented in Table 6.15. It is evident that the carbon membranes have quite high carbon content. Most of hydrogen and nitrogen atoms were burn out during carbonization, which resulting to the small amount of hydrogen and quite few nitrogen left in carbon membranes. There is, however, still some oxygen left in the carbon matrix, additionally

some CO<sub>2</sub> may also be adsorbed in the carbon membrane due to the CO<sub>2</sub> as purge gas for the carbonization procedure.

Table 6.15 Results from element analysis for carbon membranes

Samples	Element content (%)			
	C	H	N	O
HFCM-A	86.03	3.48	0.14	7.37
HFCM-B	87.35	3.48	0.11	6.34

## 6.6 Gas sorption

The CO<sub>2</sub> and N<sub>2</sub> gravimetric sorption onto the carbon membrane were executed by Robutherm magnetic suspension balance (MSB). The equilibrium adsorption data were used to estimate the micropore volume and average pore size of the carbon matrix. The kinetic measurements were conducted to investigate the kinetic rate constants when gas transport through the carbon membranes.

### 6.6.1. Structure characterization

The adsorption data of CO<sub>2</sub> and N<sub>2</sub> onto the carbon membranes were obtained at 298 K and medium pressure as shown in Fig. 6.14. A type I equilibrium isotherm was found according to the IUPAC definition for adsorption isotherms.

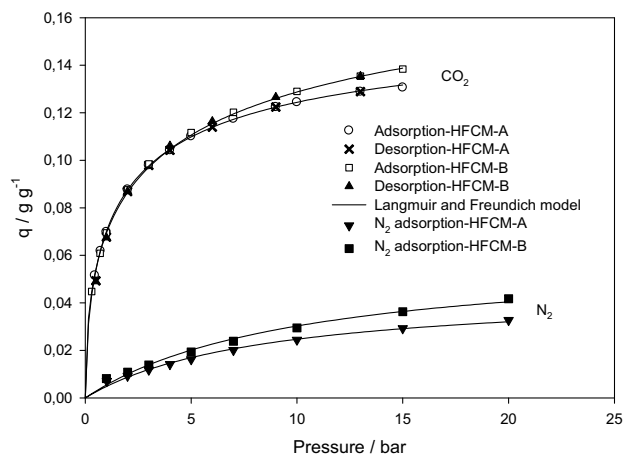


Fig. 6.14 Equilibrium adsorption isotherm at 298 K on HFCM-A ((○) CO<sub>2</sub> adsorption; (×) CO<sub>2</sub> desorption; (▼) N<sub>2</sub> adsorption) and HFCM-B ((□) Adsorption; (▲) CO<sub>2</sub> desorption; (■) N<sub>2</sub> adsorption), and the solid line corresponds to the Langmuir-Freundlich model

The Langmuir-Freundlich model was used to fit the experimental data, and described as follows:

$$q = \frac{bq_m p^{1/n}}{1 + bp^{1/n}} \quad (6.8)$$

where  $q$  is the adsorption amount at pressure ( $p$ ),  $b$  and  $q_m$  are the Langmuir affinity parameter and the maximum adsorption amount, and  $n$  is the Langmuir-Freundlich coefficient. A high coincidence was found between the Langmuir-Freundlich model fitting and the adsorption equilibrium data as can be seen from Fig. 6.14. Table 6.16 summarizes the adsorption equilibrium parameters for the carbon membranes.  $N_2$  has lower Langmuir adsorption parameter ( $b$ ) which indicates a relative weak adsorption in relation to  $CO_2$ . The coincidence of  $CO_2$  adsorption and desorption for both carbon membranes indicates a reversible  $CO_2$  adsorption process at 298 K as shown in Fig. 6.14. In order to determine the sample micropore volume, it is necessary to know the density of adsorbed  $CO_2$  in the carbon membrane. The values of density that can be used at this temperature fall within the range of 0.7-1.03 g/cm<sup>3</sup> [16]. A 0.85 g/cm<sup>3</sup> was used in this work. The Dubinin-Radushkevitch (DR) equation was used to fit the  $CO_2$  isotherm adsorption data as follows:

$$\frac{w}{w_0} = \exp\left(-\left(\frac{RT \ln(p_0/p)}{\beta E_0}\right)^2\right) \quad (6.9)$$

where  $w$  is the volume adsorbed at a pressure  $p$ ,  $w_0$  is the micropore volume of carbon membrane,  $E_0$  is the adsorption activation energy dependent on the pore structure, and  $\beta$  is the affinity coefficient that is the characteristics of the adsorption capacity used in this case is 0.35 [16]. For the non-ideal gas of  $CO_2$  in high pressure, the fugacity was used instead of pressure,  $(RT \ln(f_0/f))^2$ . The relative fugacity used in the isotherms is the fugacity divided by the saturation fugacity of 42 bar for  $CO_2$  at 298 K [16]. Fig. 6.15 shows the characteristic curves of the carbon membranes (plots of  $\ln(w)$  versus  $(RT \ln(f_0/f))^2$ ), and the similar slopes at high and low pressures indicate that the carbon membranes have quite homogeneous porosity. Moreover, the average micropore width can be roughly estimated from Stoeckli equation when the DR equation applied [17].

$$L_0 = \frac{10.8(nm \cdot kJ \cdot mol^{-1})}{E_0 - 11.4(kJ \cdot mol^{-1})} \quad (6.10)$$

The sample true density ( $\rho_s$ ) was determined by buoyancy measurements with non-adsorbable gas molecules of helium. The experimental data and linear fitting were illustrated in Fig. 6.16. The decrease (negative slope) of the measured mass of sample and sample container with increase pressure (density) of the gas phase is due to the buoyancy acting. The true densities for the samples were obtained according to the

description in Section 4.2.11. Based on the sample micropore volume and true density, the bulk density ( $\rho_b$ ) of the sample was calculated using the following equation:

$$\frac{1}{\rho_b} = \frac{1}{\rho_s} + w_0 \quad (6.11)$$

The structural parameters for the carbon membranes were measured and estimated based on the above expression, and summarized in Table 6.17. The HFCM-B shows a lower density than that of HFCM-A due to the higher weight loss during the carbonization process, which was proved from the TGA results in Fig. 6.7. A relative large micropore volume was also found for HFCM-B compared to the HFCM-A.

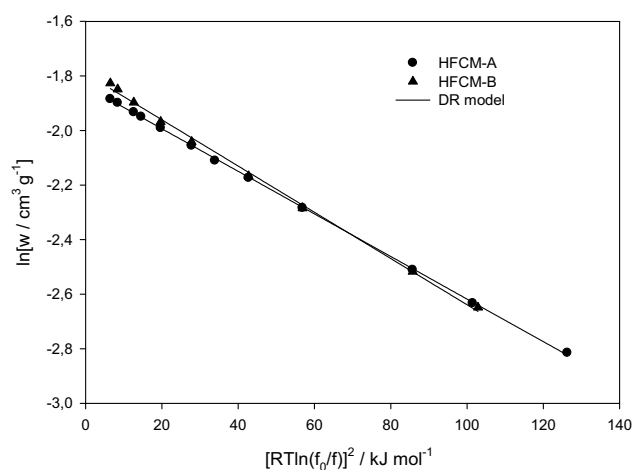


Fig. 6.15 Characteristic curves for HFCM-A (●) and HFCM-B (▲) by CO<sub>2</sub> adsorption at 298 K, solid line corresponds to the DR model

Table 6.16 Equilibrium isotherm parameters for CO<sub>2</sub> and N<sub>2</sub> on HFCMs at 298K

Samples	T (K)	Gas species	Langmuir-Freundlich model			Reference
			b (bar <sup>-1</sup> )	q <sub>m</sub> (g g <sup>-1</sup> )	n	
HFCM-A	298	CO <sub>2</sub>	0.73	0.17	1.65	This work
		N <sub>2</sub>	0.12	0.046	1	
HFCM-B	298	CO <sub>2</sub>	0.48	0.21	2	This work
		N <sub>2</sub>	0.098	0.061	1	
CMSM2	303	CO <sub>2</sub>	0.93	0.15	1.34	[18]

Table 6.17 Structural parameters of carbon membranes

Carbon membranes	$\rho_s$ (g cm <sup>-3</sup> ) <sup>a</sup>	$\rho_b$ (g cm <sup>-3</sup> )	DR model		$L_0$ (Å)	Reference
			$W_0$ (cm <sup>3</sup> g <sup>-1</sup> )	$E_0$ (kJ mol <sup>-1</sup> )		
HFCM-A	1.53	1.24	0.15	32.2	5.2	This work
HFCM-B	1.38	1.12	0.17	30.8	5.6	
CMSM1	1.6	1.1	0.28	31.6	5.5	[18]
CM-V823	-	-	0.16	22.75	-	[19]

<sup>a</sup> Density of carbons is 1.3-1.8 g/cm<sup>3</sup> as compared to 2.2 g/cm<sup>3</sup> for graphite [20]

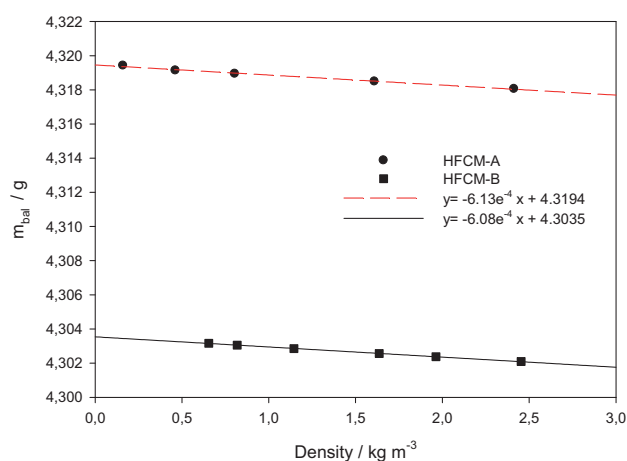


Fig. 6.16 Buoyancy measurements with helium for HFCM-A (●) and HFCM-B (■) at 298K and constant feed flow rate of 100 ml/min, solid lines correspond to the linear regressions

### 6.6.2. Kinetic measurements

The experimental kinetic data of CO<sub>2</sub> adsorption onto the carbon membranes at 298 k and 1 bar were shown in Fig. 6.17. Due to the lack control of high pressure measurements, a desired low pressure of 1bar was set for the all kinetic adsorption experiments. CO<sub>2</sub> with different flow rate of 100, 200 and 300 ml/min were fed into the sorption system to determine the actual kinetic curves. The linear driving force (LDF) model was introduced to fit the experimental data, which has been well used for the determination of mass transfer coefficient of different gases on various materials [21-22]. The LDF model is described as follows:

$$\frac{q_t}{q_e} = 1 - \exp(-kt) \quad (6.12)$$

where the  $q_t$  and  $q_e$  are the gas sorption amount onto the carbon matrix in time  $t$  and the equilibrium,  $k$  is the mass transfer coefficient or the simplified kinetic rate constant ( $s^{-1}$ ). The LDF model is used to fit the experimental data and obtain the kinetic rate constant. As summarized in Table 6.18, the kinetic rate constants for the HFCM-A and HFCM-B are compared to several literature results of Zeolite 13X [23] and carbon membrane of CMSM3 [18]. The higher kinetic rate constant of HFCM-B comparing to the HFCM-A is associated with its more open structure due to the larger average pore size as given in Table 6.17.

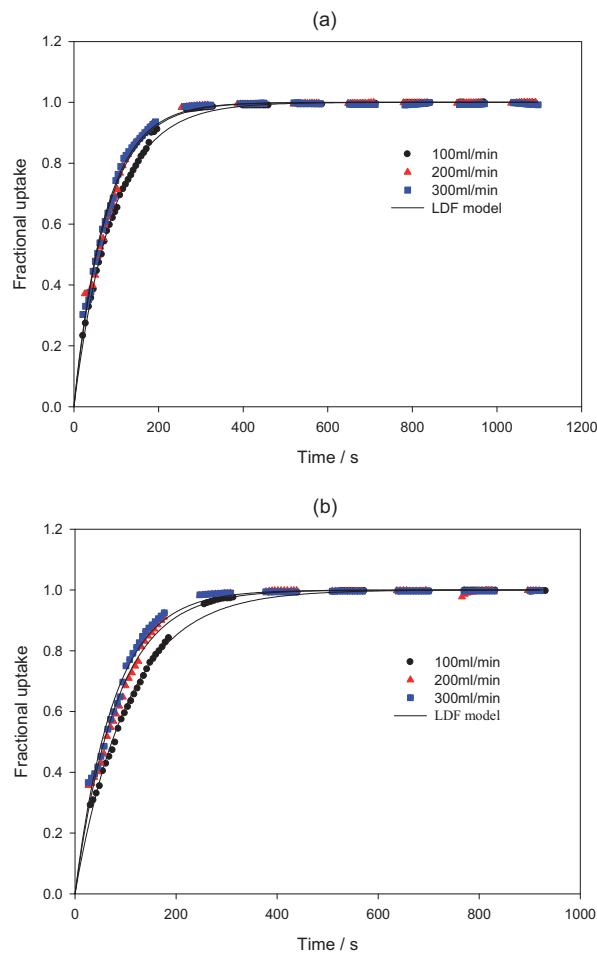


Fig. 6.17 Fractional uptake of CO<sub>2</sub> adsorption on HFCM-A (a) and HFCM-B (b) at 298K and 1bar with different flow rates: (●) 100 ml/min; (▲) 200 ml/min; (■) 300 ml/min, solid lines correspond to the LDF model

Table 6.18 Kinetic rate constant for carbon membranes and benchmark materials

Materials	$k (\times 10^{-2} \text{ s}^{-1})$	References
HFCM-A	1.10 ~ 1.34	This work
HFCM-B	0.95 ~ 1.31	This work
13X	1.23	[23]
CMSM3*	0.43	[18]

\*: calculated from the data at pressure 0.048 bar and temperature 303 K

## 6.7 Single gas tests

In order to characterize the separation performance for the prepared carbon membranes, the single gas permeation tests were conducted at different conditions such as various temperatures, feed pressures, and humidity. The aging and durability of the carbon membranes were also investigated over long time.

### 6.7.1. Effects of temperature

The gas permeabilities of the carbon membrane HFCM-A were tested with various single gases ( $\text{CO}_2$ ,  $\text{N}_2$ ,  $\text{CH}_4$  and  $\text{O}_2$ ). The testing process is illustrated in Appendix A. Fig. 6.18 indicates the dependency of permeability values of different gases on the temperature in the range of 30 - 70 °C, and at constant feed pressure of 2 bar. Moreover, the HFCM-B was also tested and the results are represented in Appendix F.

The apparent transport activation energy,  $E_a$ , and  $P_0$  ( $P = P_0 \exp(-E_a/RT)$ ) can be obtained from these data with varying temperature. Fig. 6.18 shows the logarithmic Arrhenius plot with  $\ln P$  as a function of  $1000/T$  [24], and  $E_a$  was obtained from the slope of the respective curves, which are shown in Table 6.19. The activation energy is an indicator of the probability of a molecular passing a constriction, thus, the lower activation energy relates to a higher permeability. For the large  $E_a$ , the larger effect temperature will have on the permeability. This can be seen from Fig. 6.18 where the permeabilities of the other gas molecules increase faster with increasing temperature than that of  $\text{CO}_2$ . It can be concluded that the transport can be enhanced with increase of temperature, but slightly decrease the  $\text{CO}_2$  selectivity of carbon membranes. Moreover, Suda et. al reported that the activation energy were correlated linearly with kinetic diameter [7]. Therefore, we assumed:

$$E_a = a_1 d_k + b_1 \quad (6.13)$$

A linear regression between  $E_a$  and  $d_k$  was also conducted, as shown in Fig. 6.19. The high consistency between the experiment results and the assumption validates the diffusion is dominating diffusion is dominated by a molecular sieving process and sorption has a relative small influence for carbon membrane as described in Section 6.3.

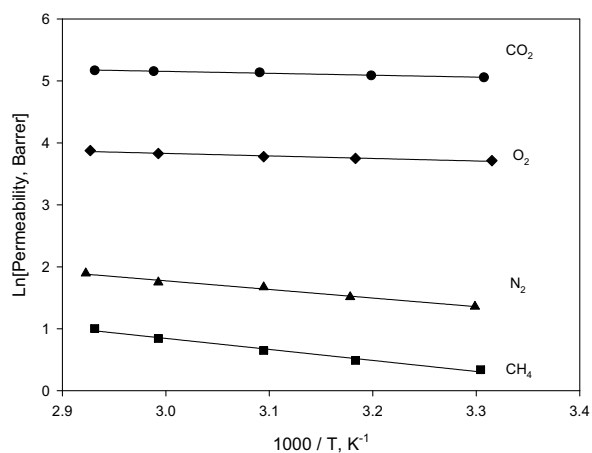


Fig. 6.18 Dependency of gas permeabilities on temperature for HFCM-A at feed pressure 2 bar

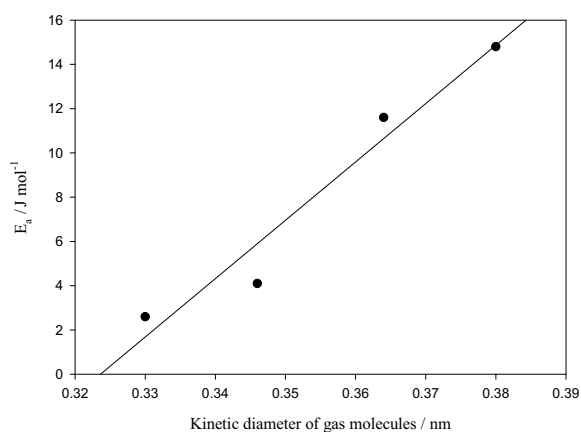


Fig. 6.19 Relationship between activation energy and gas molecule kinetic diameter

Table 6.19 Kinetic parameters for gas permeation through HFCM-A

Gas molecules	$d_k$ (nm)	$\epsilon/k$ (K)	$E_a$ (kJ mol <sup>-1</sup> )	$P_0$ (Barrer)
CO <sub>2</sub>	0.33	195.0	2.6	437.6
O <sub>2</sub>	0.346	107.0	3.4	156.6
N <sub>2</sub>	0.364	71.4	11.6	382.3
CH <sub>4</sub>	0.38	136.0	14.8	483.7

### 6.7.2. Effects of pressure

Fig. 6.20 presents the results for gas permeability of carbon membrane (HFCM-B) measured at 303 and 323 K while the feed pressure varied from about 1.5 bar up to 6 bar. The permeability of both gas species decreases with increasing feed pressure in this narrow region. The strongly adsorbed CO<sub>2</sub> shows a more significant decrease of permeability with pressure compared to the N<sub>2</sub>, which reflecting a more strong concentration dependence for the diffusion coefficient. For N<sub>2</sub>, the adsorption interaction is much weaker and the permeability values are less pressure dependent.

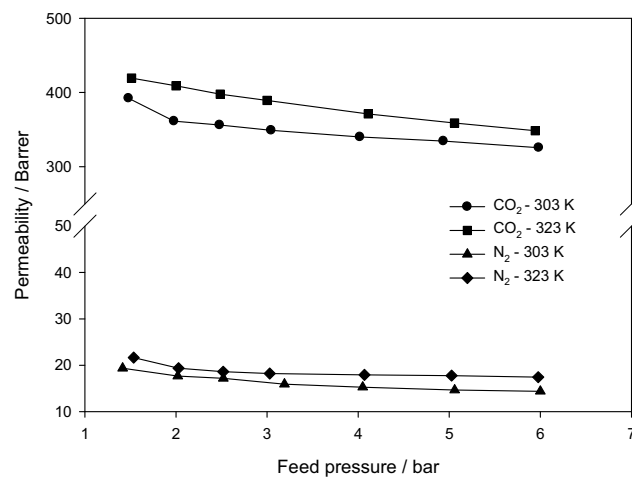


Fig. 6.20 Dependency of the feed pressure on the carbon membrane (HFCM-B) performance

### 6.7.3. Effects of humidity

The significant effects of humidity (i.e. water vapor) on the carbon membrane (HFCM-A) separation performances are also investigated. The gas permeability will decrease with increasing the humidity as can be seen from Fig. 6.21, which might be caused by the pore blocking due to the formation of hydrogen bonds between the water and carbon matrix. However, after being exposed to water vapor, the gas permeability values can be basically recovered to initial permeability values by thermal regeneration (e.g. feed N<sub>2</sub> at 100 °C overnight).

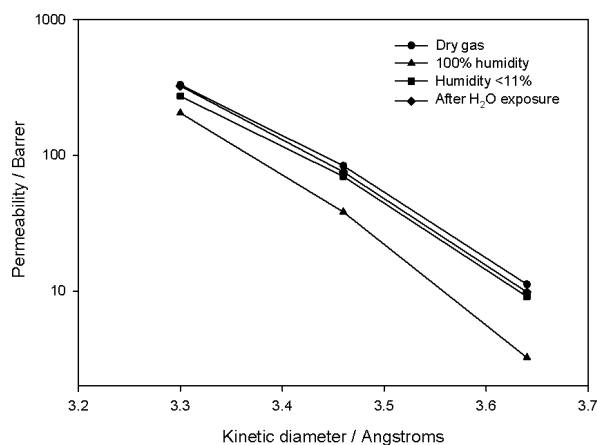


Fig. 6.21 Single gas permeability with different humidity at 303K and feed pressure of 2bar

#### 6.7.4. Aging and durability tests

A challenge for most membranes, are often the lack of long-term stability; this relates both to organic (polymeric) and inorganic (ceramic, CMS) membranes. In order to investigate the durability of carbon membrane, and long term stability (aging) tests were conducted. The HFCM-A was statically exposed to laboratory air (i.e. not in any way protected over time), and Fig. 6.22 shows the aging test results. From this figure, we can find that the permeability values decreased for both gases over ~7 months, especially for CO<sub>2</sub>. No regeneration was performed during this time. The aging may be caused by the chemisorption of O<sub>2</sub> into the carbon matrix when exposed to air. The membrane durability tests were also conducted by exposing the carbon membranes to the real flue gas steam (See Appendix B). Some regeneration methods such as thermal, chemical and electrothermal techniques have been investigated by several [25-27], these are not discussed here.

### 6.8 Gas mixture tests

The single gas tests are mainly used to characterize the ideal separation performance for the carbon membranes. However, the separation properties will be affected by the presence of other penetrants in a gas mixture. The gas transports in gas mixture are different from that in single gas, especially for the existing of strong absorbable gas like CO<sub>2</sub> (See Appendix C: Carbon membrane tests at ITM-CNR). Hence, the gas mixture tests were executed in different operating condition in order to understand their effects.

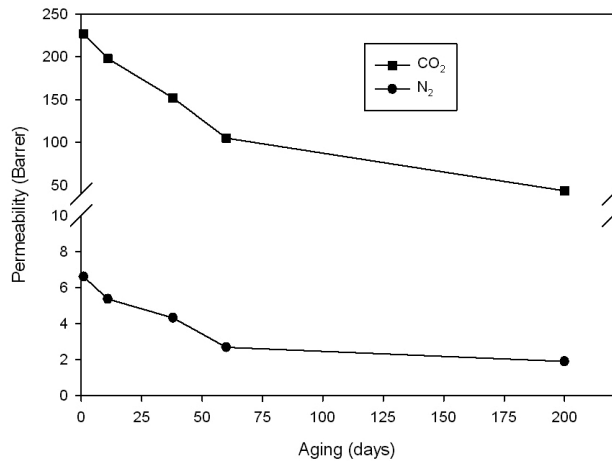


Fig. 6.22 Aging of HFCM-A by exposure to laboratory atmosphere at room temperature

## 6.9 Gas mixture tests

The single gas tests are mainly used to characterize the ideal separation performance for the carbon membranes. However, the separation properties will be affected by the presence of other penetrants in a gas mixture. The gas transports in gas mixture are different from that in single gas, especially for the existing of strong absorbable gas like CO<sub>2</sub> (See Appendix C: Carbon membrane tests at ITM-CNR). Hence, the gas mixture tests were executed in different operating condition in order to understand their effects.

### 6.9.1. CO<sub>2</sub> separation from synthetic flue gas

CO<sub>2</sub> separation from the synthetic flues gas (15% CO<sub>2</sub> - 4% O<sub>2</sub> - 81 %N<sub>2</sub>) and (10% CO<sub>2</sub> - 90% N<sub>2</sub>) by the carbon membranes (HFCM-B) were systematically investigated. In order to optimize the process operating conditions, the fractional factorial design combined with statistical analysis was employed to investigate the influences of the different operating parameters such as temperature, feed pressure, retentate flow rate and CO<sub>2</sub> feed composition, as presented in Table 6.20. A total of eight batch experiments were conducted, and the test results are given in Table 6.21. Based on the experimental data, the importance of the various operating parameters was evaluated by hypothesis testing. The type I error, if a null hypothesis is rejected when it is true and the probability of a type I error is  $\alpha$ . The value of this probability is usually called significance level of the test. The  $p$ -value approach has been widely used for practical application and the  $p$ -value is defined as the smallest level of significance that would lead to rejection of the null hypothesis. A commercial software Minitab<sup>®</sup> is used to execute the statistical analysis. The hypothesis testing with a significance level of

$\alpha=0.05$  is used to evaluate the importance of the operating parameters to the carbon membrane separation performances. The estimates of the parameter effects, coefficient, and the p-values are given in Table 6.22. The main effects plots are shown in Figs. 6.23 and 6.24 representing the influences of different operating parameters. The feed pressure and retentate flow rate give lower  $p$  values ( $< 0.05$ ) for both permeate flux and CO<sub>2</sub> recovery, which indicates the significant influence on the carbon membrane separation performance. Therefore, the parameter of feed pressure ( $B$ ) and retentate flow rate ( $C$ ) may control the membrane separation performances. The steeper slopes for the plots of the feed pressure ( $B$ ) and the retentate flow rate ( $C$ ) are additional proof of their significances. Moreover, the analysis results also indicate that the temperature ( $A$ ) in these ranges has only little effects on both permeate flux and CO<sub>2</sub> recovery. Due to the large  $p$  value for the CO<sub>2</sub> recovery and lower  $p$  value for the CO<sub>2</sub> permeance for the parameter ( $D$ ), the CO<sub>2</sub> feed composition will be important to meet the specific requirement of CO<sub>2</sub> flux (Productivity).

Table 6.20 The operating parameters and levels used in the factorial design

Factor	Operating parameter	High level (+1)	Low level (-1)
A	Temperature (°C)	50	30
B	Feed pressure (bar)	5	3
C	FR (ml min <sup>-1</sup> )	12	6
D	CO <sub>2</sub> feed composition	CO <sub>2</sub> / O <sub>2</sub> / N <sub>2</sub> : 15% / 4% / 81%	CO <sub>2</sub> /N <sub>2</sub> : 10% / 90%

Table 6.21 2<sup>4+1</sup> fractional factorial design and experiment results

Run order	A	B	C	D	Permeate flux (ml min <sup>-1</sup> )	Stage-cut (%)	CO <sub>2</sub> purity (%)	CO <sub>2</sub> Recovery (%)
1	-1	-1	-1	-1	0.46	7.15	72.6	51.7
2	+1	-1	-1	+1	0.696	10.4	70.5	58.9
3	-1	+1	-1	+1	1.07	13.8	76.9	70.9
4	+1	+1	-1	-1	0.746	12	63.8	76.8
5	-1	-1	+1	+1	0.865	6	74.6	29.7
6	+1	-1	+1	-1	0.586	4.9	72.7	35.8
7	-1	+1	+1	-1	0.806	6.3	75	47.2
8	+1	+1	+1	+1	1.22	9.26	76	46.8

Table 6.22 Results of statistical analysis by Minitab

Parameter	Permeate flux			CO <sub>2</sub> recovery		
	Effect	Coefficient	p-value	Effect	Coefficient	p-value
Constant	0.806	0.020	0	52.23	0.9936	0
Temperature	0.012	0.006	0.785	4.7	2.35	0.099
Feed pressure	0.309	0.154	0.004	16.4	8.2	0.004
Retentate flow rate	0.126	0.063	0.049	-24.7	-12.35	0.001
CO <sub>2</sub> feed composition	0.313	0.157	0.004	-1.3	-0.65	0.560

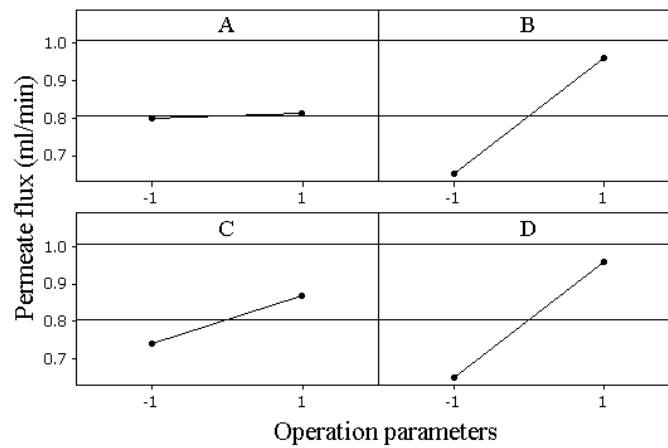


Fig. 6.23 The main influence plots by Minitab<sup>®</sup> for permeate flux, A (Temperature), B (Feed pressure), C (Retentate flow rate) and D (Feed CO<sub>2</sub> composition)

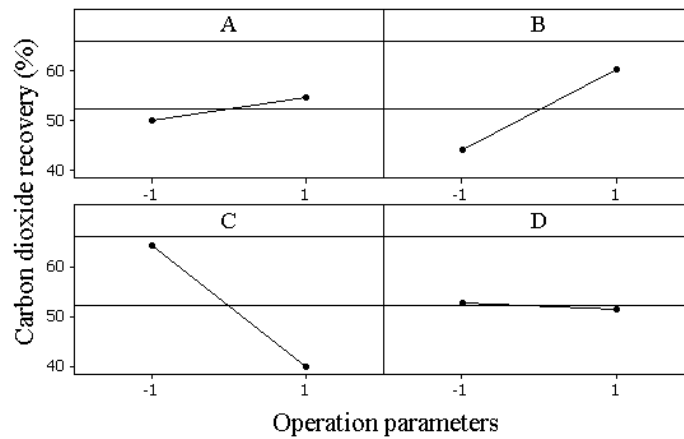


Fig. 6.24 The main influence plots by Minitab<sup>®</sup> for CO<sub>2</sub> recovery, A (Temperature), B (Feed pressure), C (Retentate flow rate) and D (Feed CO<sub>2</sub> composition)

Based on the above results, it can be concluded that the temperature has no significant effects on the separation performance within this narrow region. Moreover, for a specific application, the CO<sub>2</sub> feed concentration and feed volume flow rate are almost constant. The main operating parameter of the driving force (pressure ratio between the feed stream and permeate stream) and the flow rate in retentate (related to the stage-cut) may have significant influences on the membrane separation performances. Therefore, CO<sub>2</sub> separation from synthetic flue gas (15% CO<sub>2</sub> - 81% N<sub>2</sub> - 4% O<sub>2</sub>) using HFCM-B at different feed pressures, was also conducted. The experiments were executed at 303 K with a constant feed flow rate of 30 ml/min, while the feed pressure increase from 2 bar to 4 bar. The CO<sub>2</sub> composition in permeate and retentate, and the CO<sub>2</sub> recovery (ratio of CO<sub>2</sub> flow rate in permeate and feed stream) are given in Fig. 6.25. The CO<sub>2</sub> purity in permeate and the CO<sub>2</sub> recovery increase following the increase of the feed pressure for a given membrane area. However, a higher feed pressure will result in a higher energy demand for the compressors. Therefore, the economic cost estimation should be executed on the basis of process simulation to optimize the operating condition for the specific application and evaluate the process feasibility-this is described in Chapter 7.

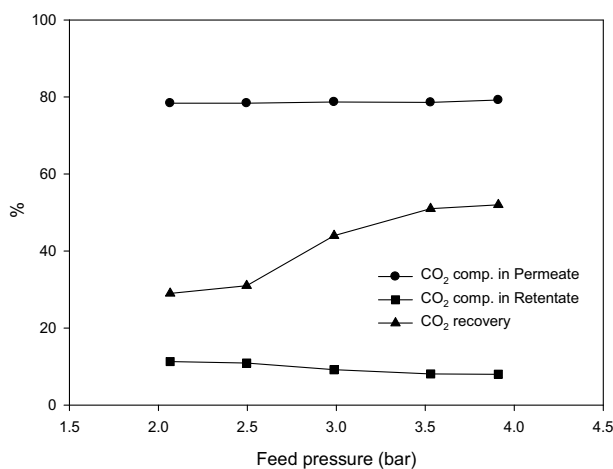


Fig. 6.25 Dependency of CO<sub>2</sub> separation performance on the feed pressure at 303 K and a feed flow rate of 30 ml/min: (●) CO<sub>2</sub> composition in permeate; (■) CO<sub>2</sub> composition in retentate; (▲) CO<sub>2</sub> recovery

#### 6.9.2. CO<sub>2</sub> separation from sythetic biogas

A module mounted with 79 HFCM-B fibers (membrane area: 86 cm<sup>2</sup>) was constructed for the testing of CO<sub>2</sub> separation from the synthetic biogas (35% CO<sub>2</sub>-65% CH<sub>4</sub>). The

gas mixture with a constant flow rate of 60 ml/min was fed into the module from the shell side with different feed pressures at 30 °C, and the results are given in Table 6.23. The stage-cut ( $\theta$ ) and CO<sub>2</sub> recovery increased with increasing feed pressure from 3 bar to 5 bar while keeping quite similar CO<sub>2</sub> purity in the permeate side.

Table 6.23 Results for CO<sub>2</sub>/CH<sub>4</sub> separation through carbon membranes at 30 °C

Feed pressure (bar)	$\theta$ (%)	Recovery (%)	CO <sub>2</sub> composition (%)		Permeability (Barrer)		Process selectivity CO <sub>2</sub> /CH <sub>4</sub>
			Permeate	Retentate	CO <sub>2</sub>	CH <sub>4</sub>	
3	9.4	25.4	94.8	28.8	321.6	9.5	33.9
4	11.8	31.9	94.9	25.4	318.1	9.2	34.6
5	14.1	38.3	94.9	25.2	284.4	8.1	35.1

## 6.10 Conclusions

Hollow fiber carbon membranes (HFCMs) were prepared from deacetylated CA precursors by controlling a multi-dwell carbonization protocol. The precursors showed a significant influence on the carbon membrane separation performances. The HFCM-2 which was fabricated from the precursor with the optimal deacetylation time of 2h, showed the best permeability for the tested gas molecules. Moreover, the membrane properties were also found to be affected greatly by the carbonization parameters. The carbonization parameters were optimized in order to obtain a high performance carbon membrane. Based on the orthogonal experimental design, an optimal carbonization procedure with CO<sub>2</sub>-823K-4K/min-2h was obtained, and the importance for the investigated carbonization parameters was sorted out with respect to their influence on carbon membrane separation performances. The order of importance was found to be: purge gas > final temperature > heating rate > final soak time. It was concluded that the purge gas was the most important parameter affecting the final carbon membrane performance, and CO<sub>2</sub> was found to be the most effective purge gas for preparation of the high performance cellulose derived carbon membranes.

The morphology and structure for the prepared carbon membranes were characterized by SEM, FTIR, XRD and element analysis. The results indicate that the carbon membranes (carbon content > 86 %) show a symmetric structure with a typical thickness of 25  $\mu\text{m}$  and d-spacing of 4.2Å. A micropore volume of 0.15 g/cm<sup>3</sup> and average pore size of 5Å were also obtained based on the gas sorption measurement.

The gas permeability of the prepared carbon membranes for different gases H<sub>2</sub>, CO<sub>2</sub>, N<sub>2</sub> and CH<sub>4</sub> were in accordance to the kinetic diameters of the gas molecules (<4Å), which indicated that the molecular sieving mechanism was dominating the transport process.

The results also showed that the kinetic diameter has a larger effect than the Lennard-Jones well depth, which indicates that the diffusion is dominated by a molecular sieving process and that the sorption has relatively little influence.

The single gas test results at different temperatures indicate that the CO<sub>2</sub> has much lower activation energy compared to O<sub>2</sub>, N<sub>2</sub>, and CH<sub>4</sub>, which is resulting in a higher selectivity of CO<sub>2</sub> over the other gases. The gas permeability will decrease with the presence of water vapor which may be caused by the pore blocking. The aging test result indicates that the permeability of carbon membrane will decrease over time when exposed to air. The operating parameters were systematically investigated by factorial design and statistical analysis. The feed pressure and retentate flow rate showed to be the most significant factors influencing the carbon membrane separation performance.

## 6.11 References

- [1] Robeson LM. Correlation of separation factor versus permeability for polymeric membranes. *J Membr Sci.* 1991;62(2):165-85.
- [2] Robeson LM. The upper bound revisited. *J Membr Sci.* 2008;320(1-2):390-400.
- [3] Wu Q, Pan N, Deng K, Pan D. Thermogravimetry-mass spectrometry on the pyrolysis process of Lyocell fibers with and without catalyst. *Carbohydr Polym.* 2008;72(2):222-8.
- [4] Prachayawarakorn S, Mann R. Effects of pore assembly architecture on catalyst particle tortuosity and reaction effectiveness. *Catal Today.* 2007;128(1-2):88-99.
- [5] Hagg M-B, Lie JA, Lindbrathen A. Carbon Molecular Sieve Membranes. A Promising Alternative for Selected Industrial Applications. *Ann Ny Acad Sci.* 2003;984(1):329-45.
- [6] Glasstone S, Laidler KJ, Eyring H. *The Theory of Rate Processes.* 1 ed. New York: McGraw-Hill Book Co. 1941.
- [7] Suda H, Haraya K. Gas Permeation through Micropores of Carbon Molecular Sieve Membranes Derived from Kapton Polyimide. *J Phys Chem B.* 1997;101(20):3988-94.
- [8] Kiyono M, Williams PJ, Koros WJ. Effect of pyrolysis atmosphere on separation performance of carbon molecular sieve membranes. *J Membr Sci.* 2010;359(1-2):2-10.
- [9] Su J, Lua AC. Influence of carbonisation parameters on the transport properties of carbon membranes by statistical analysis. *J Membr Sci.* 2006;278(1-2):335-43.
- [10] Geiszler VC, Koros WJ. Effects of Polyimide Pyrolysis Conditions on Carbon Molecular Sieve Membrane Properties. *Ind Eng Chem Res.* 1996;35(9):2999-3003.
- [11] David LIB, Ismail AF. Influence of the thermastabilization process and soak time during pyrolysis process on the polyacrylonitrile carbon membranes for O<sub>2</sub>/N<sub>2</sub> separation. *J Membr Sci.* 2003;213(1-2):285-91.
- [12] Lie JA, Hagg M-B. Carbon membranes from cellulose and metal loaded cellulose. *Carbon.* 2005;43(12):2600-7.
- [13] Tin PS, Chung T-S, Liu Y, Wang R. Separation of CO<sub>2</sub>/CH<sub>4</sub> through carbon molecular sieve membranes derived from P84 polyimide. *Carbon.* 2004;42(15):3123-31.
- [14] Yoshimune M, Fujiwara I, Haraya K. Carbon molecular sieve membranes derived from trimethylsilyl substituted poly(phenylene oxide) for gas separation. *Carbon.* 2007;45(3):553-60.

- [15] Fialkov A, Dobryakov S, Khorkhorin A, Tyan L, Polyakova N, Kuznetsov Y, et al. Structure of the residual carbon made by fluorocarbon pyrolysis. *J Struct Chem*. 1990;31(3):413-6.
- [16] Cazorla-Amoros D, Alcaniz-Monge J, Linares-Solano A. Characterization of Activated Carbon Fibers by CO<sub>2</sub> Adsorption. *Langmuir*. 1996;12(11):2820-4.
- [17] Stoeckli F, Slassi A, Hugi-Cleary D, Guillot A. The characterization of microporosity in carbons with molecular sieve effects. *Micropor Mesopor Mat*. 2002;51(3):197-202.
- [18] Lagorsse S, Magalhães FD, Mendes A. Carbon molecular sieve membranes: Sorption, kinetic and structural characterization. *J Membr Sci*. 2004;241(2):275-87.
- [19] Lua AC, Su J. Effects of carbonisation on pore evolution and gas permeation properties of carbon membranes from Kapton® polyimide. *Carbon*. 2006;44(14):2964-72.
- [20] Koresh JE, Soffer A. Molecular sieve carbon membrane Part I: Presentation of a new device for gas mixture separation. *Separ Sci Technol*. 1983;18:723-34.
- [21] Belmabkhout Y, Serna-Guerrero R, Sayari A. Adsorption of CO<sub>2</sub> from dry gases on MCM-41 silica at ambient temperature and high pressure. 1: Pure CO<sub>2</sub> adsorption. *Chem Eng Sci*. 2009;64(17):3721-8.
- [22] Berenguer-Murcia Á, Fletcher AJ, García-Martínez J, Cazorla-Amorós D, Linares-Solano Á, Thomas KM. Probe Molecule Kinetic Studies of Adsorption on MCM-41. *J Phys Chem B*. 2003;107(4):1012-20.
- [23] Cavenati S, Grande CA, Rodrigues AE. Separation of CH<sub>4</sub>/CO<sub>2</sub>/N<sub>2</sub> mixtures by layered pressure swing adsorption for upgrade of natural gas. *Chem Eng Sci*. 2006;61(12):3893-906.
- [24] Rafizah WAW, Ismail AF. Effect of carbon molecular sieve sizing with poly(vinyl pyrrolidone) K-15 on carbon molecular sieve-polysulfone mixed matrix membrane. *J Membr Sci*. 2008;307(1):53-61.
- [25] Jones CW, Koros WJ. Carbon molecular sieve gas separation membranes-II. Regeneration following organic exposure. *Carbon*. 1994;32(8):1427-32.
- [26] Menendez I, Fuertes AB. Aging of carbon membranes under different environments. *Carbon*. 2001;39(5):733-40.
- [27] Lie JA, Hagg M-B. Carbon membranes from cellulose: Synthesis, performance and regeneration. *J Membr Sci*. 2006;284(1-2):79-86.

## 7 Process simulation

This chapter describes the process simulation for CO<sub>2</sub> capture from flue gas in post combustion power plants by the carbon membranes based on HYSYS integrated with ChemBrane. The capital cost estimation was also conducted to evaluate the process feasibility and the potential commercial application of the carbon membranes for gas separation. This work has been partly included in the articles “*Hollow Fiber Carbon Membranes: Investigations for CO<sub>2</sub> Capture*” (see Appendix G) and “*Hollow Fiber Carbon Membranes: from Material to Application*” (see Appendix H)

### 7.1 Process design and simulation basis

Post-combustion CO<sub>2</sub> capture is a “tail-end” process. This means that the unit operation for CO<sub>2</sub> separation should be located in the downstream of the flue gas desulphurization (FGD) absorber for a fossil fuel fired power plant. The existing and fairly mature technology (e.g. chemical absorption) features efficient CO<sub>2</sub> capture at low temperature from the flue gas with relative low concentration, but requires large-scale columns and equipment and energy at high costs. It also reduces the thermal efficiency. An alternative way may be the use of membrane separation units. A typical schematic diagram for post-combustion power plant integrates with a carbon membrane separation unit is shown in Fig. 7.1 [1]. However, there are some challenges need to be considered for this application.

- The low pressure and low CO<sub>2</sub> concentration in feed (10-15% vol.) give very low driving force unless compression is applied
- The actual gas volume to be treated is very high, and large membrane areas are needed
- Trace impurities in the flue gas tend to reduce the efficiency of the CO<sub>2</sub> separation processes
- Compressing the captured CO<sub>2</sub> in permeate stream from low pressure (atmosphere or vacuum) to high pressure for pipeline transport (80–150 bar) represents large energy demands

The process design was based on a typical coal fired power plant (400MW). In addition to the main components of N<sub>2</sub>, CO<sub>2</sub>, water vapor and O<sub>2</sub>, relatively small concentrations of aggressive and harmful substances such as SO<sub>2</sub>, NO<sub>x</sub>, traces of metals, volatile organic compounds (VOC) and fly ash are also present in the flue gas. In order to simplify the process simulation, only the main components were considered here. The

simulation basis was chosen based on the characteristic membrane data from dry gas permeation tests and specific boundary conditions for the CO<sub>2</sub> separation process, as listed in Table 7.1. The scenarios of CO<sub>2</sub> capture by hollow fiber carbon membrane unit were simulated by Aspen HYSYS<sup>®</sup> integrated with an in-house simulation tool, ChemBrane [2]. Since the presence of water vapor will reduce the carbon membrane separation performance significantly (discussed in section 6.7.3), a dehydration unit was placed after the flue gas desulfurization (FGD) and before the carbon membrane units.

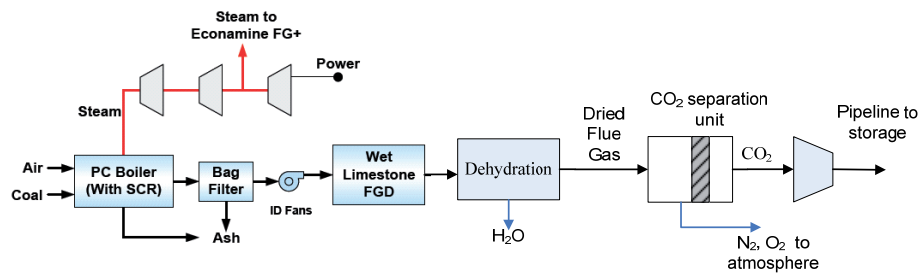


Fig. 7.1 Process flow diagram for a post-combustion power plant

Table 7.1 Simulation basis for CO<sub>2</sub> separation from flue gases through carbon membranes

Process	Carbon membrane			
		Performance	Experimental data <sup>*</sup>	Assumed performance <sup>†</sup>
Feed flow rate (Nm <sup>3</sup> h <sup>-1</sup> )	1 × 10 <sup>6</sup>	Permeance of CO <sub>2</sub> (Nm <sup>3</sup> · m <sup>-2</sup> · h <sup>-1</sup> · bar <sup>-1</sup> )	0.0395	0.1
Pressure (bar)	1.013	Selectivity of CO <sub>2</sub> /N <sub>2</sub>	41	41
Temperature (°C)	80	Selectivity of CO <sub>2</sub> /O <sub>2</sub>	6.85	6.85
CO <sub>2</sub> purity (%)	> 90			
CO <sub>2</sub> recovery (%)	> 80			
CO <sub>2</sub> transport pressure (bar)	110			
Composition (vol %, dry base)	CO <sub>2</sub> 15 N <sub>2</sub> 81 O <sub>2</sub> 4			

<sup>\*</sup>HFCM-B tested at 323K and feed pressure of 2 bar as shown in Fig. 6.20, <sup>†</sup> reducing the thickness from 25 to 10 μm

A single stage membrane unit process was firstly simulated to investigate the influence of operating conditions on the carbon membrane separation performances. The driving force across the membrane module was provided by compression of the feed stream

(configuration A) or vacuum on permeate side (configuration B). The schematic of single stage membrane separation process is shown in Fig. 7.2, which was used to investigate the influences of operating parameters such as feed and permeate pressure on the separation efficiency as well as to obtain the characteristic diagrams. Moreover, a two-stage cascade membrane process, as shown in Fig. 7.3, was also conducted to evaluate the process feasibility based on the capital cost estimation of the key equipments.

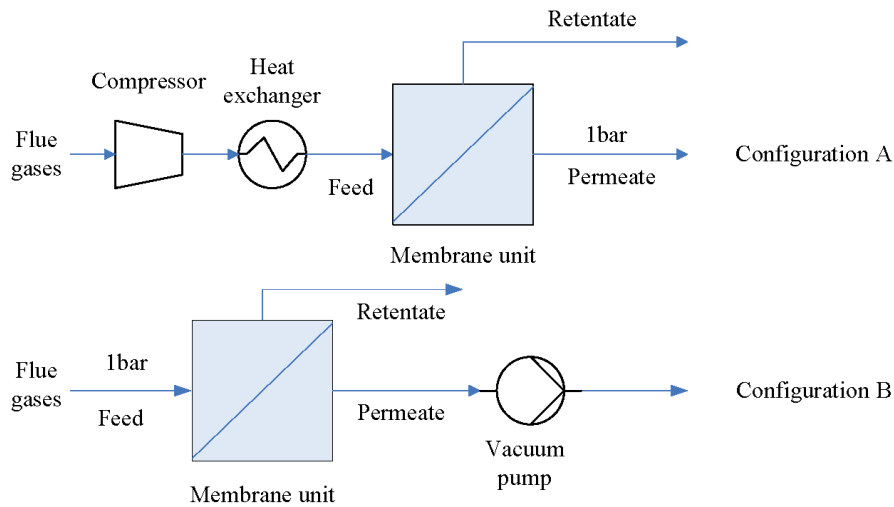


Fig. 7.2 The schematic of the two configurations for a single stage carbon membrane separation process

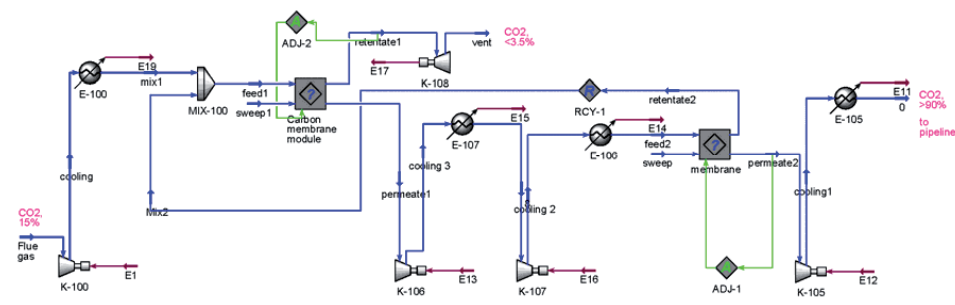


Fig. 7.3 Simulation PFD for two stage cascade carbon membrane separation process

## 7.2 Capital cost evaluation

The estimate for the capital costs is based on the evaluation of the major equipment in the process (e.g. pumps, compressors, heat exchangers, membrane units), which can be provided with an accuracy in the range from -25% to 40%, typically used for a

preliminary feasible estimate of different process alternatives [3]. The bare module costing ( $C_{BM}$ ) technique accounts to the purchased cost ( $C_p^0$ ) for the equipment in base conditions (carbon steel material and near ambient pressure), and a multiplying bare module factor ( $F_{BM}$ ) is used. This factor will consider the specific equipment type, specific materials of construction and operating pressure. The bare module cost ( $C_{BM}$ ) of each piece of equipment is the sum of the direct and indirect costs,

$$C_{BM} = C_p^0 F_{BM} \quad (7.1)$$

The excel program of CAPCOST 2008 is used to estimate the capital cost based on the equipment module approach [3]. The total capital cost ( $C_{TM}$ ) includes the contingency and contractor fee in addition to the direct and indirect cost, which is calculated as follows:

$$C_{TM} = 1.18 \sum_{i=1}^n C_{BM,i} \quad (7.2)$$

Where  $n$  is the total number of individual units. A chemical engineering plant cost index (CEPCI) of 500 is adopted for all inflation adjustments. Due to the carbon membrane cost is still unknown, an assumed 45 \$/m<sup>2</sup> (estimated polymeric membrane cost 20 \$/m<sup>2</sup> as reported by Koros [4]) with an average lifetime of 5 years for the carbon membranes was used to calculate the capital cost of carbon membrane unit. The capital costs of the compressors and heat exchangers were obtained by CAPCOST. Therefore, the specific capital costs for per ton CO<sub>2</sub> avoided ( $C_{CO_2}$ ) was calculated based on a project lifetime of 20 years together with the annual CO<sub>2</sub> avoided amount (330 days per year), as follows:

$$C_{CO_2} = \frac{C_{TM}}{20 \times F_{CO_2} \times 24 \times 330} \text{ (\$/t CO}_2 \text{ avoided)} \quad (7.3)$$

where  $F_{CO_2}$  is the mass flow of CO<sub>2</sub> to pipeline (t/h).

### 7.3 Results and discussion

#### 7.3.1. Effect of feed and permeate pressures

The single stage membrane unit with an assumed membrane area of  $2 \times 10^7$  m<sup>2</sup> was executed for the process simulation with a cross flow configuration [5]. Figs. 7.4 and 7.5 illustrate the dependency of CO<sub>2</sub> purity, recovery and specific energy demands for CO<sub>2</sub> capture with two different process configurations. For the configuration A with a constant permeate pressure of 1bar, and compression of the feed side (3-12 bar), the results showed high CO<sub>2</sub> recovery in Fig. 7.4, but lower CO<sub>2</sub> purity in permeate side.

For configuration B with a constant feed pressure of 1bar and vacuum on the permeate side (75-300 mbar), which shows higher CO<sub>2</sub> purity but relative lower CO<sub>2</sub> recovery. However, the specific energy demands for configuration A is much higher than that of configuration B.

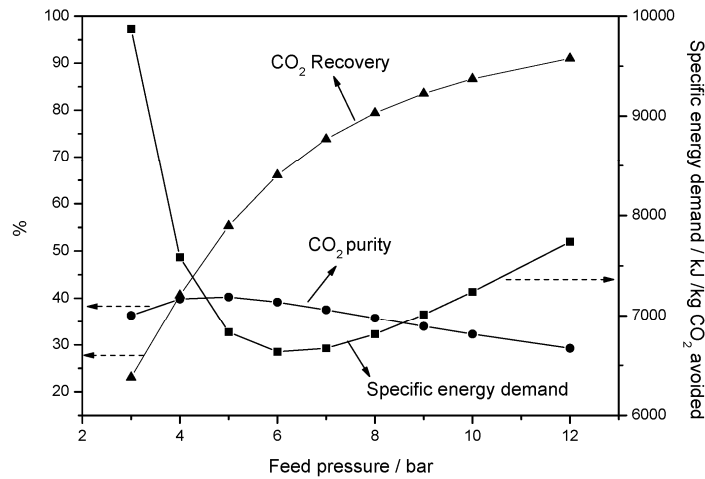


Fig. 7.4 Gas separation performance and specific energy demands with different feed pressure at constant permeate pressure of 1bar and 303K-configuration A

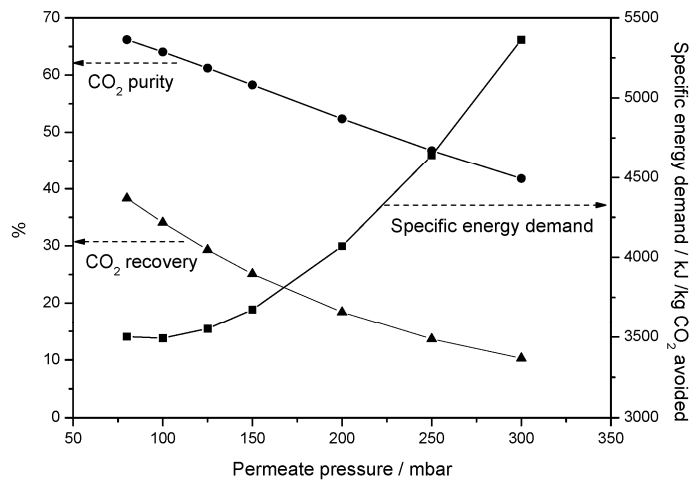


Fig. 7.5 Gas separation performance and specific energy demands with different permeate pressure at constant feed pressure of 1bar and 303K-configuration B

In order to obtain the optimal process configuration, the combination of these two configurations (feed compression and vacuum in permeate side) was also investigated. There is a trade off between the CO<sub>2</sub> recovery, CO<sub>2</sub> purity and specific energy demands under different operating conditions as shown in Fig. 7.6. It can be seen that the single stage membrane process cannot achieve high product quality (e.g. 90% CO<sub>2</sub>) and CO<sub>2</sub> recovery (e.g. 80%) simultaneously. Therefore, a multi-stage membrane unit needed to be designed for a specific application.

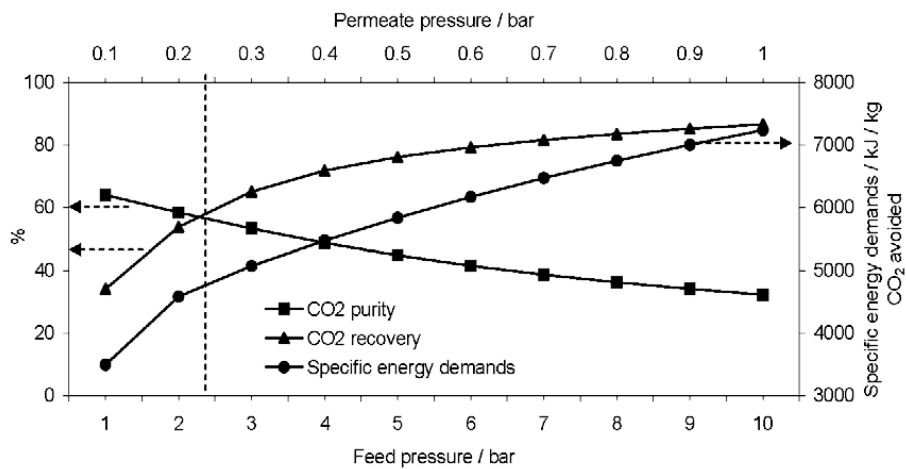


Fig. 7.6 Gas separation performance and specific energy demands with the combination of compression and evacuation of feed and permeate sides at 303K, (■) CO<sub>2</sub> purity, (▲) CO<sub>2</sub> recovery, (◆) specific energy demands-combination of configurations A and B

### 7.3.2. Characteristic diagrams

Two dimensionless parameters are derived applying the Buckingham  $\pi$  theorem to characterize the performance of single stage or multi-stage membrane separation processes.

$$\Pi = \frac{P_{CO_2} A p_F}{V_F} = b p_F \quad (7.4)$$

$$\phi = \frac{p_F}{p_P} \quad (7.5)$$

Where  $\Pi$  is the dimensionless permeation number,  $V_F$  is the feed volume flow (Nm<sup>3</sup>/h).  $P_{CO_2}$  and  $A$  are the permeance of CO<sub>2</sub> (Nm<sup>3</sup> / (m<sup>2</sup>.h.bar)) and the required membrane area (m<sup>2</sup>), respectively.  $p_F$  and  $p_P$  are the feed and permeate pressure (bar) separately.  $b$  is a simplified process parameter ( $b = P_{CO_2} A / V_F$ , bar<sup>-1</sup>).  $\Phi$  is the pressure ratio between

feed and permeate side. The flue gas was compressed to appropriate pressures (various  $\Phi$ ) and cooled down to 30 °C before fed into the membrane separation unit. The permeate pressure of 0.25 bar was used for the simulation based on the consideration of the capacity for the large-scale industrial vacuum pumps. The process simulation was executed with different pressure ratios,  $\Phi$  (5-20) and process parameters,  $b$  (0.15-1.5 bar<sup>-1</sup>). The characteristic diagrams for the different separation processes were obtained from the simulation results of CO<sub>2</sub> recovery, permeate CO<sub>2</sub> purity, specific energy demands and required membrane areas, which are shown in Figs. 7.7 to 7.10.

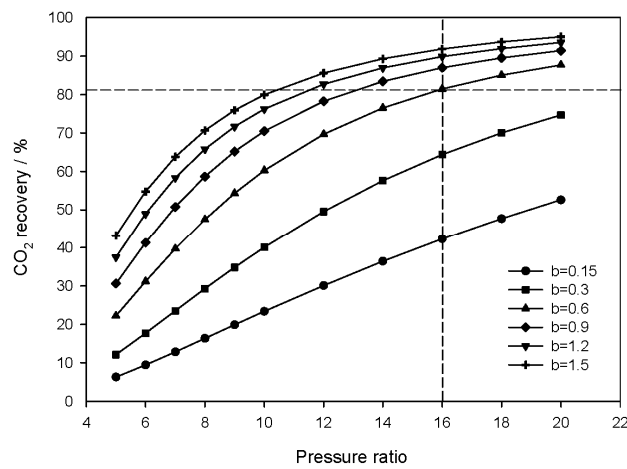


Fig. 7.7 CO<sub>2</sub> recovery as function of pressure ratio at 303k and permeate pressure of 0.25 bar

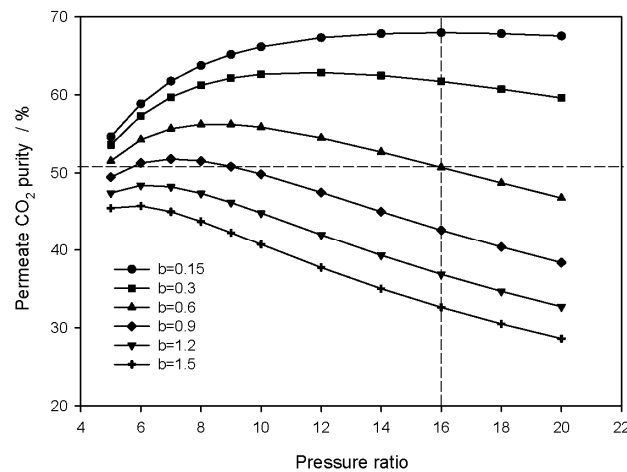


Fig. 7.8 Permeate CO<sub>2</sub> purity as function of pressure ratio at 303k and permeate pressure of 0.25bar

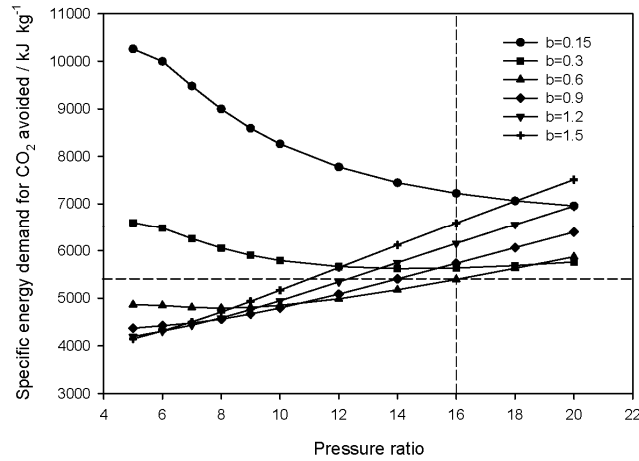


Fig. 7.9 Specific energy demands for CO<sub>2</sub> avoided as function of pressure ratio at 303k and permeate pressure of 0.25bar

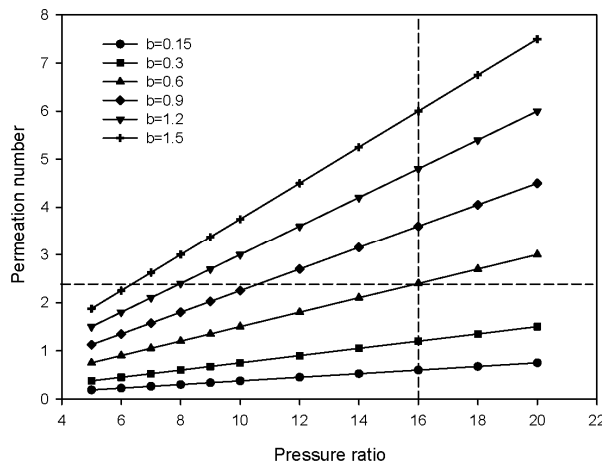


Fig. 7.10 Permeation number as function of pressure ratio at 303k and permeate pressure of 0.25bar

One can easily obtain all process parameters by drawing an appropriate line in these characteristic diagrams based on the given requirements (e.g. CO<sub>2</sub> recovery of 81.5% and pressure ratio of 16). By drawing the lines in Fig. 7.7, the parameter line of  $b=0.6$  was identified. The CO<sub>2</sub> purity in permeate side was then determined as 51 % from Fig. 7.8 by the intersection plot of the pressure ratio line ( $\Phi=16$ ) and parameter line ( $b=0.6$ ). Moreover, the specific energy demands and permeation number were also obtained

from Figs. 7.9 and 7.10 using the same procedure, and the values were 5400 kJ/kg CO<sub>2</sub> avoided and 2.4 respectively. Hence, the characteristic diagrams can be used to determine the required operating conditions and the carbon membrane areas to meet the specific constraints.

### 7.3.3. Process feasibility evaluation

Gas membrane separation process is typically designed with equipments such as compressors, coolers and membrane units; arranged, controlled, and operated in a particular way, to capture CO<sub>2</sub> which must meet a certain specification (e.g. 90%) at a constant feed flow rate (10<sup>6</sup> Nm<sup>3</sup>/h) and composition (15% CO<sub>2</sub> - 4% O<sub>2</sub> - 81 %N<sub>2</sub>) as given in Table 7.1. The minimization of capital cost was employed to conduct process optimization. Since the process with single stage membrane unit cannot achieve the specification as described in section 7.3.1, a two stage cascade membrane process with counter-current configuration was designed as shown in Fig. 7.3. A feed pressure of 4 bar was set to attain a minimum recovery of 80 % in the 1<sup>st</sup> stage, and a 90 % of CO<sub>2</sub> purity in permeate stream in the 2<sup>nd</sup> stage was subsequently achieved by optimization of the process operating conditions. The retentate stream comes out from the 2<sup>nd</sup> stage was recycled and mixed with the feed stream. The captured CO<sub>2</sub> was then compressed to 110 bar for pipeline transportation to the storage site. The purity of CO<sub>2</sub> and % CO<sub>2</sub> captured will be influenced by the pressure ratio over the membrane. As already stated, a permeate pressure of 250 mbar was chosen based on capacity for the large-scale industrial vacuum pumps. A 100 mbar permeate pressure would have shown better theoretical results, but might have been less realistic for installation at a power plant. The specific capital costs were calculated from the required membrane area and the duty of the compressors and the coolers. The optimal operating parameters and simulation results are given in Table 7.2. Based on the capital cost estimation for the major equipment which includes the membrane unit, compressor and heat exchanger, a specific capital cost of 100 \$/tonne CO<sub>2</sub> avoided was determined with the two-stage cascade membrane process. Comparing to the previous work[1], the specific capital cost was significantly reduced by increasing the carbon membrane permeance (from 0.022 to 0.0395 Nm<sup>3</sup>. m<sup>-2</sup>. h<sup>-1</sup>.bar<sup>-1</sup>) even through the carbon membrane cost was set much higher in this work (45 \$/m<sup>2</sup> comparing to 15 \$/m<sup>2</sup>). Moreover, the cost of carbon membrane unit was found to be the major part of total capital costs, which could be greatly reduced by improving the carbon membrane performance and simplifying the membrane production process although the carbon membrane/module cost is still unknown today [5].

Table 7.2 Simulation results of CO<sub>2</sub> capture by membrane process

Parameter		First stage	Second stage
CO <sub>2</sub> composition (%)	Feed	15	62.8
	Retentate	3.3	14.5
	Permeate	62.8	92.5
Feed temperature (°C)		50	50
Feed pressure (bar)		4	4
Permeate pressure (bar)		0.25	0.25
Membrane area (m <sup>2</sup> )		1.40×10 <sup>7</sup>	1.678×10 <sup>6</sup>
Total CO <sub>2</sub> recovery (%)		81.1	
Feed CO <sub>2</sub> mass flow (kg/h)		2.28×10 <sup>5</sup>	
Captured CO <sub>2</sub> mass flow (kg/h)		1.57×10 <sup>5</sup>	
Total carbon membrane cost (M\$)		2820	
Total compressor duty GJ / t CO <sub>2</sub> avoided		4.82	
Specific capital cost \$ / t CO <sub>2</sub> avoided		100	

An assumed membrane permeance, based on the reduction of wall thickness from 25 to 10 μm (see Table 7.1), was also employed for process simulation based on the same operating conditions. The results are given in Table 7.3. (Experimentally it is considered to be realistic to prepare carbon membranes with wall thickness of 10 μm – this was proven by previous company Carbon Membranes Ltd., Israel.) It was found that the total carbon membrane cost was reduced significantly from 2820 M\$ to 1280 M\$, due to the increased carbon membrane permeance, while the capital costs (\$/ t CO<sub>2</sub> avoided) now was down to 46. Ho et al. reported that the capital cost was 70 \$ / tonne CO<sub>2</sub> avoided using traditional chemical absorption method with monoethanolamine (MEA) for CO<sub>2</sub> capture from a 500MW pulverised coal power plant [6]. It can thus be concluded that the carbon membrane technology is quite promising also compared to the chemical absorption methods. Hence, this environmental friendly technology could also promote the hollow fiber carbon membranes to become a potential candidate for CO<sub>2</sub> capture in future.

Table 7.3 Simulation results based on the assumed carbon membranes\*

Parameter		First stage	Second stage
CO <sub>2</sub> composition (%)	Feed	15	62.3
	Retentate	2.7	23.3
	Permeate	62.3	93.6
Membrane area (m <sup>2</sup> )		6.47×10 <sup>6</sup>	6.13×10 <sup>5</sup>
Total CO <sub>2</sub> recovery (%)		84.2	
Total carbon membrane cost (M\$)		1280	
Total compressor duty GJ / t CO <sub>2</sub> avoided		4.84	
Specific capital cost \$ / t CO <sub>2</sub> avoided		46	

\*: Operating condition is the same with Table 7.2

#### 7.4 Conclusions

The single stage carbon membrane processes for CO<sub>2</sub> separation from flue gas with feed compression, permeate evacuation, and their combination was investigated by using Aspen HYSYS simulation tool integrated with an in-house membrane simulation model. The simulation results indicated that the single stage membrane process cannot achieve high CO<sub>2</sub> purity and CO<sub>2</sub> recovery simultaneously using these hollow fiber carbon membranes. The characteristic diagrams which were plotted can be easily used by end users to identify the required operating conditions and membrane areas so as to meet the given targets. The capital cost estimation for the two-stage cascade membrane process indicated that the cost of carbon membrane technology may be compared to the chemical absorption method. Although the cost of carbon membranes is still unknown, the membrane/module cost can be greatly reduced by improving the membrane separation performance (especially increasing the gas permeance by reducing the wall thickness of the hollow fiber carbon membranes) and simplifying the membrane production process. These hollow fiber carbon membranes will be further investigated for a potential application for CO<sub>2</sub> capture.

## 7.5 References

- [1] He X, Lie JA, Sheridan E, Hägg M-B. CO<sub>2</sub> capture by hollow fibre carbon membranes: Experiments and process simulations. *Energy Procedia*. 2009;1(1):261-8.
- [2] Grainger D. Development of carbon membranes for hydrogen recovery. Norwegian University of Science and technology, PhD thesis. 2007:195.
- [3] Turton R, Bailie RC, Whiting WB, Shaeiwitz JA. *Analysis, Synthesis, and Design of Chemical Processes*, Third Edition. Prentice Hall, New Jersey. 2008.
- [4] Koros WJ. Membrane Opportunities and Challenges for Large Capacity Gas and Vapour Feeds. European Membrane Society's 20th Summer School NTNU Trondheim, Norway. 2003.
- [5] He X, Hägg M-B. Hollow fiber carbon membranes: Investigations for CO<sub>2</sub> capture. *J Membr Sci*. In Press, Corrected Proof.
- [6] Ho MT, Allinson GW, Wiley DE. Comparison of MEA capture cost for low CO<sub>2</sub> emissions sources in Australia. *IJGGC*. 2011;5(1):49-60.

## 8 Conclusions

The focus for this work is to prepare a suitable hollow fiber carbon membrane with high gas separation properties for a specific industrial application, i.e. CO<sub>2</sub> capture from flue gases. The total CO<sub>2</sub> emissions could be reduced significantly on the basis of CO<sub>2</sub> capture and storage.

The hollow fibers were spun from a dope solution consists of CA/PVP/NMP (22.5% / 5% / 72.5%). The spinning parameters were investigated systematically based on the orthogonal experimental design method and statistical analysis, and an optimal spinning condition of a bore fluid (water+NMP (85%)), air gap (25 mm), bore flow rate (40% of dope flow rate) and temperature of quench bath (50 °C) was obtained. The spun CA hollow fibers were further deacetylated using an optimal deacetylation condition with a 0.075M NaOH in 96% ethanol solution for 2h.

The hollow fiber carbon membranes were fabricated from the deacetylated cellulosic precursors by controlling the carbonization procedures. The carbonization parameters, such as purge gas, heating rate, final temperature and soak time, were investigated systematically, and an optimal carbonization procedure with CO<sub>2</sub>-823K-4K/min -2h was obtained for preparation of high performance carbon membranes. The morphology and structure for the prepared hollow fiber carbon membranes were characterized by various techniques such as TGA, FTIR, SEM, XRD and gas gravimetric sorption. The carbon membranes showed a typical thickness of 25 μm and an average d-spacing of 4 Å. The prepared carbon membranes showed a symmetric structure with an average micropore size of 5 Å.

The gas separation performance for the prepared carbon membranes were tested on the basis of gas permeation tests with different single gases (H<sub>2</sub>, CO<sub>2</sub>, N<sub>2</sub>, CH<sub>4</sub> and O<sub>2</sub>) and gas mixtures (15% CO<sub>2</sub> - 4% O<sub>2</sub> - 81 %N<sub>2</sub>, 10% CO<sub>2</sub> - 90% N<sub>2</sub> and 35% CO<sub>2</sub>-65% CH<sub>4</sub>) at different operating conditions. The prepared carbon membrane showed quite good gas separation performance both for permeability and selectivity of CO<sub>2</sub> over the other gases. The gas permeability transport through the carbon membranes for different gases H<sub>2</sub>, CO<sub>2</sub>, N<sub>2</sub> and CH<sub>4</sub> were in accordance with the kinetic diameters of the gas molecules (< 4Å), which indicated that the molecular sieving mechanism was dominating the transport process. The results also showed that the kinetic diameter has a larger effect than the Lennard-Jones well depth, which indicated that the diffusion was dominated by a molecular sieving process and that the sorption had a relatively little influence. The gas permeability increased with increasing temperature, but slightly decreased with increasing pressure within the investigated narrow region. The experimental results also indicated that the gas permeability decreased with increasing

the humidity, which could probably be caused by the pore blocking due to the formation of hydrogen bonds between the water molecules and carbon matrix. The aging test results showed that the permeability of carbon membrane decreased slightly over time exposed to the O<sub>2</sub> atmosphere. The aging could be caused by the chemisorption of O<sub>2</sub> onto the carbon matrix. The gas mixture test results indicated that the operating parameters such as pressure, feed composition and flow rate in retentate had significant effects on the separation performances, while the temperature had relatively little influences within the tested region.

Process simulation was conducted to investigate CO<sub>2</sub> capture from flue gases through the hollow fiber carbon membranes. The single stage membrane processes with feed compression, permeate evacuation, and their combination were investigated on the basis of Aspen HYSYS integrated with an in-house membrane simulation unit. The simulation results indicated that the single stage membrane process could not achieve high CO<sub>2</sub> purity and CO<sub>2</sub> recovery simultaneously using these hollow fiber carbon membranes. The obtained characteristic diagrams could be used to identify and determine the required operating conditions and membrane areas to achieve the given targets in a given process. The capital cost estimation for a two-stage cascade membrane process indicated that the cost of the carbon membrane unit may be compared to chemical absorption. Although the cost of carbon membranes is still unknown, the membrane/module cost could be greatly reduced by improving the membrane separation performance, especially by increasing the gas permeance, and simplifying the membrane production process. The carbon membrane performance needs to be further improved before it can be brought into the commercial applications.

## 9 Future work

This chapter suggests some further work with respect to the hollow fiber carbon membranes. Based on the most experimental results and process simulations performed in the current work, the author would like to suggest the following work for future investigation.

Improving the separation performance, the carbon membrane separation performance, especially for the gas permeance should be further increased before it can be brought into the commercial applications. The following suggestions may be used to improve the gas permeance.

- a. A small dimension spinneret could be used to spin the hollow fiber precursors with reduced wall thickness. But the mechanical stability could be reduced significantly, therefore, the trade-off between the gas permeance and the mechanical stability should be considered.
- b. Two different polymer materials could be used to produce the asymmetric dual layer hollow fibers, which can be further used to prepare the asymmetric hollow fiber carbon membranes with reduced thickness of the selective layer. However, a new spinning process needs to be further investigated and optimized.
- c. Changing the carbon membrane structure by controlling the carbonization procedure. The structure parameters such as micropore volume, average pore size and pore size distribution will significantly affect the membrane separation performance. However, this work has already been well investigated within this PhD research, thus it could be quite challengeable to improve further.

Membrane performance tests exposed to the real flue gas or to the other industrial streams should be executed to investigate the membrane performance and durability under some specific conditions.

Molecular simulation could be used to investigate the gas molecule transport through the carbon membranes, and give an insight into the transport mechanism, which is difficult to achieve by the experiments.

Carbon membrane application, other specific applications for the carbon membranes could be further developed, e.g. high temperature carbon membrane reactors (CMR).

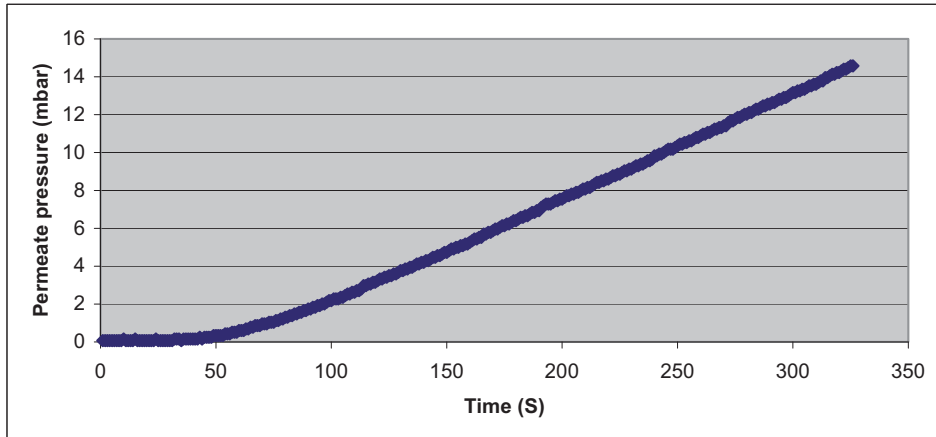
## Appendix list

- Appendix A: Example of the measurement for single gas permeability
- Appendix B: Durability test for the carbon membranes, NanoGlowa report
- Appendix C: Carbon membrane tests at ITM-CNR, NanoGlowa report
- Appendix D: Preparation and Characterization of Hollow Fiber Carbon Membranes from Cellulose Acetate Precursors (published article in *I&EC Res.*)
- Appendix E: Optimization of Carbonization Process for Preparation of High Performance Hollow Fiber Carbon Membranes (article submitted to *I&EC Res.*)
- Appendix F: Structural, Kinetic and Performance Characterization of Hollow Fiber Carbon Membranes (article submitted to *J. Membr. Sci.*)
- Appendix G: Hollow Fiber Carbon Membranes: Investigations for CO<sub>2</sub> Capture (published article in *J. Membr. Sci.*)
- Appendix H: Hollow Fiber Carbon Membranes: from Material to Application (article submitted to *AIChE Journal*)

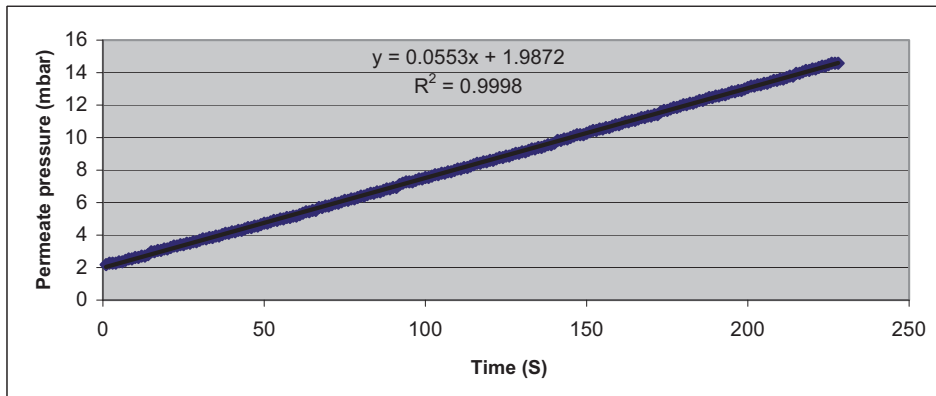


## Appendix A: Example of the measurement for single gas permeability

- CO<sub>2</sub> permeation test at 30 °C and 2 bar for a small carbon membrane module with membrane area of 8.63 cm<sup>2</sup>



- Regression of the experimental data from the steady-state (100 s) to get the  $dp/dt = 0.0553$  mbar/s



- Calculate the CO<sub>2</sub> permeability

$$P_{CO_2} = \frac{273 \times 10^7 V l (dp/dt)}{76 \Delta p A T_{exp.}} = \frac{273 \times 10^7 \times 171 \times 25 \times 10^{-4} \times 0.0553}{76 \times 2 \times 8.63 \times 303} = 162.4 \text{ Barrer}$$

The permeate volume is 171 cm<sup>3</sup>, and the membrane thickness is 25 μm.

Table 1 Gas permeabilities for HFCMs prepared from different precursors at 30 °C and 2bar

Carbon membranes	Permeability (Barrer)			
	H <sub>2</sub>	CO <sub>2</sub>	N <sub>2</sub>	CH <sub>4</sub>
HFCM-0.5	513.6	62.5	2.7	0.3
HFCM-1	618.5	124.8	3.4	1.0
HFCM-2	937.7	259.8	7.6	2.2
HFCM-4	535.0	74.7	1.9	0.5
HFCM-8	278.0	31.3	0.8	0.3

Table 2 Gas permeabilities for HFCMs at a feed pressure 2 bar and different temperatures

Temperature (°C)	Permeability of HFCM-A (Barrer)				Permeability of HFCM-B (Barrer)			
	CO <sub>2</sub>	O <sub>2</sub>	N <sub>2</sub>	CH <sub>4</sub>	CO <sub>2</sub>	O <sub>2</sub>	N <sub>2</sub>	CH <sub>4</sub>
30	157.2	41.0	3.9	1.4	405.4	62.6	9.1	4.0
40	162.0	42.5	4.5	1.6	415.9	63.5	9.7	5.1
50	170.6	43.7	5.3	1.9	433.2	65.3	10.6	6.2
60	173.6	46.0	5.8	2.3	443.6	67.2	11.5	7.3
70	176.0	48.2	6.7	2.7	450.6	69.5	12.2	9.1

Table 3 Gas permeabilities for HFCM-B at different pressures and temperatures

Pressure (Bar)	CO <sub>2</sub> permeability (Barrer)		N <sub>2</sub> permeability (Barrer)	
	30 °C	50 °C	30 °C	50 °C
1.5	392.2	419.4	19.4	21.6
2	361.5	409.1	17.7	19.4
2.5	356.2	397.9	17.2	18.6
3	349.0	389.3	15.9	18.2
4	340.1	371.1	15.3	17.9
5	334.6	358.9	14.7	17.8
6	325.7	348.7	14.4	17.4

## Appendix B: Durability test for carbon membranes

- Tested by NanoGlowa partner IEC in Israel

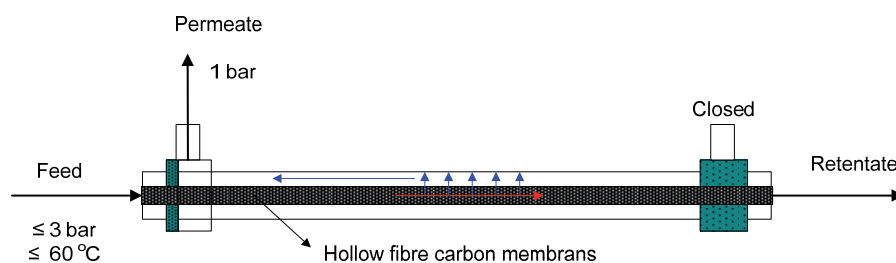
### 1. Characteristics of membranes

Hollow fibre carbon membranes were mounted into a module and tested with the utilities at Rutenberg power plant (Israel Electric Corporation, IEC) using a by-pass stream coming downstream of the FGD unit. The carbon membrane module used for testing is described in Table 1.

Table 1 Description of membrane exposed to flue gas at IEC

Membrane	Hollow fibre carbon membranes		Producer:	NTNU
Precursors	DCA		Sent on	26/10/08
Carbonization condition	CO <sub>2</sub> -1K/min-650°C-2h		Date	11/10/08
Geometry				Membrane area, 30 cm <sup>2</sup>
Hollow fibres	Fibre length, mm	200	Useful fibre length, mm	100
	OD fibre, micron	250	ID fibre, micron	160
Average Thickness (separating layer), micron		45	Self supported (Yes/No)	Yes
				Feed from bore side

### Configuration



For continuous operation : Feed from bore side, and permeate from shell side

## 2. Characteristics of flue gas

The flue gas is extracted after the FGD from the Rutenberg power plant, and the characteristics for flue gas is given in Table 2.

Table 2 Characteristics of the flue gas

Date	07/01/2009	Component	Content
Time	21:02	CO <sub>2</sub>	12.39 %
Type of coal	South Africa 21	O <sub>2</sub>	4.52 %
Excess Air	1.29	N <sub>2</sub>	70.08 %
Unit load (MW)	544	H <sub>2</sub> O	13.01 %
Temperature (°C)	51.1	SO <sub>2</sub>	89 mg/dNm <sup>3</sup>
		NO <sub>x</sub>	246 mg/dNm <sup>3</sup>

## 3. Results expected

When the carbon membrane is exposed to the real flue gas, the following results may happen

- The flux of carbon membrane may decrease due to partly pore blocking by water and/or particles.
- The hollow fibre carbon membrane may break down, why? Pressure shocks?
- The SO<sub>2</sub> and NO<sub>x</sub> may adsorb onto and react with the carbon matrix, hence reducing the flux.

## 4. Results obtained

Carbon membrane durability was tested at 303K with high vacuum at permeate stream, and feed pressure of ca. 1 bar. The results are given in Table 3. The degree of aging is in accordance with normal aging of carbon membranes in use or under storage in air, e.g.

Table 3 Carbon membrane gas permeation test results

Pure gas tests	$\frac{dp}{dt} \cdot \frac{1}{\Delta p}$ , mbar.s <sup>-1</sup> .bar <sup>-1</sup>			Aging, %
	Initial test on Oct 17-22, 2008, (P <sub>1</sub> )	After expose to the flue gas, test on Apr. 16-20, 2009, (P <sub>2</sub> )	Heating 80°C overnight with high vacuum (thermal regeneration)	
CO <sub>2</sub>	2.76e-2	1.67e-2	1.64e-2	39.5
N <sub>2</sub>	9.23e-4	5.35e-4	5.26e-4	42.0

due to formation of oxygen-containing groups at the edge of the graphene sheets in the carbon. This demonstrates the inertness or the chemical stability of the carbon membranes. Moreover, the normal thermal regeneration method is found to be no useful to these carbon membranes.

The aging is calculated as follows:

$$Aging, \% = \frac{(P_1 - P_2)}{P_1} \times 100\% \quad (1)$$

where  $P_1$  and  $P_2$  correspond to the gas permeability measured before and after the exposure to the flue gas, respectively. A brief summary for the durability test results was given in Table 4. It can be assumed that the carbon membranes have an acceptable durability in the aggressive environment where they are expected to work.

Table 4 Carbon membrane durability test results

Testing time	3 weeks
Acidic water condensation	Normal
Solid particle deposition	Normal
Breakage	No
Stability under flue gas conditions	Normal

##### 5. Pictures/appearance

SEM images for the carbon membrane before exposing to the flue gas are given in Fig. 1. Ordinary photos were not taken after exposure, since the information from this is regarded limited due to the inherent black appearance of carbon membranes.

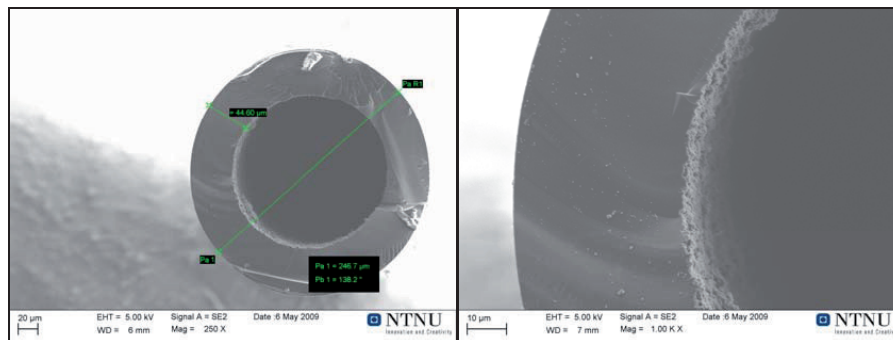


Fig. 1 SEM images for the cross section of the carbon membrane

### Appendix C: Carbon membrane tests at ITM-CNR

A lab-scale hollow fiber carbon membrane module (Fig. 1) was constructed and sent to ITM-CNR central test lab for gas separation measurements. The initial test results conducted at NTNU are listed in Table 1.

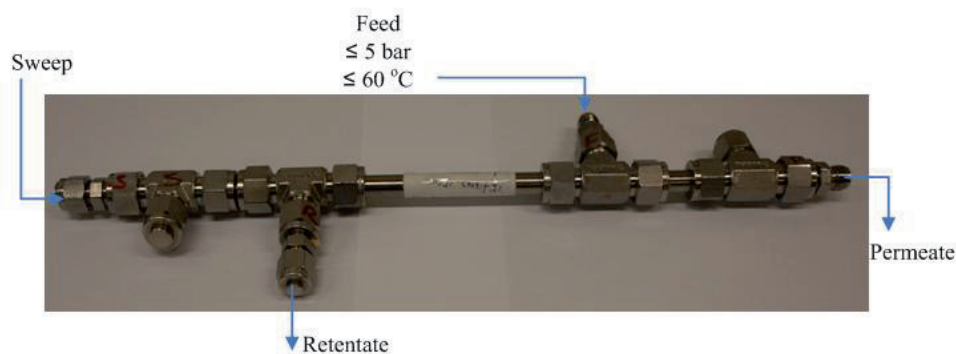


Fig. 1 A lab-scale hollow fiber carbon membrane module

Table 1 Permeance and selectivity values tested by NTNU

Carbon membrane module: membrane area 14.5 cm <sup>2</sup> , 15 fibers, Thickness= 30 μm, length =15 cm							
Pure gas test 30 °C and 2 bar							
Feed	Permeance, m <sup>3</sup> (STP)/(m <sup>2</sup> .h.bar)			Ideal selectivity		Remark	
	CO <sub>2</sub>	N <sub>2</sub>	O <sub>2</sub>	CO <sub>2</sub> /N <sub>2</sub>	CO <sub>2</sub> /O <sub>2</sub>		
Shell side	47.8E-3	2.03E-3	10.6E-3	24.0	4.5	From bore side, membrane area= 10.3 cm <sup>2</sup>	
Bore side	42.0E-3	2.61E-3	13.4E-3	16.1	3.1		
Gas mixture feed 10%CO <sub>2</sub> - 90%N <sub>2</sub>							
Temp. (°C)	Pressure (bar)	Permeance, m <sup>3</sup> (STP)/(m <sup>2</sup> .h.bar)		Selectivity of CO <sub>2</sub> /N <sub>2</sub>	Stage-cut (%)	Purity (Permeate), %	
		CO <sub>2</sub>	N <sub>2</sub>			CO <sub>2</sub>	N <sub>2</sub>
30	3.5	4.48E-2	1.81E-3	25	5.4	73.4	26.6
60	5	4.38E-2	1.92E-3	23	9.5	71.6	28.4

The module was also tested in central test lab at ITM-CNR with a feed pressure ca. 2-5 bar, 30 °C and permeate pressure as 1bar, using 2 ml/min CH<sub>4</sub> as sweep gas, and Table 2 shows the test results.

Table 2 Experimental results for carbon membrane performance tested at ITM-CNR

Temperature (°C)	Single gas	Nanoglowa Mixture (CO <sub>2</sub> :N <sub>2</sub> :O <sub>2</sub> =17% / 78% / 5%) Gas mixture CO <sub>2</sub> :N <sub>2</sub> =10% / 90%									
		CO <sub>2</sub> /N <sub>2</sub>		Permeance,		CO <sub>2</sub> /N <sub>2</sub>		Permeance,		CO <sub>2</sub> /N <sub>2</sub>	
		Selectivity	m <sup>3</sup> (STP) / (m <sup>2</sup> .h.bar)	m <sup>3</sup> (STP) / (m <sup>2</sup> .h.bar)	m <sup>3</sup> (STP) / (m <sup>2</sup> .h.bar)	Selectivity	m <sup>3</sup> (STP) / (m <sup>2</sup> .h.bar)	m <sup>3</sup> (STP) / (m <sup>2</sup> .h.bar)	m <sup>3</sup> (STP) / (m <sup>2</sup> .h.bar)	Selectivity	m <sup>3</sup> (STP) / (m <sup>2</sup> .h.bar)
		CO <sub>2</sub>	N <sub>2</sub>	CO <sub>2</sub>	N <sub>2</sub>	CO <sub>2</sub>	N <sub>2</sub>	CO <sub>2</sub>	N <sub>2</sub>	CO <sub>2</sub>	N <sub>2</sub>
30		53E-3	1.0E-3	53	160E-3	2.9E-3	21E-3	55	276E-3	4.9E-3	56
50		31E-3	1.1E-3	28	149E-3	3.7E-3	23E-3	40	263E-3	6.3E-3	42

Acknowledge to the Central test lab, Institute for Membrane Technology (ITM-CNR)



## **Appendix D**

Preparation and Characterization of Hollow Fiber Carbon  
Membranes from Cellulose Acetate Precursors

Article published in *Industrial & Engineering Chemistry Research*

Is not included due to copyright



## **Appendix E**

### Optimization of Carbonization Process for Preparation of High Performance Hollow Fibre Carbon Membranes

Article submitted to *Industrial & Engineering Chemistry Research*



# Optimization of Carbonization Process for Preparation of High Performance Hollow Fiber Carbon Membranes

*Xuezhong He, May-Britt Hägg\**

Department of Chemical Engineering, Norwegian University of Science and Technology, N-7491 Trondheim, Norway

Abstract: Orthogonal experimental design (OED) was employed to study the influences of carbonization process on the transport properties of hollow fiber carbon membranes (HFCMs). The conjoint analysis method was applied for the statistical analysis of OED results, and the importance of the investigated carbonization parameters on the performance of carbon membrane was found to be: purge gas > final carbonization temperature > heating rate > final soak time. A high performance hollow fiber carbon membrane (HFCM-5) was prepared from the optimal carbonization process. The carbon membrane structure and morphology were characterized by a Fourier transform infrared spectroscopy and a scanning electron microscope. The influences of the operating parameters such as temperature, pressure, and stage-cut on the carbon membrane performances were investigated by the single gas and gas mixture tests.

Keywords: hollow fiber carbon membrane; carbonization; orthogonal experimental design; permeability

\* Corresponding author. Fax: +47 73594080.

E-mail address: may-britt.hagg@chemeng.ntnu.no (M.-B. Hägg)

## 1 Introduction

Polymeric membranes have been commercially available for selected industrial gas applications since the 1980s, and are then applied as an alternative and competitive technology for conventional processes like distillation and adsorption [1-2]. There are, however, two main challenges faced by polymeric membranes; these are to achieve both high permeability and selectivity above the Robeson upper bound [3] and to maintain durability in aggressive (solvent or acids or bases) and adverse (high temperature and pressure) environments. With respect to the limitation of polymeric membranes, the carbon molecular sieve membranes have been presented as an alternative and promising candidate for gas separation, especially for CO<sub>2</sub> separation [4-8] and H<sub>2</sub> recovery [9]. Recently, strong interest has been shown in the preparation of hollow fiber carbon membranes (HFCMs) for gas separation based on improved selectivity and improved thermal, mechanical and chemical stability compared to membranes already in use [5, 7, 10-14]. From the standpoint of large-scale application, the hollow fiber geometry will be preferable to spiral wound membranes because of high packing density (membrane area per unit volume of vessel) and easy module assembly.

Carbon membranes are fabricated by the carbonization of polymeric membranes in a special carbonization procedure ("carbonization protocol"). The choice of precursor will greatly affect the prepared carbon membranes. Saufi et al [15] reviewed various precursors like polyimide, polyacrylonitrile (PAN), poly(phthalazinone ether sulfone ketone) and poly(phenylene oxide) which were reported in the open literature. Most HFCMs are rigid and have high microporosity which provides the high productivity and the molecular sieving mechanism exhibit the high selectivity. Hence it has been documented that carbon membranes may exceed the Robeson upper bound and show higher separation performance [5] [16]. The focus was to find a commercially available and cheap polymeric precursor material which could be used for preparation of high performance carbon membranes. Beside the choice of precursor, the carbon membrane performance will also depend on the carbonization parameters. In literature it has been reported the influences of carbonizing atmosphere, flow rate of purge gas, heating rate, final thermal temperature and soak time on the carbon membrane properties [16-19]. To the knowledge of the authors of the current paper, there has, however, not been reported a systematic approach for optimization of carbonization conditions as presented in the current work.

In this work, the cellulose acetate (CA) hollow fiber membranes were spun based on the well-known dry-wet spinning method [20-21]. The spun hollow fiber membranes were then pretreated by deacetylation as described elsewhere [22-23]. The HFCMs were prepared by carbonization of the deacetylated CA precursor which was found to be

suitable, and cheap, commercial available. The four carbonization parameters of atmosphere, heating rate, final temperature and final soak time were optimized by orthogonal experimental design (OED) method. The OED method is also being used in much of chemical process industry [24-25]. The OED method can be used to investigate the effects of multi-variable factors systematically, hence reducing the needed number of experiments greatly. This method is used widely in Chemometrics and the market decision area. The conjoint analysis has, in a relatively short time, become a popular research tool for statistical analysis. Green and Srinivasan provided a state-of-the-art review of the research activities and developments in the market area [26-28]. The conjoint analysis was employed to analyze the orthogonal experimental results and investigate the influence of carbonization parameters on the transport properties of the prepared carbon membranes. The high performance carbon membranes were fabricated under the optimal carbonization condition, and the membrane structure and morphology were characterized by various analysis techniques such as Fourier transform infrared (FTIR) spectroscopy and scanning electron microscope (SEM). The single gas and gas mixture measurements were also used to characterize the prepared carbon membrane performances of permeability and selectivity.

## **2 Experimental Section**

### **2.1 Materials**

The polymeric precursor material, cellulose acetate (CA, MW 100,000) with an average acetyl content of 39.8% was purchased from the ACROS (USA). Polyvinylpyrrolidone (PVP, MW 10,000) was supplied by Sigma. The solvent, N-methyl-2-pyrrolidone (NMP, >99.5%) was purchased from Merck (Darmstadt, Germany). NaOH (>99%) was used in for deacetylation of hollow fiber precursors and purchased from Merck. The materials were used as supplied without further purification.

### **2.2 Preparation of hollow fiber precursors**

The spinning dope consisting of CA/PVP/NMP (22.5% / 5% / 72.5%) was prepared by the following procedure [21]. Firstly, the solvent, NMP and the additive, PVP, were well mixed by mechanical stirring. The polymer CA was then added gradually into the mixture, after which the mixture was stirred for 24 h to ensure a homogenous dope solution. The dope solution and bore fluid were fed into the spinneret by gearwheel pumps. A double spinneret (ID/OD, 0.5/0.7mm) was employed for the spinning by dry-wet method. The spinning conditions were studied and subsequently optimized using an orthogonal experimental design (OED) method as reported elsewhere [29]. The resulting optimal spinning parameters were found to be: 1) an air gap of 25 mm, 2) a dope flow rate of (2.2 ml/min), 3) a bore fluid composition of water+NMP (85 %), 4) a

bore flow rate (40 % of dope flow rate) and 5) a water quench bath maintained at 50 °C. Following the hollow fiber spinning, the fibers were placed in a water bath with a flowing stream of water in order to remove excess NMP solvent. The spun hollow fiber precursors were then treated by deacetylation using a 0.075 M NaOH (96 % ethanol) solution for 2h.

### 2.3 Fabrication of Hollow fiber carbon membranes

The deacetylated precursors were carbonized in a tubular furnace (Carbolite® HZS 12/600E) using a working tube of quartz and a quartz container, which are described elsewhere [30]. The HFCMs were prepared under different carbonization protocols with various operation modes such as vacuum, inert gas or CO<sub>2</sub> atmosphere, different heating rate, final temperature and soak time. The protocol was optimized with respect to the carbon membranes separation performances for single gas and gas mixture using OED method.

### 2.4 Characterization of precursor and carbon membranes

Gas separation performance for carbon membranes was measured using single gas (N<sub>2</sub>, O<sub>2</sub>, CO<sub>2</sub>, CH<sub>4</sub>) and binary gas mixture (10% CO<sub>2</sub> and 90% N<sub>2</sub>). For single gas tests, a standard pressure-rise setup (MKS Baratron® pressure transducer, 0–100 mbar range) with LabView® data logging was conducted to measure the permeability ( $P = 273 \times 10^7 VI(dp/dt) / (76 \Delta p AT_{exp.})$ ), Barrer, 1 Barrer = 10<sup>-10</sup> cm<sup>3</sup> (STP).cm / (cm<sup>2</sup>.s.cmHg) and ideal selectivity ( $\alpha_{A/B} = P_A / P_B$ ), which was described elsewhere [5, 31-32]. The gas will feed from shell side and permeate from bore side, and the carbon membrane module was shown in Fig. 1.

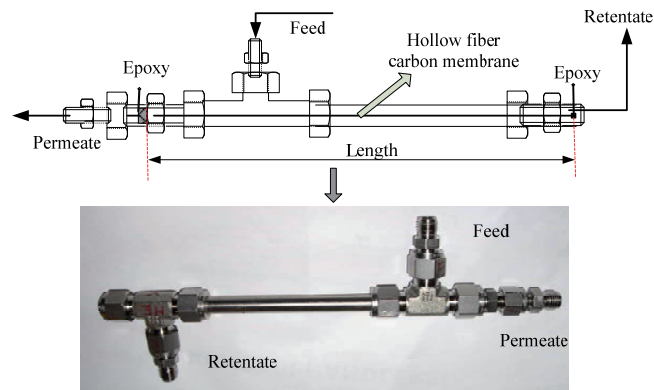


Fig. 1. Schematic and lab-scale hollow fiber carbon membrane module

For binary gas mixture measurements, a gas chromatograph (GC) of Agilent 6890N was applied to measure the gas composition in permeate and retentate stream. The dependency

of gas separation performance on the temperature and stage-cut (ratio of permeate flow rate to feed flow rate) were investigated. Considering the partial pressure of downstream gas is much lower than the upstream partial pressure, the permeability of the gas mixture in steady state can be calculated according to the following equations:

$$P_{CO_2} = \frac{273 \times 10^7}{76} \cdot \frac{y_{P,CO_2} V l (dp/dt)}{x_{CO_2} p_H A T_{exp.}} \quad (1)$$

$$P_{N_2} = \frac{273 \times 10^7}{76} \cdot \frac{(1 - y_{P,CO_2}) V l (dp/dt)}{(1 - x_{CO_2}) p_H A T_{exp.}}$$

$$\bar{x}_{CO_2} = \frac{x_{F,CO_2} - x_{R,CO_2}}{\ln \left( \frac{x_{F,CO_2}}{x_{R,CO_2}} \right)} \quad (2)$$

where  $V$  (cm<sup>3</sup>) and  $T_{exp.}$  (K) are the test volume and temperature.  $A$  (cm<sup>2</sup>) and  $l$  (cm) are the outer surface area and wall thickness of carbon membrane,  $dp/dt$  is the collection volume pressure increase rate (mbar/s).  $P_{CO_2}$  and  $P_{N_2}$  are the respective permeability values of gas CO<sub>2</sub> and N<sub>2</sub> through carbon membrane.  $p_H$  and  $x_{F,CO_2}$  are the pressure (bar) and CO<sub>2</sub> composition in feed side.  $x_{R,CO_2}$  and  $y_{P,CO_2}$  are the molar fraction of CO<sub>2</sub> in retentate and permeate stream respectively, measured by the GC. The selectivity ( $\alpha$ ) for the gas mixture was calculated using the following equation:

$$\alpha_{CO_2/N_2} = \frac{P_{CO_2}}{P_{N_2}} \quad (3)$$

The spectra for the precursor and the prepared HFCMs were obtained by using Bruker Tensor 27 FTIR. A scanning electron microscope (SEM) (Zeiss SUPRA 55VP) and element analysis were used to characterize the morphology, structure and composition of the carbon membranes.

## 2.5 Design of experiments

In order to investigate the carbonization parameter systematically and reduce the number of experiments but still keep sufficient information, the statistical analysis together with OED method was applied to study the influences of carbonization parameter on the transport properties of carbon membranes. The carbonization parameters of purge gas, heating rate, final temperature and final soak time were examined. Table 1 gives the OED's factors and levels of the carbonization protocol for fabrication of HFCMs. A  $L_4^3$  orthogonal experimental design was generated by Statistical Product and Service Solutions (SPSS) software and shown in Table 2. (A brief introduction to the SPSS is summarized in section 2.6) A total of nine and four

batches of carbon membranes were prepared, named as HFCM1-HFCM13. Cases A and B were only used as simulation and prediction.

Table 1 The factors and levels for orthogonal experimental design

Level	Purge gas	Heating rate (K min <sup>-1</sup> )	Final temperature (K)	Final soak time (h)
1	Vacuum	1	823	0
2	Nitrogen	2	923	2
3	Carbon dioxide	4	1023	4

Table 2 Experimental plan

No.	Purge gas	Heating rate (K min <sup>-1</sup> )	Final temperature (K)	Final soak time (h)	Carbon membranes
1	Vacuum	2	923	2	HFCM-1
2	Nitrogen	1	1023	2	HFCM-2
3	Nitrogen	4	923	0	HFCM-3
4	Nitrogen	2	823	4	HFCM-4
5	Carbon dioxide	4	823	2	HFCM-5
6	Carbon dioxide	1	923	4	HFCM-6
7	Vacuum	1	823	0	HFCM-7
8	Vacuum	4	1023	4	HFCM-8
9	Carbon dioxide	2	1023	0	HFCM-9
10(a)	Vacuum	1	1023	0	HFCM-10
11(a)	Vacuum	2	1023	0	HFCM-11
12(a)	Nitrogen	1	1023	0	HFCM-12
13(a)	Vacuum	1	823	4	HFCM-13
14(b)	Nitrogen	4	823	2	A
15(b)	Carbon dioxide	4	923	4	B

a: Holdout, b: Simulation

### 3 Theoretical Basis

Statistical experimental design methods have been widely employed in process engineering and product design area because these methods provide a systematic and efficient plan for experimentation under the consideration of the interactive effects among the control factors. Therefore, many factors can be studied and optimized simultaneously [24]. Among these methods, the orthogonal experimental design (OED) method, developed by Taguchi [33], possesses the advantage that many factors can be examined simultaneously and much quantitative information can be extracted by only a few experimental runs. The variables that have been chosen for an experiment are commonly termed as factors. The number of factors differs from experiment to experiments. Levels of factors can be decided more freely when adjustment by designer. When the factors and levels are both set, the orthogonal array can be generated by SPSS software. The conjoint analysis method is employed to analyze the experimental results, and the Kendall's tau coefficient is used to characterize the statistical dependence. The utilities (part-worth) present the importance for each factor level. The range (highest minus lowest) of the utility values for each factor provides a measurement of how important the factor was to overall preference. Factors with greater utility ranges play a more significant role than those with smaller ranges. The importance score (IMP) for factor  $i$  (%) is calculated:

$$IMP_i = 100 \frac{Range_i}{\sum_{i=1}^p Range_i} \quad \text{where } p = \text{factor number} \quad (4)$$

If there are several subjects used for analysis, the importance for each factor is calculated separately for each subject, and these are then averaged. For prediction, the probability of each simulation ( $\pi_i$ ) can be estimated according to following methods: The Maximum utility model determines the probability as the number of respondents predicted to choose the case divided by the total number of respondents. The BTL (Bradley-Terry-Luce) model determines the probability as the ratio of one case utility to that for all simulation cases. The Logit model is similar to BTL but uses the natural log of the utilities instead of the utilities.

## 4 Results and discussion

### 4.1 Analysis for OED

The single gas tests were executed at 30 °C with a feed pressure of 2 bar for all prepared carbon membranes. The resulting membrane performances are shown in Fig. 2. As can be seen, the results for the carbonized cellulosic-based membranes are for most part of the experiments well above the polymeric precursor with respect to selectivity and also permeability, although not yet above the Robeson upper bond. By

inclusion of metal salts in the matrix, the separation performance may be lifted above the mentioned upper bound [32]

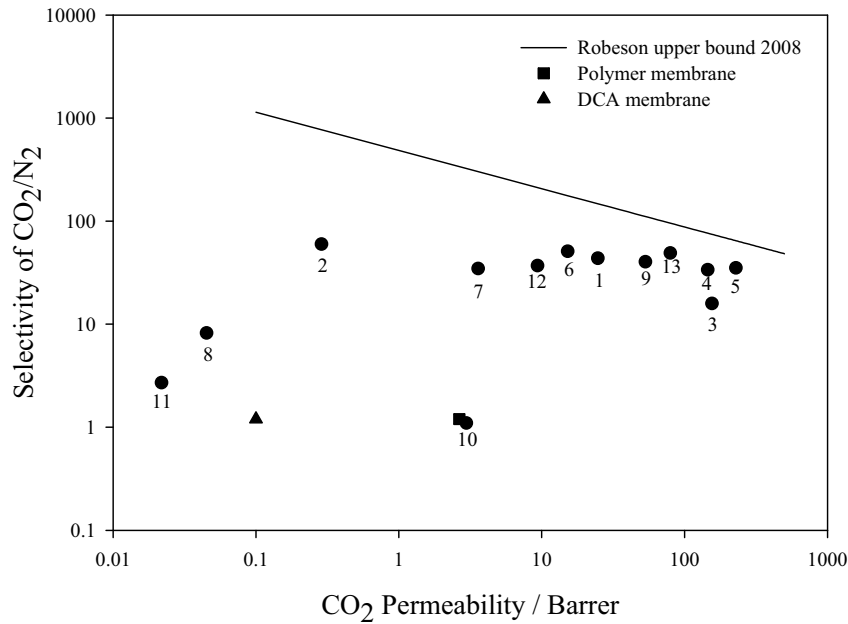


Fig. 2. Single gas permeation test results for the OED experiments at 30 °C and 2 bar (●) carbon membranes, (▲) deacetylated precursor, (■) polymer membrane, and solid line corresponds to upper bound 2008

A statistical analysis method of conjoint analysis in SPSS software (see details in section 2.6) was employed for modeling based on the experimental results presented in Fig. 2. The conjoint procedure is used to estimate the utility (part worth) of the contribution for each factor's level. Two subjects of permeability and selectivity for the prepared HFCMs were used to estimate the membrane performances. The importance for each factor was calculated separately for each subject, and then averaged. The model relationship coefficient was estimated by Pearson's R and Kendall's tau values (0.97 and 0.83 respectively), which indicates that it keeps good consistency between the estimated preferences and experiment results. The Kendall's tau coefficient for the holdout experiments displays 0.67, which is only used to check on the validity of the utilities. Table 3 shows the utilities (part-worth) for each factor level and averaged importance scores for all factors. Higher utility values indicate greater preference. From Table 3, we can find that the importance for these four factors is sorted as follows:

Purge gas > Final temperature > Heating rate > Final soak time

Table 3 Utilities and averaged importance scores for different factors

Factor	Level	Utility Estimate	Average importance scores (%)
Purge gas	Vacuum	-2.333	36.1
	Nitrogen	0.970	
	Carbon dioxide	1.364	
Heating rate (K min <sup>-1</sup> )	1	0.364	21.9
	2	0.727	
	4	1.091	
Final temperature (K)	823	1.000	22.5
	923	0.061	
	1023	-1.061	
Final soak time (h)	0	-0.545	19.5
	2	1.121	
	4	-0.576	
(Constant)		4.273	

So the parameter of *purge gas* will greatly affect the carbon membrane performances, and the parameter of *final soak time* effect has relatively little effect. The optimal carbonization condition of CO<sub>2</sub>-823K-4K/min -2h was hence obtained. Therefore, the CO<sub>2</sub> was used as the most effective purge gas for preparation of cellulose derived carbon membranes. Since the utilities are all expressed in a common unit, they can be added together to give the total utility of any combination. Table 4 gives a simple comparison for the two combinations of different factor levels and the optimal deacetylation condition. Averaged importance score provides a measure of how important the factor is to overall preference.

Factors with greater averaged importance score play a more significant role than those with smaller values, which indicates the carbon membrane prepared from condition 2 will have better performance than that from condition 1.

Table 4 An example for different carbonization conditions

Case	Utility (Purge gas)	Utility (Heating rate)	Utility (Final temperature)	Utility (Final soak time)	Utility (Constant)	Total utility
1	Vacuum (-2.333)	2K min <sup>-1</sup> (0.727)	823k (1.000)	4h (-0.576)	4.273	3.091
2	Nitrogen (0.970)	2K min <sup>-1</sup> (0.727)	823k (1.000)	2h (1.121)	4.273	8.091

The real power of conjoint analysis is the ability to predict preference for product profiles that were not rated by the subjects. Based on the conjoint analysis results of orthogonal experiment design, one can predict the carbon membrane performances under the other carbonization conditions which are not included in the plan and holdout experiments within the level's range of each factor. These are here referred to as simulation cases A and B in Table 2. The simulation results were given in Table 5. Across the 2 subjects (permeability and selectivity) in this study, all three models of Maximum utility, BTL and Logit indicated that simulation case A would be preferred. In order to validate this simulation result, the carbon membranes were carbonized under both conditions. The membrane performances tested and illustrated in Table 5. It can be found that the permeability for case A is around two times higher than that of case B, and the selectivity is only a little bit lower than that of case B, which kept the consistency with the simulation results by conjoint analysis- higher score corresponds to higher performance. Therefore, the prediction results based on conjoint analysis could be well used to guide for the preparation of high performance carbon membranes.

Table 5 Simulation and experimental results by conjoint analysis

Case	Score	Preference Probabilities of Simulations			Experimental results		
		Maximum utility	Bradley-Terry-Luce	Logit	Permeability of CO <sub>2</sub> (Barrer)	Selectivity of CO <sub>2</sub> /N <sub>2</sub>	Average weight loss (%)
A	8.455	90.9%	57.2%	85.9%	96.6	36.9	73.5
B	6.212	9.1%	42.8%	14.1%	45.2	45.4	75.9

## 4.2 FTIR analysis

The FTIR spectra of precursor and carbon membranes (HFCM-5) from optimal carbonization temperatures procedure are shown in Fig. 3. For the deacetylated cellulose acetate precursor, the characteristic absorption peaks of 1030, 1230, and 1740 $\text{cm}^{-1}$  attribute to the ether group ( $\nu_{\text{C-O-C}}$ ), acetyl ester group ( $\nu_{\text{CH}_3\text{-C=O}}$ ) and carbonyl group ( $\nu_{\text{C=O}}$ ) of CA respectively. The C-H bond stretching (2950 $\text{cm}^{-1}$ ) and hydroxy group (3400 $\text{cm}^{-1}$ ) are also shown in the precursor spectra. The characteristic peak 1665  $\text{cm}^{-1}$  attributes to the carbonyl group of PVP which was used as the additive in the precursor. After the carbonization and heat treatment, the intensities of most peaks decreased and disappeared completely due to the decomposition and break down the chemical groups mentioned above, which caused by the release of gases such as CO, CO<sub>2</sub>, H<sub>2</sub> reported by Wu et. al [34]. For the carbon membranes, the new characteristic absorption peaks were found at 2350  $\text{cm}^{-1}$  and 670  $\text{cm}^{-1}$ , which contribute to the CO<sub>2</sub> absorbed in carbon matrix and the aromatic =C-H out of plane deformation as reported by Tin [6].

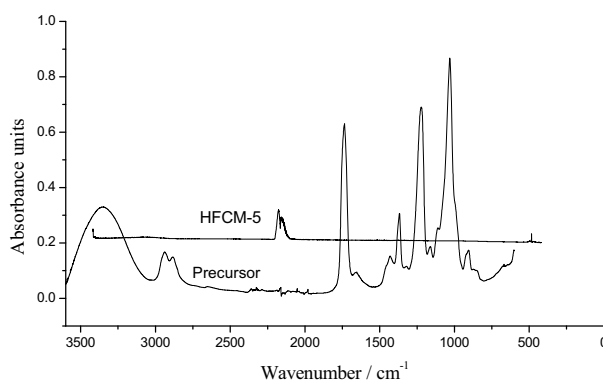


Fig. 3. FTIR spectra for precursor and HFCM-5 obtained at final temperature of 550 °C

## 4.3 SEM characterization

Using examination by SEM images it was documented that the HFCMs form a symmetric structure and the dimensions were now significantly smaller than the precursor fibers due to shrinkage occurred upon carbonization. Fig. 4 shows the cross section and inside surface of the carbon membrane of HFCM-5. The outer diameter and wall thickness of the carbonized hollow fiber membrane were typically around 250  $\mu\text{m}$  and 30  $\mu\text{m}$  respectively. This shows a significant shrinkage of the precursor which had an outer diameter of 400  $\mu\text{m}$  and wall thickness of 50  $\mu\text{m}$ .

#### 4.4 Element analysis

The results for HFCM-5 membranes obtained from the element analysis are presented in Table 6. It is clear from the table that the membrane is high in carbon content, while most of the hydrogen and nitrogen were burned out during carbonization. Moreover, there are approximate 6 % oxygen still present in the carbon membrane which could be caused by some CO<sub>2</sub> adsorbed in the matrix as explained from the FTIR spectrum in Fig. 3.

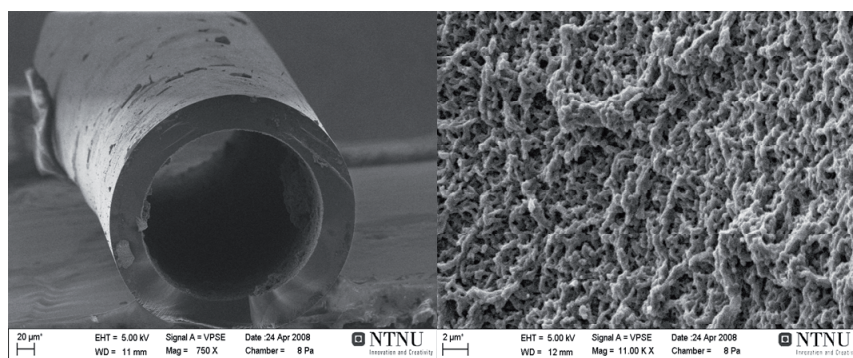


Fig. 4. SEM image of cross section and inside of HFCM-5

Table 6 Results from element analysis for HFCM-5

Sample	Element content (%)			
	C	H	N	O
HFCM-5	87.35	3.48	0.11	6.34

#### 4.5 Single gas tests

The carbon membrane HFCM-5 was tested with various single gases (CO<sub>2</sub>, N<sub>2</sub>, CH<sub>4</sub> and O<sub>2</sub>). Fig. 5 indicates the dependency of permeability values of different gases on the temperature in the range of 30-70 °C, and at constant feed pressure of 2bar.

The apparent transport activation energy,  $E_a$ , and  $P_0$  ( $P = P_0 \exp(-E_a/RT)$ ) can be obtained from these data with varying temperature. Fig.5 shows the logarithmic Arrhenius plot with  $\ln P$  plotted as function of  $1000/T$  [35], and  $E_a$  can be found from the slope of the respective curves. Results are presented in Table 7. The activation energy is an indicator of the probability of a molecular passing a constriction, thus, the lower activation energy relates to a higher permeability. For the large  $E_a$ , the larger

effect temperature will have on the permeability. This can be seen from the Fig. 5 where the permeability of other gas molecules increased faster than that of CO<sub>2</sub>, which results in the slight decrease of selectivity for CO<sub>2</sub> over the other gas molecules. Therefore, the increase of temperature will enhance the transport process, but slightly decrease the gas selectivity of carbon membranes, so the trade-off of the separation performance should be determined for carbon membrane application.

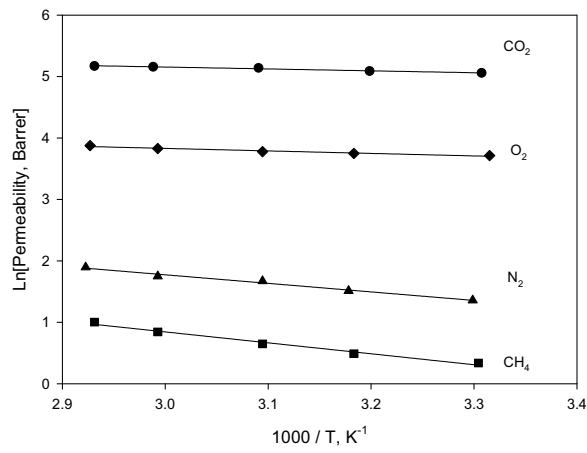


Fig. 5. Dependency of gas permeabilities on temperature for HFCM-5 at feed pressure 2 bar

Table 7 Kinetic parameter for gas permeation of carbon membrane- HFCM-5

Gas molecules	$d_k$ (nm)	$\epsilon/k$ (K)	$E_a$ (kJ mol <sup>-1</sup> )	$P_0$ (Barrer)
CO <sub>2</sub>	0.33	195.0	2.6	437.6
O <sub>2</sub>	0.346	107.0	3.4	156.6
N <sub>2</sub>	0.364	71.4	11.6	382.3
CH <sub>4</sub>	0.38	136.0	14.8	483.7

Suda et. al reported that the activation energy were correlated linearly with kinetic diameter [36]. Therefore, we assumed:

$$E_a = a_1 d_k + b_1 \quad (5)$$

A linear relationship between  $E_a$  and  $d_k$  was also conducted, which can be seen from Fig. 6. These results show high consistency between the experiment results with the assumption.

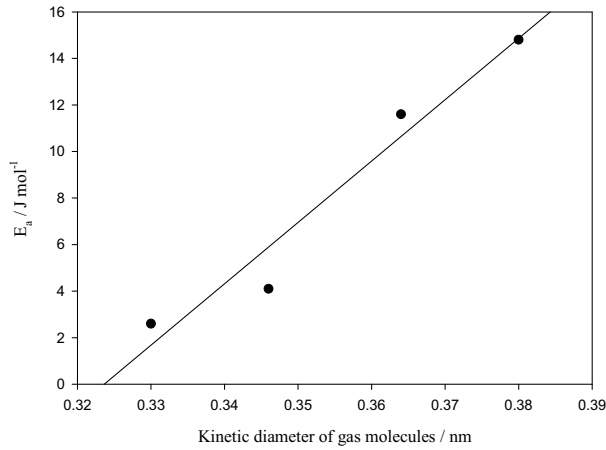


Fig. 6. Relationship between activation energy and gas molecule kinetic diameter

The feed pressure can also affect the membrane performances. Fig. 7 shows the dependency of permeability of CO<sub>2</sub> and N<sub>2</sub> on the feed pressure. The permeability increases with feed pressure in region A since the adsorption is dominating in low driving force, while in region B the permeability becomes mostly independent of pressure due to the diffusion is dominating and the adsorption has relative small influences.

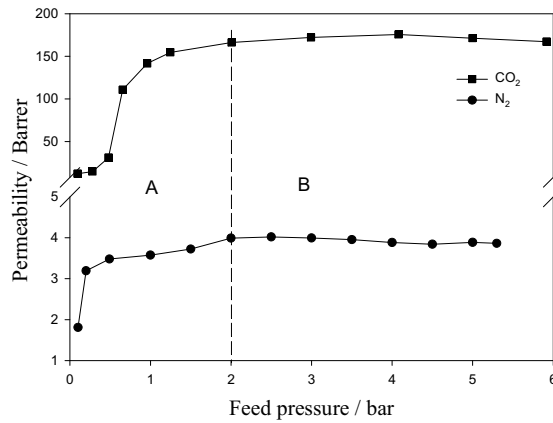


Fig. 7. Dependency of single gas permeability on the feed pressure for HFCM-5 at 30 °C, (●) N<sub>2</sub>, (■) CO<sub>2</sub>

#### 4.6 Gas mixture test

The single gas tests are normally used to indicate the ideal separation performance for carbon membranes. However, the separation properties will be affected by the presence of other penetrants in a gas mixture. The transport of gas mixture will be different from that in single gas, especially for the existing of strong adsorbable gas like CO<sub>2</sub>, so the separation of a gas mixture with 10 % CO<sub>2</sub> and 90 % N<sub>2</sub> was also investigated. Table 8 summarizes the gas mixture test results for different temperature. The permeability for CO<sub>2</sub> and N<sub>2</sub> were both improved due to the transport was enhanced with the increase of temperature from 40 °C to 70 °C, which indicated the increase of temperature can enhance the gas molecules transport through the membranes, while the CO<sub>2</sub> purity has no significant change may due to the selectivity has no obvious decrease within the temperature range 30-70 °C as shown in Table 7 and Fig. 5. Besides the temperature, the stage-cut (the ratio between permeate flux and feed flow rate) was changed by adjusting the flow rate of retentate, which will also affect the carbon membrane separation performance. The dependency of recovery and purity of CO<sub>2</sub> in permeate stream on the stage-cut at constant temperature and pressure of 30 °C and 3.5 bar was also tested, and the results was shown in Fig. 8. It can be seen that the increase of stage-cut leads to higher CO<sub>2</sub> recovery, but lower CO<sub>2</sub> purity. Therefore, the optimal operation condition should be further optimized according to the economic evaluation in future.

Table 8 Effect of temperature on membrane separation performance

Temperature (°C)	Composition in permeate (%)		Permeability (Barrer)	
	CO <sub>2</sub>	N <sub>2</sub>	CO <sub>2</sub>	N <sub>2</sub>
40	76.5	23.5	268.5	9.2
50	77.2	22.8	323.3	10.5
60	79.1	20.9	361.7	10.6
70	79.0	21.0	368.3	10.8

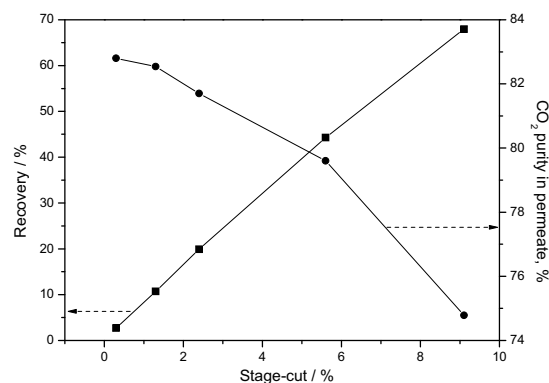


Fig. 8. Dependency of CO<sub>2</sub> recovery and purity on stage-cut at 30 °C and feed pressure of 3.5 bar, (■) CO<sub>2</sub> recovery, (●) CO<sub>2</sub> purity in permeate

## 5 Conclusions

The hollow fiber carbon membranes were prepared by the carbonization of deacetylated cellulose acetate precursor. Based on the orthogonal experimental design, an optimal carbonization procedure with CO<sub>2</sub>-823K-4K/min-2h was obtained, and the importance for the investigated carbonization parameters was sorted out with respect to their influence on carbon membrane separation performances. The order of importance was found to be: purge gas > final temperature > heating rate > final soak time. It was concluded that the purge gas was the most important parameter affecting the final carbon membrane performance, and CO<sub>2</sub> seems to be the most effective purge gas for preparation of high performance cellulose derived carbon membranes. The carbon membrane HFCM-5 prepared from the optimal carbonization process forms a symmetric structure from the SEM images and shows great shrinkage compared to the precursor by carbonization. FTIR spectra showed the decomposition and break down of the chemical groups in precursors in various carbonization environments, which leading to the release of small volatile gas molecules. The single gas test results indicate that the CO<sub>2</sub> has much lower activation energy comparing to O<sub>2</sub>, N<sub>2</sub>, and CH<sub>4</sub>, which resulting to the high selectivity of CO<sub>2</sub> over the other gases. The separation performance was also influenced by operating pressure, especially when the transport driving force was quite low and the adsorption was dominated in low pressure. The gas mixture measurements showed that the operating parameters of temperature and stage-cut for carbon membrane separation process need to be optimized.

### *Acknowledgements*

The authors want to acknowledge the NanoGloWa project for the funding (EUs 6<sup>th</sup> framework program) of the current work

### References

- [1] Baker RW. Future Directions of Membrane Gas Separation Technology. *Ind Eng Chem Res.* 2002;41(6):1393-411.
- [2] Yan S, Fang M, Zhang W, Zhong W, Luo Z, Cen K. Comparative analysis of CO<sub>2</sub> separation from flue gas by membrane gas absorption technology and chemical absorption technology in China. *Energy Convers Manage.* 2008;49(11):3188-97.
- [3] Robeson LM. The upper bound revisited. *J Membr Sci.* 2008;320(1-2):390-400.
- [4] He X, Lie JA, Sheridan E, Hägg M-B. CO<sub>2</sub> Capture by Hollow Fibre Carbon Membranes: Experiments and Process Simulations. *Conf. on GHGT-9; 2008; Washington DC USA; 2008.*
- [5] Lie JA. Synthesis, performance and regeneration of carbon membranes for biogas upgrading-a future energy carrier [PhD]. Trondheim: Norwegian University of Science and technology; 2005.
- [6] Tin PS, Chung T-S, Liu Y, Wang R. Separation of CO<sub>2</sub>/CH<sub>4</sub> through carbon molecular sieve membranes derived from P84 polyimide. *Carbon.* 2004;42(15):3123-31.
- [7] Favvas EP, Kapantaidakis GC, Nolan JW, Mitropoulos AC, Kanellopoulos NK. Preparation, characterization and gas permeation properties of carbon hollow fiber membranes based on Matrimid(R) 5218 precursor. *J Mater Process Tech.* 2007;186(1-3):102-10.
- [8] Ogawa M, Nakano Y. Separation of CO<sub>2</sub>/CH<sub>4</sub> mixture through carbonized membrane prepared by gel modification. *J Membr Sci.* 2000;173(1):123-32.
- [9] Grainger D. Development of carbon membranes for hydrogen recovery. Norwegian University of Science and technology, PhD thesis. 2007.
- [10] He X, Lie JA, Sheridan E, Hägg M-B. Preparation and Characterization of Hollow Fiber Carbon Membranes from Cellulose Acetate Precursors. *Ind Eng Chem Res.* 2011;50(4):2080-7.
- [11] Steel KM, Koros WJ. An investigation of the effects of pyrolysis parameters on gas separation properties of carbon materials. *Carbon.* 2005;43(9):1843-56.
- [12] Singh-Ghosal A, Koros WJ. Air separation properties of flat sheet homogeneous pyrolytic carbon membranes. *J Membr Sci.* 2000;174(2):177-88.

- [13] Barsema JN. Carbon membranes precursor, preparation and functionalization [PhD]. Enschede: University of Twente; 2007.
- [14] Vu DQ, Koros WJ, Miller SJ. High Pressure CO<sub>2</sub>/CH<sub>4</sub> Separation Using Carbon Molecular Sieve Hollow Fiber Membranes. *Ind Eng Chem Res.* 2001;41(3):367-80.
- [15] Saufi SM, Ismail AF. Fabrication of carbon membranes for gas separation--a review. *Carbon.* 2004;42(2):241-59.
- [16] Kiyono M, Williams PJ, Koros WJ. Effect of pyrolysis atmosphere on separation performance of carbon molecular sieve membranes. *J Membr Sci.* 2010;359(1-2):2-10.
- [17] Su J, Lua AC. Influence of carbonisation parameters on the transport properties of carbon membranes by statistical analysis. *J Membr Sci.* 2006;278(1-2):335-43.
- [18] Geiszler VC, Koros WJ. Effects of Polyimide Pyrolysis Conditions on Carbon Molecular Sieve Membrane Properties. *Ind Eng Chem Res.* 1996;35(9):2999-3003.
- [19] David LIB, Ismail AF. Influence of the thermastabilization process and soak time during pyrolysis process on the polyacrylonitrile carbon membranes for O<sub>2</sub>/N<sub>2</sub> separation. *J Membr Sci.* 2003;213(1-2):285-91.
- [20] Chung TS, Hu X. Effect of air-gap distance on the morphology and thermal properties of polyethersulfone hollow fibers. *J Appl Polym Sci.* 1997;66:1067.
- [21] Qin J-J, Li Y, Lee L-S, Lee H. Cellulose acetate hollow fiber ultrafiltration membranes made from CA/PVP 360 K/NMP/water. *J Membr Sci.* 2003;218(1-2):173-83.
- [22] Liu H, Hsieh Y-L. Ultrafine fibrous cellulose membranes from electrospinning of cellulose acetate. *J Polym Sci Part B: Polym Phys.* 2002;40(18):2119-29.
- [23] Son WK, Youk JH, Lee TS, Park WH. Electrospinning of Ultrafine Cellulose Acetate Fibers: Studies of a New Solvent System and Deacetylation of Ultrafine Cellulose Acetate Fibers. *J Polym Sci Part B: Polym Phys.* 2004;42:5-11.
- [24] Houg J-Y, Liao J-H, Wu J-Y, Shen S-C, Hsu H-F. Enhancement of asymmetric bioreduction of ethyl 4-chloro acetoacetate by the design of composition of culture medium and reaction conditions. *Process Biochem.* 2007;42(1):1-7.
- [25] Rao RS, Prakasham RS, Prasad KK, Rajesham S, Sarma PN, Rao LV. Xylitol production by *Candida* sp.: parameter optimization using Taguchi approach. *Process Biochem.* 2004;39(8):951-6.
- [26] Green PE, Srinivasan V. Conjoint Analysis in Consumer Research: Issues and Outlook. *J Cons Res.* 1978;5:103-23.

- [27] Green PE, Srinivasan V. Conjoint Analysis in Marketing: New Developments Implications for Research and Practice. *J Marketing*. 1990; 54:3-19.
- [28] Akaah IP, Korgaonkar PK. A Conjoint Investigation of the Relative Importance of Risk Relievers in Direct Marketing. *J Advertising Res*. 1988;28:38-44.
- [29] He X, Hägg M-B. Using orthogonal experimental design for spinning defect-free hollow fiber membranes. *Advanced Membrane Technology IV: Membranes for Clean and Sustainable Processes*. Trondheim 2009.
- [30] Cavenati S, Grande CA, Rodrigues AE. Separation of CH<sub>4</sub>/CO<sub>2</sub>/N<sub>2</sub> mixtures by layered pressure swing adsorption for upgrade of natural gas. *Chem Eng Sci*. 2006;61(12):3893-906.
- [31] He X, Lie JA, Sheridan E, Hägg M-B. Preparation and Characterization of Hollow Fibre Carbon Membranes based on a Cellulosic Precursor. *Conf. on ICOM 2008*. Honolulu, Hawaii USA 2008.
- [32] Lie JA, Hagg M-B. Carbon membranes from cellulose and metal loaded cellulose. *Carbon*. 2005;43(12):2600-7.
- [33] Taguchi G. System of experimental design. In: Engineering methods to optimize quality and minimize costs. New York: Kraus International Publications Of The Astronomical Society Of Australia. 1987.
- [34] Wu Q, Pan N, Deng K, Pan D. Thermogravimetry-mass spectrometry on the pyrolysis process of Lyocell fibers with and without catalyst. *Carbohydr Polym*. 2008;72(2):222-8.
- [35] Rafizah WAW, Ismail AF. Effect of carbon molecular sieve sizing with poly(vinyl pyrrolidone) K-15 on carbon molecular sieve-polysulfone mixed matrix membrane. *J Membr Sci*. 2008;307(1):53-61.
- [36] Suda H, Haraya K. Gas Permeation through Micropores of Carbon Molecular Sieve Membranes Derived from Kapton Polyimide. *J Phys Chem B*. 1997;101(20):3988-94.



## **Appendix F**

Structural, Kinetic and Performance Characterization of Hollow  
Fibre Carbon Membranes

Article submitted to *Journal of Membrane Science*



## Structural, Kinetic and Performance Characterization of Hollow Fiber Carbon Membranes

Xuezhong He, May-Britt Hägg\*

Department of Chemical Engineering, Norwegian University of Science and Technology, N-7491 Trondheim, Norway

**Abstract:** The hollow fiber carbon membranes (HFCMs) were prepared from different deacetylated cellulose acetate precursors by controlled carbonization procedure with CO<sub>2</sub> purge gas, a heating rate of 4 K/min, a final temperature of 550 °C and a final soak time 2 h. The SEM images and TGA analysis indicated that the carbon membranes form a symmetric structure and a high average weight loss during the carbonization process. The Langmuir affinity parameters of the carbon membranes were estimated by the CO<sub>2</sub> and N<sub>2</sub> adsorption equilibrium data. The membrane structure parameters of micropore volume, average pore size and d-spacing were determined by the CO<sub>2</sub> adsorption experiments combined with XRD characterization. The kinetic rate constants were also obtained from the CO<sub>2</sub> kinetic adsorption experiments. Single gas permeation tests of H<sub>2</sub>, CO<sub>2</sub>, O<sub>2</sub>, N<sub>2</sub> and CH<sub>4</sub> were conducted to investigate the transport mechanism in the carbon membrane separation process. Moreover, the influences of temperature and feed pressure on the gas separation performances were also studied on the basis of the single gas and gas mixture (synthetic flue gas, CO<sub>2</sub>-N<sub>2</sub>-O<sub>2</sub>) measurements.

**Keywords:** hollow fiber carbon membrane; adsorption; kinetic; permeability; selectivity;

---

\* Corresponding author. Tel.: +47 73594033; fax: +47 73594080.  
E-mail address: may-britt.hagg@chemeng.ntnu.no (M.-B. Hägg)

## 1 Introduction

Membrane process is considered to be a suitable technology for gas separation due to high efficiency, simple operation and low costs. Although the gas separation membranes are mostly based on the polymeric membranes, the trade-off of permeability / selectivity as well as the limitation of operation temperature directs the polymeric membrane development into the alternative inorganic membranes. The ultramicroporous carbon membranes (pore size in the range of 3-5 Å) are promising candidates for gas separation due to the high performance above the Robeson upper bound [1]. Considering their narrow pore size distribution in the range of gas molecular size, these carbon membranes are suitable for the separation of gas pairs with quite similar kinetic diameter such as CO<sub>2</sub>-N<sub>2</sub>, O<sub>2</sub>-N<sub>2</sub> and CO<sub>2</sub>-CH<sub>4</sub> (small variations of 0.2-0.5 Å), where the slightly smaller molecule in the gas pair (O<sub>2</sub> and CO<sub>2</sub>) can preferentially pass through the carbon membrane. The first carbon membranes was prepared by pyrolysis of cellulosic and phenolic resin [2]. Since then, various polymeric precursors such as polyimide [3-5], polyacrylonitrile (PAN) [6], poly(phthalazinone ether sulfone ketone) [7] and poly(phenylene oxide) [8-9] and cellulose [10] have been used as precursors for preparation of carbon membranes. A more detail review for the development of carbon membranes (until 2004) can be found in the literature of Saufi [11].

In the past research has mostly focused on the development of novel carbon membranes in order to improve the separation performance. There is a considerable amount of literature published reporting permeation data for single gases or gas mixtures through carbon membranes. However, relatively few efforts have been taken on the investigation of other important aspects of the carbon membranes. Koros analyzed the humidity effects on the membrane performance [12]. Lagorsse studied the aging of the carbon molecular sieve membranes exposed to water vapor and different dry environments (air, oxygen, nitrogen, propylene, etc.) [13]. A simple, energy effective and rapid electrothermal regeneration technique used for carbon membranes was reported by Lie [14]. There are also some reports on the characterization of micropore structure and kinetic measurements of carbon membranes, especially for hollow fiber carbon membranes (HFCMs). Lagorsse used the gas sorption and permeation tests to characterize the micropore structure of the commercial HFCMs produced by Carbon Membrane Ltd and the flat carbon membranes [15-16]. Nguyen reported the estimation of the pore size distribution based on the gas adsorption equilibrium data [17]. Sedigh reported to use gas adsorption techniques to relate the microstructure characteristics of the carbon membranes to their transport and separation properties [18].

Based on the findings reported above, some fundamental researches related to the materials properties seem still to be lacking. Therefore, this work will mainly focus on

the preparation and characterization of hollow fiber carbon membranes from deacetylated cellulose acetate precursors by a specific multi-dwell carbonization protocol. The gas sorption and permeation experiments were conducted to give insight to the micropore structure of the carbon membranes, and to try to understand the relationship between the pore structure and the gas separation performance.

## **2 Experimental**

### **2.1 Materials**

The polymer material, cellulose acetate (CA, MW 100 000) with an average acetyl content of 39.8% was purchased from the ACROS (USA). Polyvinylpyrrolidone (PVP, K10) was supplied by Sigma. The solvent, N-methyl-2-pyrrolidone (NMP, >99.5%) was purchased from Merck (Darmstadt, Germany). The glycerol (>98%) was purchased from BDH / VWR used for solvent exchange, and the NaOH (>99%) used for deacetylation was also supplied from Merck. The materials were used as supplied without further treatment.

### **2.2 Preparation of hollow fiber carbon membranes**

The cellulose acetate hollow fiber (HF) membranes were spun by well known dry-wet spinning technique from a dope solution of CA / PVP / NMP (22.5% / 5% / 72.5%) and a bore fluid of H<sub>2</sub>O/NMP (15 % / 85 %) [19]. Two batches of hollow fibers (HF-1 and HF-2) were prepared from different spinning conditions, include the spinneret dimension, air gap, flow rate of dope and bore fluid, and coagulation bath temperature as listed in Table 1. The spun fibers were placed in the fresh water bath overnight, and subsequently soaked in a 10 % glycerol solution for solvent exchange to remove the residual NMP from the fibers. The CA hollow fibers were then deacetylated by immersion in a 0.075 M NaOH (solvent: 96% ethanol) solution for 2 h to obtain the precursors of DHF-1 and DHF-2 separately. The hollow fiber carbon membranes (HFCMs) of HFCM-1 and HFCM-2 were fabricated via the controlled carbonization procedure with CO<sub>2</sub> purge gas, a heating rate of 4 °C/min, a final thermal temperature of 550 °C and a final soak time of 2 h from the precursors of DHF-1 and DHF-2, respectively. The detail carbonization procedure was described elsewhere [14].

### **2.3 Membrane Characterization**

A thermogravimetric analyzer (TGA) from TA Instruments (New Castle, DE, USA) model Q500 was used to characterize the weight loss of the precursors of DHF-1 and DHF-2 during the pyrolysis process. Helium was introduced as purge gas with a constant flow rate of 90 ml/min. The experimental data was processed with Universal Analysis 2000 software. A Zeiss SUPRA 55VP scanning electron microscopy (SEM)

was used to qualitatively assess the structure and morphology of the precursors and the prepared HFCMs. Backscatter and secondary electron images were obtained using an acceleration potential of 5 keV. The samples measured had not been used in gas permeation tests, but were taken from the same carbonization batch as those used for the sorption and permeation tests. The element analysis was also conducted to determine the composition of carbon membranes by combustion of the samples in Analytische Laboratorien (Germany). A wide-angle X-ray diffraction (WAXD) of Bruker AXS D8 Focus X-ray was used to characterize the d-spacing of membranes. A  $\text{CuK}\alpha$  radiation (1.54 Å) was performed to record the WAXD pattern with  $2\theta$  from  $15^\circ$  to  $70^\circ$ .

Gas adsorption equilibrium data for the samples were obtained by a RobuTherm magnetic suspension balance (MSB) having a 0.01 mg resolution and 0.02 mg reproducibility. The MSB overcomes some disadvantages of other conventional gravimetric sorption instruments by separating the microbalance from the sample and adsorbed gases [20]. The sample is placed in a suspended basket by a permanent magnet through an electromagnet in a closed system. The MSB instrument can perform the sorption measurements within a pressure range from vacuum to 35 bar and 150 bar for  $\text{CO}_2$  and  $\text{N}_2$ , respectively. Moreover, the temperature can be well controlled within the range from 298 K to 423 K using a Julabo thermostatic circulator. The system can automatically measure the weight change of the samples over time at a certain temperature and pressure according to the measurement procedure described elsewhere [21]. The sample density was determined based on the buoyancy measurement with helium by increasing the pressure from 1 bar to 30 bar (change the gas density). The linear regression of the measured balance masses ( $m_{bal}$ ) versus the helium density was carried out to obtain the true density of the sample as follows:

$$m_{bal} = m_{SC+S} - \rho V_{SC+S} \quad (1)$$

where the  $m_{SC+S}$  and  $V_{SC+S}$  are the mass and volume of the sample container together with the sample, respectively, which was determined from the intercept and slope of the linear regression. By subtraction of the mass ( $m_{SC} = 4.2249$  g) and volume ( $V_{SC} = 0.55$  ml) for the sample container based on the blank experiments, the mass ( $m_S$ ) and volume ( $V_S$ ) of the sample was obtained. Therefore, the true density of the samples can be calculated ( $\rho_S = m_S/V_S$ ). The  $\text{CO}_2$  and  $\text{N}_2$  adsorption onto the carbon membranes were executed at a constant temperature (298 K) and a flow rate of 100 ml/min with pressure up to 15 bar and 20 bar, respectively. In addition, the kinetic measurements were conducted at a constant pressure 1 bar with different  $\text{CO}_2$  feed flow rates (100, 200 and 300 ml/min). The weight change, pressure and temperature were measured continuously until the sorption equilibrium was achieved.

Three membrane modules consisting of varying numbers of hollow carbon fibers were constructed by ¼ inch stainless steel tube, Swagelok tees and unions. The schematic of the carbon membrane module is shown in Fig. 1. The characteristics of these in-house modules are given in Table 2. Single gas permeation tests were executed at 303 K and a feed pressure of 2 bar from shell side (maximum 20 mbar in permeate side) in a standard pressure-rise setup (MKS Baratron® pressure transducer, 0~100 mbar range) with LabView® data logging. The gas permeation test setup has been described elsewhere [22]. The order of testing was always H<sub>2</sub>, N<sub>2</sub>, O<sub>2</sub>, CH<sub>4</sub> and finally CO<sub>2</sub> in order to prevent the strongly adsorbing gases from disturbing the performance of the more ideal or non-interacting gases in carbon membranes [22]. The tests were run from several minutes to several hours to ensure that the transient phase of diffusion was passed and a steady state had been obtained ( $dp/dt$  tends to a constant). The gas permeability,  $P$  (Barrer, 1Barrer= $10^{-10}$  cm<sup>3</sup> (STP).cm / (cm<sup>2</sup>.s.cmHg)) was calculated using the following equation:

$$P = \frac{273 \times 10^7 V l (dp/dt)}{76 \Delta p A T_{exp.}} \quad (2)$$

where  $V$  is the collection volume (cm<sup>3</sup>) that can be measured with a pre-calibrated permeation cell reported elsewhere [22-23],  $dp/dt$  is the collection volume pressure increase rate (mbar/s),  $l$  and  $A$  are thickness (cm) and total active membrane area (cm<sup>2</sup>) respectively,  $\Delta P$  (bar) is the pressure drop cross the membrane and  $T_{exp}$  the experimental temperature (K). In this work, the ideal selectivity is defined as the ratio of the pure gas permeability values which is evaluated as follows:

$$\alpha_{A/B} = \frac{P_A}{P_B} \quad (3)$$

For mixed gas separation measurements, a permeation cell and a gas chromatograph (GC) were combined to analyze the gas composition and calculate the permeability of gas component. A detailed description for the gas mixture measurements has been reported elsewhere [24].

### 3 Results and Discussion

#### 3.1 TGA and SEM characterizations

The weight loss for the precursors during the carbonization process was assessed by TGA with a dry helium flow rate of 90 ml/min, as shown in Fig. 2. About 70 % weight loss was found following the final temperature up to 550 °C. SEM was used to characterize the structure and morphology of the materials, and Fig. 3 shows the cross section images of the precursors and carbon membranes. The SEM images document a nice symmetric structure of the HFCMs. The outer diameter and wall thickness of the

carbon membranes are much smaller compared to the precursors due to the shrinkage of precursors during the carbonization process, which was supported by the high weight loss on the basis of the TGA analysis.

### 3.2 Element analysis

The results for the carbon membranes obtained from the element analysis are presented in Table 3. It is evident that the carbon membranes have quite high carbon content. Most of hydrogen and nitrogen atoms were burned out during carbonization, resulting in that only a small amount of hydrogen and nitrogen are left in the carbon membranes. There is, however, still some oxygen left in the carbon matrix, additionally some CO<sub>2</sub> may also be adsorbed in the carbon membrane due to the CO<sub>2</sub> as purge gas for the carbonization procedure.

### 3.3 XRD characterization

The XRD patterns of the carbon membranes are shown in Fig. 4. The average d-spacing ( $d_{002}$ ) values were calculated based on the Bragg's equation ( $n\lambda=2d\sin\theta$ ), determining the interlayer distance of carbon matrix. The d-spacing is considered to be an efficient diffusion path for gas molecules through the carbon membranes, which can be used to evaluate the membrane microstructure [8]. The d-spacing values for HFCM-1 and HFCM-2 were found to be 4 Å and 4.2 Å with the broad asymmetric peaks located in  $2\theta = 21.1^\circ$  and  $22.2^\circ$ , respectively, which is larger than the typical graphitic and turbostratic d-spacing of 3.4 - 3.8 Å. The significant difference characterizes linearly organized aliphatic carbon with sp hybridization [25], which indicates the carbon membrane forms an amorphous carbon matrix with a mixture of sp<sup>2</sup> and sp carbon components. The XRD patterns of the carbon membranes exhibit another very weak peak around  $2\theta = 43^\circ$  with a d-spacing value of 2.1 Å, which is also the characteristic peak of the (100) plane in graphite.

### 3.4 Gas sorption measurements

The adsorption data of CO<sub>2</sub> and N<sub>2</sub> onto the carbon membranes were obtained at 298 K and medium pressure as shown in Fig. 5. A type I equilibrium isotherm was found according to the IUPAC definition for adsorption isotherms. The Langmuir-Freundlich model was used to fit the experimental data, and is described as follows [26]:

$$q = \frac{bq_m P^{1/n}}{1 + bP^{1/n}} \quad (4)$$

where  $q$  is the adsorption amount at pressure ( $p$ ),  $b$  and  $q_m$  are the Langmuir affinity parameter and the maximum adsorption amount,  $n$  is the Langmuir-Freundlich coefficient. A strong correlation was found between the Langmuir-Freundlich model fitting and the adsorption equilibrium data. Table 4 summarizes the adsorption

equilibrium parameters for different carbon membranes. N<sub>2</sub> has lower Langmuir adsorption parameter (*b*) which indicates a relative weak adsorption in relation to CO<sub>2</sub>. The coincidence of CO<sub>2</sub> adsorption and desorption for both carbon membranes indicates a reversible CO<sub>2</sub> adsorption process at 298 K as shown in Fig. 5. In order to determine the sample micropore volume, it is necessary to know the density of adsorbed CO<sub>2</sub> in the carbon membrane. The values of density that can be used at this temperature fall within the range of 0.7-1.03 g/cm<sup>3</sup> [27]. An average of 0.85 g/cm<sup>3</sup> was used in this work. The Dubinin-Radushkevitch (DR) equation was used to fit the CO<sub>2</sub> isotherm adsorption data as follows:

$$\frac{w}{w_0} = \exp\left(-\left(\frac{RT \ln(p_0/p)}{\beta E_0}\right)^2\right) \quad (5)$$

where *w* is the volume adsorbed at a pressure *p*, *w*<sub>0</sub> is the micropore volume of carbon membrane, *E*<sub>0</sub> is the adsorption activation energy dependent on the pore structure, and β is the affinity coefficient that is the characteristics of the adsorption capacity used in this case is 0.35 [27]. For the non-ideal gas of CO<sub>2</sub> in high pressure, the fugacity was used instead of pressure,  $(RT \ln(f_0/f))^2$ . The relative fugacity used in the isotherms is the fugacity divided by the saturation fugacity of 42 bar for CO<sub>2</sub> at 298 K [27]. Fig. 6 shows the characteristic curves of the carbon membranes (plots of  $\ln(w)$  versus  $(RT \ln(f_0/f))^2$ ), and the similar slopes at high and low pressures indicate that the carbon membranes have quite homogeneous porosity. Moreover, the average micropore width can be roughly estimated by Stoeckli equation when the DR equation applied [28].

$$L_0 = \frac{10.8(nm \cdot kJ \cdot mol^{-1})}{E_0 - 11.4(kJ \cdot mol^{-1})} \quad (6)$$

The structural parameters for the carbon membranes were measured and estimated based on the above expression, and summarized in Table 5.

The sample true density ( $\rho_s$ ) was determined by buoyancy measurements with the non-absorbable gas helium. The experimental data and linear fitting are illustrated in Fig. 7. The decrease (negative slope) of the measured mass of sample and sample container with increase pressure (density) of the gas phase is due to the buoyancy force. The true densities for the samples were obtained according to the description given in Section 2.3. Based on the sample micropore volume and true density, the bulk density ( $\rho_b$ ) of the sample was calculated by the following equation:

$$\frac{1}{\rho_b} = \frac{1}{\rho_s} + w_0 \quad (7)$$

The true and bulk densities of the samples are presented in Table 5. The HFCM-2 shows a lower density than that of HFCM-1 due to the higher weight loss during the

carbonization process, as proved from the TGA results in Fig. 2. Moreover, some results reported in the literature ([15, 29]) are also given in Table 5 for the comparison.

The experimental kinetic data of CO<sub>2</sub> adsorption in the carbon membranes at 298 k and 1 bar are shown in Fig. 8. Due to the lack of control for high pressure measurements, a desired low pressure of 1bar was set for the all kinetic adsorption experiments. CO<sub>2</sub> with different flow rate of 100, 200 and 300 ml/min were fed into the sorption system to determine the actual kinetic curves. The linear driving force (LDF) model was introduced to fit the experimental data, which has been often used for the determination of mass transfer coefficient of different gases in various materials [21, 30]. The LDF model is described as follows:

$$\frac{q_t}{q_e} = 1 - \exp(-kt) \quad (8)$$

where the  $q_t$  and  $q_e$  are the gas sorption amount onto the carbon matrix in time  $t$  and the equilibrium,  $k$  is the mass transfer coefficient or the simplified kinetic rate constant (s<sup>-1</sup>). The LDF model is used to fit the experimental data and obtain the kinetic rate constant. As summarized in Table 6, the kinetic rate constants for the HFCM-1 and HFCM-2 are compared to some literature results of Zeolite 13X [31] and carbon membrane of CMSM3 [15]. The higher kinetic rate constant of HFCM-2 comparing to the HFCM-1 is associated with its more open structure due to the larger average pore size as given in Table 5.

### 3.5 Single gas test

Fig. 9 illustrates the gas permeability values of H<sub>2</sub>, CO<sub>2</sub>, O<sub>2</sub>, N<sub>2</sub> and CH<sub>4</sub> at 303 K versus the gas molecule kinetic diameters of module M1 and M2 constructed by HFCM-1 and HFCM-2, respectively. The gas permeability values of the selected gases are in this order: H<sub>2</sub> (2.89 Å) > CO<sub>2</sub> (3.3 Å) > O<sub>2</sub> (3.46 Å) > N<sub>2</sub> (3.64 Å) > CH<sub>4</sub> (3.8 Å). The permeability values are decreasing with increasing kinetic diameter of the gases, indicating that molecular sieving mechanism is dominated for carbon membrane transport processes. Moreover, the higher permeability of HFCM-2 comparing to the HFCM-1 is caused by the higher micropore volume and average pore size of HFCM-2 as documented by gas adsorption results in Table 5. In order to investigate the effects of temperature on gas separation performance, the permeability values of CO<sub>2</sub>, O<sub>2</sub>, N<sub>2</sub> and CH<sub>4</sub> for both membranes were tested with different temperatures and kept the constant feed pressure at 2 bar, which are shown in Fig. 10. The apparent transport activation energy,  $E_a$ , and  $P_0$  ( $P = P_0 \exp(-E_a/RT)$ ) was obtained by linear regression of  $\ln(p)$  versus  $T$  based on the experiment data are presented in Table 7. The activation energy is an indicator of the probability of a molecular passing a constriction, thus, a larger

activation energy shows a lower gas permeability. A more significant effect of temperature on the gas permeability can be found with a large  $E_a$ , as proved by the results in Fig. 10. The permeability of other gas molecules increased faster than CO<sub>2</sub> with the increase of temperature, which resulted in a slight decrease for the selectivity of CO<sub>2</sub> over other gas species within this temperature range.

### 3.6 Gas mixture separation

The CO<sub>2</sub> separation from synthetic flue gas (15% CO<sub>2</sub> - 81% N<sub>2</sub> - 4% O<sub>2</sub>) by the module M3 mounted with the carbon membranes of HFCM-2 was investigated. The characteristic of the module is given in Table 2. The gas mixture separation experiments were conducted at 303 K and a constant feed flow rate of 30 ml/min, while the feed pressure was increased from 2 to 4 bar. The CO<sub>2</sub> composition in permeate and retentate (measured by GC), and the CO<sub>2</sub> recovery (ratio of CO<sub>2</sub> flow rate in permeate and feed stream) are given in Fig. 11. The CO<sub>2</sub> purity in permeate and the CO<sub>2</sub> recovery increase as the feed pressure is increased for a given membrane area. However, a higher feed pressure will cause an increase in the energy demand for the compressor. Therefore, the capital cost estimation for the key equipment including the compressor and the membrane unit, should be executed to optimize the operating condition – this is described elsewhere [19].

## 4 Conclusions

The hollow fiber carbon membranes were prepared from different deacetylated cellulose acetate precursors by controlled carbonization procedure with CO<sub>2</sub> purge gas, a heating rate of 4 K/min, a final temperature of 550 °C and a final soak time 2h. A symmetric carbon matrix was documented by SEM images. The prepared carbon membrane showed a significant shrinkage with a weight loss about 70 % during the carbonization procedure.

CO<sub>2</sub> and N<sub>2</sub> adsorption equilibrium isotherms were obtained by the gravimetric sorption measurements, and the Langmuir-Freundlich model was used to fit the experimental data. The higher adsorption affinity of CO<sub>2</sub> clearly indicated that the CO<sub>2</sub> is more adsorbable than that of N<sub>2</sub>. Such investigations are very useful to document the competitive adsorption effects in gas mixture separation process. Moreover, the gas sorption experiments combined with XRD were used to determine the carbon membrane porous structure. The micropore volume and average pore size for the carbon membrane of HFCM-2 were found to be 0.17 cm<sup>3</sup>/g and 5.6 Å, respectively, which were slightly larger than that of the HFCM-1 (0.15 cm<sup>3</sup>/g and 5.2 Å). In addition, the average d-spacing of the carbon membranes was found to be 4 Å. The kinetic rate constants were

also determined from the CO<sub>2</sub> kinetic adsorption experiments, and the higher kinetic rate constant of HFCM-2 indicated its more open structure.

Single gas permeation tests of H<sub>2</sub>, CO<sub>2</sub>, O<sub>2</sub>, N<sub>2</sub> and CH<sub>4</sub> showed clearly that the molecular sieving mechanism was dominated in the carbon membrane separation processes, as the permeability values decreased with increasing kinetic diameter of the gas species. It was also observed that the permeability increased with temperature due to the activated transport process for the molecular sieve mechanism. Activation energies were calculated, and the gas molecules with the larger activation energy (e.g. CH<sub>4</sub> and N<sub>2</sub>) are affected significantly by the temperature, compared to the gas with lower activation energy (e.g. CO<sub>2</sub>). The gas mixture tests indicated that the operating parameters (e.g. feed pressure) need to be optimized in order to find the best trade-off between the membrane separation performance and process energy demands.

#### *Acknowledgements*

The authors want to acknowledge the NanoGloWa project for the funding (EUs 6<sup>th</sup> framework program). Appreciation also goes to the Analytische Laboratorien in Germany for the element analysis.

#### References

- [1] Robeson LM. The upper bound revisited. *J Membr Sci.* 2008;320(1-2):390-400.
- [2] Koresh JE, Soffer A. Molecular sieve carbon membrane Part I: Presentation of a new device for gas mixture separation. *Separ Sci Technol.* 1983;18:723-34.
- [3] Favvas EP, Kapantaidakis GC, Nolan JW, Mitropoulos AC, Kanellopoulos NK. Preparation, characterization and gas permeation properties of carbon hollow fiber membranes based on Matrimid(R) 5218 precursor. *J Mater Process Tech.* 2007;186(1-3):102-10.
- [4] Suda H, Haraya K. Gas Permeation through Micropores of Carbon Molecular Sieve Membranes Derived from Kapton Polyimide. *J Phys Chem B.* 1997;101(20):3988-94.
- [5] Steel KM, Koros WJ. Investigation of porosity of carbon materials and related effects on gas separation properties. *Carbon.* 2003;41(2):253-66.
- [6] David LIB, Ismail AF. Influence of the thermastabilization process and soak time during pyrolysis process on the polyacrylonitrile carbon membranes for O<sub>2</sub>/N<sub>2</sub> separation. *J Membr Sci.* 2003;213(1-2):285-91.

- [7] Zhang B, Wang T, Zhang S, Qiu J, Jian X. Preparation and characterization of carbon membranes made from poly(phthalazinone ether sulfone ketone). *Carbon*. 2006;44(13):2764-9.
- [8] Yoshimune M, Fujiwara I, Haraya K. Carbon molecular sieve membranes derived from trimethylsilyl substituted poly(phenylene oxide) for gas separation. *Carbon*. 2007;45(3):553-60.
- [9] Lee H-J, Suda H, Haraya K, Moon S-H. Gas permeation properties of carbon molecular sieving membranes derived from the polymer blend of polyphenylene oxide (PPO)/polyvinylpyrrolidone (PVP). *J Membr Sci*. 2007;296(1-2):139-46.
- [10] Lie JA, Hagg M-B. Carbon membranes from cellulose and metal loaded cellulose. *Carbon*. 2005;43(12):2600-7.
- [11] Saufi SM, Ismail AF. Fabrication of carbon membranes for gas separation--a review. *Carbon*. 2004;42(2):241-59.
- [12] Jones CW, Koros WJ. Characterization of Ultramicroporous Carbon Membranes with Humidified Feeds. *Ind Eng Chem Res*. 1995;34(1):158-63.
- [13] Lagorsse S, Magalhaes FD, Mendes A. Aging study of carbon molecular sieve membranes. *J Membr Sci*. 2008;310(1-2):494-502.
- [14] Lie JA, Hagg M-B. Carbon membranes from cellulose: Synthesis, performance and regeneration. *J Membr Sci*. 2006;284(1-2):79-86.
- [15] Lagorsse S, Magalhães FD, Mendes A. Carbon molecular sieve membranes: Sorption, kinetic and structural characterization. *J Membr Sci*. 2004;241(2):275-87.
- [16] Lagorsse S, Campo MC, Magalhaes FD, Mendes A. Water adsorption on carbon molecular sieve membranes: Experimental data and isotherm model. *Carbon*. 2005;43(13):2769-79.
- [17] Nguyen C, Do DD, Haraya K, Wang K. The structural characterization of carbon molecular sieve membrane (CMSM) via gas adsorption. *J Membr Sci*. 2003;220(1-2):177-82.
- [18] Sedigh MG, Jahangiri M, Liu PKT, Sahimi M, Tsotsis TT. Structural characterization of polyetherimide-based carbon molecular sieve membranes. *AIChE J*. 2000;46(11):2245-55.
- [19] He X, Lie JA, Sheridan E, Hägg M-B. CO<sub>2</sub> capture by hollow fibre carbon membranes: Experiments and process simulations. *Energy Procedia*. 2009;1(1):261-8.
- [20] Dreisbach F, H. RSA, Lösch HW. Gravimetric Measurement of Adsorption Equilibria of Gas Mixture CO/H<sub>2</sub> with a Magnetic Suspension Balance. *Chem Eng Technol*. 2002;25(11):1060-5.

- [21] Belmabkhout Y, Serna-Guerrero R, Sayari A. Adsorption of CO<sub>2</sub> from dry gases on MCM-41 silica at ambient temperature and high pressure. 1: Pure CO<sub>2</sub> adsorption. *Chem Eng Sci.* 2009;64(17):3721-8.
- [22] Lie JA. Synthesis, performance and regeneration of carbon membranes for biogas upgrading-a future energy carrier [PhD]. Trondheim: Norwegian University of Science and technology; 2005.
- [23] Lin W-H, Vora RH, Chung T-S. Gas transport properties of 6FDA-durene/1,4-phenylenediamine (pPDA) copolyimides. *J Polym Sci Part B: Polym Phys.* 2000;38(21):2703-13.
- [24] He X, Lie JA, Sheridan E, Hägg M-B. Preparation and Characterization of Hollow Fiber Carbon Membranes from Cellulose Acetate Precursors. *Ind Eng Chem Res.* 2011;50(4):2080-7.
- [25] Fialkov A, Dobryakov S, Khorkhorin A, Tyan L, Polyakova N, Kuznetsov Y, et al. Structure of the residual carbon made by fluorocarbon pyrolysis. *J Struct Chem.* 1990;31(3):413-6.
- [26] Yu J, Neretnieks I. Single-component and multicomponent adsorption equilibria on activated carbon of methylcyclohexane, toluene, and isobutyl methyl ketone. *Ind Eng Chem Res.* 1990;29(2):220-31.
- [27] Cazorla-Amoros D, Alcaniz-Monge J, Linares-Solano A. Characterization of Activated Carbon Fibers by CO<sub>2</sub> Adsorption. *Langmuir.* 1996;12(11):2820-4.
- [28] Stoeckli F, Slasli A, Hugli-Cleary D, Guillot A. The characterization of microporosity in carbons with molecular sieve effects. *Micropor Mesopor Mat.* 2002;51(3):197-202.
- [29] Lua AC, Su J. Effects of carbonisation on pore evolution and gas permeation properties of carbon membranes from Kapton® polyimide. *Carbon.* 2006;44(14):2964-72.
- [30] Berenguer-Murcia Á, Fletcher AJ, García-Martínez J, Cazorla-Amorós D, Linares-Solano Á, Thomas KM. Probe Molecule Kinetic Studies of Adsorption on MCM-41. *J Phys Chem B.* 2003;107(4):1012-20.
- [31] Cavenati S, Grande CA, Rodrigues AE. Separation of CH<sub>4</sub>/CO<sub>2</sub>/N<sub>2</sub> mixtures by layered pressure swing adsorption for upgrade of natural gas. *Chem Eng Sci.* 2006;61(12):3893-906.

## List of figure and table captions

### Figures

Fig. 1 Schematic diagram of the carbon membrane module

Fig. 2 Weight loss of precursors from TGA analysis

Fig. 3 SEM images of the cross section for precursors and carbon membranes: (A) DHF-1, (B) DHF-2, (C) HFCM-1 and (D) HFCM-2

Fig. 4 XRD Patterns of (a) HFCM-1, (b) HFCM-2 and (c) graphite

Fig. 5 Equilibrium adsorption isotherm at 298K on HFCM-1 ((○) CO<sub>2</sub> adsorption; (×) CO<sub>2</sub> desorption; (▼) N<sub>2</sub> adsorption) and HFCM-2 ((□) Adsorption; (▲) CO<sub>2</sub> desorption; (■) N<sub>2</sub> adsorption), and the solid line corresponds to the Langmuir-Freundlich model

Fig. 6 Characteristic curves for HFCM-1 (●) and HFCM-2 (▲) by CO<sub>2</sub> adsorption at 298K, Solid line corresponds to the DR model

Fig. 7. Buoyancy measurements with helium for HFCM-1 (●) and HFCM-2 (■) at 298K and constant feed flow rate of 100 ml/min, solid lines correspond to the linear regression.

Fig. 8 Fractional uptake of CO<sub>2</sub> adsorption on HFCM-1 (a) and HFCM-2 (b) at 298K and 1bar with different flow rates: (●) 100 ml/min; (▲) 200 ml/min; (■) 300 ml/min, solid lines correspond to the LDF model

Fig. 9 Single gas permeability values of HFCM-1(●) and HFCM-2 (▲) against the gas molecular kinetic diameters at 303K and feed pressure of 2bar

Fig. 10 Dependency of gas permeability on the temperature of HFCM-1 (a) and HFCM-2 (b) at constant feed pressure of 2bar

Fig. 11 Dependency of CO<sub>2</sub> separation performance on the feed pressure at 303K and a feed flow rate of 30 ml/min: (●) CO<sub>2</sub> composition in permeate; (■) CO<sub>2</sub> composition in retentate; (▲) CO<sub>2</sub> recovery

### Tables

Table 1 Characteristics of hollow fiber membranes and various spinning parameters

Table 2 Characteristics of in-house hollow fiber carbon membrane modules

Table 3 Results from element analysis for carbon membranes

Table 4 Equilibrium isotherm parameters for CO<sub>2</sub> and N<sub>2</sub> on carbon membranes at 298K

Table 5 Structural parameters of carbon membranes

Table 6 Kinetic rate constant for carbon membranes and benchmark materials

Table 7 Kinetic parameter for gas permeation through carbon membranes

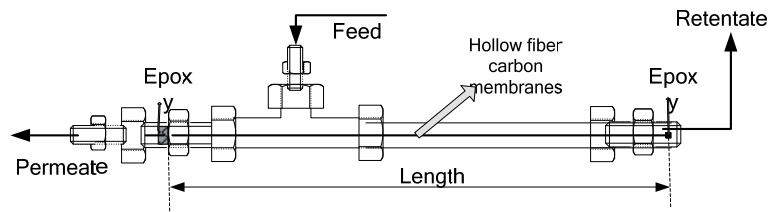


Fig. 1. Schematic diagram of the carbon membrane module

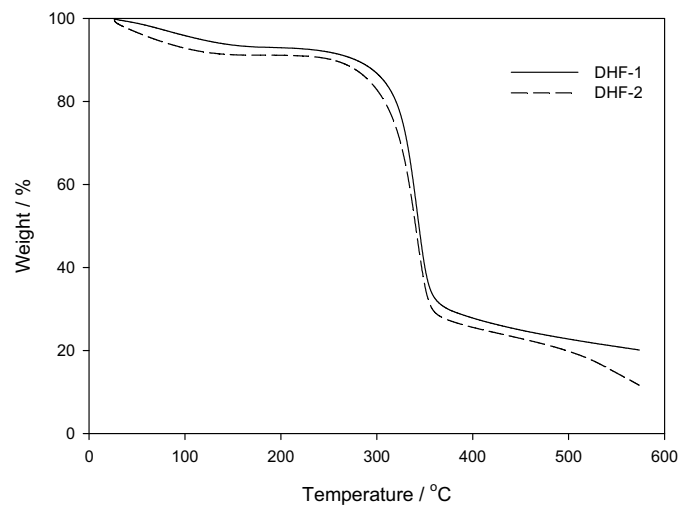


Fig. 2. Weight loss of precursors from TGA analysis

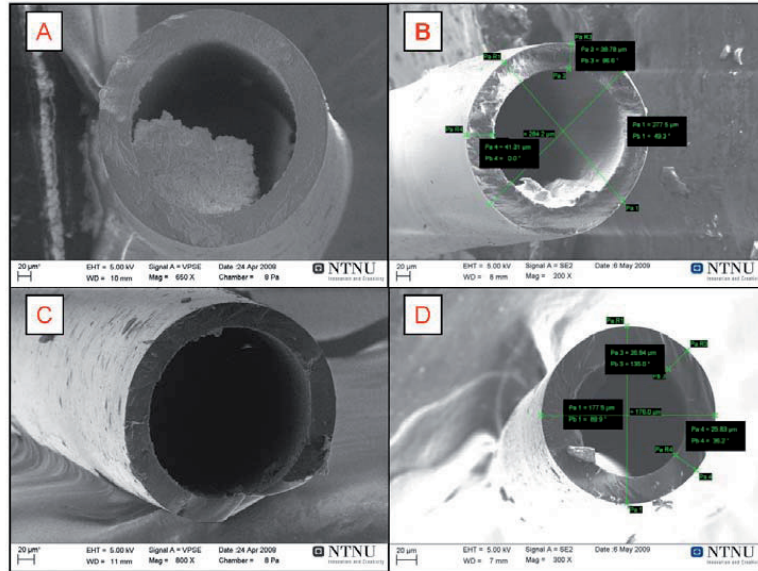


Fig. 3. SEM images of the cross section for precursors and carbon membranes: (A) DHF-1, (B) DHF-2, (C) HFCM-1 and (D) HFCM-2

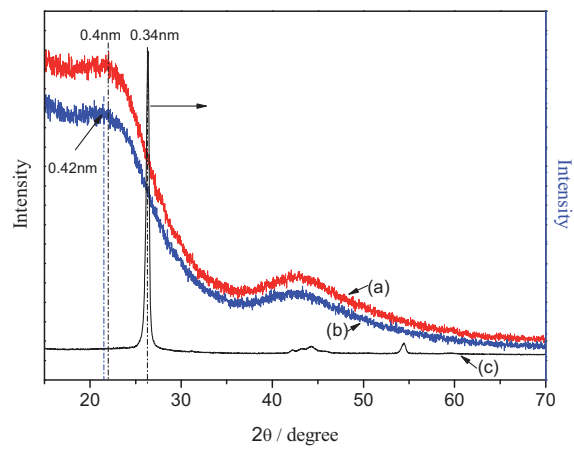


Fig. 4. XRD Patterns of (a) HFCM-1, (b) HFCM-2 and (c) graphite

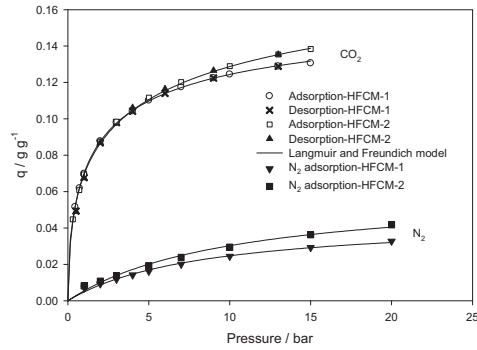


Fig.5. Equilibrium adsorption isotherm at 298 K on HFCM-1 (( $\circ$ )  $\text{CO}_2$  adsorption; ( $\times$ )  $\text{CO}_2$  desorption; ( $\blacktriangledown$ )  $\text{N}_2$  adsorption) and HFCM-2 (( $\square$ ) Adsorption; ( $\blacktriangle$ )  $\text{CO}_2$  desorption; ( $\blacksquare$ )  $\text{N}_2$  adsorption), and the solid line corresponds to the Langmuir-Freundlich model

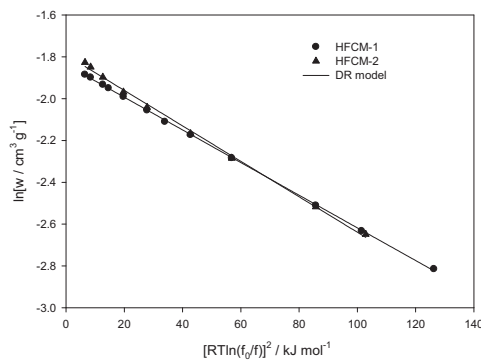


Fig. 6. Characteristic curves for HFCM-1 ( $\bullet$ ) and HFCM-2 ( $\blacktriangle$ ) by  $\text{CO}_2$  adsorption at 298 K, solid line corresponds to the DR model

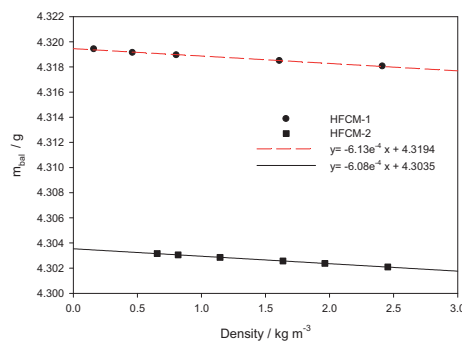


Fig. 7. Buoyancy measurements with helium for HFCM-1 ( $\bullet$ ) and HFCM-2 ( $\blacksquare$ ) at 298K and constant feed flow rate of 100 ml/min, solid lines correspond to the linear regressions.

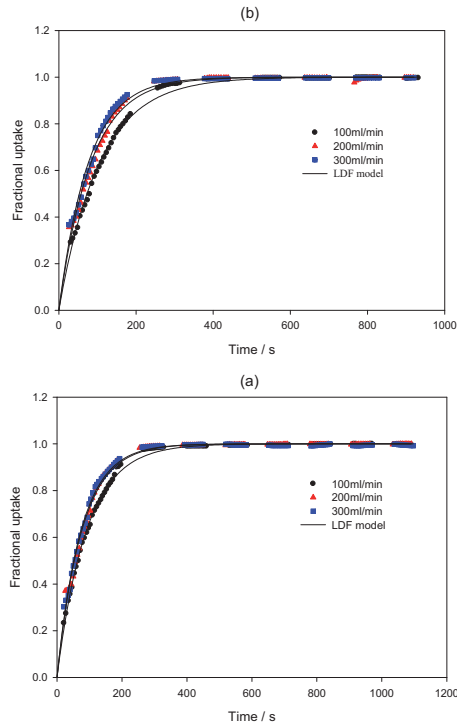


Fig. 8. Fractional uptake of CO<sub>2</sub> adsorption on HFCM-1 (a) and HFCM-2 (b) at 298K and 1bar with different flow rates: (●) 100 ml/min; (▲) 200 ml/min; (■) 300 ml/min, solid lines correspond to the LDF model

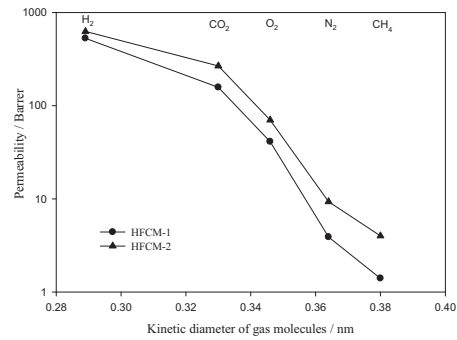


Fig. 9. Single gas permeability values of HFCM-1(●) and HFCM-2 (▲) against the gas molecular kinetic diameters at 303 K and feed pressure of 2 bar

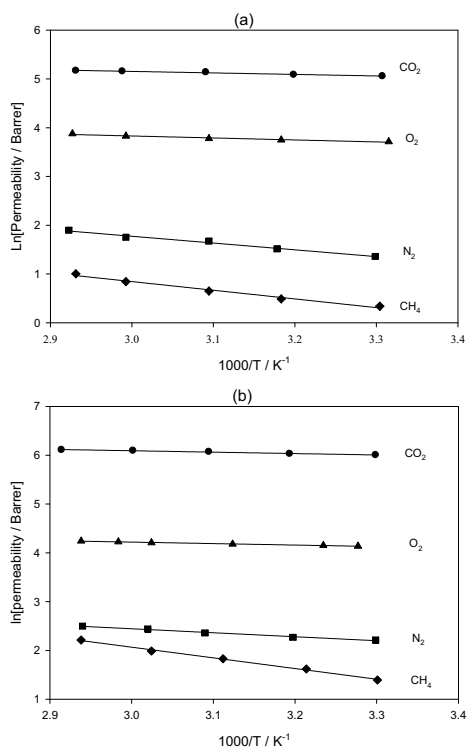


Fig. 10. Dependency of gas permeability on the temperature of HFCM-1 (a) and HFCM-2 (b) at constant feed pressure of 2 bar

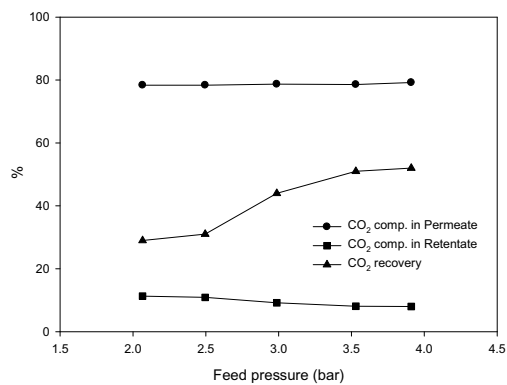


Fig. 11. Dependency of CO<sub>2</sub> separation performance on the feed pressure at 303 K and a feed flow rate of 30 ml/min: (●) CO<sub>2</sub> composition in permeate; (■) CO<sub>2</sub> composition in retentate; (▲) CO<sub>2</sub> recovery

Table 1 Characteristics of hollow fiber membranes and various spinning parameters

Membrane	Spinneret inner/outer diameter (mm )	Dope flow rate (ml min <sup>-1</sup> )	Bore flow rate (% of dope)	Air gap (mm)	Coagulation bath temp. (°C)
HF-1	0.5/0.7	2.2	40	25	50
HF-2	0.1/0.2	0.9	140	15	50

Table 2 Characteristics of in-house hollow fiber carbon membrane modules

Module	Carbon membrane	Membrane amount	Effective membrane area (cm <sup>2</sup> )	Membrane dimensions (average)		
				Outer diameter ( $\mu$ m)	Effective length (cm)	Thickness ( $\mu$ m)
M1	HFCM-1	5	8.6	250	22	25
M2	HFCM-2	5	6.7	200	21.5	25
M3	HFCM-2	91	86	200	15	25

Table 3 Results from element analysis for carbon membranes

Samples	Element content (%)			
	C	H	N	O
HFCM-1	86.03	3.48	0.14	7.37
HFCM-2	87.35	3.48	0.11	6.34

Table 4 Equilibrium isotherm parameters for CO<sub>2</sub> and N<sub>2</sub> on carbon membranes at 298K

Samples	T (K)	Gas species	Langmuir-Freundlich model			Reference
			b (bar <sup>-1</sup> )	q <sub>m</sub> (g g <sup>-1</sup> )	n	
HFCM-1	298	CO <sub>2</sub>	0.73	0.17	1.65	This work
		N <sub>2</sub>	0.12	0.046	1	
HFCM-2	298	CO <sub>2</sub>	0.48	0.21	2	[14]
		N <sub>2</sub>	0.098	0.061	1	
CMSM2	303	CO <sub>2</sub>	0.93	0.15	1.34	[14]
		N <sub>2</sub>	0.19	0.07	1	

Table 5 Structural parameters of carbon membranes

Carbon membranes	True density $\rho_s$ ( $\text{g cm}^{-3}$ ) <sup>a</sup>	Bulk density, $\rho_b$ ( $\text{g cm}^{-3}$ )	DR model		Average micropore width ( $\text{\AA}$ )	Reference
			$W_0$ ( $\text{cm}^3 \text{g}^{-1}$ )	$E_0$ ( $\text{kJ mol}^{-1}$ )		
HFCM-1	1.53	1.24	0.15	32.2	5.2	This work
HFCM-2	1.38	1.12	0.17	30.8	5.6	This work
CMSM1	1.6	1.1	0.28	31.6	5.5	[14]
CM-V823			0.16	22.75		[27]

<sup>a</sup> Density of carbons is 1.3-1.8  $\text{g/cm}^3$  as compared to 2.2  $\text{g/cm}^3$  for graphite [1]

Table 6 Kinetic rate constant for carbon membranes and benchmark materials

Materials	$k$ ( $\times 10^{-2} \text{s}^{-1}$ )	References
HFCM-1	1.10 ~ 1.34	This work
HFCM-2	0.95 ~ 1.31	This work
13X	1.23	[29]
CMSM3*	0.43	[14]

\* Calculated from the data at pressure 0.048 bar and temperature 303 K

Table 7 Kinetic parameter for gas permeation through carbon membranes

Gas molecules	$d_k$ ( $\text{\AA}$ )	$\epsilon/k$ (K)	$E_a$ ( $\text{kJ mol}^{-1}$ )		$P_0$ (Barrer)	
			HFCM-1	HFCM-2	HFCM-1	HFCM-2
CO <sub>2</sub>	3.3	195.0	2.6	2.4	437.6	1049.4
O <sub>2</sub>	3.46	107.0	3.4	2.5	156.6	168.2
N <sub>2</sub>	3.64	71.4	11.6	6.8	382.3	133.6
CH <sub>4</sub>	3.8	136.0	14.8	18.2	483.7	5602.7

## **Appendix G**

Hollow Fiber Carbon Membranes: Investigations for CO<sub>2</sub> Capture

*Journal of Membrane Science*, Article in Press





Contents lists available at ScienceDirect

Journal of Membrane Science

journal homepage: [www.elsevier.com/locate/memsci](http://www.elsevier.com/locate/memsci)

## Hollow fiber carbon membranes: Investigations for CO<sub>2</sub> capture

Xuezhong He, May-Britt Hägg\*

Department of Chemical Engineering, Norwegian University of Science and Technology, N-7491 Trondheim, Norway

### ARTICLE INFO

#### Article history:

Received 13 August 2010

Received in revised form 22 October 2010

Accepted 29 October 2010

Available online xxx

#### Keywords:

Hollow fiber carbon membrane

CO<sub>2</sub> capture

Process simulation

### ABSTRACT

Hollow fiber carbon membranes were prepared from the cellulosic precursors by controlling the carbonization protocol of CO<sub>2</sub> using 823–4 K/min for 2 h. The prepared carbon membranes presented a symmetric structure and a much smaller wall thickness of 25 μm compared to the precursor (40 μm) from the SEM images. Single gas (i.e. O<sub>2</sub>, N<sub>2</sub>, CO<sub>2</sub>) permeation tests indicated that the molecular sieve mechanism was the dominating transportation mechanism for the gas species through the carbon membranes. The influences of operating parameters on the carbon membrane separation performance include pressure, temperature, retentate flow rate and feed CO<sub>2</sub> composition. These parameters were systematically investigated by factorial design method. The experimental and process simulation results indicated that the CO<sub>2</sub> purity can only achieve ca. 75% with one stage membrane configuration. Therefore, a simple two stage cascade configuration without sweep was designed for the process optimization based on the capital cost estimation of the major equipments. A CO<sub>2</sub>-purity of 90% was then achieved with 60% CO<sub>2</sub> capture. Although the specific capital cost for carbon membrane technology is still high compared to the traditional chemical absorption method, simulation results also proved that the costs can be significantly decreased by reducing the carbon membrane wall thickness from 25 to 10 μm—this is considered to be a realistic option. Therefore, the prepared hollow fiber carbon membranes needs to be further optimized in order to be a potential candidate for CO<sub>2</sub> capture.

© 2010 Elsevier B.V. All rights reserved.

### 1. Introduction

Energy Information Administration (EIA) 2010 predicted a 49% increase of energy demand from 2007 to 2035 following more and more countries becoming industrialized [1]. The International Energy Outlook 2010 (IEO2010) reference case reported that the world energy-related carbon dioxide (CO<sub>2</sub>) emissions increased from 29.7 billion metric tons in 2007 to 33.8 billion metric tons in 2020 and 42.4 billion metric tons in 2035 [1]. The control of anthropogenic emissions of greenhouse gases (GHG) is one of the most challenging environmental issues owing to the implications of GHG for global climate change. Among these GHG, CO<sub>2</sub> is the largest contributor in regard of its amount present in the atmosphere contributing to 60% of global warming effects, although methane and chlorofluorocarbons have much higher greenhouse effect as per mass of gases [2]. Three options were reported to reduce the total CO<sub>2</sub> emission into the atmosphere, such as to reduce energy consumption, to reduce fossil fuel usage, and to capture and store the CO<sub>2</sub>. The first two options require efficient usage of energy and switch to using non-fossil fuels such as hydrogen and renewable energy, respectively, while the third option requires the develop-

ment of new efficient technologies for CO<sub>2</sub> capture and storage (CCS). The key attraction for CCS is that we may continue to use fossil fuels but without causing significant CO<sub>2</sub> emissions.

The main application of CO<sub>2</sub> capture is likely to be at large point sources: fossil fuel power plants, oil refineries, and industrial plants, particularly for the manufacture of iron, steel, cement and chemicals. Such plants emit large quantities of CO<sub>2</sub>, for example the fossil fuel power plants are responsible for roughly 40% of total CO<sub>2</sub> emissions, and coal-fired plants being the main contributor. Clearly, coal-fired plants need to be addressed first, especially by retrofitting existing plants. However, it will result in higher costs and lower efficiency to retrofit the existing plants compared to new plants with the CO<sub>2</sub> capture system integrated in the design [3]. Hence, the CO<sub>2</sub> capture may be an option to reduce the CO<sub>2</sub> emission from today's industries.

There are many dedicated researches trying to improve the current technologies or develop new methods for CO<sub>2</sub> capture. There are several different techniques which can be used for CO<sub>2</sub> capture, such as chemical and physical absorption, adsorption, cryogenics and membrane separation, but the choice of a suitable method will, to a large extent, mainly depend on the characteristics of the gas to be treated as well as the process conditions. Membranes are already an alternative and competitive technology for selected gas separation processes such as air separation, natural gas and biogas upgrading, and hydrogen production during the last

\* Corresponding author. Tel.: +47 73594033; fax: +47 73594080.  
E-mail address: [may-britt.hagg@chemeng.ntnu.no](mailto:may-britt.hagg@chemeng.ntnu.no) (M.-B. Hägg).

two decades. It will become steadily more attractive due to the energy efficiency and low economical costs. Yang et al. reviewed the progress in CO<sub>2</sub> separation, and they concluded that membrane process are basically energy-saving, space-saving, easy to scale-up, and could be the future technology for CO<sub>2</sub> separation [4]. There are many authors reporting research work on CO<sub>2</sub> capture by membrane technology, examples are: [4–12]. Although the polymeric membranes are dominating the current industrial use for gas separation, the trade-off of permeability/selectivity as well as the limitation of operation temperature and adverse conditions such as the presence of acid gases SO<sub>2</sub> and NO<sub>x</sub>, may direct the polymeric membrane development into the alternative carbon membranes. The carbon membranes are readily prepared by pyrolysis of polymer precursors and show promising applications for gas separation especially for CO<sub>2</sub> removal from natural gas and flue gas, oxygen enriched air and purification of H<sub>2</sub>. Up to now, different precursor materials such as polyimide [13,14], polyacrylonitrile (PAN) [15], poly(phthalazinone ether sulfone ketone) (PPESK) [16], poly(phenylene oxide) (PPO) [17] have been tested for fabrication of carbon membranes. Recently, there has been taken strong interests in preparation of hollow fiber carbon membranes (HFCMs) for gas separation, which based on the hollow fiber precursor membranes that provide better selectivity, thermal and chemical stability than those that already used [18–21]. From the standpoint of large-scale application, hollow fibers will be preferable because of its high packing density (membrane area per unit volume of vessel) and easier module assembly.

The deacetylated cellulose acetate (CA) was found to be one of the most suitable precursor for the preparation of carbon membranes due to the commercial availability, cheap price and easy to process [22,23]. In this work, the HFCMs were fabricated by controlling the carbonization protocol from deacetylated cellulose acetate precursors. The structure, morphology and separation performance will be investigated and discussed. Moreover, the feasibility for application of hollow fiber carbon membrane to capture CO<sub>2</sub> from flue gas is also evaluated by process simulation.

## 2. Experimental

### 2.1. Materials

The polymer precursor material, cellulose acetate (CA, MW 100,000) with average acetyl content of 39.8% was purchased from the ACROS (USA). Polyvinylpyrrolidone (PVP K10) was supplied by Sigma. The solvent, N-methyl-2-pyrrolidone (NMP, >99.5%) was purchased from Merck (Darmstadt, Germany), and the glycerol (>98%) was purchased from BDH/VWR. The NaOH (>99%) was used for the deacetylation of the fibers supplied from Merck. The materials were used as supplied without further purification.

### 2.2. Fabrication of hollow fiber carbon membranes

The spinning dope of CA/PVP/NMP (22.5%/5%/72.5%) was prepared by the following procedure [24]. The hollow fiber membranes were spun using well-known dry-wet spinning method [25,26]. The optimal condition with an air gap of 25 mm, a dope flow rate of 2.2 ml/min, a bore fluid composition of water + NMP (85%), a bore flow rate (40% of dope flow rate) and a water quench bath maintained at 50 °C was controlled for the whole spinning process. The spun hollow fibers were subsequently soaked in the fresh water and 10% glycerol solution overnight to remove the residual NMP from the fibers. The hollow fiber was then deacetylated with 0.075 M NaOH (96% ethanol) solution for 2 h to prepare the precursors for carbon membranes. The deacetylated precursors were then carbonized in a tubular furnace (Carbolite® TZF 12/100/900) using a

**Table 1**

Operating parameters and levels used in the factorial design.

Factor	Operating parameter	High level (+1)	Low level (−1)
A	Temperature (°C)	50	30
B	Feed pressure (bar)	5	3
C	Retentate flow rate (ml/min)	12	6
D	CO <sub>2</sub> feed composition	CO <sub>2</sub> /O <sub>2</sub> /N <sub>2</sub> : 15%/4%/81%	CO <sub>2</sub> /N <sub>2</sub> : 10%/90%

working tube of alumina and a quartz container, which is describe elsewhere [20]. A multi-dwells carbonization protocol with CO<sub>2</sub> purge gas, a heating rate of 4 °C/min and a final temperature 550 °C and soak time 2 h, was executed to prepare the hollow fiber carbon membranes (HFCM).

### 2.3. Scanning electron microscope

A Zeiss SUPRA 55VP scanning electron microscope (SEM) was used to qualitatively assess structural and morphological characteristics of the precursor and the produced HFCMs. Backscatter and secondary electron images were obtained using an acceleration potential of 5 keV. The samples measured had not been used in gas permeation tests, but were taken from the same carbonization batch as those used for permeation.

### 2.4. Gas permeation tests

The prepared HFCMs (27 fibers) were mounted in a module (shown in Fig. 1). Single gas permeation tests were conducted at 30 °C and a feed pressure of 2 bar (permeate side evacuated) in a standard pressure-rise setup (MKS Baratron® pressure transducer, 0–100 mbar range) with LabView® data logging as described elsewhere [27]. The gas mixture separation (10% CO<sub>2</sub>–90% N<sub>2</sub> and 15% CO<sub>2</sub>–4% O<sub>2</sub>–81% N<sub>2</sub>) through the carbon membranes were also measured with a gas permeation setup fitted with online gas chromatograph (GC) for analysis. The fractional factorial design combined with statistical analysis was employed to investigate the influence of the different operating parameters such as temperature, feed pressure, flow rate of retentate (FR) and CO<sub>2</sub> feed composition on the separation performance. The parameters and levels used for factorial design are listed in Table 1. Each parameter has two levels in which the high level (+1) and the low level (−1) are selected values. For a 2<sup>4−1</sup> fractional factorial design, the defining relation used to produce the aliases is I = ABCD, the main factors are aliased with the three-factor interactions, e.g. A.I = A.BCD, or A = BCD. A total of eight experiments with different combinations of the operating parameters were investigated.

## 3. Process simulation

### 3.1. Process design and simulation basis

Post-combustion CO<sub>2</sub> capture is a “tail-end” process. This means that the unit operation for CO<sub>2</sub> separation should be located in the downstream of the flue gas desulphurization (FGD) absorber for a fossil fired power plant. The existing and fairly mature technology (e.g. chemical absorption) features efficient CO<sub>2</sub> capture at low temperature from the flue gas with relative low concentration, but requires large-scale columns and equipment at high costs. It also reduces the thermal efficiency. An alternative way may be the use of membrane separation units. A typical schematic diagram for post-combustion power plant integrates with a carbon membrane separation unit was described elsewhere [27]. However, there are some challenges which need to be considered for this application.

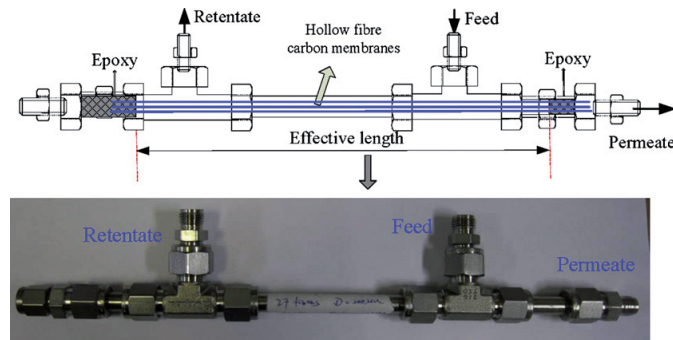


Fig. 1. Lab-scale hollow fiber carbon membrane module.

- The low pressure and low CO<sub>2</sub> concentration in feed (10–15 vol.%) give very low driving force unless compression is applied;
- The actual gas volume to be treated is very high, and large membrane areas are needed;
- Trace impurities in the flue gas tend to reduce the efficiency of the CO<sub>2</sub> separation processes;
- Compressing the captured CO<sub>2</sub> in permeate stream from low pressure (atmosphere or vacuum) to high pressure for pipeline transport (80–150 bar) represents a large energy demands.

The process design was based on a typical coal fired power plant (400 MW). In addition to the main components of N<sub>2</sub>, CO<sub>2</sub>, water vapor and O<sub>2</sub>, relatively small concentrations of aggressive and harmful substances such as SO<sub>2</sub>, NO<sub>x</sub>, traces of metals, volatile organic compounds (VOC) and fly ash are present in the flue gas. In order to simplify the process simulation, only the main components were considered here. The simulation basis was chosen based on the characteristic membrane data from dry gas permeation tests and specific boundary conditions for the CO<sub>2</sub> separation process, as listed in Table 2. The scenarios of CO<sub>2</sub> capture by hollow fiber carbon membrane unit were simulated by Aspen HYSYS® integrated with an in-house simulation tool, ChemBrane [28]. Since the presence of water vapor may reduce the carbon membrane separation performance significantly (discussed in Section 4.2), a dehydration unit was placed after the FGD and before the carbon membrane units.

A single stage membrane unit process was firstly simulated to investigate the influence of operating conditions on the carbon membrane separation performances. The driving force across the membrane module was provided by compression of the feed stream (here called configuration A) and vacuum on permeate side (configuration B). The schematic of single stage membrane separation process is shown in Fig. 2, which was used to investigate the influences of operating parameters such as feed and permeate pressure on the separation efficiency as well as to obtain the characteristic diagrams. Moreover, a two-stage cascade membrane process, as shown in Fig. 3, was also conducted to evaluate the process feasibility based on the capital cost estimation of the key equipments.

### 3.2. Economic estimation of capital costs

The estimate for the capital costs is based on the evaluation of the major equipment in the process (e.g. pumps, compressors, heat exchangers, membrane units), which can be provided with an accuracy in the range from –25% to 40%, typically used for a preliminary feasible estimate of different process alternatives [29]. The bare module costing ( $C_{BM}$ ) technique accounts to the purchased cost

( $C_p^0$ ) for the equipment in base conditions (carbon steel material and near ambient pressure), and a multiplying bare module factor ( $F_{BM}$ ) is used. This factor will consider the specific equipment type, specific materials of construction and operating pressure. The bare module cost ( $C_{BM}$ ) of each piece of equipment is the sum of the direct and indirect costs:

$$C_{BM} = C_p^0 F_{BM} \quad (1)$$

The excel program of CAPCOST 2008 is used to estimate the capital cost based on the equipment module approach [29]. The total capital cost ( $C_{TM}$ ) includes the contingency and contractor fee in addition to the direct and indirect cost, which is calculated as follows:

$$C_{TM} = 1.18 \sum_{i=1}^n C_{BM,i} \quad (2)$$

where  $n$  is the total number of individual units. A chemical engineering plant cost index (CEPCI) of 500 is adopted for all inflation adjustments. Due to the carbon membrane cost is still unknown, an assumed 45 \$/m<sup>2</sup> (estimated polymeric membrane cost 20 \$/m<sup>2</sup> as reported by Koros [30]) with an average lifetime of 5 years for the carbon membranes was used to calculate the capital cost of carbon membrane unit. The capital costs of the compressors and heat exchangers were obtained by CAPCOST. Therefore, the specific capital costs for per ton CO<sub>2</sub> avoided ( $C_{CO_2}$ ) was calculated based on a project lifetime of 20 years together with the annual CO<sub>2</sub> avoided amount (330 days per year), as follows:

$$C_{CO_2} = \frac{C_{TM}}{20 \times F_{CO_2} \times 24 \times 330} (\$/t \text{ CO}_2 \text{ avoided}) \quad (3)$$

where  $F_{CO_2}$  is the mass flow of CO<sub>2</sub> to pipeline (t/h).

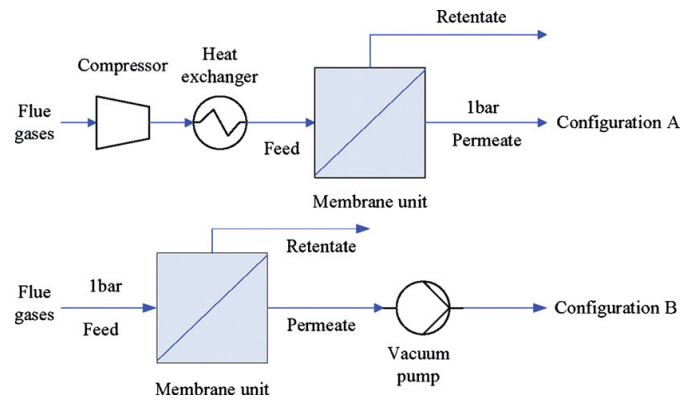
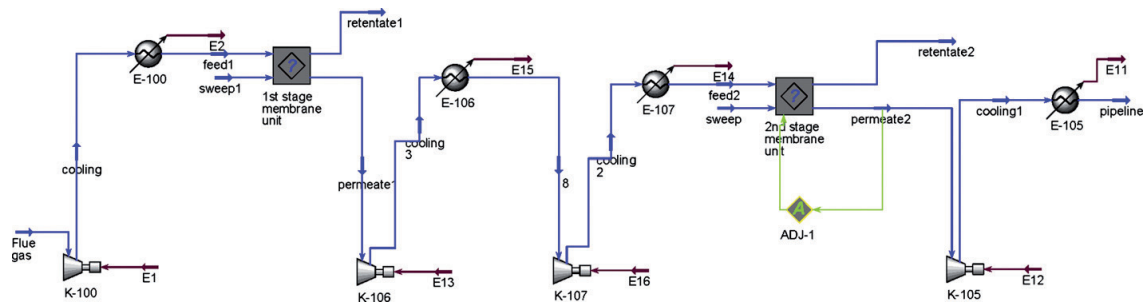
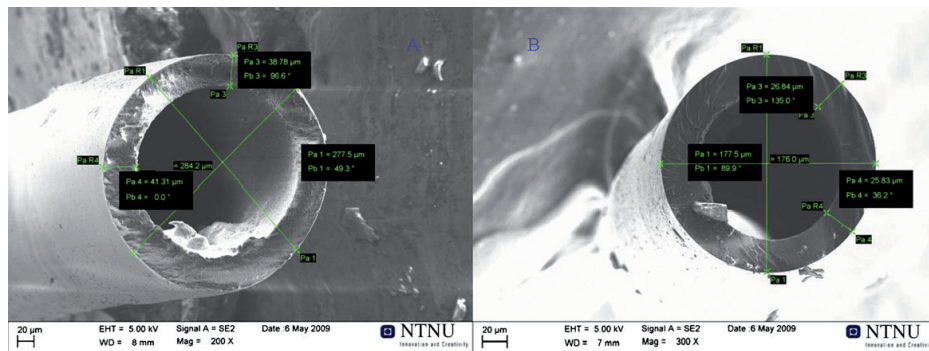
## 4. Results and discussion

### 4.1. Membrane structure and morphology

Fig. 4 shows the cross section of the precursor and the hollow fiber carbon membrane, respectively. The HFCM forms the symmetric structure and shows a dramatic shrinkage (ca. 70%) comparing to the precursor. For instance, the outer diameter and wall thickness of the HFCM are approximately 180 μm and 25 μm, which are significantly smaller than that of the precursor with 280 μm and 40 μm, respectively.

**Table 2**Simulation basis for CO<sub>2</sub> separation from flue gases through carbon membranes.

Process	Carbon membrane		
	Performance	Experimental data <sup>a</sup>	Assumed by reducing thickness
Feed flow rate (Nm <sup>3</sup> h <sup>-1</sup> )	1 × 10 <sup>6</sup>	Permeance of CO <sub>2</sub> (Nm <sup>3</sup> m <sup>-2</sup> h <sup>-1</sup> bar <sup>-1</sup> )	0.03
Pressure (bar)	1.013	Selectivity of CO <sub>2</sub> /N <sub>2</sub>	29.5
Temperature (°C)	80	Selectivity of CO <sub>2</sub> /O <sub>2</sub>	3.9
CO <sub>2</sub> transport pressure (bar)	110		
Composition (vol.%, dry base)			
CO <sub>2</sub>	15		
N <sub>2</sub>	81		
O <sub>2</sub>	4		

<sup>a</sup> Tested at 303 K and feed pressure of 2 bar.**Fig. 2.** The schematic of the two configurations for a single stage carbon membrane separation process.**Fig. 3.** Simulation PFD for two stage cascade carbon membrane separation process.**Fig. 4.** SEM imaged of cross section for precursor and carbon membranes.

Please cite this article in press as: X. He, M.-B. Hägg, Hollow fiber carbon membranes: Investigations for CO<sub>2</sub> capture, J. Membr. Sci. (2010), doi:10.1016/j.memsci.2010.10.070

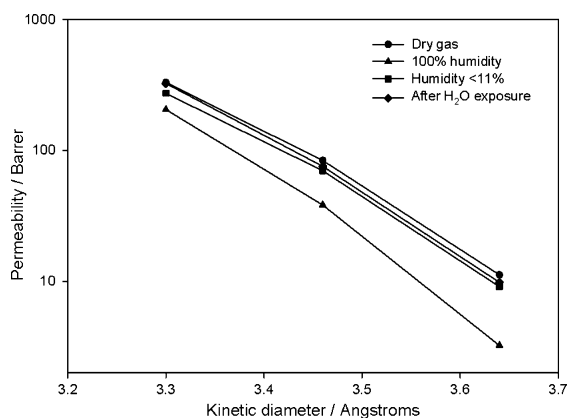


Fig. 5. Single gas permeability with different humidity at 303 K and feed pressure of 2 bar.

#### 4.2. Single gas test

Fig. 5 illustrates the gas permeabilities of  $\text{CO}_2$ ,  $\text{O}_2$  and  $\text{N}_2$  versus the gas molecular kinetic diameters for the prepared HFCMs under different humidity at  $30^\circ\text{C}$  and feed pressure of 2 bar. The gas permeability values of the selected gases were found to be in the following order:  $\text{CO}_2$  (3.3 Å) >  $\text{O}_2$  (3.46 Å) >  $\text{N}_2$  (3.64 Å). The permeability values are decreasing with increasing kinetic diameter of the gas molecules, indicating that the main transport mechanism of HFCMs is dominated by molecular sieving. Moreover, the significant effects of humidity (i.e. water vapor) on the carbon membrane separation performances are also found to all tested gases. The gas permeability will decrease with increasing the humidity as can be seen from Fig. 5, which may be caused by the pore blocking due to the formation of hydrogen bonds between the water and carbon matrix. However, after being exposed to water vapor, the gas permeability values can be basically recovered to initial permeability values by thermal regeneration (e.g. feed  $\text{N}_2$  at  $100^\circ\text{C}$  overnight).

#### 4.3. Gas mixture tests

The single gas tests are mainly used to characterize the ideal separation performance for the carbon membranes. However, the separation properties will be affected by the presence of other penetrants in a gas mixture. The transport of gas mixture will be different from that in single gas, especially for the existing of strong adsorbable gas like  $\text{CO}_2$ , hence the separation of the gas mixtures of (15%  $\text{CO}_2$ –4%  $\text{O}_2$ –81%  $\text{N}_2$ ) and (10%  $\text{CO}_2$ –90%  $\text{N}_2$ ) were also investigated. In order to optimize the process operating conditions, the fractional factorial design combined with statistical analysis was employed to investigate the influences of the different operating parameters such as temperature, feed pressure, retentate flow rate and  $\text{CO}_2$  feed composition. A total of eight batch experiments were conducted, and the test results are given in Table 3. Based on the experimental data, the importance of the various operating parameters was evaluated by hypothesis testing. The type I error, if a null hypothesis is rejected when it is true and the probability of a type I error is  $\alpha$ . The value of this probability is usually called significance level of the test. The  $p$ -value approach has been widely used for practical application and the  $p$ -value is defined as the smallest level of significance that would lead to rejection of the null hypothesis. A commercial software Minitab® is used to execute the statistical analysis. The hypothesis testing with a significance level of  $\alpha = 0.05$  is used to evaluate the importance of the operating

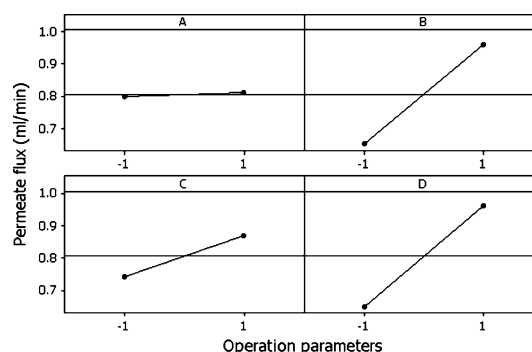


Fig. 6. The main influence plots by Minitab® for the permeate flux, A (temperature), B (feed pressure), C (retentate flow rate) and D (feed  $\text{CO}_2$  composition).

parameters to the carbon membrane separation performances. The estimates of the parameter effects, coefficient, and the  $p$ -values are given in Table 4. The main effects plots are shown in Figs. 6 and 7 representing the influences of different operating parameters. The feed pressure and retentate flow rate give lower  $p$  values (<0.05) for both permeate flux and  $\text{CO}_2$  recovery, which indicates the significant influence on the carbon membrane separation performance. Therefore, the parameter of feed pressure (B) and retentate flow rate (C) may control the membrane separation performances. The steeper slopes for the plots of the feed pressure (B) and the retentate flow rate (C) are additional proof of their significances. Moreover, the analysis results also indicate that the temperature (A) in these ranges has only little effects on both permeate flux and  $\text{CO}_2$  recovery. Due to the large  $p$  value for the  $\text{CO}_2$  recovery and lower  $p$  value for the  $\text{CO}_2$  permeance for the parameter (D), the  $\text{CO}_2$  feed composition will be important to meet the specific requirement of  $\text{CO}_2$  flux (Productivity).

#### 4.4. Effect of feed and permeate pressures

The single stage membrane unit with an assumed membrane area of  $2 \times 10^7 \text{ m}^2$  was executed for the process simulation with a cross flow configuration. Figs. 8 and 9 illustrate the dependency of  $\text{CO}_2$  purity, recovery and specific energy demands for  $\text{CO}_2$  capture with two different process configurations. For the configuration A with a constant permeate pressure of 1 bar, and compression of the feed side (3–12 bar), the results showed high  $\text{CO}_2$  recovery in Fig. 8, but lower  $\text{CO}_2$  purity on permeate side. For configuration B with a constant feed pressure of 1 bar and vacuum on the perme-

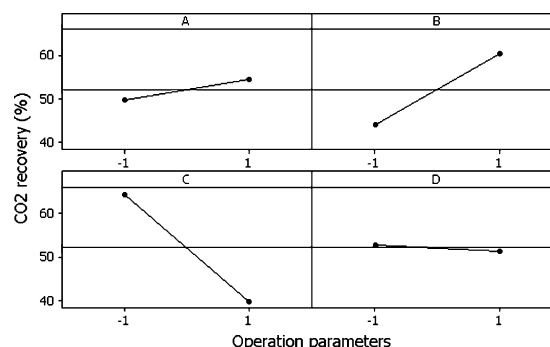


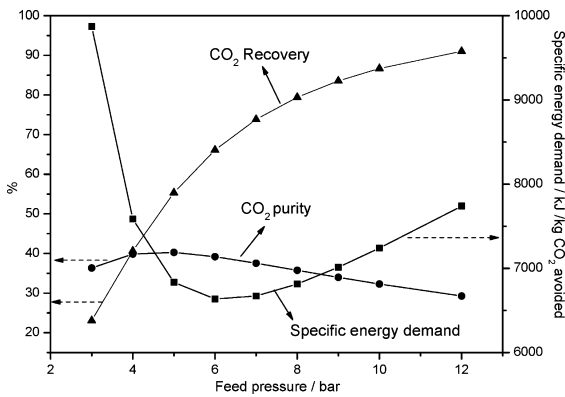
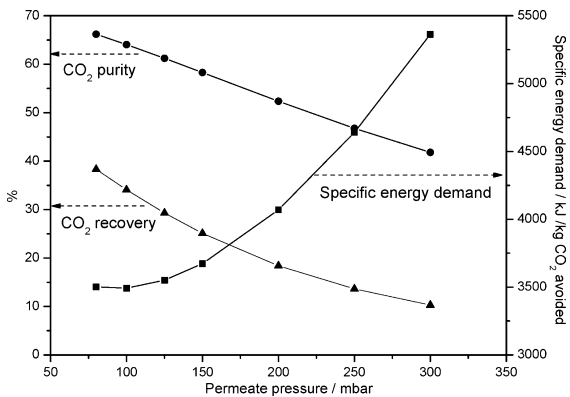
Fig. 7. The main influence plots by Minitab® for  $\text{CO}_2$  recovery, A (temperature), B (feed pressure), C (retentate flow rate) and D (feed  $\text{CO}_2$  composition).

**Table 3**  
2<sup>4</sup>-1 fractional factorial design and experiment results.

Run order	A	B	C	D	Permeate flux (ml min <sup>-1</sup> )	Stage-cut (%)	CO <sub>2</sub> purity (%)	CO <sub>2</sub> Recovery (%)
1	-1	-1	-1	-1	0.46	7.15	72.6	51.7
2	+1	-1	-1	+1	0.696	10.4	70.5	58.9
3	-1	+1	-1	+1	1.07	13.8	76.9	70.9
4	+1	+1	-1	-1	0.746	12	63.8	76.8
5	-1	-1	+1	+1	0.865	6	74.6	29.7
6	+1	-1	+1	-1	0.586	4.9	72.7	35.8
7	-1	+1	+1	-1	0.806	6.3	75	47.2
8	+1	+1	+1	+1	1.22	9.26	76	46.8

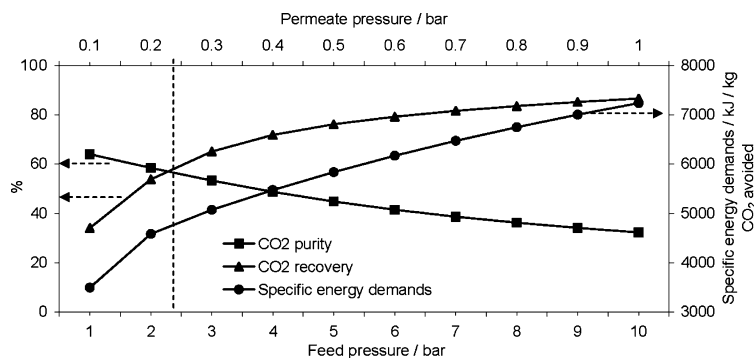
**Table 4**  
Results of statistical analysis by Minitab®.

Term	Permeate flux			CO <sub>2</sub> recovery		
	Effect	Coefficient	p-Value	Effect	Coefficient	p-Value
Constant	0.806125	0.01972	0	52.23	0.9936	0
Temperature	0.01175	0.005875	0.785	4.7	2.35	0.099
Feed pressure	0.30875	0.154375	0.004	16.4	8.2	0.004
Retentate flow rate	0.12625	0.063125	0.049	-24.7	-12.35	0.001
CO <sub>2</sub> feed composition	0.31325	0.156625	0.004	-1.3	-0.65	0.56

**Fig. 8.** Gas separation performance and specific energy demands with different feed pressure at constant permeate pressure of 1 bar and 303 K.**Fig. 9.** Gas separation performance and specific energy demands with different permeate pressure at constant feed pressure of 1 bar and 303 K.

ate side (75–300 mbar), which shows higher CO<sub>2</sub> purity but relative lower CO<sub>2</sub> recovery. However, the specific energy demands for configuration A is much higher than that of configuration B. In order to obtain the optimal process configuration, the combination of

these two configurations (feed compression and vacuum in permeate side) was also investigated. There is a trade off between the CO<sub>2</sub> recovery, CO<sub>2</sub> purity and specific energy demands under different operating conditions as shown in Fig. 10. It can be seen that

**Fig. 10.** Gas separation performance and specific energy demands with the combination of compression and evacuation of feed and permeate sides at 303 K, (■) CO<sub>2</sub> purity, (▲) CO<sub>2</sub> recovery, (◆) specific energy demands.

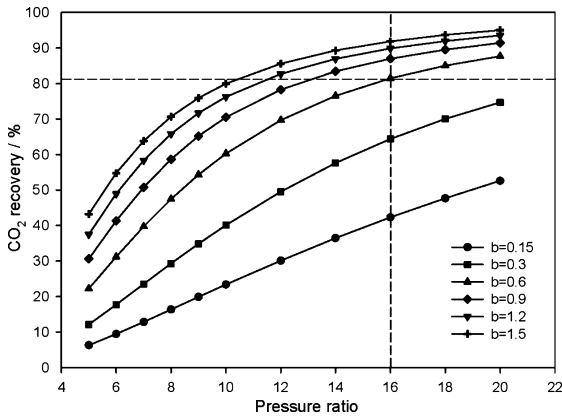


Fig. 11. CO<sub>2</sub> recovery as function of pressure ratio at 303 K and permeate pressure of 0.25 bar.

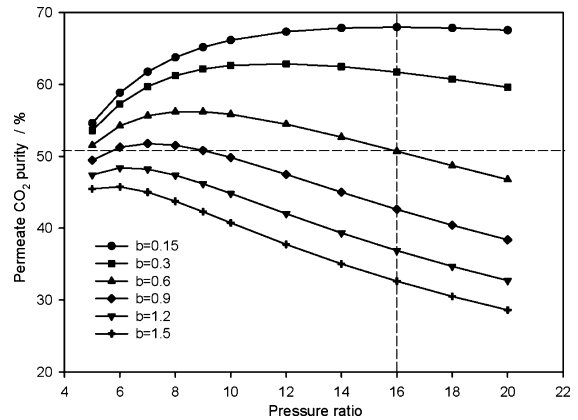


Fig. 12. Permeate CO<sub>2</sub> purity as function of pressure ratio at 303 K and permeate pressure of 0.25 bar.

the single stage membrane process cannot achieve high product quality (e.g. 90% CO<sub>2</sub>) and CO<sub>2</sub> recovery (e.g. 60%) simultaneously. A minimum recovery of 60% was chosen as a starting point for the simulation based on the current performance data. Hence a multi-stage membrane units needed to be designed for the specific application.

#### 4.5. Characteristic diagrams

Two dimensionless parameters are derived applying the Buckingham  $\pi$  theorem to characterize the performance of single stage or multi-stage membrane separation processes.

$$\Pi = \frac{P_{\text{CO}_2} A p_F}{V_F} = b p_F \quad (4)$$

$$\phi = \frac{p_F}{p_P} \quad (5)$$

where  $\Pi$  is the dimensionless permeation number,  $V_F$  is the feed volume flow (Nm<sup>3</sup>/h).  $P_{\text{CO}_2}$  and  $A$  are the permeance of CO<sub>2</sub> (Nm/(m<sup>2</sup> h bar)) and the required membrane area (m<sup>2</sup>), respectively.  $p_F$  and  $p_P$  are the feed and permeate pressure (bar) separately.  $b$  is a simplified process parameter ( $b = P_{\text{CO}_2} A / V_F$ , bar<sup>-1</sup>).  $\Phi$  is the pressure ratio between feed and permeate side. The flue gas was compressed to appropriate pressures (various  $\Phi$ ) and cooled down to 30 °C before fed into the membrane separation unit. The permeate pressure of 0.25 bar was used for the simulation based on the consideration of the capacity for the large-scale industrial vacuum pumps. The process simulation was executed with different pressure ratios,  $\Phi$  (5–20) and process parameters,  $b$  (0.15–1.5 bar<sup>-1</sup>). The characteristic diagrams for the different separation processes were obtained from the simulation results of CO<sub>2</sub> recovery, permeate CO<sub>2</sub> purity, specific energy demands and required membrane areas, which were shown in Figs. 11–14. One can easily obtain all process parameters by drawing an appropriate line in these characteristic diagrams based on the given requirements (e.g. CO<sub>2</sub> recovery of 81.5% and pressure ratio of 16). By drawing the lines in Fig. 11, the parameter line of  $b = 0.6$  was identified. The CO<sub>2</sub> purity in permeate side was then determined as 51% from Fig. 12 by the intersection plot of the pressure ratio line ( $\Phi = 16$ ) and parameter line ( $b = 0.6$ ). Moreover, the specific energy demands and permeation number were also obtained from Figs. 13 and 14 using the same procedure, and the values were 5400 kJ/kg CO<sub>2</sub> avoided and 2.4, respectively. Hence, the characteristic diagrams can be used to determine the required operating

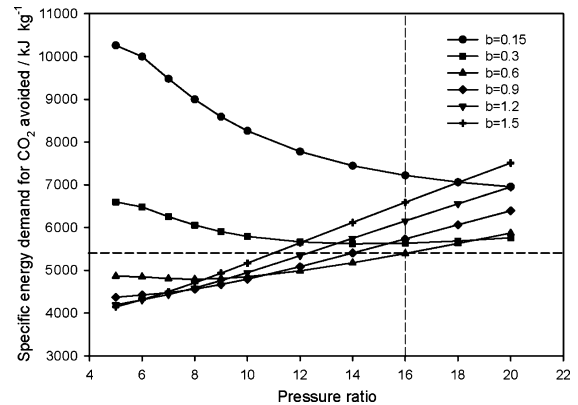


Fig. 13. Specific energy demands for CO<sub>2</sub> avoided as function of pressure ratio at 303 K and permeate pressure of 0.25 bar.

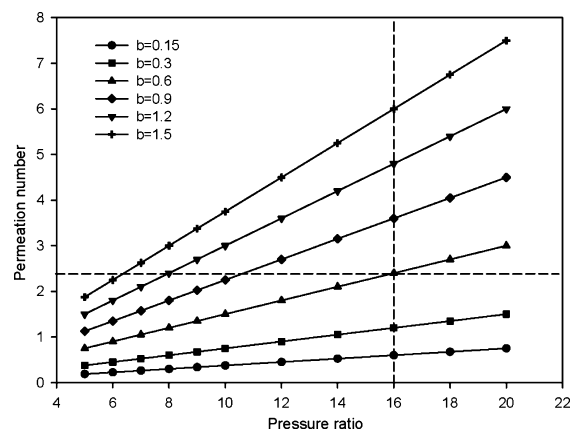


Fig. 14. Permeation number as a function of pressure ratio at 303 K and permeate pressure of 0.25 bar.

**Table 5**Simulation results of CO<sub>2</sub> capture by membrane process.

Parameter	First stage	Second stage
Feed pressure (bar)	4	3.75
Permeate pressure (bar)	0.25	0.25
CO <sub>2</sub> composition (%)		
Feed	15.0	57.9
Retentate	3.5	26.2
Permeate	57.9	90.3
Feed temperature (°C)	30	30
Stage CO <sub>2</sub> recovery (%)	81.6	77.2
Membrane area (m <sup>2</sup> )	1.50 × 10 <sup>7</sup>	1.66 × 10 <sup>6</sup>
Total CO <sub>2</sub> recovery (%)	63.0	
Feed CO <sub>2</sub> mass flow (kg/h)	2.28 × 10 <sup>5</sup>	
Captured CO <sub>2</sub> mass flow (kg/h)	1.43 × 10 <sup>5</sup>	
Total carbon membrane cost (M\$)	3000	
Total compressor duty GJ/t CO <sub>2</sub> avoided	6.32	
Specific capital cost \$/t CO <sub>2</sub> avoided	136	

conditions and the carbon membrane areas in order to meet the specific constraints.

#### 4.6. Process feasibility evaluation

Gas membrane separation process is typically designed with equipments such as compressors, coolers and membrane units; arranged, controlled, and operated in a particular way, to capture CO<sub>2</sub> which must meet a certain specification as given in Table 2. The minimization of capital cost was employed to conduct the process optimization. Since the process with single stage membrane unit cannot achieve the specification as described in Section 4.4, a two stage cascade membrane process with counter-current configuration was designed and investigated. A feed pressure of 4 bar was set to attain a minimum recovery of 80% in the 1st stage, and a 90% of CO<sub>2</sub> purity in permeate stream and 75% CO<sub>2</sub> recovery in the 2nd stage was subsequently achieved by optimize the process operating conditions. The captured CO<sub>2</sub> was then compressed to 110 bar for sequestration. The purity of CO<sub>2</sub> and % CO<sub>2</sub> captured will be influenced by the pressure ratio over the membrane. As already stated, a permeate pressure of 250 mbar was chosen based on capacity for the large-scale industrial vacuum pumps. A 100 mbar permeate pressure would have shown better theoretical results, but might have been less realistic for installation at a power plant. The specific capital costs were calculated from the required membrane area and the duty of the compressors and the coolers. The optimal operating parameters and simulation results are given in Table 5. Based on the capital cost estimation for the major equipment which includes the membrane unit, compressor and heat exchanger, a specific capital cost of 136 \$/tonne CO<sub>2</sub> avoided was determined with the two-stage cascade membrane process. Comparing to the previous work [27], the specific capital cost was significantly reduced by increasing the carbon membrane permeance (from 0.022 to 0.03 Nm<sup>3</sup> m<sup>-2</sup> h<sup>-1</sup> bar<sup>-1</sup>) even through the carbon membrane cost was set much higher in this work (45 \$/m<sup>2</sup> comparing to 15 \$/m<sup>2</sup>). Moreover, the cost of carbon membrane unit was found to be the major part of the total capital cost, which could be greatly reduced by improving the carbon membrane performance and simplifying the membrane production process although the carbon membrane/module cost is still unknown today. Therefore, an assumed membrane permeance, based on the reduction of wall thickness from 25 to 10 μm (see Table 2), was also employed for the process simulation using the same operating conditions. The results are given in Table 6. (Experimentally it is considered to be realistic to prepare carbon membranes with wall thickness of 10 μm—this was proven by previous company Carbon Membranes Ltd., Israel.) It was found that the total carbon membrane cost was reduced significantly from 3000 M\$ to 1220 M\$, due to the

**Table 6**Simulation results based on the assumed carbon membranes.<sup>a</sup>

Parameter	First stage	Second stage
CO <sub>2</sub> composition (%)		
Feed	15	57.7
Retentate	3.4	25.2
Permeate	57.7	90.1
Stage CO <sub>2</sub> recovery (%)	82.1	78.2
Membrane area (m <sup>2</sup> )	6.1 × 10 <sup>6</sup>	6.9 × 10 <sup>5</sup>
Total CO <sub>2</sub> recovery (%)	64.2	
Total carbon membrane cost (M\$)	1220	
Total compressor duty GJ/t CO <sub>2</sub> avoided	6.24	
Specific capital cost \$/t CO <sub>2</sub> avoided	57	

<sup>a</sup> Operating condition is the same with Table 5.

increased carbon membrane permeance, while the capital costs (\$/t CO<sub>2</sub> avoided) now was down to 57. Ho et al. reported that the capital cost was 70 \$/tonne CO<sub>2</sub> avoided using traditional chemical absorption method with monoethanolamine (MEA) for CO<sub>2</sub> capture from a 500 MW pulverised coal power plant [31]. It can thus be concluded that the carbon membrane technology is quite promising also compared to the chemical absorption methods. Hence, this environmental friendly technology could also promote the hollow fiber carbon membranes to become a potential candidate for CO<sub>2</sub> capture in future.

## 5. Conclusions

The hollow fiber carbon membranes were prepared from the deacetylated cellulose acetate precursors by controlling the carbonization procedure with CO<sub>2</sub> as purge gas, a heating rate of 4 °C/min, a final temperature 550 °C and soak time 2 h. A typical thickness and outer diameter of 25 μm and 200 μm for the prepared carbon membranes were determined from the SEM images. The permeability for the prepared HFCEMs for different gases CO<sub>2</sub>, O<sub>2</sub> and N<sub>2</sub> were in accordance with the order of kinetic diameters for gas molecules (<4 Å), which indicated that the molecular sieving mechanism was dominated for the transport process. The gas permeability will decrease with the presence of water vapor which may be caused by the pore blocking. The operating parameters were systematically investigated by factorial design and statistical analysis. The feed pressure and retentate flow rate showed the more significant influences on the carbon membrane separation performance.

The single stage membrane processes for CO<sub>2</sub> separation from flue gas with feed compression, permeate evacuation, and their combination was investigated using Aspen HYSYS simulation tool integrated with an in-house membrane simulation model. The simulation results indicated that the single stage membrane process cannot achieve high CO<sub>2</sub> purity and CO<sub>2</sub> recovery simultaneously using these hollow fiber carbon membranes. The characteristic diagrams which were plotted can be easily used by end users to identify the required operating conditions and membrane areas so as to meet the given targets. The capital cost estimation for the two-stage cascade membrane process indicated that the cost of carbon membrane technology may be compared to the chemical absorption method. Although the cost of carbon membranes is still unknown, the membrane/module cost can be greatly reduced by improving the membrane separation performance, especially by reducing the wall thickness, and simplifying the membrane production process. These hollow fiber carbon membranes will be further investigated for a potential application for CO<sub>2</sub> capture.

## Acknowledgements

The authors want to thank the NanoGloWa project for the funding of the current work (EUs 6th framework program).

## References

- [1] International Energy Outlook 2010—Highlights, <http://www.eia.doe.gov/oi/af/ieo/highlights.html>.
- [2] A. Yamasaki, An overview of CO<sub>2</sub> mitigation options for global warming—emphasizing CO<sub>2</sub> sequestration options, *J. Chem. Eng. Jpn.* 36 (2003) 361–375.
- [3] N. Nsakala, J. Marion, C. Bozzuto, G. Liljedahl, M. Palkes, D. Vogel, J.C. Gupta, M. Guha, H. Johnson, S. Plasynski, Engineering feasibility of CO<sub>2</sub> capture on an existing US coal-fired power plant, *J. Energy Environ. Res.* 2 (2002).
- [4] H. Yang, Z. Xu, M. Fan, R. Gupta, R.B. Slimane, A.E. Bland, I. Wright, Progress in carbon dioxide separation and capture: a review, *J. Environ. Sci.* 20 (2008) 14–27.
- [5] R. Carapellucci, A. Milazzo, Membrane systems for CO<sub>2</sub> capture and their integration with gas turbine plants, *Proc. Inst. Mech. Eng. A: J. Power Energy* 217 (2003) 505–517.
- [6] R. Bredesen, K. Jordal, O. Bolland, High-temperature membranes in power generation with CO<sub>2</sub> capture, *Chem. Eng. Process.* 43 (2004) 1129–1158.
- [7] M.B. Hagg, A. Lindbrathen, CO<sub>2</sub> capture from natural gas fired power plants by using membrane technology, *Ind. Eng. Chem. Res.* 44 (2005) 7668–7675.
- [8] J. Huang, J. Zou, W.S.W. Ho, Carbon dioxide capture using a CO<sub>2</sub>-selective facilitated transport membrane, *Ind. Eng. Chem. Res.* 47 (2008) 1261–1267.
- [9] S.R. Reijerkerk, Polyether Based Block Copolymer Membranes for CO<sub>2</sub> Separation, Enschede Thesis 2010, University of Twente, pp. 245.
- [10] H. Lin, B.D. Freeman, Materials selection guidelines for membranes that remove CO<sub>2</sub> from gas mixtures, *J. Mol. Struct.* 739 (2005) 57–74.
- [11] L. Deng, T.-J. Kim, M.-B. Hägg, Facilitated transport of CO<sub>2</sub> in novel PVAm/PVA blend membrane, *J. Membr. Sci.* 340 (2009) 154–163.
- [12] M. Sandru, S.H. Haukebo, M.-B. Hägg, Composite hollow fiber membranes for CO<sub>2</sub> capture, *J. Membr. Sci.* 346 (2010) 172–186.
- [13] H. Suda, K. Haraya, Gas permeation through micropores of carbon molecular sieve membranes derived from kapton polyimide, *J. Phys. Chem. B* 101 (1997) 3988–3994.
- [14] K.M. Steel, W.J. Koros, Investigation of porosity of carbon materials and related effects on gas separation properties, *Carbon* 41 (2003) 253–266.
- [15] L.I.B. David, A.F. Ismail, Influence of the thermastabilization process and soak time during pyrolysis process on the polyacrylonitrile carbon membranes for O<sub>2</sub>/N<sub>2</sub> separation, *J. Membr. Sci.* 213 (2003) 285–291.
- [16] B. Zhang, T. Wang, S. Zhang, J. Qiu, X. Jian, Preparation and characterization of carbon membranes made from poly(phthalazinone ether sulfone ketone), *Carbon* 44 (2006) 2764–2769.
- [17] M. Yoshimune, I. Fujiwara, K. Haraya, Carbon molecular sieve membranes derived from trimethylsilyl substituted poly(phenylene oxide) for gas separation, *Carbon* 45 (2007) 553–560.
- [18] J.N. Barsema, Carbon membranes precursor, preparation and functionalization, University of Twente, Enschede, 2007.
- [19] E.P. Favvas, G.C. Kapantaidakis, J.W. Nolan, A.C. Mitropoulos, N.K. Kanellopoulos, Preparation, characterization and gas permeation properties of carbon hollow fiber membranes based on Matrimid(R) 5218 precursor, *J. Mater. Process. Technol.* 186 (2007) 102–110.
- [20] J.A. Lie, Synthesis, Performance and Regeneration of Carbon Membranes for Bio-gas Upgrading—A Future Energy Carrier, Department of Chemical Engineering, Norwegian University of Science and Technology, Trondheim, 2005.
- [21] S.M. Saufi, A.F. Ismail, Development and characterization of polyacrylonitrile (PAN) based carbon hollow fiber membrane, *Songklanakarinn J. Sci. Technol.* 24 (Suppl.) (2002) 843–854.
- [22] X. He, J.A. Lie, E. Sheridan, M.-B. Hägg, Preparation and characterization of hollow fibre carbon membranes based on a cellulosic precursor, in: *Conf. on ICOM 2008, Honolulu, Hawaii, 2008*.
- [23] X. He, J.A. Lie, E. Sheridan, M.-B. Hägg, CO<sub>2</sub> capture by hollow fibre carbon membranes: experiments and process simulations, in: *Conf. on GHGT-9, Washington, DC, 2008*.
- [24] J.-J. Qin, Y. Li, L.-S. Lee, H. Lee, Cellulose acetate hollow fiber ultrafiltration membranes made from CA/PVP 360K/NMP/water, *J. Membr. Sci.* 218 (2003) 173–183.
- [25] X.H. Tai-ShungChung, Effect of air-gap distance on the morphology and thermal properties of polyethersulfone hollow fibers, *J. Appl. Poly. Sci.* 66 (1997) 1067–1077.
- [26] J.-J. Qin, F.-S. Wong, Y. Li, Y.-T. Liu, A high flux ultrafiltration membrane spun from PSU/PVP (K90)/DMF/1,2-propanediol, *J. Membr. Sci.* 211 (2003) 139–147.
- [27] X. He, J.A. Lie, E. Sheridan, M.-B. Hägg, CO<sub>2</sub> capture by hollow fibre carbon membranes: experiments and process simulations, *Energy Procedia* 1 (2009) 261–268.
- [28] D. Grainger, Development of carbon membranes for hydrogen recovery, Norwegian University of Science and Technology, PhD Thesis, 2007.
- [29] R. Turton, R.C. Bailie, W.B. Whiting, J.A. Shaeiwitz, Analysis, Synthesis, and Design of Chemical Processes, 3rd edition, Prentice Hall, New Jersey, 2008.
- [30] W.J. Koros, Membrane Opportunities and Challenges for Large Capacity Gas and Vapour Feeds, European Membrane Society's 20th Summer School NTNU, Trondheim, Norway, 2003.
- [31] M.T. Ho, G.W. Allinson, D.E. Wiley, Comparison of MEA capture cost for low CO<sub>2</sub> emissions sources in Australia, *Int. J. Greenhouse Gas Control* (2010), doi:10.1016/j.ijggc.2010.06.004.



## **Appendix H**

Hollow Fiber Carbon Membranes: from Material to Application

Article Submitted to *AIChE Journal*



# Hollow Fiber Carbon Membranes: from Material to Application

*Xuezhong He, May-Britt Hägg\**

Department of Chemical Engineering, Norwegian University of Science and  
Technology, N-7491 Trondheim, Norway

**Abstract:** A general technical route of Design-Preparation-Construction-Operation-Integration (DPCOI) platform was firstly presented to promote the hollow fiber carbon membranes (HFCMs) from material to application. The cellulose acetate (CA) was chosen as the polymer material for spinning of hollow fibers. The cellulosic precursors were regenerated from the CA hollow fibers using an optimized deacetylation process. The HFCMs were fabricated from the cellulosic precursors with the optimal carbonization process. The structure, morphology, and gas separation performance for the prepared HFCMs were characterized on the basis of a scanning electronic microscopy (SEM) and the gas permeation tests. The process simulations were also conducted to evaluate the process feasibility for CO<sub>2</sub> capture by HFCMs on the basis of the capital cost estimation. The results indicated that the DPCOI platform could be used to guide the development of the HFCMs, and promote their commercial applications.

**Keywords:** cellulose acetate; spinning; deacetylation; hollow fiber carbon membranes; CO<sub>2</sub> capture

\* Corresponding author. Tel.: +47 73594033; fax: +47 73594080.  
E-mail: may-britt.hagg@chemeng.ntnu.no

## 1 Introduction

Carbon membranes have been studied in the last few years as a promising candidate for energy-efficient gas separation processes. Fuertes et al. reported that the carbon membranes had a potential to push the upper boundary of permeability vs. selectivity tradeoff relationship [1]. Strong interests have been shown in the preparation of the carbon membranes for gas separation [2-7], based on the improved selectivity and enhanced thermal, mechanical and chemical stability compared to polymeric membranes already in use. Moreover, the hollow fiber geometry will be preferable to spiral wound membranes due to the high packing density (membrane area per unit volume of vessel) and easy module assembly from the standpoint of large-scale application. Therefore, the development the hollow fiber carbon membranes (HFCMs) could be the potential commercial application for the carbon membranes. However, most published work are focusing on seeking for a high performance carbon membrane on the basis of the pure gas and synthetic gas mixture measurements on lab scale, and no commercial gas separation application has yet been reported for the use of HFCMs. The goal of the *fundamental* experimental research is in general to gain knowledge and understanding of a physical problem, and is not necessarily considering the practical use or implication of the findings. This is quite different from the *applied* research, in which the scientific investigation is carried out to seek for a solution to a practical problem. A typical route to bridge the fundamental and applied research is shown in Figure 1 – this is a general technical route of Design-Preparation-Construction-Operation-Integration (DPCOI) platform which was followed in the current project for promoting the HFCMs from material to industrial applications. The results reported in the current paper, is following the carbon membranes from the choice of polymer in the fundamental research through to the evaluation of separation performance of a pilot scale HFCM-module and simulations.

Material design, the chemical structure and physical properties should be primarily evaluated to choose a suitable polymer material. Previous literature reported to use different polymer materials such as polyimide, PAN and cellulose as the precursors for the carbon membranes [8-13]. Among them, cellulose is the most abundant biorenewable material for many commercial applications. The carbon membranes prepared from the cellulose precursors have proved to show good separation performances [14-15]. However, the cellulose is quite challengeable to be dissolved in the conventional solvents due to the strong inter- and intra-molecular hydrogen

bonding, which causes the potential of cellulose has not been fully exploited to be used as the precursors for the carbon membranes [16].

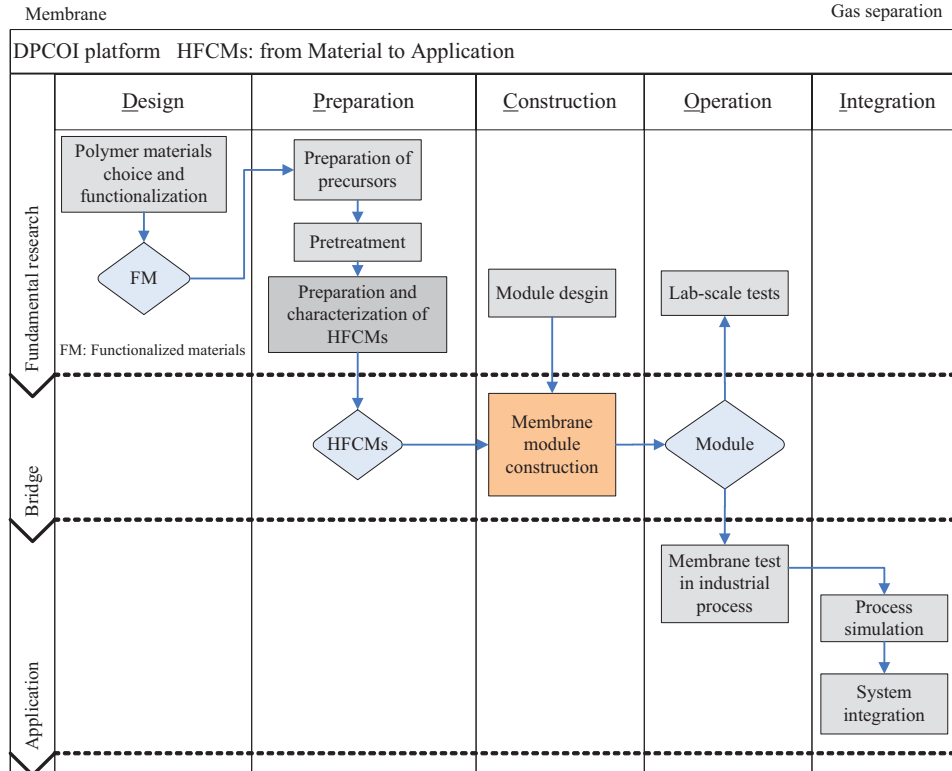


Figure 1. DPCOI platform for HFCMs from material to application.

The recently developed Lyocell process, reported to use N-methylmorpholine-N-oxide (NMMO) to dissolve cellulose directly from biomass, showed a higher efficiency compared to the other processes [17]. However, the Lyocell process embodies significant engineering challenges with regard to the solvent mentioned, such as stability, safety, and recovery. Moreover, a lot of byproducts are also formed within the process which may cause the detrimental effects such as degradation of cellulose, discoloration of the resulting fibers, significant decomposition of NMMO. Some literature also reported the use of green solvents such as ionic liquids, to dissolve the cellulose and prepare the dope solution [16, 18-19]. However, the ionic liquids are still very expensive and not commercial available now. Previous studies have already reported the spinning of cellulose acetate (CA) fibers, which are mostly used for the dialysis, reverse osmosis (RO) and ultrafiltration (UF) [20-25]. However, regenerated

cellulose acetate fibers could be used as the precursors for the preparation of hollow fiber carbon membranes. Therefore, this alternative low-cost, commercial available polymer of cellulose acetate was chosen as the material for spinning of hollow fibers in the current project.

Preparation of the precursor and carbon membranes. the well-known dry-jet wet spinning technology was used to spin the defect-free CA hollow fiber membranes. Qin [24] and Chung [26] reported that spinning parameters such as air gap, bore fluid composition, flow rate of bore fluid, and temperature of quench bath would affect the membrane properties. Hence, the spinning condition needs to be optimized to obtain the defect-free hollow fibers with the desired properties. Since the cellulose acetate hollow fibers could not be directly used for the preparation of the carbon membranes as reported in our previous work [27], therefore, the prepared CA fibers were regenerated by deacetylation to be used as the precursors for the carbon membranes. Some literature reported the use of alkali, e.g. NaOH and KOH, for deacetylation [23, 25, 28-29]. Liu et al. found that the reaction time was very important to the deacetylation results, and the deacetylation of CA membranes by immersion in a NaOH ethanol solution was more efficient than in the aqueous solution [23]. The deacetylation of the CA fibers using a 0.5M KOH ethanol solution was also investigated by Son et al [25]. They reported that the deacetylation was quite fast and almost completed within 20 min. Their results provided a valuable clue for the investigation of the deacetylation process. The regenerated cellulose fibers were then used as the precursors for the preparation of hollow fiber carbon membranes on the basis of optimized carbonization procedure.

Module construction. Saufi et al. reported that all system designs for a module must consider the factors of the production cost, maintenance, and efficiency [30]. Membrane module construction is, however, seldom referred in open literature as details on this will typically be confidential information for a company producing membrane modules. To date, only tubular and hollow fiber lab-scale modules have been reported for carbon membranes [3, 12, 31-32]. The potentially industrial use of these membranes were reported by two companies; Carbon Membranes Ltd. (Israel) in the late nineties, and later Blue Membranes GmbH (Germany). Carbon Membranes Ltd. produced hollow fibers on a pilot scale and demonstrated successfully separation for various applications, while Blue Membranes developed a new concept based on the honeycomb membrane module configuration for their carbon membranes [33]. None of these two companies succeeded in taking their carbon membranes all the way to the market. There are, however, new companies which will take advantage of the superior separation

properties the carbon membranes have, and hopefully will be able to develop them for various applications in the market, such as biogas upgrading which is the focus of the company MemfoACT in Norway.

Membrane test, the carbon membrane performance can be characterized by the gas permeation tests through the constructed module on the basis of the single gas (e.g. CO<sub>2</sub>, O<sub>2</sub>, N<sub>2</sub>, CH<sub>4</sub>) and gas mixtures of different compositions. The single gas test is typically used to characterize the ideal selectivity and gas permeability, while the gas mixture measurements are executed to investigate the effects of the operating parameters, e.g. temperature, pressure and feed composition, on the process separation performance (i.e. product recovery and purity). Moreover, the exposure of the prepared carbon membranes to a real environment in an industrial process must also be conducted to document the membrane stability and durability. At least two pilot stages with increased module size should be tested.

Process simulation and system integration, the parameters relevant to the carbon membrane separation process as well as to other membrane processes, are temperature, pressure ratio, feed concentration as well as the membrane area. These variables will significantly influence the membrane separation results. Therefore, the process simulation needs to be conducted to evaluate the process feasibility of the membrane separation unit operation based on the economic estimation. Lie et al. reported the process simulation and economic evaluation for the CO<sub>2</sub> removal in steelmaking industry by carbon membrane [34]. The process for CO<sub>2</sub> capture from flue gases using the hollow fiber carbon membranes was simulated by He et al [35-36]. Their results indicated that a high performance carbon membrane could possibly be an alternative to the traditional chemical absorption. The membrane gas separation system may also be integrated with other unit operations at a process plant, such as distillation, reactor and absorption units, for a specific industrial application. Some literature investigated the design and synthesis of membrane technology for gas separation processes [37-38]. Grainger reported the heat exchange network integration for H<sub>2</sub> / CO<sub>2</sub> separation by membrane technology in an IGCC power plant [39].

In this work, the CA hollow fibers were spun on the basis of the optimal spinning condition. The cellulosic precursors were regenerated from the CA hollow fibers by deacetylation, which were further used to prepare the hollow fiber carbon membranes. The carbon membrane properties were characterized on the basis of gas permeation tests both for single gas and gas mixture. Moreover, the process simulation was also

conducted to evaluate the process feasibility for CO<sub>2</sub> capture from flue gases by the hollow fiber carbon membranes.

## **2 Experimental Section**

### **2.1 Materials**

CA (MW 100,000) with an average acetyl content of 39.8 % was purchased from ACROS (USA). Polyvinylpyrrolidone (PVP K10) was purchased from Sigma. The solvent, N-methyl-2-pyrrolidone (NMP, >99.5 %) was purchased from Merck (Darmstadt, Germany). Glycerol (>98 %) was purchased from BDH/VWR. NaOH (>99 %) was also purchased from Merck, and was used for the deacetylation of CA hollow fibers.

### **2.2 Spinning of CA hollow fibers**

CA hollow fibers were spun from a dope solution consists of CA/PVP/NMP (22.5% / 5% / 72.5%) [3]. The solvent, NMP and the additive, PVP K10, were well mixed by mechanical stirring. The polymer CA was then added gradually into the mixture. The mixture was stirred for 24 h to ensure a homogeneous dope solution. The ultrasonic oscillator was further employed to remove the air bubbles from the dope solution. The dope solution and bore fluid (NMP+water) were fed into a double spinneret by gearwheel pumps [3]. A schematic diagram for spinning is shown in Figure 2. The extrusion rates of the dope solution and bore fluid are well controlled by two gear pumps respectively. Previous investigations in our research have shown that the high temperature of the quench bath gives an open structure with a thin skin layer, while low temperature results to forming a dense membrane with a thick skin layer (He et.al)[40]. Moreover, the bore fluid (e.g. mixture of NMP / H<sub>2</sub>O) with high water content results in internal macrovoids, while the high NMP content resulting to form a membrane with much more open sub-structure. Therefore, the spinning conditions of dope flow rate, air gap, bore fluid composition, bore flow rate and temperature of quench bath should be well controlled to prepare the even, defect-free hollow fibers.

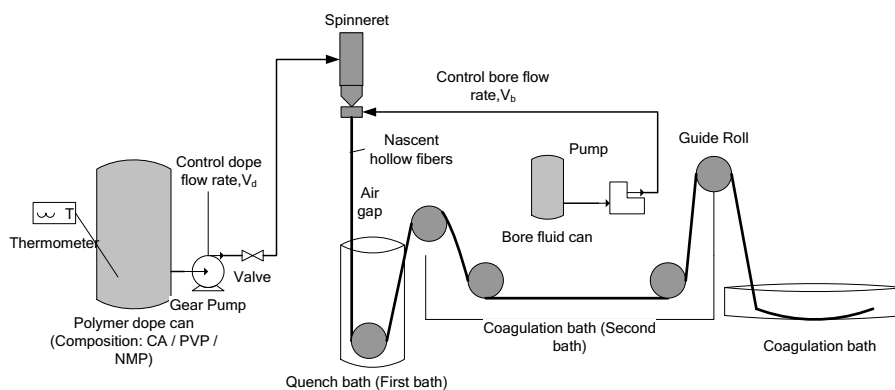
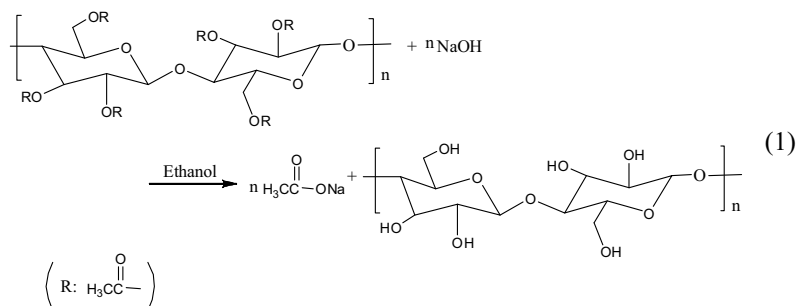


Figure 2. Schematic diagram for the spinning process.

### 2.3 Deacetylation

The spun CA hollow fibers were deacetylated by immersion in different NaOH solution at room temperature to prepare the cellulosic precursors. The deacetylation reaction of CA and NaOH is shown in eq 1.



The deacetylation was firstly conducted using a 0.5 M NaOH (50 % and 96 % ethanol) solution for various reaction times to investigate the effects of solution on the deacetylation results. The deacetylation parameters of NaOH concentration, solution, deacetylation time, and swelling (soak in a 10 % glycerol solution) time before deacetylation were then optimized on the basis of the experimental design and statistical analysis.

## **2.4 Fabrication of hollow fiber carbon membranes**

The deacetylated precursors were carbonized in a tubular furnace (Carbolite® TZF 12/100/900) using a working tube of alumina and a quartz container, which is describe elsewhere [4]. An optimized multi-dwells carbonization protocol with CO<sub>2</sub> purge gas, a heating rate of 4 °C/min and a final temperature 550 °C and soak time 2 h, was executed to prepare the hollow fiber carbon membranes [27].

## **2.5 Membrane characterization**

A Bruker Tensor 27 Fourier transform infrared (FTIR) spectroscopy was used to characterize the properties of the deacetylated cellulose precursors. The FTIR spectra was employed to determine the residual acetyl content, PVP content of the precursors. A Zeiss SUPRA 55VP scanning electron microscopy (SEM) was used to characterize the structure and morphology of the precursors and the hollow fiber carbon membranes. The prepared HFCMs were mounted in a pilot scale membrane module for the gas permeation tests, as shown in Figure 3. The carbon membrane separation performance was measured at 30 °C and a feed pressure of 2 bar (permeate side evacuated) in a standard pressure-rise setup (MKS Baratron® pressure transducer, 0–100 mbar range) with LabView® data logging as described elsewhere [3]. A gas chromatography (GC; Agilent 6890N) was combined with the permeation setup to allow online detection of gas composition in the retentate and permeate streams. The gas permeability and selectivity was calculated on the basis of the method described elsewhere [3].

# **3 Results and Discussion**

## **3.1 Morphology of hollow fibers**

The spinning condition was optimized on the basis of the of orthogonal experimental design and statistical analysis [40]. The optimal spinning condition of a bore fluid (water + NMP (85%)), an air gap (25 mm), a bore flow rate (40 % of dope flow rate) and a temperature of quench bath (50 °C) was obtained and used for spinning of defect-free CA hollow fibers. The SEM images of the cross sections for a representative CA hollow fiber are shown in Figure 4.

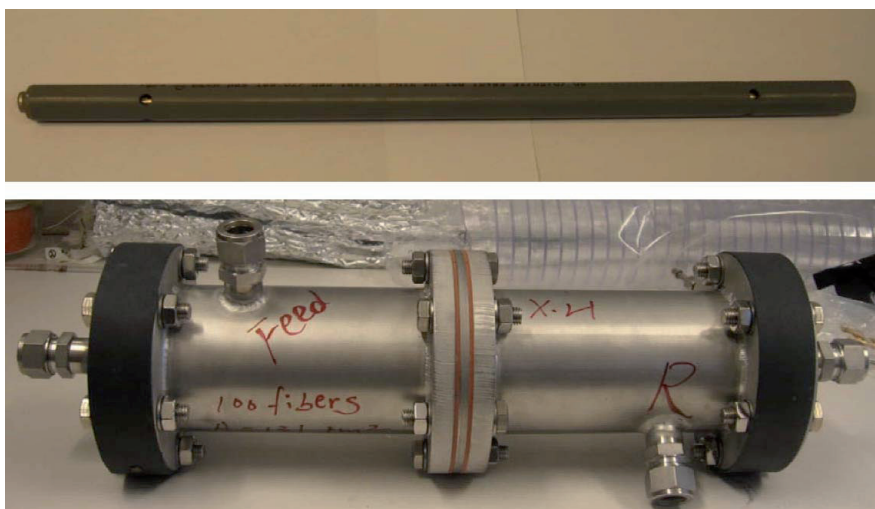


Figure 3. Hollow fiber carbon membrane module (Designed by HyGear).

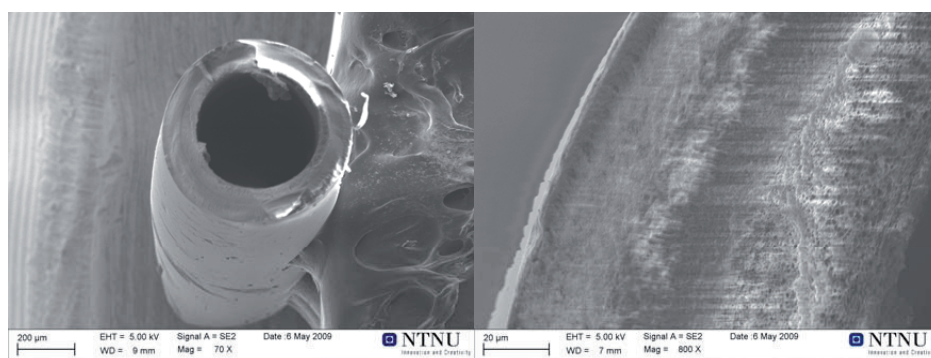


Figure 4. SEM images of the cross sections for a representative CA hollow fiber.

### 3.2 Deacetylation of CA hollow fibers

CA hollow fibers were firstly deacetylated by immersion in a 0.5 M NaOH (50 % and 96 % ethanol) solution for different reaction times. The FTIR spectroscopy was employed to determine the deacetylation results. The characteristic peaks for the pure CA, pure PVP, physical mixture of CA and PVP, and CA hollow fiber in the FTIR spectra are shown in Figure 5. The adsorption peaks  $1030$ ,  $1230$ , and  $1740\text{ cm}^{-1}$  attribute to the ether group ( $\nu_{C-O-C}$ ), acetyl ester group ( $\nu_{CH_3-C=O}$ ) and carbonyl group ( $\nu_{C=O}$ ) of CA respectively [25]. Moreover, the characteristic peak  $1665\text{ cm}^{-1}$  attributes to the carbonyl group of PVP. The residual acetyl content of the deacetylated CA fibers were

determined on the basis of the absorption intensity ratios of  $A_{1740\text{ cm}^{-1}}/A_{1030\text{ cm}^{-1}}$  from the FTIR spectra.

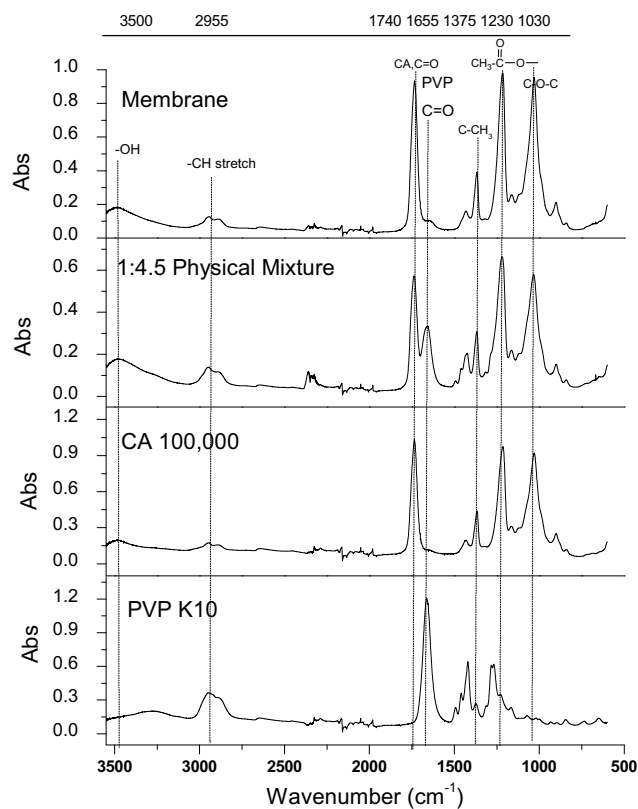


Figure 5. FTIR spectra for CA, PVP, physical mixture and membrane.

Figure 6 shows the relationship between the residual acetyl content in the deacetylated CA hollow fibers and the reaction time. It can be found that the reaction rate in a 50 % ethanol solution was faster than that in a 96 % ethanol solution. The orthogonal experimental design and statistical analysis was also conducted to optimize the deacetylation condition. The optimal deacetylation condition was found to be: swelled fibers in 10 % glycerol solution (24 h), immersion in a 0.075 M NaOH in (96 % ethanol) solution for 2 h. The CA hollow fibers treated at the optimal deacetylation condition were used as precursors for the preparation of HFCMs subsequently.

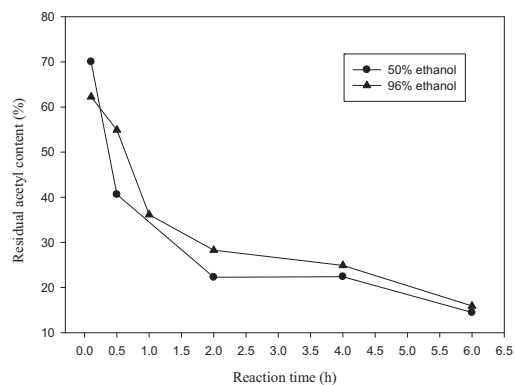


Figure 6. Dependence of residual acetyl content for hollow fibers on the deacetylation reaction time, (●) 50 % ethanol, (▲) 96% ethanol.

### 3.3 Carbon membrane structure and performance

#### 3.3.1 Membrane structure and morphology

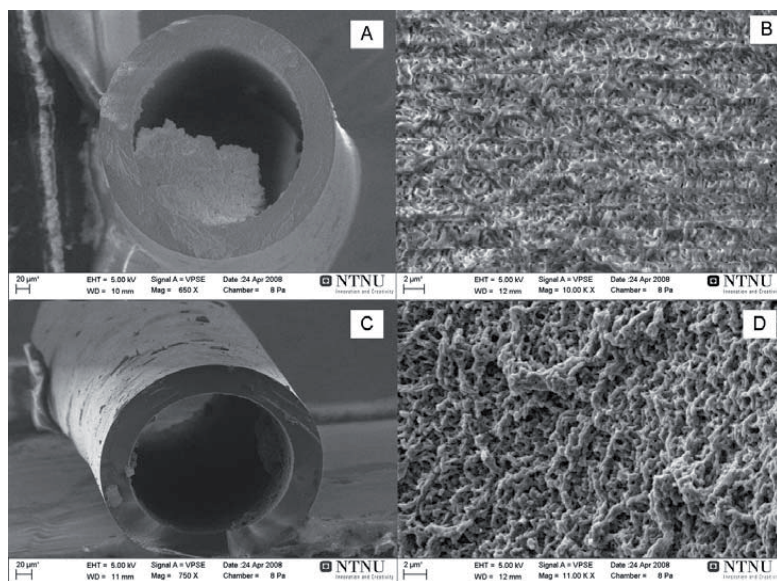


Figure 7. SEM images of cross section and inside of the precursor and carbon membrane: (A, B) cross section and inside of the precursor, (C, D) cross section and inside of the prepared carbon membrane.

SEM is used to characterize the structure and morphology of the samples, and Figure 7 shows the SEM images of the cross section and inside for the precursor and carbon membrane. Upon examination of SEM images, it was concluded that the HFCMs form a symmetric structure. The outer diameter (ca.250  $\mu\text{m}$ ) and wall thickness (ca. 25  $\mu\text{m}$ ) of the carbon membranes are much smaller compared to that of the precursors due to a significant shrinkage occurred in the carbonization process, which is consistent with the previous reported results [3].

### 3.3.2 Single gas tests

The gas permeability for the prepared HFCMs (see module in section 2.5) was tested with various single gases ( $\text{CO}_2$ ,  $\text{N}_2$ ,  $\text{CH}_4$  and  $\text{O}_2$ ). Figure 8 indicates the dependency of permeability values of different gases on the experimental temperature in the range of 30 - 70  $^\circ\text{C}$ , and at a constant feed pressure of 2 bar. The apparent transport activation energy,  $E_a$ , and  $P_0$  ( $P = P_0 \exp(-E_a/RT)$ ) was obtained from the experimental data by taking the logarithmic Arrhenius plot with  $\ln P$  as a function of  $1000/T$ , which are shown in Table 1. The activation energy is an indicator of the probability of a molecular passing a constriction, thus, the lower activation energy relates to a higher permeability. A large  $E_a$  resulting to a larger effect of temperature on the gas permeability. It can be concluded that the transport can be enhanced with increase of temperature, but slightly decrease the  $\text{CO}_2$  selectivity of carbon membranes within the experimental temperature range.

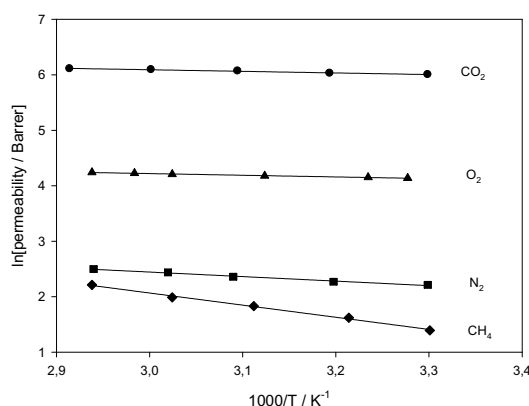


Figure 8. Dependency of gas permeability on the temperature of HFCMs at constant feed pressure 2 bar.

Table 1 Kinetic parameters for gas permeation through the HFCMs

Gas molecules	$d_k$ (nm)	$\varepsilon/k$ (K)	$E_a$ (kJ mol <sup>-1</sup> )	$P_0$ (Barrer)
CO <sub>2</sub>	0.33	195.0	2.4	1049.4
O <sub>2</sub>	0.346	107.0	2.5	168.2
N <sub>2</sub>	0.364	71.4	6.8	133.6
CH <sub>4</sub>	0.38	136.0	18.2	5602.7

Figure 9 presents the results for gas permeability of HFCMs measured at 303 and 323 K at different feed pressures from 1.5 to 6 bar. The permeability of both gas species decreases with increasing feed pressure in this narrow region. The strongly adsorbed CO<sub>2</sub> shows a more significant decrease of permeability with pressure compared to the N<sub>2</sub>, which indicating a much stronger concentration dependence for the CO<sub>2</sub> diffusion coefficient. The N<sub>2</sub> permeability is less pressure dependent due to the relative weak adsorption interaction between the nitrogen molecules and the carbon matrix.

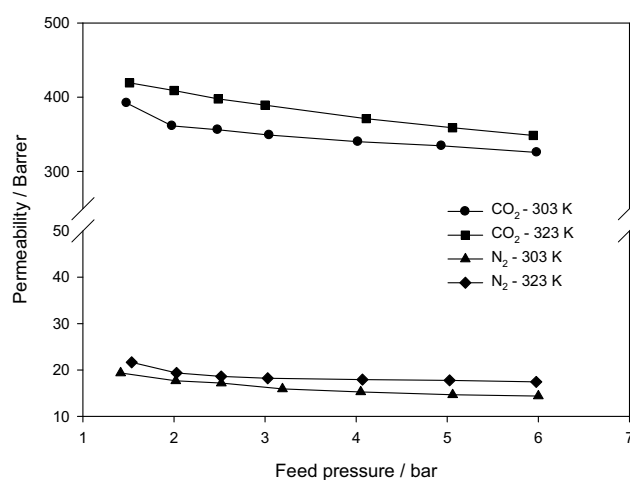


Figure 9. Dependency of the feed pressure on the performance of HFCMs at 303 and 323 K.

### 3.3.3 Gas mixture tests

The single gas tests are mainly used to characterize the ideal separation performance of the carbon membranes. However, the separation properties are usually influenced by the presence of the other penetrants in a gas mixture. Thus, a gas mixture (synthetic flue gas: 15% CO<sub>2</sub> - 81% N<sub>2</sub> - 4% O<sub>2</sub>) separation through the HFCMs was also tested at 303 K with a constant feed flow rate of 30 ml/min, while the feed pressure varied from 2 to 4 bar. The CO<sub>2</sub> composition in permeate and retentate stream as well as CO<sub>2</sub> recovery (ratio of CO<sub>2</sub> flow rate in permeate and feed stream) are given in Figure 10. The results indicates that the permeate CO<sub>2</sub> purity and CO<sub>2</sub> recovery increase following the increase of the feed pressure at a given membrane area. However, a higher energy demand for the compressors is required to reach a high feed pressure. Moreover, the influences of the operating parameters such as feed pressure and composition, temperature, and flow rate in retentate on the membrane process performances was systematically investigated in our previous work [35], and the results indicated that the operating conditions needs to be optimized for a specific application on the basis of the economic estimation from the process simulation. Moreover, the aging tests by the exposure of the HFCMs to the real flue gas needs to be also conducted to document the membrane durability, but this work has not been done so far.

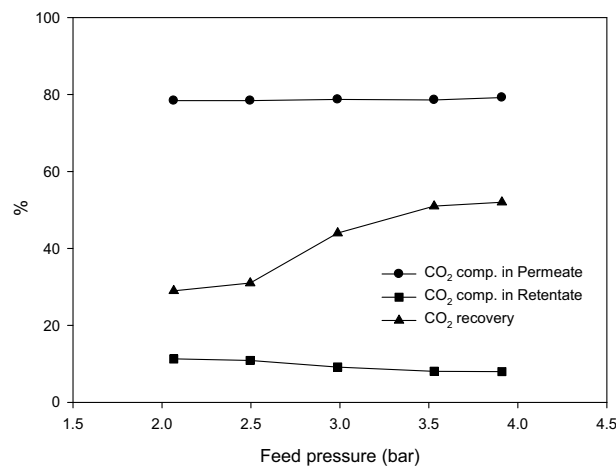


Figure 10. Dependency of CO<sub>2</sub> separation performance on the feed pressure at 303 K and a feed flow rate of 30 ml/min: (●) CO<sub>2</sub> composition in permeate; (■) CO<sub>2</sub> composition in retentate; (▲) CO<sub>2</sub> recovery.

## 4 Process simulation

The process simulation for CO<sub>2</sub> capture from flue gases in post combustion process by the HFCMs were conducted on the basis of Aspen HYSYS integrated with an in-house membrane unit. The process design was based on a typical 400MW power plant as described elsewhere [35]. To simplify the process simulation, only the main components of CO<sub>2</sub>, N<sub>2</sub>, and O<sub>2</sub> were considered here. The simulation basis was chosen on the basis of the characteristic membrane data from the dry gas permeation tests (case A) and specific boundary conditions for the CO<sub>2</sub> capture process, as listed in Table 2. Moreover, the process simulation based on an assumed carbon membrane performance (case B) by reducing the membrane thickness was also studied.

Table 2 Simulation basis for CO<sub>2</sub> capture from flue gases using HFCMs

Process	Carbon membrane			
	Performance	Case A <sup>*</sup>	Case B <sup>+</sup>	
Feed flow rate (Nm <sup>3</sup> h <sup>-1</sup> )	1×10 <sup>6</sup>	Permeance of CO <sub>2</sub> (Nm <sup>3</sup> . m <sup>-2</sup> . h <sup>-1</sup> .bar <sup>-1</sup> )	0.0395	0.1
Pressure (bar)	1.013	Selectivity of CO <sub>2</sub> /N <sub>2</sub>	41	41
Temperature (°C)	80	Selectivity of CO <sub>2</sub> /O <sub>2</sub>	6.85	6.85
CO <sub>2</sub> purity (%)	> 90			
CO <sub>2</sub> recovery (%)	> 80	Simulation condition	First stage	Second stage
CO <sub>2</sub> transport pressure (bar)	110	Feed temperature (°C)	50	50
Composition (vol %, dry base)	CO <sub>2</sub>	Feed pressure (bar)	4	4
	N <sub>2</sub>	Permeate pressure (bar)	0.25	0.25
	O <sub>2</sub>			

<sup>\*</sup>HFCMs tested at 323 K and a feed pressure of 2 bar as shown in Figure 9, <sup>+</sup> reducing the thickness from 25 to 10 μm

Since a single stage membrane process cannot achieve the specification as described elsewhere [35], a two stage cascade membrane process combined with recycling was designed for the simulation, as shown in Figure 11. The process parameters were optimized on the basis of the minimization of capital cost and the specific requirements (see Table 2). The captured CO<sub>2</sub> was then compressed to 110 bar for the pipe transportation to a sequestration site. As already stated, a permeate pressure of 250 mbar was chosen based on capacity for the large-scale industrial vacuum pumps. A 100 mbar

permeate pressure would have shown better theoretical results, but might have been less realistic for installation at a power plant. The specific capital costs are calculated from the required membrane area and the duty of the compressors and the coolers, and the simulation results of case A are given in Table 3. Comparing to the previous work [35], the specific capital cost was reduced from 136 to 100 \$/tonne CO<sub>2</sub> avoided by increasing the carbon membrane permeance (from 0.03 to 0.0395 Nm<sup>3</sup> · m<sup>-2</sup> · h<sup>-1</sup> · bar<sup>-1</sup>). Moreover, the cost of carbon membrane unit was found to be the major part of the total capital cost, which could be greatly reduced by improving the carbon membrane performance and simplifying the membrane production process although the carbon membrane/module cost is still unknown today. Therefore, an assumed membrane permeance (case B), based on the reduction of the wall thickness from 25 to 10 μm (see Table 2), was also employed for the process simulation using the same operating conditions. The results are given in Table 3. (Experimentally it is considered to be realistic to prepare carbon membranes with wall thickness of 10 μm – this was proven by previous company Carbon Membranes Ltd., Israel.) It was found that the total carbon membrane cost was reduced significantly from 2820 M\$ to 1280 M\$, due to the increased carbon membrane permeance, while the capital costs (\$/ t CO<sub>2</sub> avoided) now was down to 46. Ho et al. reported that the capital cost was 70 \$ / tonne CO<sub>2</sub> avoided using traditional chemical absorption method with monoethanolamine (MEA) for CO<sub>2</sub> capture from a 500 MW pulverised coal power plant [41]. It can thus be concluded that the carbon membrane technology is quite promising also compared to the chemical absorption methods. Hence, this environmental friendly technology could promote the hollow fiber carbon membranes to become a potential candidate for CO<sub>2</sub> capture in future.

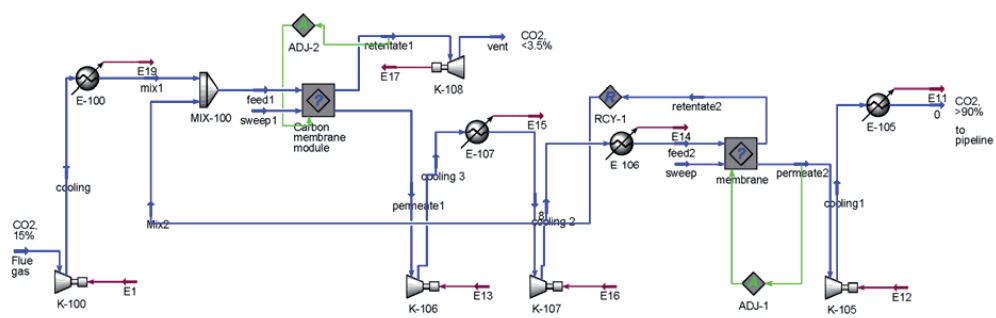


Figure 11. Simulation PFD for a two stage cascade carbon membrane units combined with recycling.

Table 3 Simulation results of CO<sub>2</sub> capture from flue gases by HFCMs

Parameter	Simulation results	
	Case A	Case B
CO <sub>2</sub> purity (%)	92.5	93.6
CO <sub>2</sub> recovery (%)	81.1	84.2
Membrane area (m <sup>2</sup> )	First stage	1.40×10 <sup>7</sup>
	Second stage	6.47×10 <sup>6</sup>
Total carbon membrane cost (M\$)	1.678×10 <sup>6</sup>	6.13×10 <sup>5</sup>
Total compressor duty GJ/ t CO <sub>2</sub> avoided	2820	1280
Specific capital cost \$ / t CO <sub>2</sub> avoided	4.82	4.84
	100	46

## 5 Conclusions

A general technical route of DPCOI platform has been presented to promote the HFCMs towards industrial. The cellulose acetate was chosen as the polymer material to prepare the hollow fibers from an optimized spinning process. The cellulosic precursors were regenerated from the CA hollow fibers on the basis of the optimal deacetylation process (i.e. the swelled CA hollow fibers were soaked in a 0.075M NaOH (96 %) solution for 2 h). The HFCMs were fabricated from the regenerated cellulosic precursors by well controlling of the carbonization procedure. The prepared HFCMs showed a good separation performance based on the single gas and gas mixture measurements. The potential industrial application of the HFCMs was also investigated on the basis of process simulation. The results indicated that the environment friendly process using high performance HFCMs, could possibly become a promising technology for CO<sub>2</sub> capture in future. It can be concluded that following the DPCOI platform for HFCM is a useful technical route for bridging fundamental and applied research with respect to the HFCMs from material to potential industrial application.

### Acknowledgements

The authors thank the NanoGloWa project (EUs 6<sup>th</sup> framework) for funding of this work and the Ugelstad lab at NTNU for the help with FTIR analysis.

## References

- [1] Fuertes AB, Centeno TA. Preparation of supported asymmetric carbon molecular sieve membranes. *J Membr Sci.* 1998;144(1-2):105-11.
- [2] Barsema JN. Carbon membranes precursor, preparation and functionalization [PhD]. Enschede: University of Twente; 2007.
- [3] He X, Lie JA, Sheridan E, Hägg M-B. Preparation and Characterization of Hollow Fiber Carbon Membranes from Cellulose Acetate Precursors. *Ind Eng Chem Res.* 2011;50(4):2080-7.
- [4] Lie JA. Synthesis, performance and regeneration of carbon membranes for biogas upgrading-a future energy carrier [PhD]. Trondheim: Norwegian University of Science and technology; 2005.
- [5] Kiyono M, Williams PJ, Koros WJ. Effect of pyrolysis atmosphere on separation performance of carbon molecular sieve membranes. *J Membr Sci.* 2010;359(1-2):2-10.
- [6] Vu DQ, Koros WJ, Miller SJ. High Pressure CO<sub>2</sub>/CH<sub>4</sub> Separation Using Carbon Molecular Sieve Hollow Fiber Membranes. *Ind Eng Chem Res.* 2001;41(3):367-80.
- [7] Vu DQ, Koros WJ, Miller SJ. Effect of Condensable Impurities in CO<sub>2</sub>/CH<sub>4</sub> Gas Feeds on Carbon Molecular Sieve Hollow-Fiber Membranes. *Ind Eng Chem Res.* 2003;42(5):1064-75.
- [8] David LIB, Ismail AF. Influence of the thermastabilization process and soak time during pyrolysis process on the polyacrylonitrile carbon membranes for O<sub>2</sub>/N<sub>2</sub> separation. *J Membr Sci.* 2003;213(1-2):285-91.
- [9] Favvas EP, Kapantaidakis GC, Nolan JW, Mitropoulos AC, Kanellopoulos NK. Preparation, characterization and gas permeation properties of carbon hollow fiber membranes based on Matrimid(R) 5218 precursor. *J Mater Process Tech.* 2007;186(1-3):102-10.
- [10] Soffer A, Koresh J, Saggy S. Separation device. US patent 4685940. 1987.
- [11] Tin PS, Chung T-S, Liu Y, Wang R. Separation of CO<sub>2</sub>/CH<sub>4</sub> through carbon molecular sieve membranes derived from P84 polyimide. *Carbon.* 2004;42(15):3123-31.
- [12] Vu DQ, Koros WJ, Miller SJ. High Pressure CO<sub>2</sub>/CH<sub>4</sub> Separation Using Carbon Molecular Sieve Hollow Fiber Membranes. *Ind Eng Chem Res.* 2002;41(3):367-80.
- [13] Das M, Perry JD, Koros WJ. Effect of processing on carbon molecular sieve structure and performance. *Carbon.* 2010;48(13):3737-49.

- [14] Lie JA, Hagg M-B. Carbon membranes from cellulose and metal loaded cellulose. *Carbon*. 2005;43(12):2600-7.
- [15] Lie JA, Hagg M-B. Carbon membranes from cellulose: Synthesis, performance and regeneration. *J Membr Sci*. 2006;284(1-2):79-86.
- [16] Sun N, Swatloski RP, Maxim ML, Rahman M, Harland AG, Haque A, et al. Magnetite-embedded cellulose fibers prepared from ionic liquid. *J Mater Chem*. 2008;18:1-9.
- [17] Rosenau T, Potthast A, Sixta H, Kosma P. The chemistry of side reactions and byproduct formation in the system NMMO/cellulose (Lyocell process). *Prog Polym Sci*. 2001;26(9):1763-837.
- [18] Swatloski RP, Spear SK, Holbrey JD, Rogers RD. Dissolution of Cellose with Ionic Liquids. *J Am Chem Soc*. 2002;124(18):4974-5.
- [19] Zhang H, Wu J, Zhang J, He J. 1-Allyl-3-methylimidazolium Chloride Room Temperature Ionic Liquid: A New and Powerful Nonderivatizing Solvent for Cellulose. *Macromolecules*. 2005;38(20):8272-7.
- [20] Edgar KJ, Buchanan CM, Debenham JS, Rundquist PA, Seiler BD, Shelton MC, et al. Advances in cellulose ester performance and application. *Prog Polym Sci*. 2001;26(9):1605-88.
- [21] Hao J-h, Dai H-p, Yang P-c, Wei J-m, Wang Z. Cellulose acetate hollow fiber performance for ultra-low pressure reverse osmosis. *Desalination*. 1996;107(3):217-21.
- [22] Jie X, Cao Y, Qin J-J, Liu J, Yuan Q. Influence of drying method on morphology and properties of asymmetric cellulose hollow fiber membrane. *J Membr Sci*. 2005;246(2):157-65.
- [23] Liu H, Hsieh Y-L. Ultrafine fibrous cellulose membranes from electrospinning of cellulose acetate. *J Polym Sci Part B: Polym Phys*. 2002;40(18):2119-29.
- [24] Qin J-J, Li Y, Lee L-S, Lee H. Cellulose acetate hollow fiber ultrafiltration membranes made from CA/PVP 360 K/NMP/water. *J Membr Sci*. 2003;218(1-2):173-83.
- [25] Son WK, Youk JH, Lee TS, Park WH. Electrospinning of Ultrafine Cellulose Acetate Fibers: Studies of a New Solvent System and Deacetylation of Ultrafine Cellulose Acetate Fibers. *J Polym Sci Part B: Polym Phys*. 2004;42:5-11.
- [26] Chung T-S, Hu X. Effect of air-gap distance on the morphology and thermal properties of polyethersulfone hollow fibers. *J Appl Polym Sci*. 1997;66(6):1067-77.

- [27] He X, Lie JA, Sheridan E, Hägg M-B. Preparation and Characterization of Hollow Fibre Carbon Membranes based on a Cellulosic Precursor. *Conf. on ICOM 2008*. Honolulu, Hawaii USA 2008.
- [28] Olaru N, Olaru L. Cellulose acetate deacetylation in benzene/acetic acid/water systems. *J Appl Polym Sci*. 2004;94(5):1965-8.
- [29] Yamashita Y, Endo T. Deterioration behavior of cellulose acetate films in acidic or basic aqueous solutions. *J Appl Polym Sci*. 2004;91(5):3354-61.
- [30] Saufi SM, Ismail AF. Fabrication of carbon membranes for gas separation--a review. *Carbon*. 2004;42(2):241-59.
- [31] Kusuki Y, Shimazaki H, Tanihara N, Nakanishi S, Yoshinaga T. Gas permeation properties and characterization of asymmetric carbon membranes prepared by pyrolyzing asymmetric polyimide hollow fiber membrane. *J Membr Sci*. 1997;134(2):245-353.
- [32] Lagorsse S, Magalhães FD, Mendes A. Carbon molecular sieve membranes: Sorption, kinetic and structural characterization. *J Membr Sci*. 2004;241(2):275-87.
- [33] Lagorsse S, Leite A, Magalhaes FD, Bischofberger N, Rathenow J, Mendes A. Novel carbon molecular sieve honeycomb membrane module: configuration and membrane characterization. *Carbon*. 2005;43(4):809-19.
- [34] Lie JA, Vassbotn T, Hägg M-B, Grainger D, Kim T-J, Mejdell T. Optimization of a membrane process for CO<sub>2</sub> capture in the steelmaking industry. *IJGGC*. 2007;1:309-17.
- [35] He X, Hägg M-B. Hollow fiber carbon membranes: Investigations for CO<sub>2</sub> capture. *J Membr Sci*. In Press, Corrected Proof.
- [36] He X, Lie JA, Sheridan E, Hägg M-B. CO<sub>2</sub> capture by hollow fibre carbon membranes: Experiments and process simulations. *Energy Procedia*. 2009;1(1):261-8.
- [37] Kookos IK. A targeting approach to the synthesis of membrane networks for gas separations. *J Membr Sci*. 2002;208(1-2):193-202.
- [38] Pettersen T, Lien KM. Insights into the design of optimal separation systems using membrane permeators. *Computers Chem Eng*. 1994;18(Suppl.):319-24.
- [39] Grainger D, Hägg M-B. Techno-economic evaluation of a PVAm CO<sub>2</sub>-selective membrane in an IGCC power plant with CO<sub>2</sub> capture. *Fuel*. 2008;87(1):14-24.
- [40] He X, Hägg M-B. Using orthogonal experimental design for spinning defect-free hollow fiber membranes. *Advanced Membrane Technology IV: Membranes for Clean and Sustainable Processes*. Trondheim 2009.
- [41] Ho MT, Allinson GW, Wiley DE. Comparison of MEA capture cost for low CO<sub>2</sub> emissions sources in Australia. *IJGGC*. 2011;5(1):49-60.

